IDŐJÁRÁS

QUARTERLY JOURNAL
OF THE HUNGARIAN METEOROLOGICAL SERVICE

CONTENTS

VOL. 97 * NO. 1 * JANUARY–MARCH 1993

IDŐJÁRÁS

Quarterly Journal of the Hungarian Meteorological Service

Editor-in-Chief
E. MÉSZÁROS

Editor
T. TÄNCZER

Technical Editor
Mrs. M. ANTAL

Editorial Office: P.O. Box 39, H–1675 Budapest

Subscription from customers in Hungary should be sent to the Financial Department of the Hungarian Meteorological Service Kitaibel Pál u. 1, 1024 Budapest. The subscription rate is HUF 2000.

Abroad the journal can be purchased from the distributor: KULTURA, P.O. Box 149, H–1389 Budapest. The annual subscription rate is USD 56.

IDŐJÁRÁS

Quarterly Journal of the Hungarian Meteorological Service
Vol. 97, No. 1, January–March 1993

Recent developments in the MAPS isentropic-sigma data assimilation system

S. G. Benjamin, T. L. Smith[1], P. A. Miller, D. Kim[2], T. W. Schlatter, D. Dévényi[3], J.-M. Carrière[4] and R. Bleck[5]

NOAA Environmental Research Laboratories
Forecast Systems Laboratory
Boulder, Colorado 80303, U.S.A.

(Manuscript received 3 September 1992; in final form 22 February 1993)

Abstract—A data assimilation system with a 3-h update frequency has been configured in hybrid isentropic-sigma coordinates. Several changes to this system have either been recently made or are now under development, including a change in the hybrid coordinate structure, addition of model physics, assimilation of satellite radiances, and improved analysis structure functions that allow explicit analysis of the divergent wind component. Short-range forecasts (3-6 hours) from this system are shown to provide improvement over longer-range forecasts (12 hours), indicating that high-frequency asynoptic observations from aircraft and wind profilers can be used successfully to update numerical predictions.

Key-words: data assimilation, isentropic coordinates, mesoscale forecasting, numerical weather prediction.

---

[1] Jointly affiliated with the Cooperative Institute for Research in the Atmosphere, Colorado State University, Ft. Collins, CO

[2] Jointly affiliated with the Cooperative Institute for Research in Environmental Sciences, University of Colorado, Boulder, CO

[3] Permanent affiliation - Hungarian Meteorological Service, Budapest

[4] Permanent affiliation - Météo France, Toulouse

[5] Permanent affiliation - University of Miami, Rosenstiel School of Marine and Atmospheric Science, Miami, Florida

---

Corresponding author address: Dr. S.G. Benjamin, NOAA/ERL/FSL,R/E/FS1, 325 Broadway, Boulder, CO 80303, U.S.A.

1. Introduction

The Mesoscale Analysis and Prediction System (MAPS), a mesoscale data assimilation system now configured in hybrid isentropic-sigma coordinates, has been under development since 1986. MAPS runs in real time at the Forecast Systems Laboratory, currently providing three-dimensional analyses and short-range forecasts over the contiguous United States and adjacent areas every 3 hours. The asynoptic analyses are supported by data from commercial aircraft, wind profilers, and surface reporting stations. Several significant changes have been made to MAPS since the original all-isentropic version was introduced in 1988 (see *Benjamin et al.*, 1991).

2. Hybrid isentropic-sigma coordinates

A hybrid isentropic-sigma ($\theta-\sigma$) coordinate was adopted to provide better resolution of the boundary layer under conditions of neutral static stability while retaining the advantages of θ coordinates in the free atmosphere. Isentropic coordinates give extra resolution in the vicinity of frontal zones and, therefore, better define gradients of temperature, moisture and momentum found in those regions. The initial version of this system, with 18 levels (5 σ levels and 13 θ levels), used a constant-depth σ domain with four layers of 50 hPa each and a fairly smooth surface terrain field. The initial hybrid coordinate configuration is illustrated in *Fig. 1a*, a depiction of analysis/model surfaces on an east-west cross section through the northwestern United States.

A variation of the hybrid coordinate was subsequently developed in which the σ domain is of variable depth, occupying the volume between a detailed surface terrain field and a smoothed $\theta-\sigma$ interface positioned approximately 150 hPa above a smoothed terrain field (*Fig. 1b*). In this variable-depth σ system, the error associated with the σ pressure gradient force is limited to a narrower vertical extent, allowing the use of high-resolution topography. A comparison of topography fields for the 80- and 60-km versions of MAPS is given in *Fig. 2*.

The pressure at the $\theta-\sigma$ interface is specified (time-independent) in the variable-depth σ system. In the original fixed-depth σ system, the interface pressure was time-dependent, a constant pressure thickness above the surface pressure. Tests with calm initial conditions show that this new formulation produces less noise than the hybrid coordinates with a constant-depth σ domain.

At the same time as the change to the variable-depth σ hybrid system, the number of levels was increased from 18 to 25 (6 σ and 19 θ levels). The spacing between isentropes below about 320 K was changed from 6 to 4 K. Also, the horizontal grid spacing was changed from 80 to 60 km. The high-resolution topography for the 60-km MAPS domain is shown in Fig. 2b.

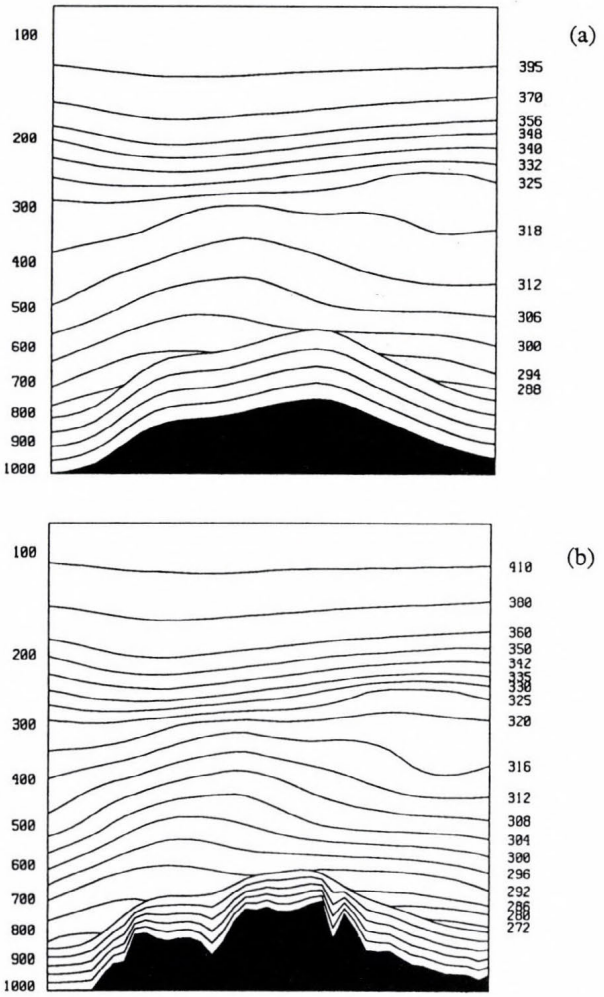

Fig. 1. East-west cross section from the Pacific Ocean off the southern Oregon coast to northern South Dakota for 1200 UTC 1 February 1991. Lines show the positions of MAPS analysis/forecast levels, including isentropic levels (labels on right) and sigma levels parallel to the model terrain. Pressure in hPa is shown on the left. Data are from gridded output of the Nested Grid Model analysis at this time. (*a*) 80-km, 18-level, fixed-σ version of MAPS, (*b*) 60-km, 25-level, variable-σ version of MAPS.

3. Observational data used in MAPS

MAPS incorporates data from several sources available within its current domain: about 80 standard 12-hourly rawinsonde (RAOB) observations, between 600 and 1200 hourly surface airways observations (SAOs), about 25 fixed buoys near the Atlantic and Pacific coastlines, and unconventional data

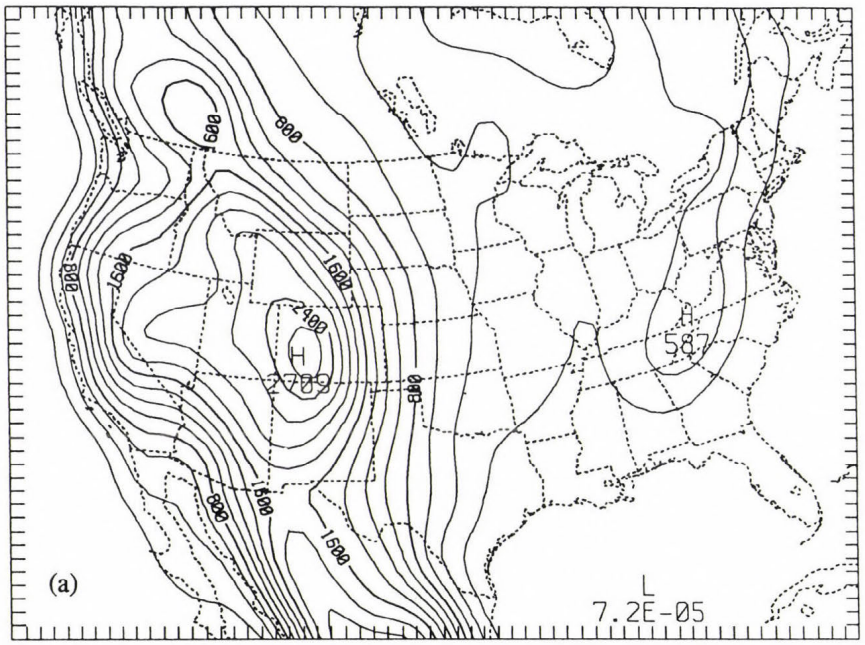

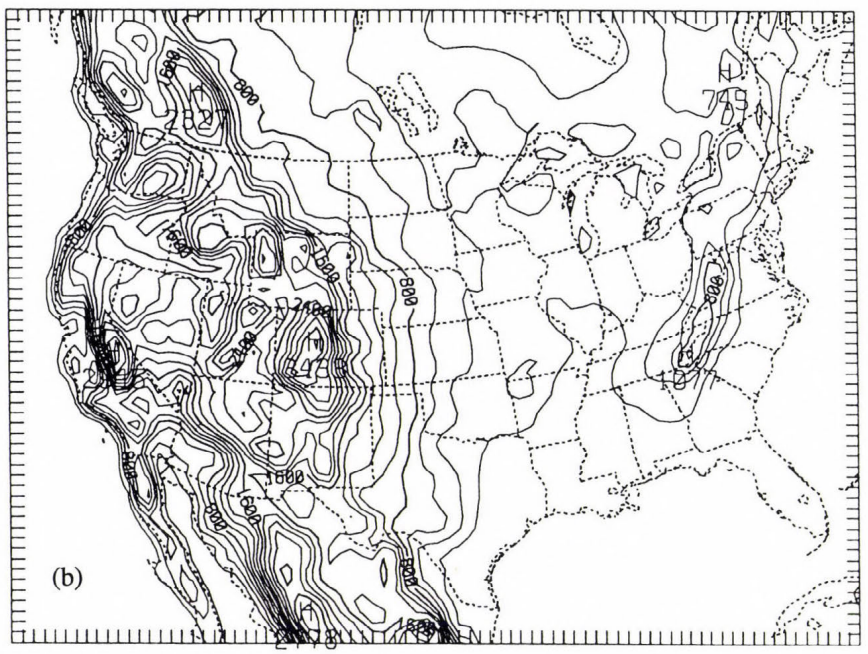

Fig. 2. Comparison of terrain fields for (*a*) 80-km and (*b*) 60-km versions of MAPS.

sources such as wind profilers and automated aircraft reports. With these observations, MAPS produces 3-hourly upper-air analyses.

The wind profiler data come from the NOAA Wind Profiler Demonstration Network, which is concentrated in the central United States (*Chadwick* and *Hassel,* 1987). As of June 1992, about 25 network profilers were operational. The data from all the profilers are 60-min averages of wind by height.

The automated aircraft reports in MAPS arrive via ACARS, the ARINC (Aeronautical Radio, Inc.) Communications, Addressing and Reporting System. Automated wind and temperature reports are typically made every 7.5 minutes by commercial aircraft that are properly equipped. The wind reports are of very high accuracy, owing to the inertial navigation systems onboard the aircraft (*Benjamin et al.,* 1991). Aircraft observations from −2 h to +1 h of the analysis time are used in the analysis. Depending on the time of day, the number of reports used in an analysis ranges from fewer than 400 at 0900 UTC to more than 1500 at 0000 UTC (*Fig. 3*). These reports, now numbering about 8500 per day over the United States, are concentrated in the middle to upper troposphere at standard flight levels.

Lateral boundary conditions for MAPS are specified from forecasts from the National Meteorological Center (NMC) Regional Analysis and Forecast System (RAFS; *Petersen et al.,* 1991). RAFS forecasts are interpolated to MAPS vertical and horizontal coordinates for this purpose.

4. Observational quality control

Incoming data are screened before assimilation into MAPS. The screening takes place in two steps: (1) vertical consistency checks performed on incoming

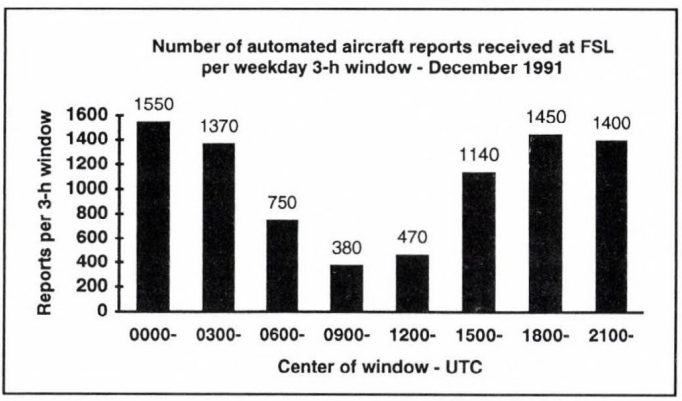

Fig. 3. Number of ACARS reports collected in 3-h intervals throughout the day in December 1991. These numbers were still representative in June 1992.

rawinsonde and wind profiler data and (2) horizontal consistency checks performed on all observations after interpolation to analysis surfaces. These checks are similar to those for the pure isentropic version of MAPS described by *Benjamin et al.* (1991).

Rawinsonde profiles are required to contain reasonable surface data and to be vertically consistent in temperature, height, pressure, and dewpoint. Hydrostatic and lapse-rate checks are employed to check the vertical consistency of heights and temperature. Corrections are made (when possible) based on ideas given in *Gandin* (1988). If correction is not possible, the erroneous levels are flagged as bad and not used in subsequent MAPS quality control, analysis, or forecast components. Wind profiler data are checked for vertical consistency using a gate-to-gate shear threshold, which is a function of height, wind speed, and wind direction. Temporal consistency is also checked by statistically comparing each profiler wind observation to winds from adjacent times and heights (*Brewster* and *Schlatter,* 1989). No corrections are attempted but, as with rawinsonde data, bad levels are flagged and ignored in later processing. After these vertical quality control checks, rawinsonde and profiler data are interpolated to MAPS hybrid coordinate levels.

Each observation is then checked for horizontal consistency by comparing it to surrounding observations at the same level. Surrounding observations are analyzed to the location of the target observation (the observation being checked) using univariate optimal interpolation and MAPS 3-h forecasts as background. If the analyzed residual (difference between observation and background value) minus the observed residual is greater than a threshold, further checking is performed to determine if the target observation or one of the surrounding observations is incorrect. The threshold is a function of analysis error and contains a factor dependent on analysis level and observation type. The factors were updated for the new MAPS domain by studying the statistical properties of the ratio of the threshold to the analysis minus observed values (*Miller* and *Benjamin,* 1991). As before, observations found bad are not used in subsequent processing. Horizontal consistency checks for surface observations are performed separately as part of the MAPS surface assimilation system (*Miller* and *Benjamin*, 1992).

5. Objective analysis in isentropic-sigma hybrid coordinates

Benjamin et al. (1991) described the original MAPS analysis in pure isentropic coordinates. The mass analysis consisted of a two-step procedure, a multivariate mass/wind initial analysis followed by a univariate analysis of mass only. The two-step analysis procedure has been extended in the MAPS hybrid analysis for the mass variable in both the θ and σ domains. Optimal interpolation (OI) is used for multivariate and univariate analyses. Up to 63

observations may influence the analyzed value at a single grid point. Observations are selected as described by *Benjamin* (1989).

In the θ domain, first an *M/u/v* multivariate analysis (where the Montgomery stream function, $M = gz + \Pi\theta$) is performed from which an increment to the Exner function,

$$\Pi = C_p \left(\frac{P}{P_0} \right)^{R/C_p} = \frac{\partial M}{\partial \theta},$$

(with $P_0 = 1000$ hPa) is calculated hydrostatically. This increment is added to the original Exner function background field, forming an updated background field for a subsequent univariate analysis of pressure on θ surfaces.

In the σ domain, a *z/u/v* multivariate analysis is performed at each level. A surface pressure increment is determined from the z increment at the lowest sigma level. A univariate analysis of θ is then performed throughout the σ domain.

One final step is performed for the wind/mass analysis in hybrid coordinates. The original M increment at a reference level in the upper troposphere is saved after the multivariate analysis. Using that updated M value, we hydrostatically integrate back down to the surface and then compare that value of M with M_{sfc} calculated directly from

$$M_{sfc} = gz_{topo} + \Pi_{sfc}\,\theta_{sfc}.$$

A temperature adjustment is then calculated and applied to the column between the surface and the reference θ level. In this manner, the original multivariate M increment at the reference level is assured even after hydrostatic integration. The reference level, chosen to be in the upper troposphere, is considered to be most reliable because it is close to the layer of dense aircraft report coverage.

The moisture variable used in MAPS is condensation pressure (P_c), which is the lifting condensation level for a given parcel of air. P_c is conserved for motion on isentropic surfaces if no condensation or evaporation occurs, and it varies much more linearly through the troposphere than water vapor mixing ratio. A univariate OI analysis of P_c is performed in which the P_c increments are streaked elliptically along the wind in a manner similar to that described by *Benjamin* and *Seaman* (1985).

Previously, the coefficients for models describing horizontal correlation of background error used in MAPS were based on statistics of 12-h errors collected by *Benjamin* (1989) from the Nested Grid Model (NGM) run at NMC. Recently, *Carrière* (1991) collected new statistics on 3-h forecast errors from the MAPS prediction model. As of March 1991, new coefficients for the

second-order autocorrelation model (SOAR) of horizontal correlation of forecast error had been implemented based on Carrière's study.

Analyses on isentropic levels may use observations both above and below the $\theta-\sigma$ interface; the position of the interface is not relevant. The σ and θ level analyses are redundant in a sense, since the domains usually overlap, and analyses are performed on both sets of surfaces separately. This is done to ensure the best possible θ analyses just above the interface by using data on both sides of the interface. Before a hybrid analysis is used to initialize the hybrid forecast model, however, information on θ levels beneath the interface is truncated and isentropic levels beneath the interface are forced to become collocated with the interface, as shown in Figs. 1 and 2.

Observation selection is done on θ surfaces in the θ domain and on σ surfaces in the σ domain. The three-dimensional correlations of forecast error are partitioned into horizontal and vertical components in both σ and θ domains, where the vertical component is based on potential temperature separation. The use of this "vertical" correlation model in the σ domain can result in sharp horizontal gradients along σ surfaces that are consistent with observed air-mass discontinuities.

6. Experiments with assimilating satellite radiances into MAPS analyses

Satellite data have not been utilized by MAPS yet in real time, but testing in this area has been conducted for the last few years. Because of complications in the temperature retrievals of satellite radiance data, a radiance assimilation scheme has been designed for MAPS based on the scheme of *Eyre* and *Lorenc* (1989). At each field of view of the Television and Infrared Observation Satellite (TIROS) pass within the MAPS analysis domain, a temperature/humidity profile from the 3-h MAPS forecast is interpolated from hybrid to pressure coordinates in order to compute radiances. Satellite radiance residuals (difference between measured and computed radiances) are calculated, from which an analysis increment field can be obtained using an off-line empirical retrieval operator.

The retrieval operator that converts radiance residuals to the temperature or humidity increment is a covariance matrix obtained from the collocated data set of (1) measured radiances, (2) computed radiances from 3-h MAPS forecast, (3) computed radiances from RAOB, (4) RAOB profiles and (5) 3-h MAPS forecast profiles. The retrieval operator is further refined by obtaining covariance matrices from smaller (in the sample size) but more homogeneous (in the distribution of errors) collocated data sets. This is achieved by classifying the data set into several clusters according to closeness in the data. Each cluster represents different covariances because of different error characteristics in the forecast field. A preliminary study of cluster analyses with a March 1991 data set was reported by *Kim* (1992).

7. Development of new structure functions for MAPS objective analyses

The MAPS wind field analysis is currently based on the geostrophic relationship using a geostrophic coupling coefficient to allow some ageostrophy. Because divergence plays an important role in mesoscale processes, use of the geostrophic approximation in a mesoscale model is questionable. Applying the kinematic theory of homogenous and isotropic turbulence, *Daley* (1985) developed a new approach to determine background error correlation functions for mass and wind forecasts that includes an explicit analysis of the divergent wind component. The European Centre for Medium-Range Weather Forecasts (ECMWF) has followed Daley's formulation in modeling wind and mass field first guess errors (*Hollingsworth* and *Lönnberg*, 1986; *Lönnberg* and *Hollingsworth*, 1986). A similar formulation is under development at MAPS for implementation in a 3-h data assimilation cycle.

Based on the Helmholtz theorem, a long but straightforward derivation (*Daley*, 1991, pp.155-169; *Schlatter* and *Carrière*, 1991) results in the following system of equations for autocorrelation and cross-correlation functions (ρ) of Montgomery stream function (M), velocity potential (χ), and stream function (ψ):

$$-\frac{1}{D^2}\left(\frac{d^2}{dx^2}+\frac{1}{x}\frac{d}{dx}\right)\left[\gamma^2\,\rho_{\psi\psi}(x)+\delta^2\,\rho_{\chi\chi}(x)\right]=\rho_{ll}(x)+\rho_{tt}(x) \tag{1}$$

$$\frac{1}{D^2}\left(\frac{d^2}{dx^2}-\frac{1}{x}\frac{d}{dx}\right)\left[\gamma^2\,\rho_{\psi\psi}(x)-\delta^2\,\rho_{\chi\chi}(x)\right]=\rho_{ll}(x)-\rho_{tt}(x) \tag{2}$$

$$-\frac{\gamma\,\delta}{D^2}\left(\frac{d^2}{dx^2}-\frac{1}{x}\frac{d}{dx}\right)\rho_{\psi\chi}(x)=\rho_{lt}(x)=\rho_{tl}(x) \tag{3}$$

$$\frac{\gamma}{D}\frac{d}{dx}\rho_{M\psi}(x)=\rho_{Mt}(x) \tag{4}$$

$$\frac{\delta}{D}\frac{d}{dx}\rho_{M\chi}(x)=\rho_{Ml}(x) \tag{5}$$

$$\rho_{MM}(x)=\rho_{MM}(x). \tag{6}$$

In the system of Eqs. (1)−(6), D signifies a distance beyond which correlations are expected to be a small constant value, giving a natural scaling for separation distance ($x=r/D$). In our investigation, a value for D of 3000 km was used. Standard deviations of background error for the stream function and velocity potential have been normalized by the standard deviation of background error for the transverse (t) wind component (or equivalently, because of isotropy, by the standard deviation of background error for the longitudinal (l) wind component), resulting in $\gamma=\sigma_\psi/\sigma_l$ and $\delta=\sigma_\chi/\sigma_l$. (The t and l wind components are defined as the wind components normal and parallel, respectively, to the line segment connecting the pair of points, as shown by *Daley* (1991, p.158).) Eq. (6) is added to the system for completeness. The background error correlations on the right-hand sides of Eqs. (1)−(6) are considered to be known. They may be computed from a sample of forecasts by the assimilating model.

The system of equations above can be solved if the unknown correlations on the left are represented by a truncated expansion of Bessel functions.

$$\rho_{unknown}(x) = \sum_{i=1}^{N} y_i^{unknown} J_0(k_i x). \tag{7}$$

The unknown coefficients y_i are to be determined, and J_0 is a Bessel function of the first kind of order zero. The coefficients k_i are the positive roots of $J_1(k)=0$, corresponding to a zero, Neumann-type boundary condition at D. Substituting expressions like (7) into the left-hand side of Eqs. (1)−(6) and the empirical correlation values into the right-hand sides yields a fully determined system for the unknown coefficients of the truncated Bessel function series. Because of unavoidable noise in the empirical correlations, it is preferable to use a least squares technique to solve for the coefficients.

To achieve this solution, knowledge of the parameters γ and δ is required. But in the case of a limited area model such as MAPS, stream function and velocity potential fields cannot be computed uniquely because they depend on actual lateral boundary conditions. Therefore the following method for iterative estimation of these parameters has been developed. In addition to the system of Eqs. (1)−(6), a diagnostic relationship can be obtained from turbulent microscale theory. To do this, a two-dimensional length scale L has been defined for any autocorrelation function ρ as

$$L^2 \equiv -2\left[\frac{\rho(r/D)}{\nabla^2 \rho(r/D)}\right]_{r\to 0}, \tag{8}$$

where, for the isotropic case,

$$\nabla^2 = \left(\frac{d^2}{dr^2} + \frac{1}{r} \frac{d}{dr} \right).$$

Using (8), (7), and (1), one can derive the following relationship between stream-function length scale L_ψ and velocity potential length scale L_χ (*Daley*, 1991, p.160):

$$\frac{\gamma^2}{L_\psi^2} + \frac{\delta^2}{L_\chi^2} = 1, \tag{9}$$

where

$$L_\psi^2 = \frac{2D^2}{\sum_{i=1}^{N} k_i^2 \psi_i}, \qquad L_\chi^2 = \frac{2D^2}{\sum_{i=1}^{N} k_i^2 \chi_i}. \tag{10}$$

The ratio $\nu^2 = \delta^2 / L_\chi^2$ in (9) is equivalent to the kinetic energy in the divergent component of the forecast error normalized by total forecast error kinetic energy.

Using (7), (9), and (10), an iterative least squares method can be developed such that the solution of (1) and (2) is represented by a convergent series of unknown coefficients ψ_i and χ_i. The value of ν is iterated until the distance between the empirical and modeled correlations is minimized.

To illustrate the results of the above procedure, *Fig. 4* shows the autocorrelation of 3-h MAPS forecast error for the Montgomery stream function on the 312 K isentropic level. Note that the sample size for all but the smallest separation distance is 3000. The correlation approaches slowly a small negative value, suggesting a slight large-scale bias in the Montgomery field. Considering the correlations ρ_{ll} and ρ_{tt} we find, similar to *Hollingsworth* and *Lönnberg* (1986), that the longitudinal correlation falls off less rapidly with distance than the transverse correlation. It does not approach zero until beyond 1000 km whereas the transverse correlation becomes negative around 500 km. Corresponding solutions of Eqs. (1) and (2) show that the original behavior of empirical correlations has been retained, but the results are corrected by zero intercept values containing the effects of measuring errors and unresolved scales in the MAPS model. The correlations ρ_{Mt} and ρ_{Ml} are illustrated in *Figs. 5a* and *5b*. The value of ρ_{Mt} reaches a minimum at r=400 km and then returns to near zero throughout the rest of its range. The fact that our ρ_{Mt} dips beyond 1000 km only to -0.25 suggests that our 3-h background errors are relatively less geostrophic than those at ECMWF (compare with Fig. 16 of *Lönnberg* and *Hollingsworth* (1986), where the $Z-t$ correlation dips to -0.55). Note that ρ_{Ml} is near zero throughout its range. *Fig. 6* (fitted $\rho_{M\psi}$) gives another illustration of

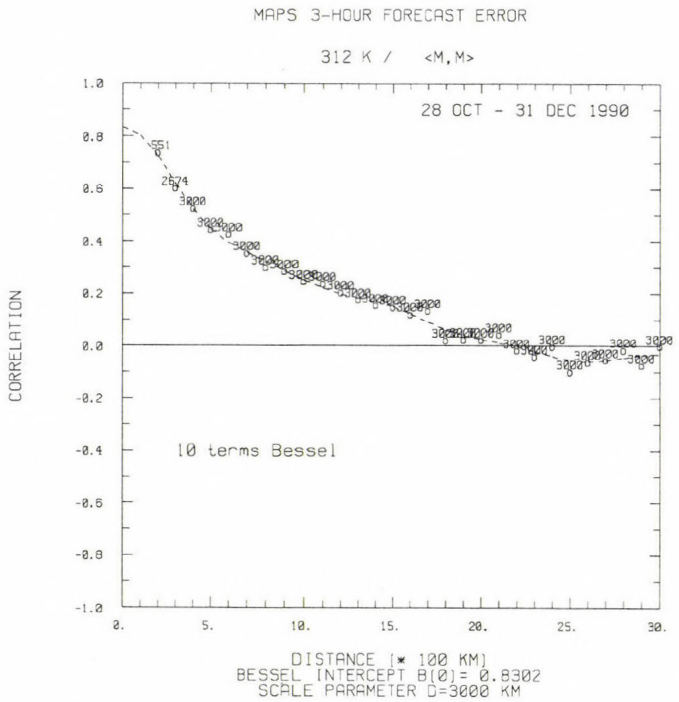

Fig. 4. Correlation of Montgomery stream function on the 312 K isentropic level. The open circles are empirical correlation values computed from 3-h MAPS forecast errors during the winter of 1990 and 1991. The dashed line depicts the fitted Bessel function expansion.

the ageostrophic character of MAPS forecast errors. If the 3-h forecast errors of the MAPS model were purely geostrophic, one would expect $\rho_{M\psi}$ to approach one at zero separation. Instead, it reaches 0.39 for the winter data, indicating substantial ageostrophy in the error field.

The statistics described above for the 312 K isentropic level have also been computed for another 12 θ and 5 σ levels in the MAPS model. Since calculating 10-term Bessel expansions for every correlation in the analysis program would be very expensive, we plan to precompute them at 1-km resolution. From these look-up tables, the correlations actually used in the analysis are easily computed.

This method for determining new forecast error structure functions and preliminary results from it are the first steps in the modernization of the MAPS objective analysis system. Determination of the vertical correlation structure for M, ψ, and χ background error fields is not yet complete. Applying new corre-

Fig. 5. Cross-correlations between the Montgomery stream function and the longitudinal and transverse wind components 3-h MAPS forecast errors on the 312 K isentropic level. Legends are as in Fig. 4. (*a*) ρ_{Mt} correlations, (*b*) ρ_{Ml} correlations.

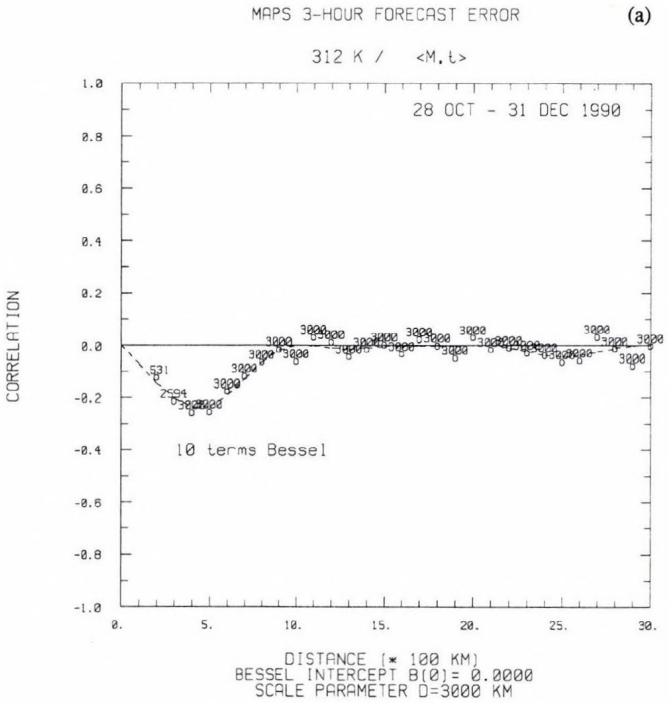
MAPS 3-HOUR FORECAST ERROR
(a)
312 K / <M,t>
28 OCT - 31 DEC 1990
CORRELATION
1.0
0.8
0.6
0.4
0.2
0.0
-0.2
-0.4
-0.6
-0.8
-1.0
0.
5.
10.
15.
20.
25.
30.
10 terms Bessel
DISTANCE (* 100 KM)
BESSEL INTERCEPT B(0)= 0.0000
SCALE PARAMETER D=3000 KM

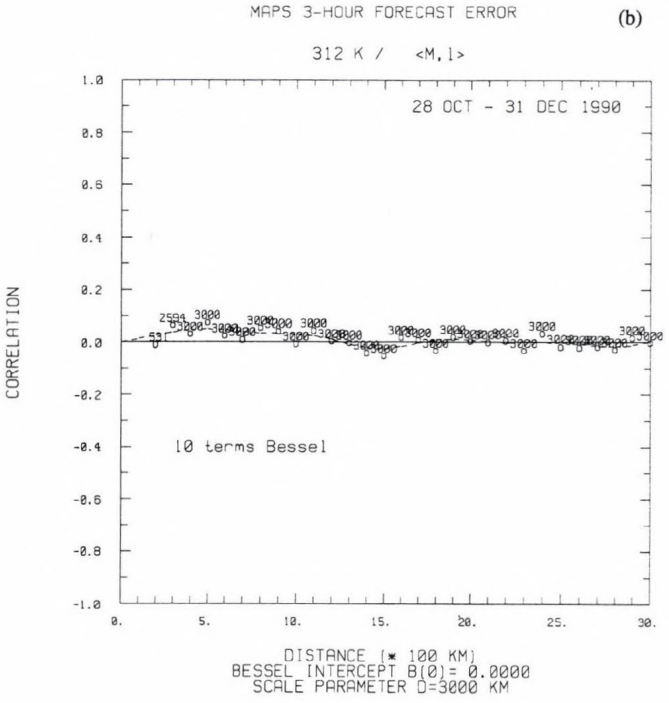
MAPS 3-HOUR FORECAST ERROR
(b)
312 K / <M,l>
28 OCT - 31 DEC 1990
CORRELATION
1.0
0.8
0.6
0.4
0.2
0.0
-0.2
-0.4
-0.6
-0.8
-1.0
0.
5.
10.
15.
20.
25.
30.
10 terms Bessel
DISTANCE (* 100 KM)
BESSEL INTERCEPT B(0)= 0.0000
SCALE PARAMETER D=3000 KM

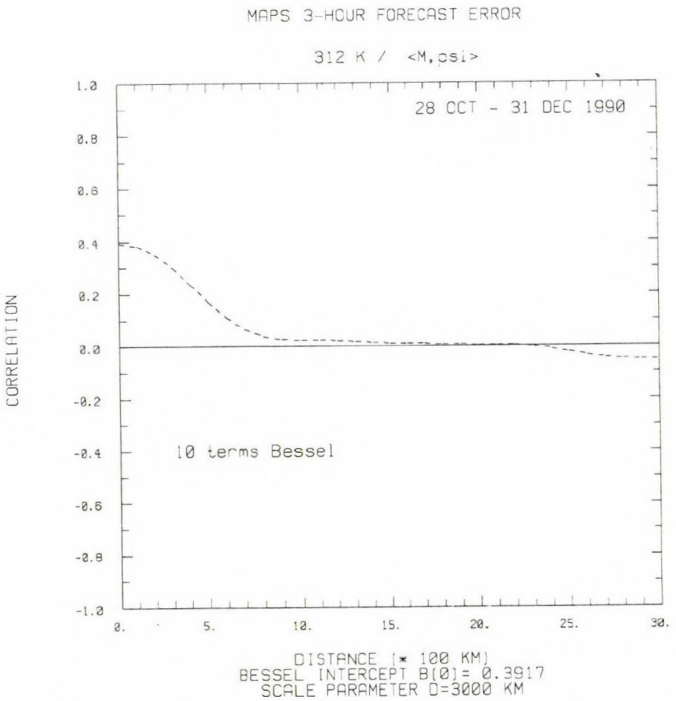

Fig. 6. $\rho_{M\psi}$ correlations on the 312 K isentrope by solution of Eq. (4). The dashed line depicts the fitted Bessel function expansion.

lation functions for dynamical variables of the MAPS objective analysis could also lead to an improved method for the humidity analysis, including application of total precipitable water information derived from GOES satellite data.

8. *Isentropic-sigma hybrid forecast model*

The forecast model used in MAPS is a descendant of the primitive equation model developed by *Bleck* (1974, 1977, 1984). The MAPS version of the Bleck model uses non-staggered vertical levels to avoid vertical interpolation between analyses and forecasts in the MAPS assimilation cycle.

The primary recent numerical innovation in the MAPS model has been the incorporation of the hybrid coordinate system. The prognostic variables are pressure thickness, P_c, and u/v wind components in the θ domain, and potential temperature, P_c, u, and v in the σ domain. Following Fig. 1, isentropic coordinate surfaces are allowed to intersect the $\sigma-\theta$ interface because θ is variable along the interface. Computationally, the interface plays a role similar to that of the ground in pure isentropic models. Isentropic layers collapse to a state of zero layer thickness on the interface.

Since the interface is not a material surface, the σ and θ domains are permitted to exchange mass (and other properties). The vertical component of motion across the interface is determined through integration of the continuity equation. The pressure thickness in isentropic layers above the interface is adjusted so that entropy and mass in the column are conserved.

Precipitation physics has also been added to the MAPS model. Stable precipitation is determined by excess moisture over saturation—saturation occurring when the condensation pressure equals the pressure at a grid point. There is currently no evaporation of stable precipitation in layers below the supersaturated level. Convective precipitation is estimated via the parameterization developed by *Grell* (1992); the effects of evaporation and convective downdrafts are included. The closure assumption in the Grell scheme is the rate of destabilization.

A scheme for vertical turbulent mixing based on the level-2.0 turbulence closure of *Mellor* and *Yamada* (1982) has also been added to MAPS. The scheme acts primarily in the boundary layer, but can also mix layers aloft with sufficiently low Richardson numbers. Even without realistic surface fluxes, the Mellor-Yamada second-order scheme produces much improved profiles of potential temperature and wind near the surface. Work is under way to add a surface energy budget and surface flux formulations to the MAPS model, including effects of cloudiness on downward shortwave and longwave fluxes.

9. Statistical verification

Statistical verification of MAPS forecasts against rawinsonde data has shown a steady improvement over the last 30 months as modeling and analysis improvements have been implemented. The changes most responsible for statistical improvement include elimination of errors in data ingest, analysis, and forecast model routines as well as planned improvements. These improvements include the implementation of the hybrid coordinate system in May 1990, the Grell convective scheme in September 1990, and the 60-km/25-level variable-σ system with the Mellor-Yamada mixing in September 1991. The volume of observations has not changed appreciably during this period.

The use of isentropic coordinates and extra aircraft observations in MAPS allows improved short-range forecasts of jet-level winds. This is evident in the recent history of verification of 250-hPa wind forecasts (*Fig. 7*). MAPS 3-h forecasts, using asynoptic observations, currently improve on NGM 12-h forecasts (not using asynoptic data) by well over 1 m s^{-1}. This margin of improvement over NGM forecasts has increased substantially during the comparison period. Six-hour forecasts from MAPS have also generally shown improvement over 12-h NGM forecasts in the upper troposphere since they started running in January 1991. The distribution of wind forecast errors with

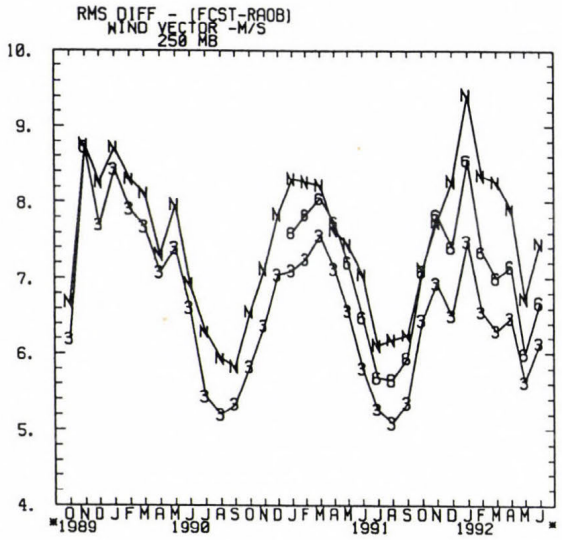

Fig. 7. RMS vector difference between forecasts and rawinsonde observations of 250-hPa winds from October 1989 to June 1992. NGM 12-h forecasts are denoted as **N**, 3-h MAPS forecasts as **3**, and 6-h MAPS forecasts as **6**.

height is shown in *Fig. 8a* for early 1992. The greatest advantage of frequent assimilation is in the high troposphere, where ACARS reports are most plentiful.

Height forecasts from MAPS with durations of 3 hours and even 6 hours currently show improvement of 1−2 m (standard deviation error) over 12-h NGM height forecasts at all mandatory levels up to 150 hPa (*Fig. 8b*). The difference is most pronounced near jet level and near the surface. During the winter of 1990-91 when the pure isentropic version of MAPS was running, 3-h MAPS forecasts were poorer than 12-h NGM forecasts of height at all mandatory levels (*Benjamin et al.*, 1991). This indicates the progress that has occurred since that time. Data sensitivity experiments done by *Benjamin* and *Stamus* (1991) show that surface observations are quite helpful in improving low-level height forecasts, and also have some positive impact in height forecasts throughout the troposphere.

10. Plans for the future

The current MAPS assimilation cycle produces upper-level analyses and forecasts every 3 hours. *Benjamin* and *Stamus* (1991) have shown that there are already sufficient asynoptic data over the United States to run an assimilation cycle at 1-h frequency with the potential for modest improvements over a 3-h cycle. Their tests were run with a case from January 1990, when wind profiler

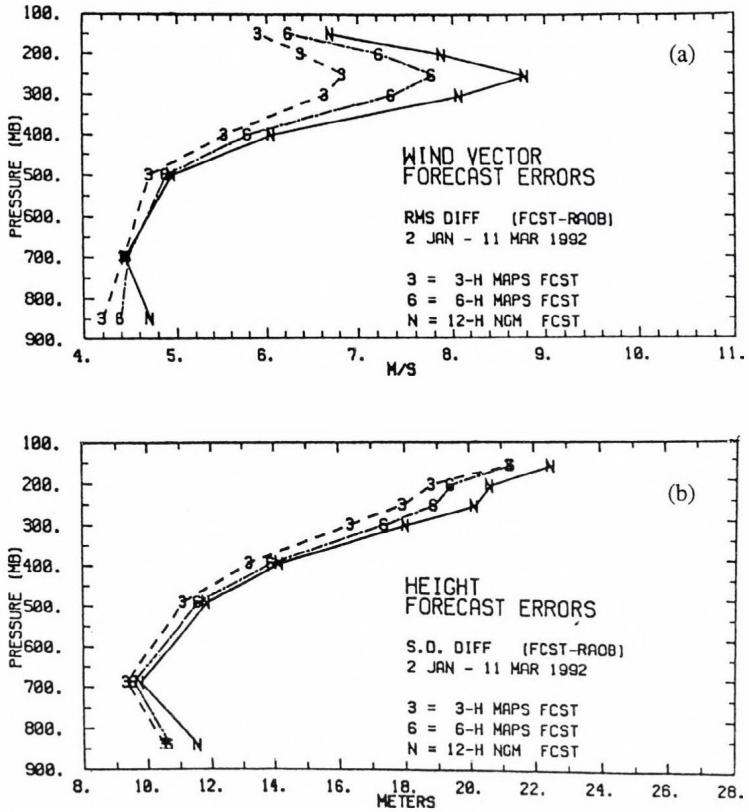

Fig. 8. Vertical profiles of forecast errors (difference from rawinsonde observations at forecast verifying time) for the period 2 January–11 March 1992. Symbols are as in Fig. 7. (*a*) Root-mean-square vector error of wind forecasts, (*b*) standard deviation error of height forecasts.

data were available only from a few experimental sites in Colorado. As the number of wind profilers producing hourly data increases, the potential improvement from a 1-h cycle will also increase.

Improvements in handling diurnal surface effects have been implemented during the remainder of 1992. In 1993, the MAPS analysis in hybrid vertical coordinates will be recast to allow explicit analysis of the divergent wind component (*Schlatter* and *Carrière,* 1991).

After real-time testing at the Forecast Systems Laboratory, these improvements will be incorporated into a version of MAPS now running experimentally at NMC. MAPS is expected to run regularly at NMC beginning in 1993.

Acknowledgments—The authors acknowledge the contributions of *Kevin Brundage* and *Pan Zaitao* in the development of MAPS. *Chris Thomas* and *Pete Stamus* gave careful reviews of the paper.

D. Dévényi's work was supported by a National Research Council (NRC) - NOAA/ERL/Forecast Systems Laboratory Research Associateship. He would like to thank the MAPS team for assistance during his visit.

References

Benjamin, S.G., 1989: An isentropic meso-alpha scale analysis system and its sensitivity to aircraft and surface observations. *Mon. Wea. Rev. 117*, 1586-1605.

Benjamin, S.G. and *Seaman, N.L.*, 1985: A simple scheme for objective analysis in curved flow. *Mon. Wea. Rev. 113*, 1184-1198.

Benjamin, S.G. and *Stamus P.A.*, 1991: Experiments with 1-h and 3-h assimilation cycles using mesoscale aircraft and surface data. *Preprints, 9th Conference on Numerical Weather Prediction*, Denver, Colorado, 14-18 October. American Meteorological Society, Boston, Massachusetts, 186-189.

Benjamin, S.G., Brewster, K.A., Brümmer, R.L., Jewett, B.F., Schlatter, T.W., Smith, T.L. and *Stamus, P.A.*, 1991: An isentropic three-hourly data assimilation system using ACARS aircraft observations. *Mon. Wea. Rev. 119*, 888-906.

Bleck, R., 1974: Short range prediction in isentropic coordinates with filtered and unfiltered numerical models. *Mon. Wea. Rev. 102*, 813-829.

Bleck, R., 1977: Numerical simulation of lee cyclogenesis in the Gulf of Genoa. *Mon. Wea. Rev. 105*, 428-445.

Bleck, R., 1984: An isentropic coordinate model suitable for lee cyclogenesis simulation. *Riv. Meteor. Aeronaut. 44*, 189-194.

Brewster, K.A. and *Schlatter, T.W.*, 1989: Recent progress in automated quality control of wind profiler data. *Preprints, 8th Conference on Numerical Weather Prediction*, Baltimore, Maryland. American Meteorological Society, Boston, Massachusetts, 331-338.

Carrière, J.-M., 1991: Statistics of horizontal correlation of errors for three-hour prediction fields in isentropic coordinates. *Preprints, 9th Conference on Numerical Weather Prediction*, Denver, Colorado, 14-18 October. American Meteorological Society, Boston, Massachusetts, 62-65.

Chadwick, R.B. and *Hassel, N.*, 1987: Profiler: the next generation surface-based atmospheric sounding system. *Preprints, Third International Conference on Interactive Information and Processing Systems for Meteorology, Oceanography and Hydrology*, 12-16 January, New Orleans, Louisiana. American Meteorological Society, Boston, Massachusetts, 15-21.

Daley, R., 1985: The analysis of synoptic scale divergence by a statistical interpolation procedure. *Mon. Wea. Rev. 113*, 1066-1079.

Daley, R., 1991: *Atmospheric Data Analysis*. Cambridge University Press, New York.

Eyre, J.R. and *Lorenc, A.C.*, 1989: Direct use of satellite sounding radiances in numerical weather prediction. *Meteor. Mag. 118*, 13-16.

Gandin, L.S., 1988: Complex quality control of meteorological observations. *Mon. Wea. Rev. 116*, 1137-1156.

Grell, G., 1992: Prognostic evaluation used by cumulus parameterization schemes. *Mon. Wea. Rev. 120*, in press.

Hollingsworth, A. and *Lönnberg, P.*, 1986: The statistical structure of short-range forecast errors as determined from radiosonde data. Part I: The wind field. *Tellus 38A*, 111-136.

Kim, D., 1992: Cluster analyses of radiance data measured from satellite and computed from forecast profiles. *Preprints, Twelfth Conference on Probability and Statistics in the Atmospheric Sciences*, 22-26 June, Toronto, Canada. American Meteorological Society, Boston, Massachusetts, J109-112.

Lönnberg, P. and *Hollingsworth, A.*, 1986: The statistical structure of short-range forecast errors as determined from radiosonde data. Part II: The covariance of height and wind errors. *Tellus 38A*, 137-161.

Mellor, G.L. and *Yamada, T.*, 1982: Development of a turbulence closure model for geophysical fluid problems. *Rev. Geophys. Space Phys. 20*, 851-875.

Miller, P.A., and *Benjamin, S.G.*, 1991: Horizontal quality control for a real-time 3-h assimilation system configured in isentropic coordinates. *Preprints, 9th Conference on Numerical Weather Prediction*, Denver, Colorado, 14-18 October. American Meteorological Society, Boston, Massachusetts, 58-61.

Miller, P.A. and *Benjamin, S.G.*, 1992: A system for the hourly assimilation of surface observations in mountainous and flat terrain. *Mon. Wea. Rev. 120*, 2342-2359.

Petersen, R.A., DiMego, G.J., Hoke, J.E., Mitchell, K.E., Gerrity, J.P., Wobus, R.L., Juang, H. and *Pecnick, M.J.*, 1991: Changes to NMC's Regional Analysis and Forecast System. *Weather and Forecasting 6*, 133-141.

Schlatter, T.W. and *Carrière, J.-M.*, 1991: A correlation model allowing for divergent wind analyses and supporting three-hour assimilation of mesoscale data. *Preprints, 9th Conference on Numerical Weather Prediction*, Denver, Colorado, 14-18 October. American Meteorological Society, Boston, Massachusetts, 58-61.

IDŐJÁRÁS

Quarterly Journal of the Hungarian Meteorological Service
Vol. 97, No. 1, January–March 1993

Effects of the large-scale circulation on local climate anomalies in relation to GCM outputs

J. Mika

Hungarian Meteorological Service, H-1525 Budapest P.O.Box 38, Hungary

(Manuscript received 2 November 1992; in final form 1 April 1993)

Abstract—A possible way to apply General Circulation Models (GCMs) in regional climate scenarios is to consider the changes in the frequency distribution of model-generated macrocirculation types, and combine them with conditional climatology of each macrotype calculated from the present climate. This can be successful, if a great part of local climate anomalies is connected to frequency anomalies of the macrotypes. To test this assumption, a diagnostic method for separation of circulation and non-circulation factors in local climate anomalies is developed (also allowing a mixed term), based on the classification of *Ambrózy et al.* (1983, 1984), which is an objective modification of that introduced by *Hess* and *Brezowsky* (1969). Results of separation for monthly temperature and precipitation anomalies for Kecskemét, Hungary (47°N 20°E) are presented, for which a secondary role of the circulation factor is experienced, except for the low precipitation anomalies. The annual course in the weight of this term (maximum in winter) is considerable, except for the high precipitation groups. Extracting more information from series of macrosynoptic types than just their monthly frequencies is recommended.

Key-words: GCM-outputs, regional climate scenarios, Hungary, macrocirculation types, temperature, precipitation.

1. Introduction

Estimation of regional features of the expected global warming is one of the actual problems in the greenhouse-gas issue. The use of General Circulation Models (coupled with ocean models, as a tendency, allowing time-dependent simulations of gradual changes) is practically the only way to get information about regional features of global changes, assumed to be larger than that covered by direct instrumental observations.

However, the spatial resolution of GCMs is constrained for practical reasons

by the speed and memory of computers. An increase in resolution not only increases the memory needs, but also leads to a reduction in the required time step. Therefore, in spite of earlier trials (e.g. *Kim et al.*, 1984), the coarsely resolved GCM-outputs cannot be directly used for this goal, while the inadequacy of pure geometrical interpolation (e.g. *Cohen* and *Allsopp,* 1988) has recently been discussed by *Grotch* and *MacCracken* (1991). It is also not a real help from the impact point of view, if climate consequences are expressed in averages for larger areas, e.g. spherical rectangles, of tens of geographical degrees wide, as defined by *Mitchell et al.* (1990). Due to the scaling problem, a visual interpolation from output maps (*Mika,* 1991), losing some information, but also smoothing the grid-specific errors of the field, might be an alternative among the one-step trials in applying GCM-outputs for regional scenarios.

More sophisticated efforts to use GCM-outputs for regional climate scenario construction can be sorted into two groups. In both approaches, however, accuracy of the large-scale flow generated in the GCM is crucial.

The first possibility is a *one way-coupling* of a limited-area model into the original sequence of GCM-fields. From this approach, which is not closely related to the subject of this paper, one can learn at least (*Giorgi et al.,* 1990) that regional climatic patterns, both of the present state and of greenhouse-gas disturbed ones, fail to be well simulated on the coarse grid, comparing to the finer one. Simulations in the latter, however, agree well with high-resolution observations and show considerable geographical details, that cannot be portrayed in original GCMs.

The second way is *to combine* larger scale averages, or main components of the *model-generated fields with empirical relationships*, learned on measured data sets between the large scale characteristics and the regional-scale climate elements. This approach has opened new perspectives for empirical analysis of synchronous processes. Limitation of the statistical approach is, however, that it can only be applied with success, if strong connections between the large-scale parameters and regional climate anomalies exist.

Not referring to earlier works on synchronous connections, generally motivated by long-range forecasting needs (e.g. *Klein* and *Yang,* 1986), there are three often quoted recent studies, representing different approaches in their details.

Karl et al. (1990) used free-atmosphere parameters in the closely located grid-points for independent variables in the belief that their fields were less sensitive to the sub-grid scale details, scarcely simulated in the GCMs. *Wigley et al.* (1990) used areal averages around the locality of interest (Oregon, USA) for the elements (temperature, precipitation) intended to estimate from outputs of a GCM. It was found, that for some locations the majority of local variance could be attributed to large scale effects, but there were wide areal variations in the extent, to which the larger scale anomalies were the determining factors.

In both approaches, a relationship between local anomalies and larger scales containing this locality are established. The third way is based on pressure fields from a wider area, containing also distant localities. *Von Storch et al.* (1991) used canonical correlation analysis relating the rainfall field over the Iberian Peninsula to the observed sea-level pressure field of the Atlantic Sector, in winter. This technique successfully reproduced the observed rainfall patterns, but only the half of the interannual variability was explained. Though the global-scale pressure pattern was fairly well simulated by the applied GCM, the model itself reproduced the precipitation fields with large deficiencies, probably due to the imperfectly treated physics of rainfall. Similar technique for the same GCM was applied by *Werner* (1992) for Central European temperatures in winter. Large part of anomalies was controlled by patterns of Northern Atlantic pressure field, however, on time scales of several decades the trends were controlled by other processes, too.

Pressure information can be related to local climate also in a different way (*Bogardi et al.*, 1992, *Matyasovszky et al.*, 1992). In these works the sequence of previously determined macrosynoptic types is coupled to the series of local weather (precipitation, or indices derived from it) through the probability distribution of conditional Markovian processes. This approach was illustrated by winter precipitation and summer drought indices, but it still has to be verified on broader set of model-generated fields and climate elements. This theoretically sophisticated method, however, requires long series of daily weather elements in order to provide well-defined probability distributions, as free from sample errors as possible.

Our *present paper*, therefore, is dedicated to a less complicated use of macrocirculation types for GCM-related regional climate scenarios. It is suggested to use just the anomalies in the frequencies for all macrotypes, assuming that they produce conditional distributions, being not so well-defined, but easier to realize in practice.

To test this approach, a method is introduced to calculate the relative weight of anomalies in the frequency of macrocirculation patterns relative to time averaged climate anomalies. After describing this method (*Section 2.1*), the applied objective macrosynoptic classification (*Section 2.2*) and the data sets used for the test (*Section 2.3*) is presented. Results for temperature (*Section 3.1*) and pressure (*Section 3.2*) are discussed in *Section 4* in relation with the suggested approach.

2. Methods and data

2.1 The method of separation

The aim of this method is to quantify, what part of climate anomalies can

be directly attributed to the anomalous frequency distribution of macrosynoptic types in the period for which the anomaly is formed. The following elementary operations will conclude at a separation of the anomalies, where this term is one of their three, non-zero components.

Let us have a macrosynoptic classification, containing M disjunct macrotypes. Assuming that the i-th day of the record is characterized by the I-th macrotype, the value of an appropriate weather element can be characterized as $A_I(i)$. The difference between this actual value and its climatological mean is $\Delta A_I(i)$, where

$$\Delta A_I(i) = A_I(i) - \{A\}. \tag{1}$$

Let us further introduce the conditional climatic average $\{A_I\}$ related to the I-th macrotype in the same period as for the unconditional $\{A\}$. Let us add to, and subtract from Eq. (1) $\{A_I\}$. Then $\Delta A_I(i)$ can be divided into two parts:

$$\Delta A_I(i) = [A_I(i) - \{A_I\}] + [\{A_I\} - \{A\}] = A_I'(i) + \{\Delta A_I\}, \tag{2}$$

where $A'_I(i)$ is the actual anomaly relative to the conditional climate average; $\{\Delta A_I\}$ is the difference between conditional and unconditional climate averages.

So the second term is the part of daily weather anomalies which is fully determined by the macrotype itself. The first term, however, is the part of anomalies which can not be estimated at all, if knowing just the actual macrotype.

Let us further have a period which is much shorter than that used for climate averages. For this period, the mean anomaly related to macrotype I is designated by $<\Delta A_I>$. Omitting (i) indices from Eq. (2), this term is averaged as

$$<\Delta A_I> = <A_I'> + \{\Delta A_I\}. \tag{3}$$

(Here and in the next formula, symbols of shorter averaging are not marked in connection with the longer-term averages.)

Within the shorter period for which components of the anomalies are being investigated, the actual relative frequency of the I-th macrotype, $<q_I>$ can also be divided into its climatological relative frequency $\{q_I\}$ and anomaly $<q'_I>$, similarly to the way followed in Eqs. (2) and (3):

$$<q_I> = \{q_I\} + <q_I'>. \tag{4}$$

Approaching to our goal, the anomaly of the whole period, $<\Delta A>$ is equal to

the sum of average conditional anomalies, weighted by relative frequencies of the specific macrotypes:

$$< \Delta A > = \sum_{I=1}^{M} < q_I > < \Delta A_I > . \tag{5}$$

Putting Eqs.(3) and (4) into Eq.(5), after elementary operations this expression can be written as

$$< \Delta A > = \sum_{i=1}^{M} \{q_I\}\{\Delta A_I\} + \sum_{I=1}^{M} <q_I'>\{\Delta A_I\} + \sum_{I=1}^{M} \{q_I\}<A_I'> + \sum_{I=1}^{M} <q_I'><A_I'>, \tag{6}$$

where the first term is equal to zero, if only $\{q_I\}$ and $\{\Delta A_I\}$ are calculated from the same reference period. The remaining three terms can be interpreted as follows:

- $\Sigma <q'_I> \{\Delta A_I\}$ is the part of the $<\Delta A>$ anomaly due to anomalous frequency distribution of macrotypes. This term of *circulation* origin is henceforth referred as *C*.
- $\Sigma \{q_I\} <A'_I>$ is the part of anomaly, directly not influenced by frequencies of macrotypes. This *physical* or *non-circulation* term, *P* will be discussed in detail below.
- $\Sigma <q'_I> <A'_I>$ is the term (*M*) due to *mixed* influence of both circulation and non-circulation (physical) origin.

So the anomaly for a given period is separated into 3 terms:

$$< \Delta A > = C + P + M . \tag{7}$$

Information contained by the distribution of macrosynoptic types, related to the expected use of GCM-outputs (see Introduction) is included in term *C* and partly in term *M*. The physical (non-circulation) term, on the other hand, is determined by processes of at least three roots.

The *first* one is the initial large-scale anomaly, compared to the climatic mean pattern of the given macrotype, which is not great enough to select this pattern into a different class. This large-scale source of term *P* can appear tendentiously parallel to climate variations and changes. The *second* source of term *P* can be originated in the local anomalies of the underlying surface (heat and moisture content) that of course might indirectly be influenced by the sequence of macrotypes within their fixed frequency distribution. *Thirdly*, term *P* may also contain the effects of scales not resolved by the horizontal grid-structure of the classification, or those connected to peculiarities of the

actual vertical profiles, which are not represented by the one vertical level, used in the classification.

The aim of our calculations is to estimate the relative weights of these terms in local climate anomalies. To do so, day-by-day sequences of meteorological elements and of actual macrotypes are needed. The method described above can be used for any individual period of interest, but we try to apply it independently of *episodic* particularities of the periods, which they are calculated for. Therefore anomalies of the whole longer-term period (see *Section 2.2*) are selected into 5 groups as extremely positive (++), positive (+), medium (=), negative (-) and extremely negative (--) ones, representing 20−20% of the frequency distribution in the arranged sample of local climate anomalies (see *Section 2.3*). Calculation of terms in Eq. (7) is performed for separate months in the groups, and results are averaged within the groups thereafter.

2.2 The macrosynoptic classification

The classification of macrosynoptic types to be applied can be chosen from a finite set of objective or expert-defined classifications covering either the whole Hemisphere or just the area, related to the given locality. There are, however, some considerations motivating the choice of classification.

First, the separation method requires a macrosynoptic classification in a limited area, because local weather anomalies and macrotypes should be considered synchronously. On the other hand, it would not be reasonable to have a horizontal resolution for the data base of classification, which were higher than in the GCM-s simulating the circulation patterns.

Ambrózy et al. (1983,1984) have published an objective macrosynoptic classification, fulfilling these two criteria, which is based on cluster-analysis ("K-means", see e.g. *Anderberg*, 1973) of the 500 hPa geopotential fields. In this study the Atlantic-European region is represented by 80 grid-points on a 5°x10° geographical grid (*Fig. 1*). The initial classification, i.e. the typical geopotential patterns, forming the cluster-centers in the 0-th step of classification was the *Hess* and *Brezowsky*'s (1969) classification (HB), being uniform in each season. However, *Ambrózy et al.* (1983, 1984) established that frequencies of the objective versions of HB-types exhibit definite annual variations. Therefore, the classification was fulfilled for all seasons separately, between 1949 and 1972.

Having the macrotypes already defined, the identification of individual days were continued also after 1972, but it was terminated in 1985 for technical reasons. In our study, macrosynoptic codes for the period 1951-1980 are used.

Numbers and average durations of macrotypes, maximum and minimum external distances between them, and also standard deviations (i.e. mean internal distances) of the macrotypes averaged to one grid-point are presented in *Table 1*, compiled according to the original papers. Short average durations

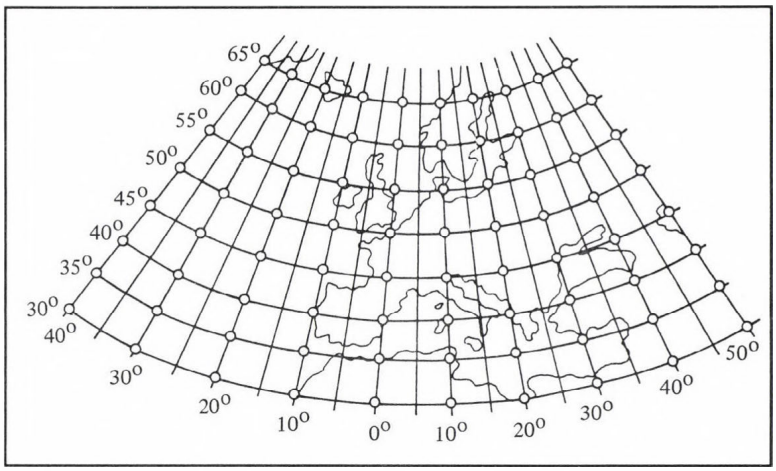

Fig. 1. The Atlantic-European sector and the 5°x10° grid of the applied macrosynoptic classification (from *Ambrózy et al.*, 1983).

of macrotypes suggest that the applied horizontal and vertical resolutions are fine enough to produce macrosynoptic patterns having the same average duration as the local weather. Advantages of the objective classification, as compared to the initial HB, can be realized (*Ambrózy et al.*, 1983) if comparing the average internal distances presented in Table 1 (8.0−10.3 gpm) with those of the original HB catalogue (14.4 gpm).

There are three advantageous properties of the applied classification, that are thought to be important for the adequate separation. First, *objectivity of the classification and day-by-day recognition* of the patterns assures the separation against (expert-induced) systematic distortions in the estimation of the terms in Eq. (7). Second, *equivalent importance of each 80 grid-points* (in contrast to

Table 1. Characteristics of the applied objective macrosynoptic classification

	Number of macrotypes	Mean duration of macrotypes (days)	Average internal distance (gpm)	Distance between macrotypes (gpm)	
				Maximum	Minimum
Winter	17	2.4	10.3	25	4
Spring	19	2.5	9.3	26	8
Summer	8	3.5	8.0	15	6
Autumn	15	2.7	9.6	26	9

classifications which emphasize one certain country or region) is crucial to assure the independence of macrosynoptic classes of the weather in the investigated locality, having influence only in a few grid-points.

Third, the classification *considers the absolute value of geopotential*, not only the qualitative features of the pattern. This makes it possible to distinct qualitatively similar situations with different temperatures (relative geopotentials) in the troposphere.

2.3 Grouping the anomalies in local climate elements

The method of separation can be applied for the whole Atlantic-European region and for all climate elements. Of course, results and conclusions concerning the use of GCM-outputs in the suggested way, may highly depend on the area and element for which the separation is carried out.

In the following we present the results of separation for monthly *temperatures* and *precipitation* anomalies for *Kecskemét*, Hungary (47°N 20°E) located in a representative plain area. This point is in the middle of the north-south, and at the eastern 2/3 of the west-east extension of the area, used for the macrosynoptic classification.

Monthly anomalies of both meteorological elements are divided into five groups, representing 20−20% of the empirical distribution, according to their sign and severity, as suggested in *Section 2.1*. So, 6−6 months from the samples containing 30 years between 1951 and 1980 are selected for each anomalygroup. Boundary values between the neighboring anomaly-groups are presented in *Figs. 2* and *3* for temperature and precipitation, respectively.

3. Results

In the following only four anomaly groups are analyzed, as for the middle group (little or no anomalies) signs of the weights are often the opposite as the anomalies themselves.

3.1 Temperature

Results of separation for the extreme categories (++ and −−) are presented in *Fig. 4*. It can be seen that relative weights of circulation, physical and mixed components have definite annual cycles. Absolute dominance of the physical component in the warm months and approximate equilibrium among the components in the cold months can be established, except for November–December in the (−−) anomalies. All components exhibit the same sign as the anomalies themselves, except for June. Main features of distributions in the (++) group are nearly the same as in the (−−) group.

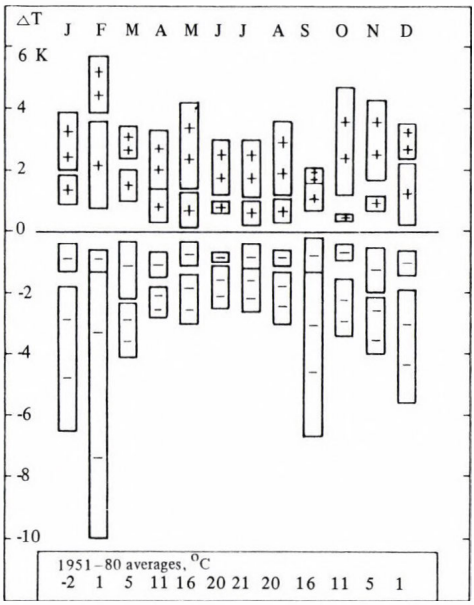

Fig. 2. Groups of monthly mean temperature anomalies (ΔT) at Kecskemét, Hungary. Average rounded values in °C are indicated at the bottom.

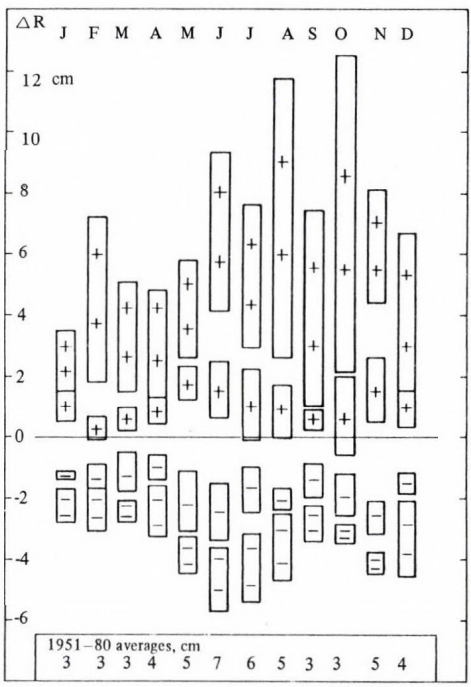

Fig. 3. The same as Fig. 2 for precipitation. Rounded averages in cm/month.

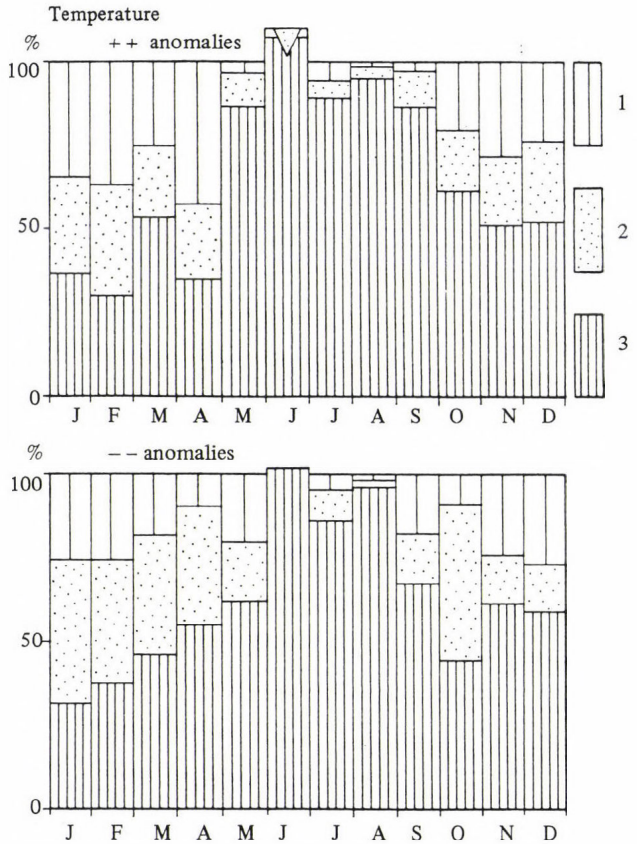

Fig. 4. Proportion of the circulation (1), mixed (2) and physical (3) terms in groups of extremely warm (+ +) and extremely cold (– –) anomalies of temperature at Kecskemét, Hungary. Triangles indicate terms of opposite sign.

To compare the extreme anomalies with moderate (+ and –) ones, seasonal and annual mean weights of the different components, averaged from their initial monthly values, are demonstrated in *Table 2*. The most plausible feature of these numbers is that the difference between relative weights in the different anomaly-groups are small. The dominance of the physical term (P) over the circulation (C) is unambiguous, even in winter. Thus, this is not only a feature of extremities, but a more general characteristic of climate in the given location. The mixed component (100-P-C%) has also just a secondary role (2–23% in annual averages).

3.2 Precipitation

The separation for the two extreme anomaly groups is presented in *Fig. 5*. There are considerable differences between the (––) and (+ +) groups, both in the terms and their annual course. (The sequence of displaying the anomaly

Table 2. Proportion of the physical (P) vs. circulation (C) terms in the temperature anomalies expressed in percents for the different seasons and anomaly groups (Kecskemét, Hungary): ++ extremely warm, + moderately warm etc. groups. The central (40–60%) group is omitted.

Temperature	DJF	MAM	JJA	SON	Year
	C/P	C/P	C/P	C/P	C/P
++	28/40	18/58	0/97	17/66	16/65
+	8/53	18/51	30/118	7/104	16/82
–	25/34	21/52	16/72	9/82	18/60
––	26/42	16/54	2/94	17/57	15/62

groups of different signs is changed with respect to the common appearance of positive temperature with negative precipitation anomalies, and vice versa.) For extreme negative anomalies (––), the physical component has a well defined annual course with a slight dominance (approx. 60%) in summer and a rather minor role in winter. The circulation term has a considerable role (40–50%) in the majority of months, except for December with very high, and for February and August with low weights. For the extremely high precipitation (++) group, a slight uneven dominance of physical components can be established, with no definite annual cycle. The circulation term plays little role in this group. The mixed term is somewhat more important, than in case of the temperature (16–36% in annual mean for the different groups). Synchronism in the sign of the three components can also be recognized, with few exceptions.

For moderate anomalies, the seasonal and annual averages are demonstrated in *Table 3*, together with those for the extreme groups. The relative weights are different for different seasons and for groups of the same strength, but different signs, especially in winter and spring. The most important feature, however, is that no great differences in (++) vs. (+) or in (––) vs. (–) groups can be identified.

4. Discussion

In the presented calculations, regarding to Kecskemét, Hungary, the most important conclusion is the relatively minor role of the circulation term, except for the low precipitation anomalies. The annual course of this term is in broad coincidence with one's *a priori* expectations, as the latter can also be confirmed

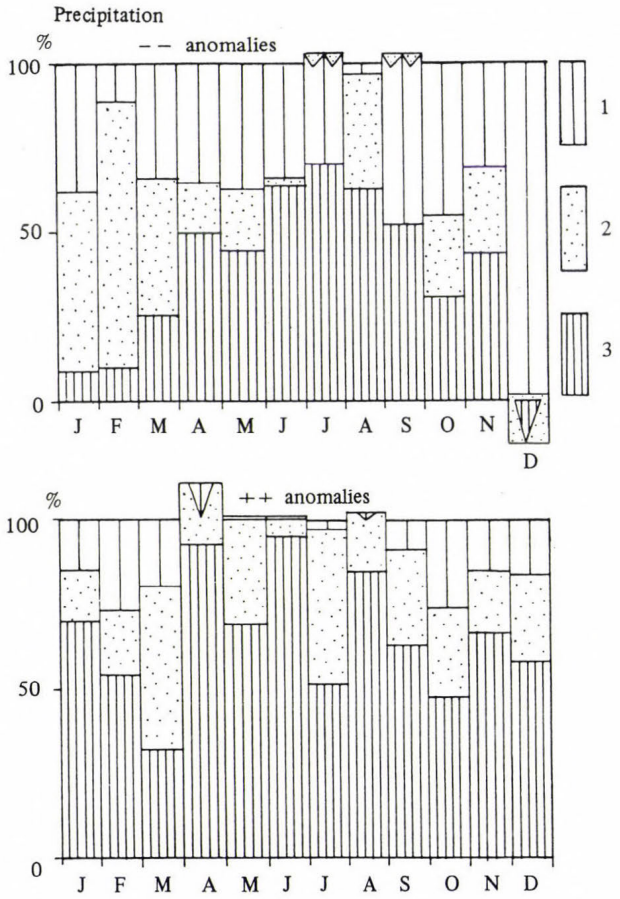

Fig. 5. The same as Fig. 4 for precipitation (e.g. – –: extremely dry).

by Table 1. Here the number of macrotypes in summer is the less in the year, and their "distance" (i.e. mean gpm difference) has also a minimum. Thus, the less the difference between the macrotypes is, the lower part of the anomalies are expected to be attributed to anomalous frequency distribution of the macrotypes.

It is impossible, however, to consider this circulation term as the maximum information contained by a series of macrotypes, because the succession of macrotypes is not taken into account by the separation. E.g. cool and wet westerlies at the beginning of the period (in summer), followed by warm and dry anticyclones could cause a much different monthly anomaly than the opposite case, although the frequency distribution of the investigated period would be the same. Effects, induced by the circulation on previous days are registered in the physical term, implicitly (see explanations of this term, in *Section 2.1*). Therefore, the approach, suggested by *Matyasovszky et al.* (1992) and *Bogardy et al.* (1992), has a reasonable physical background. Thus, it

Table 3. The same as Table 2 for precipitation: – – extremely dry, etc.

Precipitation	DJF C/P	MAM C/P	JJA C/P	SON C/P	Year C/P
– –	77/2	24/4	1/66	42/42	36/38
–	74/–16	34/30	–3/71	16/59	30/34
+	20/66	–3/93	5/65	39/53	15/69
+ +	19/61	3/65	0/77	17/59	10/65

might be worth following the sequence of macrotypes (not their frequencies only), despite the sample problems arising in connection with the more conditions considered.

The seasonal objective classification applied in this study has several advantages detailed in *Section 2.2*, but it is not proven that this were the optimal one. The separation of time averages can also be completed by applying other macrosynoptic classifications, investigating how the results are specific to the applied classification. An alternative to the applied one might be the classification, introduced by *Péczely* (1957, 1983). This, not objective classification represents smaller scale (Europe with a special attention to Hungary), but it has probably more narrow conditional distributions for the weather elements in Hungary.

Our study has been dedicated to an empirical investigation in relation to the application of GCM-outputs. This mixed, empirical-dynamical approach relies on the assumption that the response of the regional climate to a changing global flow, due either to interannual climate variability or to the longer-term changes, is the same in both cases. This assumption, however, remains unproven for any combination of circulation patterns related to the future with conditional distributions of the present climate. This uncertainty should always be taken into consideration, relying on regional climate scenarios based on this combination.

Acknowledgements – The author thanks *Ms. Judit Bartholy* for making the catalogue of the applied macrosynoptic classification and also the conditional climatological data available, and *Ms. Márta Korándi* for programming the calculations on an IBM-360 computer. Preparation of this paper was partly supported by contract OTKA-443 with the Hungarian Academy of Sciences.

References

Ambrózy, P., Bartholy, J. and *Gulyás, O.*, 1983: Determination of seasonal macro-synoptic types for the Atlantic-European region by cluster-analysis (in Hungarian).

OMSZ Kisebb Kiadványai, No. 39, Budapest.

Ambrózy, P., Bartholy, J. and *Gulyás, O.*, 1984: A system of seasonal macrocirculation patterns for the Atlantictic-European region. *Időjárás 88*, 121-133.

Anderberg, M.R., 1973: *Clusteranalysis for Applications*. Academic Press, New York.

Bogardi, I., Matyasovszky, I., Bardossy, A. and *Duckstein, L.*, 1992: Estimating space-time local hydrological quantities under climate change. In *Proc. 5th Int. Meeting on Statistical Climatology*, 22-26 June, 1992 Toronto, Canada, 95-99.

Cohen, S.J. and *Allsopp, T.R.*, 1988: The potential impacts of a scenario of CO_2-induced climatic change on Ontario, Canada. *J. Climate 1*, 669-681.

Giorgi, F., Marinucci, M.R. and *Visconti, G.*, 1990: Use of a limited area model nested in a general circulation model for regional climate simulation over Europe. *J. Geophys. Res. 95*, 18413-18431.

Grotch, S.L. and *MacCracken, M.C.*, 1991: The use of general circulation models to predict regional climate change. *J. Climate 4*, 286-303.

Hess, P. and *Brezowsky, H.*, 1969: Katalog der Grosswetterlagen Europas. *Berichte des Deutschen Wetterdienstes Bd. 15*, N. 113, Offenbach.

Karl, T.,W., Wang, W.-C., Schlesinger, M.E., Knight, R.W. and *Portman, D.*, 1990: A method of relating general circulation model simulated climate to the observed local climate. Part I: Seasonal statistics. *J. Climte 3*, 1053-1079.

Kim, W.J., Chang, T., Baker, N.L., Wilks, D.S. and *Gates, W.L.*, 1984: The statistical problem of climate inversion: Determination of the relationship between local and large-scale climate. *Mon. Wea. Rev. 112*, 2069-2077.

Klein, W.H. and *Yang, R.*, 1986: Specification of monthly mean surface temperature anomalies in Europe and Asia from concurrent 700 mb monthly mean height anomalies over the Northern Hemisphere. *J. Climatology 6*, 463-484.

Matyasovszky, I., Bogardi, I., Bardossy, A. and *Duckstein, L.*, 1992: Hydroclimatological modeling of droughts under climate change. In *Proc. 16th European Regional Conference of ICID.*, 21-27 June, 1992, Budapest, Hungary, 239-250.

Mika, J., 1991: Regional features of a stronger global warming over Hungary (in Hungarian). *Időjárás 95*, 265-278.

Mitchell, J.F.B., Manabe, S., Tokioka, T. and *Meleshko, V.*, 1990: Equilibrium climate change. In *IPCC WG-1 Report, WMO-UNEP*, 139-174 .

Péczely, G., 1957: Grosswetterlagen in Ungarn. *Kleinere Veröffentlichungen der Zentralanstalt für Meteorologie*, No. 30., Budapest.

Péczely, G., 1983: Catalogue of the macrosynoptic types for Hungary (1881-1983) (in Hungarian). *Meteorológiai Tanulmányok* 53, OMSZ, Budapest.

von Storch, H., Zorita, E. and *Cubasch, U.*, 1991: Downscaling of global climate change estimates to regional scales: An application to Iberian rainfall in wintertime. *Max Planck Inst. Meteor. Rept.* No. 64, Hamburg, June 1991.

Werner, P.C., 1992: On the relationship between the atmospheric circulation in the Atlantic-European area and some seasonal meteorological parameters in Central Europe. In *Proc. 5th International Meeting on Statistical Climatology*, 22-26 June, 1992, Toronto, Canada, 161-164.

Wigley, T.M.L., Jones, P.D., Briffa, K.R. and *Smith, G.*, 1990: Obtaining sub-grid scale information from coarse-resolution general circulation model output. *J. Geophys. Res. 95 (D2)*, 1943-1953.

IDŐJÁRÁS

Quarterly Journal of the Hungarian Meteorological Service
Vol. 97, No. 1, January–March 1993

Trace metal concentrations in atmospheric precipitation over Hungary[1]

E. Mészáros*, A. Molnár*, Zs. Horváth and A. Lásztity****

* *Department of Analytical Chemistry, University of Veszprém, H-8201 Veszprém, P.O.Box 158, Hungary*
** *Institute of Inorganic and Analytical Chemistry, Eötvös Loránd University, H-1518 Budapest, P.O.Box 112, Hungary*

(Manuscript received 11 January 1993; in final form 5 April 1993)

Abstract—The aim of this paper is to present the concentration of ten trace metals in atmospheric precipitation waters. Precipitation samples were taken by means of a wet-only collector at a regional background site in central Hungary. The water samples were analyzed by the inductively coupled plasma atomic emission spectroscopy (ICP-AES). The results obtained are discussed and compared to those published in the literature, as well as to emission information available.

Key-words: chemical composition of precipitation, wet deposition, toxic metals, Hungary.

1. Introduction

The study of the chemical composition of precipitation provides useful information for estimating the trace substance concentration and self-cleaning capacity of the atmosphere. On the other hand, such an investigation is of interest to determine the impact of atmospheric pollution on terrestrial and aquatic ecosystems.

For these reasons the chemical composition of atmospheric precipitation has been widely studied under several geographic conditions (see e.g. *Mészáros*, 1981; *Warneck*, 1988) including the central-eastern part of Europe (e.g. *Horváth* and *Mészáros*, 1984; *Malissa et al.*, 1984; *Moldan et al.*, 1987). However, in the latter studies only the concentration of inorganic ions was determined. With the exception of some alkali and alkaline earth metals, the

[1] Sponsored by the National Foundation for Scientific Research (OTKA, N° 345).

level of trace elements was not detected in spite of their importance in ecological studies. In this paper the concentrations of ten metals in precipitation are presented from the analyses of daily samples collected in the middle of Hungary under rural conditions (K-puszta station, ϕ=46°58'N λ=19°33'E H=130 m) by a wet-only sampler. These new measurements were possible through the application of the inductively coupled plasma atomic emission spectrometry (ICP-AES).

2. *Analytical technique*

Precipitation samples were acidified with HNO_3 down to pH=2 at the station immediately after collection. The samples were then transported to the laboratory and submitted to a preconcentration procedure. For this purpose a microcolumn filled with iminodiacetic acid/ethyl cellulose ion (IDAEC) exchanger was used. The samples were buffered with 1M ammonium acetate and pumped through the column in a flow system. The trace metals thus collected in the column were eluted by injection with 100 μL of 2M HNO_3 and introduced into the plasma torch of the ICP-AES device.

Fig. 1 shows the schematic diagram of the system used. Data obtained with this system show that in all cases the column uptake is directly proportional to the metal concentration in solution. Results also indicate that the reproducibility of the preconcentration process is better than 5 % (for further details including calibration see *Horváth et al.*, 1992).

In seven samples the concentration of cadmium, manganese and lead was also determined simultaneously by graphite furnace atomic absorption spectrometry widely used in environmental studies. Data gained by the two methods are in good agreement. On the basis of seven samples the ratio of the concentration measured by ICP to that detected by atomic absorption spectrometry is 1.1, 0.99 and 1.2 for Cd, Mn and Pb, respectively. The higher ratio

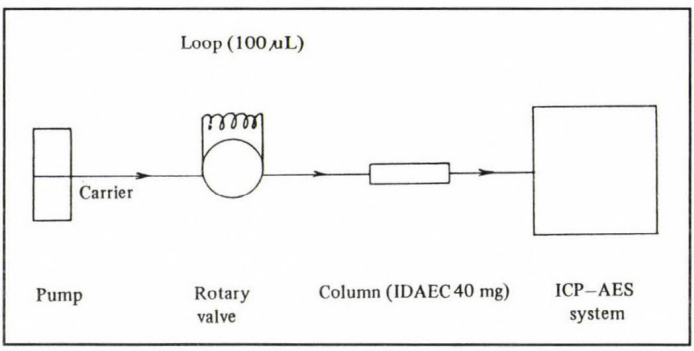

Fig. 1. Schematic diagram of the preconcentration (IDAEC) and analysis (ICP-AES) system.

for Pb is caused by differences when the concentrations are lower than 10 μgL^{-1}. Thus, it can be concluded that in the future for Pb a higher preconcentration factor should be used.

Finally we note that the analysis of calcium and magnesium was found to be possible by ICP-AES without preconcentration due to their relatively high concentration. However, in this paper the concentration of these elements is not discussed since similar results were obtained as in the case of our previous studies (*Horváth* and *Mészáros,* 1984).

3. Concentrations

The average concentrations of ten metals calculated by weighing the individual values with precipitation amount are given in the first column of *Table 1*. These data were obtained on the basis of the analysis of 46 daily samples collected between 1 July and 31 December, 1991. In the second column of the table the detection limits of the analyses are also tabulated. It can be seen that the detection limits are significantly lower than averages, except for vanadium for which the ratio of the average to the detection limit is only slightly higher than two. This means that vanadium data must be considered with some caution.

It should be noted that the scatter of data around the averages is rather large as the third line of Table 1 shows. This is due to the inverse relationship between elemental concentration and precipitation amount. Further analyses are necessary, however, to determine this relationship on solid statistical basis.

In the fourth column of Table 1 the average concentrations compiled for rural areas by *Galloway et al.* (1982) are tabulated. As in our case these data refer to regional conditions, not directly influenced by local anthropogenic emissions. The comparison of these data with our results indicate that the values measured in Hungary are rather close to word-wide average concentrations, with the exception vanadium. The detection of the latter is somewhat questionable, as was mentioned above. *Barrie et al.* (1987) noted that the trace metal concentrations reported by Galloway and his associates are unreliable because of possible sample contamination. For this reason the values reported by *Ross* (1986) for Southern Sweden are also included in Table 1 (last column). In the Swedish study, like in our case, proper precautions were taken to avoid sample contamination (samplers were acid-washed). Although for four metals (Cu, Zn, Pb and Cd) Swedish concentrations are smaller than our values, the two data sets are still comparable. It is speculated that the observed differences between Southern Sweden and Hungary are real and due to different environmental conditions. Overall we conclude that Hungarian concentrations reported in this paper do not differ significantly from concentrations observed in other regional background areas of the world.

Table 1. Concentration of metals in precipitation in Hungary and over other regions. The values are expressed in $\mu g\ L^{-1}$

Element	Concentration	Detection limit	Range of concentration	Rural average[1] word	Southern Sweden[2]
Ti	0.76	0.1	<0.1 – 3.8	–	–
V	1.9	0.9	<0.9 – 5.4	9.0	–
Mn	7.0	0.9	<0.9 – 41	5.7	6.4
Fe	70	2.0	13 – 360	–	–
Co	0.85	0.1	<0.1 – 3.6	0.75	–
Ni	1.7	0.1	<0.1 – 16	2.4	–
Cu	6.7	0.6	<0.6 – 157	5.4	1.4
Zn	46	0.9	0.8 – 96	36	16
Pb	8.9	0.4	<0.4 – 160	12	8.8
Cd	0.52	0.1	0.24 – 2.9	0.50	0.14

[1] *Galloway et al.* (1982)
[2] *Ross* (1986)

4. Scavenging coefficients and wet depositions

During the year when precipitation samples were collected the elemental composition of the aerosol particles was also measured (*Molnár et al.*, 1993). These measurements were carried out by the PIXE analysis of aerosols captured on Nuclepore filters. This makes it possible to calculate the scavenging coefficients defined as the ratio of the concentration of a given element in precipitation to that in the aerosol phase. The results obtained are listed in the first column of *Table 2.* Except for titanium the coefficients are close to 10^6 proposed as a general value for different elements by *Pacyna et al.* (1984).

The climatic average of annual precipitation amount measured in the region of our sampling station is equal to 518 mm. Using this figure and the average concentrations presented in Table 1, the wet deposition values can be calculated. The deposition rates (in mg $m^{-2}\ yr^{-1}$) are given in the second column of Table 2, while the data in the third column of the table show an extrapolation to total area of Hungary. Deposition values are high in particular for iron and zinc. For these elements the annual deposition is of the order of tens of mg $m^{-2}yr^{-1}$. In the case of iron the high deposition is at least partly caused by

Table 2. Scavenging coefficients ($x10^5$), wet deposition rates (in mg m^{-2} yr^{-1}), total wet deposition and emissions (both in t yr^{-1}) of trace metals in Hungary

Element	Scavenging coefficient	Deposition rate	Hungarian deposition	Emission[1]
Ti	0.46	0.39	36	–
V	5.9	0.98	92	389
Mn	14.3	3.6	336	160
Fe	2.7	36	33620	–
Co	3.3	0.44	41	24
Ni	5.7	0.89	83	162
Cu	7.1	3.5	323	509
Zn	12	24	22416	280
Pb	4.7	4.6	430	888
Cd	–	0.27	25	8

[1] *Pacyna et al.* (1984)

the contribution of crustal sources. This is shown by the enrichment factor of iron in aerosol samples (*Molnár et al.*, 1993) collected at the same station. However, the high deposition of Zn is at least partly due to anthropogenic sources (e.g. fossil fuel combustion, metal industry, refuse incineration) which are located mainly outside of Hungary as indicated by long-range transport model calculations (*Molnár et al.*, 1992). Further studies are needed, however, to determine the reasons for this relatively high Zn deposition.

It should be noted that although cadmium deposition is numerically low, the calculated Cd depositions might be dangerous from an environmental point of view due to the high toxicity of this element. Thus, according to *Galloway et al.* (1982) cadmium is toxic for aquatic organisms at concentrations as low as 0.2 μg L^{-1}, which is less than half of the average concentration measured (see Table 1). Pb wet deposition is important, but it is lower than the average value reported for Hungary for the period between 1984 and 1988 (*Bozó* and *Horváth*, 1992). This decrease is obviously caused by the use of gasolines with low lead content in recent years, outside and inside of the country.

Finally, in Table 2 (last column) emission values estimated by *Pacyna et al.* (1984) for Hungary are also given. It can be seen that for V, Ni, Cu and Pb the

emissions are higher than depositions. This can be probably explained by the fact that dry deposition is not included into the study. The situation is quite different for the other four elements for which the emissions are tabulated. For Mn this might be due to the contribution of crustal sources to the deposition, while for Co and Cd long-range transport is the probable origin. However, in the case of Zn this explanation does not hold since the wet deposition measured is much higher (about eight times) than the emission calculated by *Pacyna* and his co-workers. This obviously means that further, more reliable emission calculations are needed. Furthermore the more appropriate determination of the wet deposition by using several sampling sites in the country is necessary.

5. Aims of further research

On the basis of the above discussion we conclude that for a reliable calculation of the budget of different metals in the air over Hungary, the following items should be included into the study:

(a) reconsideration of emission values given for Hungary by *Pacyna et al.* (1984);
(b) estimation of the dry depositions for the country and
(c) determination of the wet deposition on the basis of samples collected at several sites.

Thus, we will continue the project in these directions.

References

Barrie, L.A., Lindberg, S.E., Chan, W.H., Ross, H.B., Arimoto, R. and *Church, T.M.*, 1987: On the concentration of trace metals in precipitation. *Atmos. Environ. 21*, 1133-1135.

Borbély-Kiss, I., Bozó, L., Koltay, E., Mészáros, E., Molnár, Á. and *Szabó, Gy.*, 1991: Elemental composition of aerosol particles under background conditions in Hungary. *Atmos. Environ. 25A*, 661-668.

Bozó, L. and *Horváth, Zs.*, 1992: Atmospheric concentration and budget of lead and cadmium over Hungary. *Ambio 21*, 324-326.

Galloway, J.N., Thornton, J.D., Norton, S.A., Volckok, H.L. and *McLean, R.A.N., 1982:* Trace metals in atmospheric deposition: a review and assessment. *Atmos. Environ. 16*, 1677-1700.

Horváth, L. and *Mészáros, E.*, 1984: The composition and acidity of precipitation in Hungary. *Atmos. Environ. 18*, 1843-1847.

Horváth, Zs., Lásztity, A. and *Varga, I.*, 1992: The role of spectrochemical analysis in the determination of the composition of atmospheric precipitation and aerosol samples in remote environment. *Microchem. J. 46*, 130-135.

Malissa, H., Puxbaum, H., Pimminger, M. and *Nikoopour, A.*, 1984: Untersuchungen des Nährstoffeintrages in der Neusiedler

See aus der Atmosphäre. In *Forschungsbericht 1981-1984.* Bundesministerien für Wissenschaft und Forschung, 41-89.

Mészáros, E., 1981: *Atmospheric Chemistry.* Elsevier, Amsterdam.

Moldan, B., Veselý, M. and *Bartoňova, A.*, 1987: Chemical composition of atmospheric precipitation in Czechoslovakia 1976-1984-I. monthly samples. *Atmos. Environ. 21,* 2383-2396.

Molnár, A., Bozó, L., Mészáros, E. and *Harris, J.M.*, 1992: Long-range transport of different elements in atmospheric aerosols: the case of Hungary. In *Nucleation and Atmospheric Aerosols* (eds.: *N. Fukuta* and *P.E. Wagner*), A. Deepak Publ., Hampton, Virginia, 473-480.

Molnár, A., Mészáros, E., Bozó, L., Borbély-Kiss, I., Koltay, E. and *Szabó, Gy.*, 1993: Elemental composition of atmospheric aerosol particles under different conditions in Hungary. *Atmosheric Environment* (submitted).

Pacyna, J.M., Semb, A. and *Hanssen, J.E.*, 1984: Emission and long-range transport of trace elements in Europe. *Tellus 36B,* 163-178.

Ross, H.B., 1986: The importance of reducing sample contamination in routine monitoring of trace metals in atmospheric precipitation. *Atmos. Environ. 20,* 401-405.

Warneck, P., 1988: *Chemistry of Natural Atmosphere.* Academic Press, New York.

IDŐJÁRÁS

Quarterly Journal of the Hungarian Meteorological Service
Vol. 97, No. 1, January–March 1993

Simulation of soil moisture dynamics

G. A. Georgiev and **V. A. Alexandrov**

Institute of Meteorology and Hydrology,
Bulgarian Academy of Sciences, Trakia Blvd.66, Sofia, Bulgaria

(Manuscript received 18 June 1992; in final form 22 March 1993)

Abstract—One of the most important factors determining the productiveness of the plants is the soil moisture. The knowledge of wetting conditions is helpful in planning of meliorative activities. The paper presents a model for calculating the dynamics of soil moisture during the vegetation period between wilting point and fully saturated soil. The blocks of evapotranspiration calculation with using a modified Penman-Monteith equation, precipitation assimilation and soil moisture movement in different layers are concerned. Data of comparison between measured and simulated values of soil moisture content under the maize plants are presented. Daily average meteorological data of air temperature, air humidity deficit, sunshine duration and precipitation quantity are used for calculating of soil moisture profile.

Key-words: Penman-Monteith equation, effective rainfall, agrometeorological modelling.

1. Introduction

The moisture is one of the irreplaceable life factors for agricultural crops. The soil moisture is practically the single water source of plants. The water takes part in the next processes: photosynthesis, thermoregulation of the crop and its mineral nutrition. Different values of soil moisture are observed from year to year in many regions and areas all over the world. The dependence between the yield and the soil moisture is very favourable for assessment of the expected yield.

2. Analysis and methods

The water balance equation, applicable to every soil layer, is basic part of the our model

$$W_i^{j+1} = W_i^j - \lambda E_i^j + q_{i-1}^j - q_i^j, \tag{1}$$

where W_i^j, W_i^{j+1} moisture content of i-th soil layer in the j day and the next $j+1$ day; q_{i-1}^j, q_i^j amount of passed water through i-th layer's boundary per day; λE_i^j evapotranspiration. We suppose that the plant roots reach 100 cm soil depth, arbitrarily divided into ten discrete layers (i=1,2,3,..,10). We use an eleventh layer (100–110 cm) too, whose moisture content is constant. The formula, for determination of water flux through the soil layers, is established by means of the theory describing the water streams in unsaturated soil (*Sirotenko*, 1981)

$$q_i^j = \sqrt{K_i^j K_{i+1}^j} \left[\left(\frac{\psi_{si+1}^j - \psi_{si}^j}{h_s} \right) + 1 \right], \tag{2}$$

where K_i^j water conductivity of the soil, ψ_{si}^j soil moisture pressure, h_s thickness of the soil layer. The soil moisture pressure during the period between wilting point and fully saturated soil was presented by *Mitchurin* (1975) with empirical equation

$$\psi_{si}^j = 15 \exp\left(- 7.76 \frac{W_i^j - W_i^{wp}}{W_i^{fs} - W_i^{wp}} \right), \tag{3}$$

where ψ_{si}^j water potential (10^5 Pa), W_i^{fs}, W_i^{wp} moisture of fully saturated soil and wilting point at i-th layer. When the soil saturation approximates 1, $\psi_{si}^j \to 0$, and when it equals to 0, $\psi_{si}^j = 15$. For the connection between hydraulic conductivity and soil moisture the following relationship (*Sirotenko*, 1981), is used

$$K_i^j = \bar{K}_{oi} \left(W_i^j - \frac{W_i^{wp}}{W_i^{fs} - W_i^{wp}} \right)^F, \tag{4}$$

where $\bar{K}_{oi}$ hydraulic conductivity (filtering coefficient) of saturated soil, F parameter. Using Karman–Kozen's formula (*Mitchurin*, 1975) we obtain

$$\bar{K}_{oi} = \frac{K_o \left(0.01\, W_i^{fs}\right)^3}{\left(W_i^{wp}\right)^2 \left(1 - 0.01\, W_i^{fs}\right)^2}, \tag{5}$$

where K_o empirical parameter.

The Penman-Monteith equation (*Thompson et al.*, 1981) provides a rational, physically-based procedure for calculating the water loss from any surface. The equation is

$$\lambda E = \frac{\Delta (R_N - G) + \rho c_p (e_s - e)/r_a}{\Delta + \gamma (1 + r_s/r_a)}, \tag{6}$$

where E rate of water loss (Kg m^{-2} s^{-1}), Δ rate of change of saturated vapour pressure with temperature (hPa $°C^{-1}$), R_N net radiation (W m^{-2}), G soil heat flux (W m^{-2}), ρ air density (Kg m^{-3}), c_p specific heat of air at constant pressure (1005 J Kg^{-1}), e_s saturation vapour pressure at screen temperature (hPa), e screen vapour pressure (hPa), λ latent heat vaporization ($\approx$ 2465000 J Kg^{-1}), γ psychromatic constant=0.66 for temperatures in deg C and vapour pressures in (hPa), r bulk surface resistance (s m^{-1}), r_a bulk aerodynamic resistance (s m^{-1}). This formula may be written thus as follows

$$\lambda E = - \frac{\Delta (R_{NE} - G) + \rho c_p \delta q (1 + b r_a/\rho c_p)/r_a}{\Delta + \gamma (1 + r_s/r_a)(1 + b r_a/\rho c_p)}, \tag{7}$$

where R_{NE} is R_N calculated assuming $T_o = T_{SCR}$, T_o bulk surface temperature, T_{SCR} screen temperature, ϵ emissivity of surface, $b = 4\,\epsilon\sigma\,(273.1 + T_{SCR})^3$, σ Stefan-Boltzman's constant, δq specific humidity deficit at screen height. This is the combination used in our model.

Prof. *J. L. Monteith* of the University of Nottingham provided constructive suggestion for aerodynamic resistance as the sum of momentum and bluff-body terms (*Choudhury* and *Idso*, 1985)

$$r_a = \frac{\ln^2((z - d)/z_o)}{k^2 u} + \frac{4 \cdot \ln((z - d)/z_o)}{ku}, \tag{8}$$

where k=0.4 the Karman constant, u wind speed at height z, d and z_o are the zero-plane displacement and the roughness height, respectively, calculated from the crop height (H) as: d=0.56H, z=0.13H.

For seasonal crops the surface will range from bare soil, to moderately or densely foliated. Water may be extracted directly from both the soil and the crop, and the surface resistance has to be calculated by taking both these processes into account. The basics scheme is based on suggestion by *Grant* (*Thompson et al.*, 1981) and uses the expression

$$1/r_s = (1 - A)/r_{sc} + A/r_{ss}, \quad (9)$$

where r_{ss} surface resistance of the crop, freely supplied with water, and dense enough for evaporation from the soil to make a negligible contribution, r surface resistance of bare soil (assumed to be 100 s m^{-1} for wet soil), $A=f^L$ (where L leaf area index). *Grant* found that f for barley was about 0.7, and this value has been assumed to apply to all the crops treated by our model. The last Eq. (9) has been derived for daytime conditions, assuming the parallel contributions of soil and crop resistance to their combined resistance to be roughly proportional to the amount of incident radiation which is absorbed by each of them. At night the leaf stomata are closed and the crop resistance r_{sc} is assumed to be the sum of the individual leaf (cuticular) resistances in parallel. These in turn are taken to be directly in parallel to the soil resistance so that

$$1/r_s = 2L/r_{sc}\,(\text{night}) + 1/r_{ss}. \quad (10)$$

A typical leaf resistance when stomata are closed, is about five thousand s m^{-1}, consequently Eq. (10) assumes the next form

$$1/r_s = L/2500 + 1/r_{ss}. \quad (11)$$

It is not possible to justify this last equation convincingly since it ignores the effects of turbulent resistances in the crop canopy. However, evaporation is usually small at night so errors introduced by Eq. (11) will also be small.
From concurrent data of stomatal conductance of sunlit leaves (C_1;mm s^{-1}), leaf water potential (ψ;m) and net radiation (R_N;W m^{-2}) *Choudhury* and *Idso* (1985) derived the empirical relationship

$$C_l = (0.986 + 0.025\,R_N) f_2\,. \quad (12)$$

The function f_2 was proposed by *Fisher* (*Fisher et al.*, 1981)

$$f_2 = 1/(1 + (\psi/q)^p), \quad (13)$$

where q and p are adjustable parameters. The Eq. (12) may be applied only to sunlit leaves. For a wheat canopy, however, all leaves are not likely to be sunlit. If leaf stomatal conductances were measured within various strata of a canopy to account for varied radiation regimes and leaf ages then canopy conductances (g_c) could be obtained as (*Roberts et al.*, 1980; *Choudhury* and *Idso*, 1985)

$$g_c = \sum_{j=1}^{n} L_j C_{lj} = (0.986L + R_N(1 - \tau))f_2, \quad (14)$$

where $j=1$ to n represents canopy strata having a leaf area index of L_j and leaf stomatal conductance of C_{lj}, τ an exponential function (*Denmead* and *Millar*, 1976): $\tau=\exp(-L/(2 \sin \Theta))$, Θ is solar elevation. Now the canopy resistance r_{sc} (s m^{-1}) follows from Eq. (14) as

$$r_{sc} = 1000/g_c. \quad (15)$$

The following plan for accounting the effective precipitation is suggested. At first, the rainfall sums are determined. The rainfall is effective when the daily sum is bigger than 0.2 mm until tasseling (0.9 mm after tasseling). The effective rainfall (*Sirotenko*, 1981), when $R^j \neq 0$, may be presented with equation

$$R_{ef}^j = R^j \left\{ 1 - \left[1 - \left(\frac{W_{fs}^{50} - W_{50}^j}{W_{fs}^{50} - W_{wp}^{50}} \right)^{1.5} \right]^2 \right\}, \quad (16)$$

where R^j, R_{ef}^j measured rainfall sum and effective rainfall sum per day (mm), W_{fs}^{50}, W_{wp}^{50} moisture of fully saturated soil and wilting point at 0–50 cm layer, W_{50}^j current soil moisture. Eq. (16) allows to account the precipitation loss of the soil surface. So, if $W_{50}^j = W_{fs}^{50}$ then $R_{ef}^j=0$, but when $W_{50}^j = W_{wp}^{50}$ then $R_{ef}^j=R^j$.

The procedure describing the precipitation assimilation is organized by the following steps: the effective rainfall sum is added to moisture of the first soil layer. If $(R_{ef}^j + W_i^j) > WW_i$ then the difference $(R_{ef}^j + W_i^j) - WW_i$ is combined with the next soil layer and it is "effective rainfall" for this layer. The procedure is repeated down to tenth soil layer inclusive. If the last layer is fully saturated, the excess water is added to ninth layer. When the ninth layer is saturated too, the excess water is added to eight soil layer etc. – inclusive of the first soil layer.

3. Results and discussion

The model permits to calculate the distribution of soil moisture from 10 cm to 100 cm depth. The root distribution, soil aeration, physical structure of the soil, underground water, water movement in the soil and root age are very

important elements in this model. We assume that the root distribution of maize is reduced according to the exponential law and the root mass decreases with the depth. It is supposed that the capillary water motion from underground water is absent. The means of agrophysical constants describe the soil structure. Dynamics of soil moisture during the vegetation period between wilting point and fully saturated soil is calculated. The values of soil moisture, which were up or down this interval, were equalized to them. In *Figs. 1a, 1b* and *2a, 2b* the comparison between calculated and measured values of soil moisture in the layers 0–10 cm, 30–40 cm, 60–70 cm, 90–100 cm is shown. Used data were measured in agrometeorological station Knezha (43.50°N, 24.08°E), Bulgaria, in 1982. In *Table 1* the monthly average values of the air temperature (T), air humidity deficit (D) and sunshine duration (S) are shown at meteorological station Knezha in the same year. The soil of the experimental field is typical chernozem.

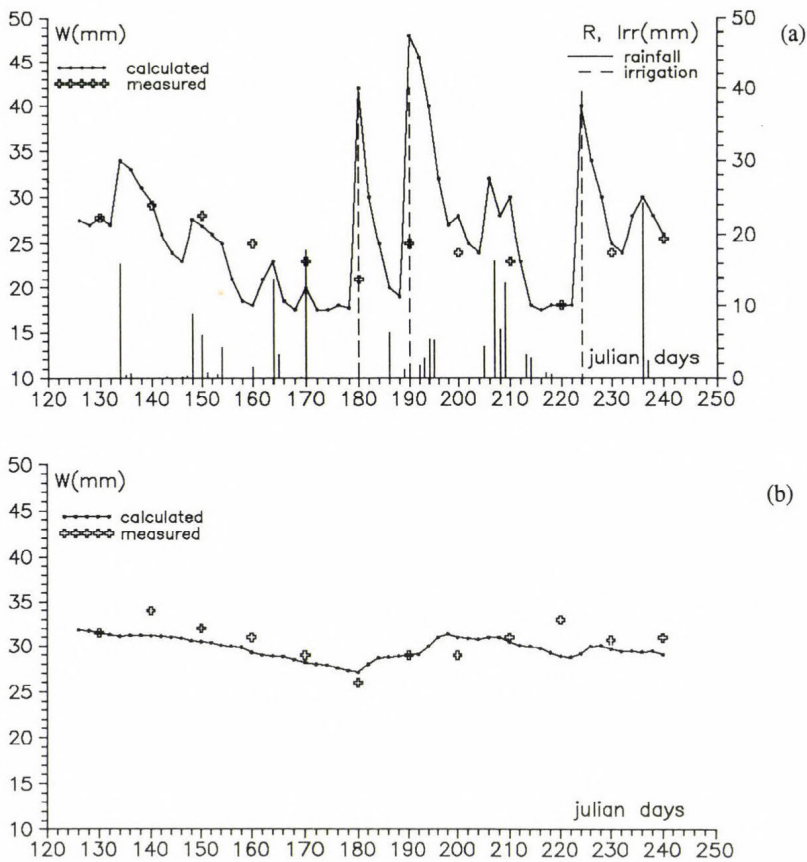

Fig. 1. Comparison between dynamics of calculated and measured soil moisture in layer (*a*) 0–10 cm, (*b*) 30–40 cm under maize.

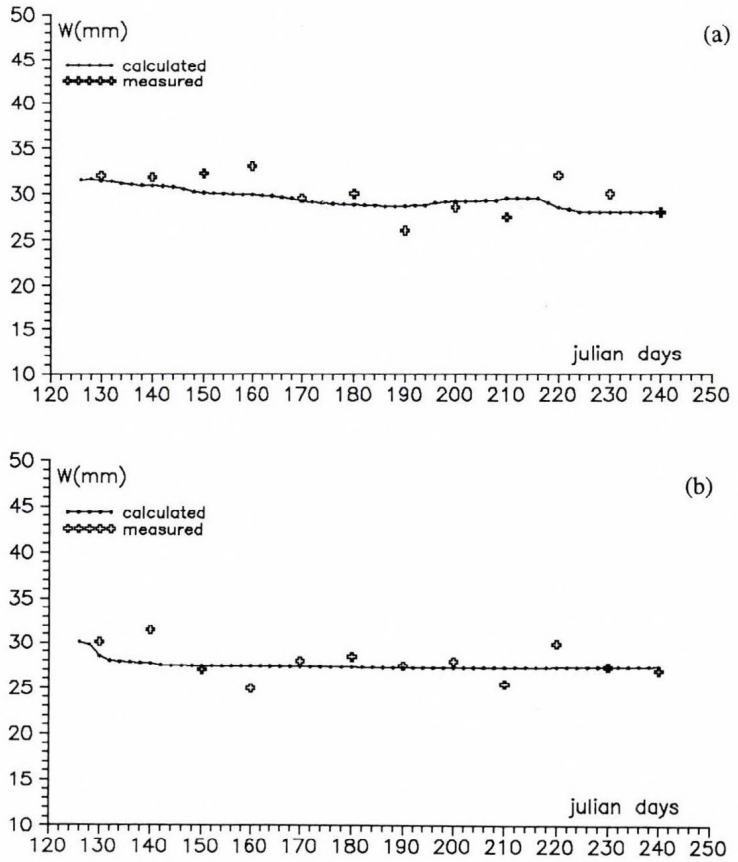

Fig. 2. Comparison between dynamics of calculated and measured soil moisture in layer (*a*) 60–70 cm, (*b*) 90–100 cm under maize.

The calculations for all over the vegetation period without input corrections were done. It is necessary to remark that when the depth increases the instability of soil moisture decreases and there are very small trend in the last layer. In this case, the maximum error is less than 20% and it is within the error's interval of the method of experimental measuring of the soil moisture. The calculated soil moisture is well correlated with atmospheric conditions. The sudden raise of soil moisture in the surface layer coincides with date of irrigation. It is necessary to remark that the maximum deviation of calculated values is observed in these moments. It is explained with the imperfect methods (as the bulk density core method, which we were used) of measuring the soil moisture and the incorrectly chosen place. Assuming the soil moisture below 100 cm as a constant brings to small variation of calculated values and big errors for 90–100 cm layer. Excluding the relationship between the age and the

Table 1. Monthly average values of air temperature (T), air humidity deficit (D) and sunshine duration (S)

	J	F	M	A	M	J	J	A	S	O	N	D
T (°C)	-2.8	-0.7	5.7	14.2	17.0	22.6	22.2	21.3	14.4	8.3	5.8	-0.7
D (hPa)	0.4	0.5	3.5	6.9	7.8	13.8	8.8	10.7	4.2	2.2	2.4	0.6
S (h)	0.6	1.3	5.6	6.5	8.1	10.5	8.4	8.7	4.9	3.8	4.8	1.4

water assimilation abilities of the roots provokes an incorrect calculation of the soil moisture in depth. On the other hand, we consider the soil moisture below 100 cm as a constant.

Nevertheless, this model adequately responds to variation of the atmospheric conditions and may be used for determination of the soil moisture during the vegetation period between the wilting point and the fully saturated soil.

References

Choudhury, J. and *Idso B.*, 1985: An empirical model for stomatal resistance of field-grown wheat. *Agricultural and Forest Meteorology 36*, 65-82.

Denmead, O. and *Millar, B.*, 1976: Field studies of the conductance of wheat leaves and transpiration. *Agronomy Journal 68*, 307-311.

Fisher, M., Charles-Edwards, D. and *Ludlow M.*, 1981: An analysis of the effects of repeated short-term water deficits on stomatal conductance to carbon dioxide and leaf photosynthesis by the legume *Macroptilium atropurpureum* cv.Sirato. *Australian Journal of Plant Physiology 8*, 347-357.

Mitchurin, B., 1975: *Power of soil moisture* (in Russian). Gidrometeoizdat, Leningrad.

Roberts, J., Pymer, C., Wallace, J. and *Pitman, R.*, 1980: Seasonal changes in leaf area, stomatal and canopy conductances and transpiration from bracken below a forest canopy. *J. Applied Ecology 17*, 409-422.

Sirotenko, O., 1981: *Mathematical modelling of water-heat regime and crop productivity* (in Russian). Gidrometeoizdat, Leningrad.

Thompson, N., Barrie, I.A. and *Ayles, M.*, 1981: The Meteorological Office rainfall and evaporation calculation system. *Hydrological Memorandum*, No.45, England.

IDŐJÁRÁS

Quarterly Journal of the Hungarian Meteorological Service
Vol. 97, No. 1, January—March 1993

On the determination of vapour's molecular diffusion constant

F. Thoma

Consulting Engineer
Bimbó út 190/192, H-1026 Budapest, Hungary

(Manuscript received 17 December 1992; in final form 9 February 1993)

Abstract—In connection with the study of the individual characteristics of the water vapour's molecular diffusion constant D_m, which was published in the recent past (*Thoma*, 1991 b), some further questions may be arise. Accordingly, it is aimed to make clear that of the three parameters T_w (water temperature), T_a (air temperature) and R (relative humidity), respectively, which one is those having the greatest influence on the magnitude of D_m.

The author illustrates and analyses the effects of T_w as well as T_a on the molecular diffusion constant by the distribution function of $D_m = f(T_w)$ and $D_m = f(T_a)$, respectively. The effect of the relative humidity is still illustrated and analysed by the function of $D_m = f(R)$,—namely in the three cases of different water temperature, regarding four-four air temperatures for each case—i.e. by 3x4=12 function-curves, using a common system of co-ordinates.

Comparing the effects of different parameters one by one it seems that the magnitude of the relative humidity has the greatest influence on the magnitude of D_m above all. In the second place there may be mentioned the effect of the water temperature. The effect of the air temperature may be neglected.

Key-words: molecular diffusion constant, evaporating water surface, sprinkler irrigation.

1. Introduction

For the planning operations of the floating valve sheets (in the patent specification written as "coverplates") being used as an evaporation reduction apparatus (*Thoma*, 1967, 1971,1973, 1992), it is absolutely necessary to know, in the given case, the accurate value of the water-vapour's molecular diffusion constant D_m. (In this paper expression *molecular diffusion constant* is used because its values is rather constant compared to the turbulent diffusion coefficient, see *Thoma*, 1982.)

During the research work, have performed for long years, first the diffusion

constant's determination method has been developed (*Thoma*, 1982). On the basis of this method the functions of $D_m=f(T_w)$, $D_m=f(T_a)$ and $D_m=f(R)$ have been sketched out (*Thoma*, 1987). Hereupon, the individual characteristics of the molecular diffusion function of $D_m=f(T_w)$ have been analysed in detail (*Thoma*, 1991b).

From both theoretical and practical view points some further questions may be raised up. For example, of the three—in our opinion the most important—parameters, i.e. the water temperature T_w, the air temperature T_a and the relative humidity R, which one is that, having the greatest influence on the most-probable value of molecular diffusion constant $D_{m(m.p.)}$. It is thought that these questions may be answered correctly, first of all, by the application of distribution functions.

In the course of this study there will be presented:

(a) the distribution functions of the $D_m=f(T_w)$ and $D_m=f(T_a)$, using generally their values No. "n", in three-three cases; namely for the $D_m=f(T_w)$ function, when $T_a=16°C$ and 24°C, 30°C, respectively; and for the $D_m=f(T_a)$ function, when $T_w=16°C$, 24°C and 32°C, respectively,

(b) the linear functions of $D_m=f(R)$—using generally their values No."n" and No. "n_2"—to discuss the curves more precisely, similarly in three cases; namely when $T_w=16°C$, 24°C and 32°C, respectively.

Knowing these distribution functions and linear functions, we analyse the effects of the three most important parameters on the value of D_m functions. The investigations comprise the determination of values of the vapour's molecular diffusion constant, the magnitude of which depends on the air temperature and the evaporating water temperature between 0°C and 50°C (i.e. in the so called "middle range", *Thoma*, 1987, 1991b).

The aim of this study is to demonstrate the effect of the above mentioned parameters acting on the value of the molecular diffusion constant.

2. *Distribution function of vapour's molecular diffusion constant*

For the distribution function of vapour's molecular diffusion constant the normal, Gaussian distribution function has been adopted, which is defined (*Csoma* and *Szigyártó*, 1975) as

$$F(x) \equiv P(\xi<x) \equiv \Phi(x) = \frac{1}{\sigma\sqrt{2\pi}} \int_{-\infty}^{x} e^{-\frac{t-m}{2\sigma^2}} dt, \qquad (1)$$

where $F(x)$ is the distribution function, P the probability, ξ random variable, x

independent variable of the distribution function as well as of the empirical distribution function, $\Phi(x)$, σ standard deviation, σ^2 variance, m probable value.

The random variable ξ is, in the present case, equivalent the molecular diffusion constant. The undistorted estimation of variance of the sample-set is given by formula

$$\sigma^2 = \frac{\sum_{i=1}^{n} (x_i - \bar{x})^2}{n - 1}, \tag{2}$$

where n is the number of samples, x independent variable, $\bar{x}$ arithmetical mean of the independent variable.

The basic importance of the distribution originates from the thesis that the random variable ξ characterizing the phenomenon, may be written as a sum of several other ξ_i random variables

$$\xi^{(n)} = \xi_1 + \xi_2 + \ldots + \xi_n, \tag{3}$$

which will converge to the normal distribution,—in case of very common conditions—with the increase of the number of sample, symbolically

$$\lim_{n \to \infty} F(x)^{(n)} = \Phi x^{(n)}, \quad \text{if } x^{(n)} = \sum_{i=1}^{n} x_i. \tag{4}$$

The dependent variables belonging to the values of the different independent variables of this distribution function may be determined using the well known table by *Csoma* and *Szigyártó* (1975).

The table contains values of the distribution function $F(x)$ for the $x=x_t$ values in the region of $0 < x_t \leq 3$ with accuracy of 0.02, and in the region of $x_t > 3$ with accuracy of 0.2 under the conditions, $m=0$, $\sigma=1$, $x_t \geq 0$.

3. Individual characteristics of the distribution functions of vapour's molecular diffusion constant

3.1. Dependence on the evaporating water temperature

The first comparative, analytical examinations were carried out by distribution functions determined for three cases. The parameters, serving as starting-points, are summarized in *Table 1.*

Table 1. Parameters for the calculation of every single point of the three $D_m=f(T_w)$ functions as well as the values of the random variable $D_{m(m.p.)}$ (n is number of cases)

Individual cases	T_a	ΔT_a	R	T_w	n	$D_{m(m.p.)}$	$10^3\Delta D_{m(m.p.)}$
	°C	°C	%	°C		$cm^2\ s^{-1}$	$cm^2\ s^{-1}$
I	16		75	12-50	23	0,483	
		8					0,715
II	24		75	20-50	23	0,489	
		6					3,931
III	30		75	26-50	17	0,492	

As may be seen, the air temperature-differences ΔT_a—considering T_a as constant value for the individual cases—are close to each other, i.e. $\Delta T_a=8°C$ and 6°C, respectively. The relative humidity is, in all three cases, the same, i.e. $R=75\%$. The values of evaporating water temperatures—as the values of selected samples—were always chosen from the so called "working section" (by the number of specimen as : $n=23$, 23 and 17, respectively). In the last column of Table 1 the most probable values of the molecular diffusion constant are shown, which are deduced using the No. "n" molecular diffusion constant values of D_m given by equation

$$D_{m(m.p.)} = \frac{\sum D_m}{n}. \tag{5}$$

The values of $D_{m(m.p.)}$ are strikingly close to each other.

The three distribution functions are presented in *Fig. 1* using a common system of co-ordinates, in order to ensure the easier compatibility of the three distribution functions. The axis of abscissas represents the scale of the random variable, in this case, the values of the molecular diffusion constant, while the axis of ordinates represents the scale of the values of the empirical distribution function, at present, the values of $\Phi(x)=1-x$.

The three distribution functions show great similarity as it is expected. All the three curves may be characterized by strongly straddling bell-shaped curves. The bell-shaped curves and the places of their summits are located shifting to the right, in a very small degree, depending on the increasing air-temperature. These, relatively very small displacements mean that the air-temperature above the evaporating water surface has only small effect on the most probable value $D_{m(m.p.)}$ of the molecular diffusion constant (e.g. the increase of 8 °C and 6 °C,

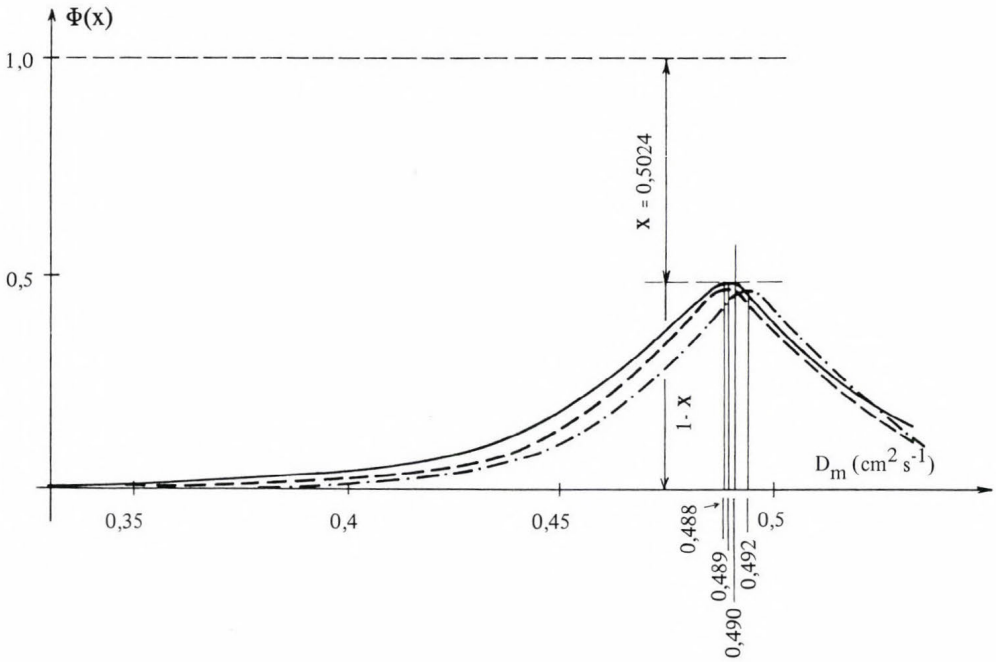

Fig. 1. Distribution functions of D_m as a function of T_w for different $T_a = 16°C$ (solid), 24°C (dashed) and 30°C (dot-dashed), respectively. The R is equal to 75% in all the three cases.

in the value of T_a will raise the value of $D_{m(m.p.)}$ by only 0,146% and 0,803%, respectively).

3.2. Dependence on the air temperature above the evaporating water surface

The next comparative, analytical examinations were carried out—similarly as in the Section 3—by distribution functions determined for the three cases. The values of parameters, serving as starting-points for calculation of $D_m = f(T_a)$ functions, are summarized in *Table 2*.

The water temperature differences ΔT_w—considering T_w as constant value for the individual cases—are equivalent, i.e. $\Delta T_w = 8°C$. Moreover, the relative humidities are, in all three cases, similarly equivalent, i.e. $R = 75\%$. While the values of air temperatures above the water, T_a —as the values of selected samples—are always chosen from the so called "working section" (by the number of specimen as $n = 21$, 23 and 23, respectively). In the last column of Table 2 there are shown the most probable values of the molecular diffusion constant which are deduced by using the No "n" molecular diffusion constant values of D_m as well as by the application of Eq. 5.

Table 2. Parameters for the calculation of every single point of the three $D_m = f(T_a)$ functions as well as the values of the random variable $D_{m(m.p.)}$ (n is number of cases)

Individual cases	T_w	ΔT_w	R	T_a	n	$D_{m-(m.p.)}$	$10^3 \Delta D_{m(m.p.)}$
	°C	°C	%	°C		$cm^2\ s^{-1}$	$cm^2\ s^{-1}$
I	16		75	0-20	21	0,460	
		8					17,103
II	24		75	6-28	23	0,477	
		8					12,702
III	32		75	14-36	23	0,489	

The three distribution functions are presented in *Fig. 2.* These distribution functions show also great similarity to those in Section 3. All the three curves are of bell-shaped similarly to Section 3.1. But here the right side of the curve is open from its half height downwards. The bellshaped curves and their culmination's points are shifting to the right (as compared with each others), in the same degree, depending on the increase of the water temperature. These relatively conspicuos displacements indicate how intense and determining is the effect of the evaporating water temperature on the most probable value $D_{m(m.p.)}$ of the molecular diffusion constant (e.g.: the increase of 8°C in the value of T_w will raise the value of $D_{m(m.p.)}$ by 3.7% and 2.7%, respectively).

Concerning the effect of T_w,—its determining character coming from above mentioned conclusion—it is reasonable to give a more detailed and correct explanation based on the mechanism of this physical phenomenon, showing which process produces this significant effect.

Earlier it has been mentioned (*Thoma*, 1974), that the water molecules, due to their kinetic energy in the evaporating water, are moving in different directions and with different velocity (Brownian/colloidal movement), depending on the actual water temperature. Some water molecules,—if their moving direction is perpendicular to the water surface—in case of suitable velocity, break through the pellicle of water surface influenced by the surface-tension and penetrate into the so called boundary layer next to the water surface (thickness of which equals to about 100 μm (*Katsaros et al.*, 1977).

It is well known that the colloidal-movement is proportional to the temperature of the elementary particles. The change of state between the water surface and boundary layer, intensifies in the case of increasing water temperature, as long as the boundary layer with the increased temperature will be

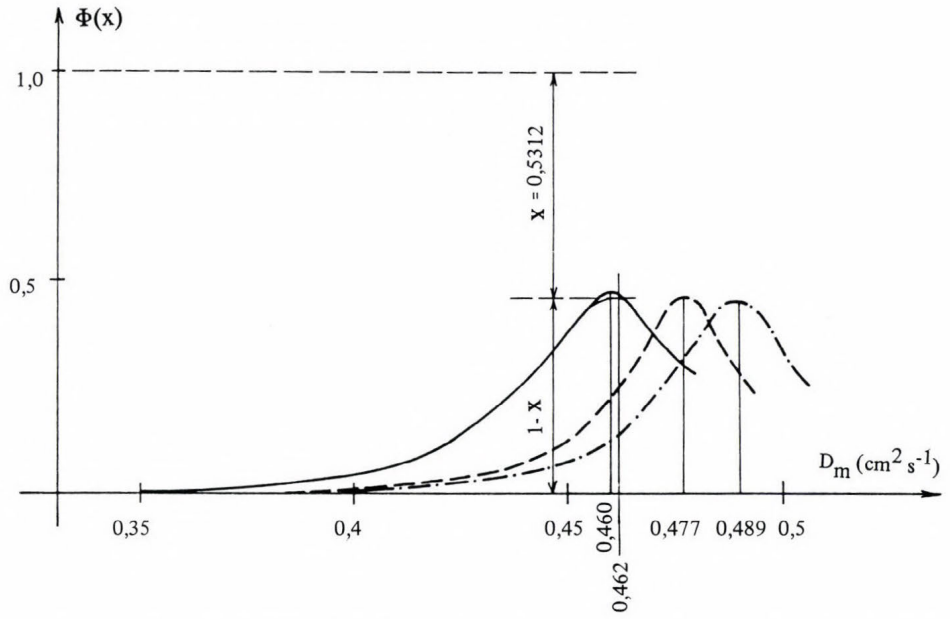

Fig. 2. Distribution functions of D_m as a function of T_a for different $T_w = 16°C$ (solid), 24°C (dashed) and 32°C (dot-dashed), respectively. The R is equal to 75% in all the three cases.

saturated again. This will induce a higher vapour-pressure in the boundary layer which leads to a higher vapour pressure difference as compared to the vapour pressure of the air layer being above the boundary layer. Consequently, the rate of molecular diffusion will increase between the two layers.

The distribution function's sample numbers "n" shown in Table 2 are near-by each others. While the relative humidity values of the air above the evaporating water having different temperatures T_a are equivalent (i.e. 75%) in each case. Thus, the shifting of the most probable value $D_{m(m.p.)}$ of the molecular diffusion constant is no doubt the consequence of change in the water temperature.

4. Individual characteristics of the functions $D_m = f(R)$ of vapour's molecular diffusion constant against the relative humidity of the air

4.1 Determination of the $D_m = f(R)$ curves

The investigations are based on three individual cases again, now instead of distribution functions simple function-groups are used. The parameters concerned are summarized in *Table 3*.

Table 3. Parameters used for the determination of individual points of the three function groups $D_m = f(R)$ and the values of molecular diffusion constants $D_{m(sing.)}$ of singular straights for different T_w, T_a and R.

Individual cases	T_w	T_a	R	n_1	n	n_2	$D_{m(sing)}$
	°C	°C	%	(left side)		(right side)	$cm^2\ s^{-1}$
		20,0	0- 75	4			
		19,0	0- 75	4			
		17,0	0- 93	6			
I	16	16,0	0-100		5		0,462
		15,8	0-100			4	
		15,4	0-100			5	
		13,0	0-100			5	
		10,0	0-100			5	
		27,0	0- 83	6			
		26,0	0- 85	4			
		25,0	0- 94	5			
II	24	24,0	0-100		5		0,475
		23,5	0-100			5	
		20,0	0-100			5	
		12,0	0-100			5	
		4,0	0-100			5	
		35,0	0- 80	5			
		34,0	0- 87	5			
		33,0	0- 93	6			
III	32	32,0	0-100		5		0,488
		31,8	0-100			6	
		31,4	0-100			5	
		30,0	0-100			5	
		29,0	0-100			5	

Three water temperatures (i.e. $T_w = 16$, 24 and 32°C) were associated with n_1+n+n_2 (generally $3+1+4$) and the air temperatures and the values of molecular diffusion coefficients were determined by an earlier introduced method (*Thoma*, 1987) for 4–6 different relative humidity data.

The pair of values, i.e. D_m against R obtained in this way are shown in *Fig. 3*. This figure is identical in principle but more detailed and complete as compared to the Fig. 1c of an earlier work published already in 1987 (*Thoma*, 1987). At that time we aimed merely to present the constructing possibility of the linear function R against D_m in case of different air temperatures, further, to draw some inferences.

In the present case Fig. 3 will give presumably several more interesting information which are taken into account below.

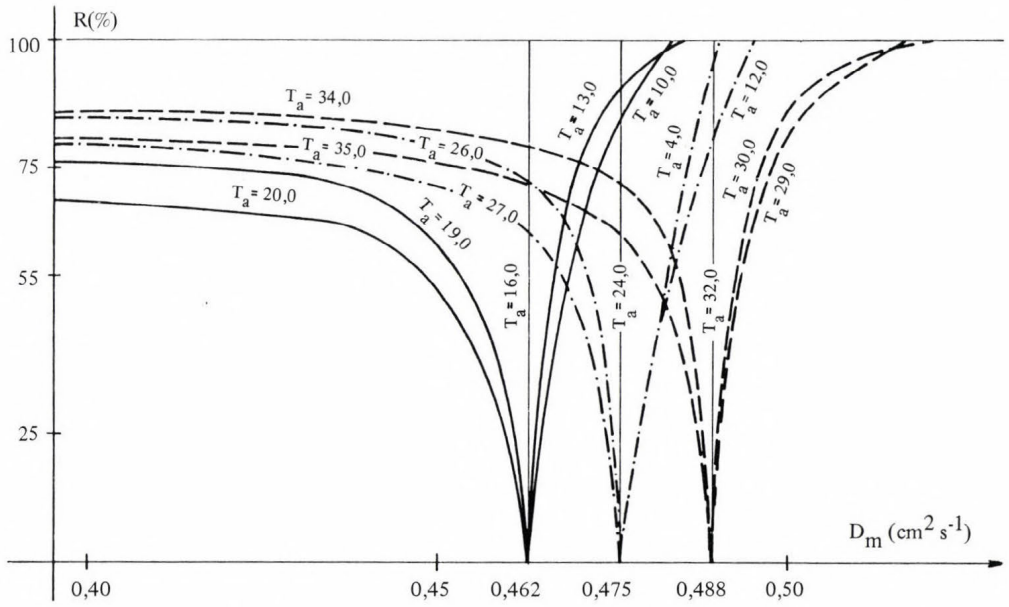

Fig. 3. Functions of D_m against R for different T_a (written on the curves) and $T_w = 16$°C (solid), 24°C (dot-dashed) and 32°C (dashed), respectively.

4.2 Individual characteristics of the $D_m = f(R)$ function curves

Analysing the function curves in Fig. 3, we have to notice three typical characters. To the water temperature's each fixed value (i.e. to $T_w = 16$, 24 and 32°C, respectively) two so-called "functiongroups" belong one of which opens on the left side and an other on the right side. Through the center of this function-group a vertical straight (a singular function-line) passes to which we shall refer later in more detailed. For example, selecting one of the function-group, to which the water temperature of $T_w = 24$ °C belongs, it may be seen that:

(1) If the function group located on the right side, i.e. when the water temperature, $T_w = 24$°C is fixed and the air temperatures are smaller than the fixed water temperature (i.e. $T_a = T_w - \Delta T$, and the curves belong to air temperatures of 23, 20 and 12°C, respectively), then it will be seen that the value of D_m does not increase uniformly with the increasing R value, but it increases in more and more degree.

However, as compared with the increase of the function-group being on the left side of the straight of the air temperature of $T_a = 24$°C the increasing is slow enough.

(2) On the contrary of the above statement if the water temperature is fixed, i.e. $T_w = 24$°C, and the function-group on the left of straight of the air

temperature of T_a=24°C is examined, (i.e. the $T_a=T_w+\Delta T$ curves, and T_a 26, 27 and 28°C, respectively), then it may be seen, that the value of D_m will decrease with the increase of the relative humidity not uniformly but in more and more degree.

However, as compared with the increase of the function-group on the right side of the straight of the air temperature of T_a=24°C the decreasing is slow enough.

This latter decrease takes place more rapidly than the increase mentioned in point 4.2(1) as it may be seen very well in Fig. 3.

4.3 Individual characteristics of the $D_{m(sing.)}$ singular straight in case of $T_w=T_a$

As an introduction it should be mentioned that the water temperature has always to be measured at the water surface because of the heat abstraction. According to the researches (*Katsaros*, 1977) the water temperature is higher by 1.0°C if measured at 0.5 cm below the water surface compared to the temperature measured immediately at the surface. This difference was determined by an experiment performed at 29°C water temperature.

During the designing of the function-lines it has been noticed that in case of $T_w=T_a$ the function's shape is a straight. This means that the same singular value of $D_{m(sing.)}$ belongs to any relative humidity values (e.g. in case of $T_w=T_a$=16°C the $D_{m(sing.)}$=0.462 cm^2 s^{-1}). Well then the question is how this is possible?

In order to answer this, let us adopt Eq. (4) in our recently published study concerning the value of vapour's molecular diffusion constant (*Thoma*, 1991 b):

$$D_m = k \frac{E(T_w) - RE(T_a)}{a(T_w) - Ra(T_a)}, \tag{6}$$

where D_m molecular diffusion constant (cm^{2}s^{-1}), k constant (4,633.10^{-7} s^{-1}), $E(T_w)$ vapour pressure of boundary layer (Hg mm), R relative humidity of the air (%), $E(T_a)$ air vapour pressure (Hg mm), $a(T_w)$ vapour concentration (g/cm^3), $a(T_a)$ air density (g/cm^3).

In our case—since the boundary layer's temperature (the vapour saturated layer's temperature) and the air layer's temperature above it are the same—the vapour pressure of $E(T_w)$ as well as $E(T_a)$ used in Eq. (6) are equivalent. Therefore, let us denote them generally by $E(T)$. For the vapour concentration the same situation is valid consequently its values will be denoted by $a(T)$.

Accordingly, the value of this special singular molecular diffusion constant will be as follows

$$D_{m(sing.)} = k \frac{E(T) - R \cdot E(T)}{a(T) - R \cdot a(T)}, \tag{7}$$

and after simplification

$$D_{m(sing.)} = k \frac{E(T)}{a(T)}, \tag{8}$$

which is after all visibly independent of the relative humidity and thus it assumes a fixed value indeed.

This value of $D_{m(sing.)}$ is a singular value for each temperature-pair of $T_w \equiv T_a$, and the function $D_{m(sing.)} = f(E(T)/a(T))$ belonging to them represents straights perpendicular to the axis of abscissas.

5. Possible practical application of the results

Drop and sprinkler irrigations are used all over the world. One of the most wide-spread irrigation method is the sprinkler-irrigation. But this has a drawback with regards to the drop-irrigation. Namely, the outcoming water (water drops, jet etc.) from the sprinkler-head suffer loss because of the evaporation before it reaches the soil. This is well known by the hydrologists (*Antal*, 1965). This loss is at least 30–40% which is more than has been supposed so far (generally 2–25%) which may be decreased in the future by selecting the right time and day's period, according to the present research.

Using meteorological forecastings there is given the possibility to choose the optimum irrigation period from the 24 hours of a day, based on $D_m = f(R)$ curves.

Accordingly, beside the temperature of the water sprinkled out from the head, which changes practically very small for 1 or 2 days it is possible to choose the most favorable air temperature and relative humidity in order to get the minimum value of the molecular or turbulent diffusion, $D_{m(min.)}$ or $D_{t(min.)}$. The optimum periods for irrigation will be most probably at the terms of dawn, sun-rise and at the beginning of night, after sunset.

6. Conclusions

(1) In case of constant air temperature and variable water temperature the curve of the molecular diffusion constant's distribution function is bell-shaped, ogival above and diverging underneath. The summits of these distribution curves, the most probable values of the molecular diffusion constant are located

very close to each other. It may be said that the air temperature does not influence the most probable value of the molecular diffusion constant considerably.

(2) In case of constant water temperature and variable air temperature the curve of the molecular diffusion constant's distribution function is bell-shaped, downward diverging at the top and defective in its right lower half. These distribution functions are shifting to the right considerably, depending on the increasing water temperature assumed to be constant value. Accordingly, the values of $D_{m(m.p.)}$ are increasing remarkably in the right direction. From these characteristics the conclusion can be drawn that the evaporating water temperature influences the most probable value of the molecular diffusion constant considerably.

(3) Comparing points (1) and (2), it can be stated that the water temperature has essentially higher effect on the value of the molecular diffusion constant than the air temperature does.

(4) In case of the functions $D_m=f(R)$, associating three constant water temperatures and variable air temperatures with them, the effect of relative humidity is relatively small on the molecular diffusion constant, in the section of $R=0$–55% it is nearly symmetrical to the left and right of the singular straight. But above 55% relative humidity, to the left of the singular straight the increase of the relative humidity has a rapidly decreasing effect on the molecular diffusion constant. At the same time to the right of the singular straight, the values of relative humidity above 55% increase the values of D_m but only in a moderate degree as compared to the case mentioned before.

(5) When examining the values of the distribution functions, it may be seen that the summits of independent variable x are found between the values of 0.5024 and 0.5312. This means a difference of cca. 5.42%. From this small difference a conclusion may be drawn that the choosing of the sample's number as well as the accuracy of the calculation method are correct enough.

(6) Among the functions of $D_m=f(R)$ there is a special one, namely when the two parameters, i.e. the values of temperatures T_w and T_a are equivalent. In this case the shape of the $D_m=f(R)$ function is straight vertical to the axis of abscissa, so called "singular straight". Accordingly, one singular straight belongs to each $T_w=T_a$ temperature-pair which is independent of the relative humidity.

(7) The conclusion from points 1–6 indicates that the relative humidity plays so important role in the formation of the value of the molecular diffusion constant. This effect of the relative humidity is larger as compared to that of temperatures T_w or T_a.

(8) The saturated "air cushion" mentioned in the English Patent (*Thoma*, 1971) and the physical explanation of the cushion's development formulated earlier (*Thoma*, 1980) demonstrate the primary effect of R as well. Namely, in connection with the vapour hydraulic theory of different valve sheets it came

to light that assuming the relative humidity of the air to be $R=40\%$ the relative humidity $R_{thicked}$ of the artifically thicked air-layer between the valve-sheet and the evaporating water surface, increased by the following degree:

(a) in case of rectangular valve sheet and reducing the evaporation by 84% the $R_{thicked}=95\%$ (*Thoma*, 1989),

(b) in case of triangle-formed valve sheet and reducing the evaporation by 79%, the $R_{thicked}=98\%$ (*Thoma*, 1991a).

(9) Similarly to the curves outlined in Fig. 3., there may be drawn further innumerable function-groups of $D_m=f(R)$. Based on these function groups we can choose the time-table for sprinkler-irrigation taking into consideration the evaporation loss of delivered irrigation water in a more economically way (*Dobos*, 1992, personal consultation).

The values of the air temperature and relative humidity are predicted for several days by the meteorological services (*Antal*, 1992, personal consultation).

References

Antal, E., 1965: Irrigation and meteorology (in Hungarian). *Időjárás 69*, 248-257.

Csoma, J. and *Szigyártó, Z.*, 1975: *Adoption of mathematical statistics in hydrorlogy* (in Hungarian). VITUKI publication Budapest, 1-220.

Katsaros, K., Liu, W. Businger, T. Joost, A. and *Tillman, J. E.*, 1977: Heat transport and thermal structure in the international boundary layer measured in an open tank of water in turbulent free convention. *J. Fluid Mech. 83*, Part 2, 311-335.

Thoma, F., 1967: Evaporation model tests (in Hungarian). *Hidrológiai Tájékoztató*, November, 34-41.

Thoma, F., 1971: Apparatus for Reducing Evaporation from a Liquid Surface. No. 1, 229 852, The Patent Office, London, Filed 22 May 1968, 1-3.

Thoma, F., 1973: Model tests with thin sheets to reduce evaporation. *J. of the Irrigation and Drainage Division*, ASCE, *Vol. 99*, No. IR 2, Proc. Paper 9779, June, 1973, 117-131.

Thoma, F., 1974: Property of vapour's elementary particles originating at vaporization (in Hungarian). *Hidrorlógiai Tájékoztató*, 40-44.

Thoma, F., 1980: Motion of vapour and the forcess inducing of that (in Hungarian). *Hidrológiai Tájékoztató*, October, 14-15.

Thoma, F., 1982: Vapour's diffusion constant and its numerical determination (in Hungarian). *Hidrológiai Tájékoztató*, October, 6-9.

Thoma, F., 1987: Function of vapour's diffusion constant and its Gaussian-distribution (in Hungarian). *Hidrológiai Tájékoztató*, April, 15-18.

Thoma, F., 1989: Numerical determination of on one or on two oposite sides open rectangle-formed sheet's characteristic--curve, in case of meteorological circumstances given in advance (in Hungarian). *Hidrológiai Tájékoztató*, October, 22-25.

Thoma, F., 1991a: Numerical determination of on one or two sides open equilateral

triangle-formed sheet's characteristic-curve, in case of meteorlological circumstances given in advance (in Hungarian). *Hidrológiai Tájékoztató*, April, 37-39.

Thoma, F., 1991b: Individual characteristics of the vapour molecular diffusion function (in Hungarian). *Időjárás 95*, 245-257.

Thoma, F., 1992: Evaporation Reduction with Floating Sheets. International Commission on Irrigation and Drainage. *Proc. of the Rapport of the 16th European Regional Conference*, 21-27 June, Budapest. Vol. I. Drough Phenomena, 501-515.

BOOK REVIEW

F. Fliri: **The Snow in North- and East-Tyrol 1895–1991** (in German). Universitätsverlag Wagner, Innsbruck, 1992 (Vol. I: pp. 593, Vol. II: pp. 553).

As a climatologist–retired since 1977–and an old-timer researcher of the snow conditions of Hungary, I took this work in my hand with a great deal of genuine interest.

The title and the size of the two volumes already gave me an advance hint of the level of detail, and rightly so. *Most probably no one in the worlds has ever produced such an exhausting and carefully prepared monography about the snow cover of a relatively small area.*

The two volumes comprise the observations of snow conditions carried out at 80 stations all over *North-, Central-* and *East-Tyrol*, through a period of nearly 100 years. Among the 80 stations there were 44 with observations from 1895 onwards, with only minor gaps (at 20 stations) during World Wars I and (particularly) II. From 1950 onwards the observation series are uninterrupted at all of the 80 stations.

Firstly a short, general historical overview is given about snow observations in Tyrol. Then, following some statistical information about the observation network, the *average snow cover data* are presented in figures and diagrams.

Next, a particularly interesting part deals with *snow cover data in summer*, from 65 stations. Between altitudes of 490 and 1950 metres above sea level, snow cover–as we see–is a familiar phenomenon in the May–June and September–October periods. Above 1000 metres an unbroken snow cover is a relatively frequent–although not very long-lived–phenomenon.

For the 95 winters between 1895 and 1991, a graphical presentation is given of snow cowers deeper than 1 cm (these figures may be called: "snow assurances"). Next, we find tabulations of dates marked with maximum snow depths, showing that below 2000 metres these maxima occur in February, while above 2000 metres in March.

The most voluminous part of the work contains the *chronological diagrams* of snow depths. This part of the work is the novelty of the whole monography. The presentation is very instructive. The snow cover builds up before our eyes–like in a movie–, reaches its maximum depth, and then–more slowly–it recedes. It is experimental to follow the story of 95 winters in the light of these snow cover data. Watching the unfolding story of snow in Austria, as it is presented in Professor Fliri's work, this Hungarian reviewer can only admire the substance (namely the snow), which has become one of the great assets of Austrian tourist industry in our age.

M. Kéry

ATMOSPHERIC ENVIRONMENT

an international journal

To promote the distribution of Atmospheric Environment *Időjárás* publishes regularly the *contents* of this important journal. For further information the interested reader is asked to contact *Dr. P. Brimblecombe,* School for Environmental Sciences, University of East Anglia, Norwich NR 7TJ, U.K.

Volume 26A Number 16 1992

Volume 26A Number 17 1992

R.I. Sykes and *D.S. Henn*: Large-eddy simulation of concentration fluctuations in a dispersing plume, 3127-3144.

D.S. Henn and *R.I. Sykes*: Large-eddy simulation of dispersion in the convective boundary layer, 3145-3159.

K. Ruoss, R. Dlugi, C. Weigl and *G. Hänel*: Intercomparison of different aethalometers with an absorption technique: laboratory calibrations and field measurements, 3161-3168.

D. Knotková and *K. Barton*: Effects of acid deposition on corrosion of metals, 3169-3177.

G.H.L. Verver and *F.A.A.M. De Leeuw*: An operational puff dispersion model, 3179-3193.

A. Bytnerowicz, P.J. Dawson, C.L. Morrison and *M.P. Poe*: Atmospheric dry deposition on pines in the Eastern Brook Lake Watershed, Sierra Nevada, California, 3195-3201.

A.S. Mason and *F.A. Gifford*: Atmospheric tracer dispersion over a 24-h time span, 3203-3205.

G. Hacisalihoglu, F. Eliyakut, I. Olmez, T.I. Balkas and *G. Tuncel*: Chemical composition of particles in the Black Sea atmosphere, 3207-3218.

R. Mathur, L.K. Peters and *R.D. Saylor*: Sub-grid representation of emission source clusters in regional air quality modeling, 3219-3238.

Volume 26A Number 18 1992

R. Kozlowski, A. Hejda, S. Cęckiewicz and *J. Haber*: Influence of water contained in porous limestone on corrosion, 3241-3248.

M. Bennett, S. Sutton and *D.R.C. Gardiner*: An analysis of Lidar measurements of buoyant plume rise and dispersion at five power stations, 3249-3263.

M. Luria, J.F. Boatman, D.L. Wellman, R.L. Gunter, B.A. Watkins, S.W. Wilkison and *C.C. Van Valin*: Lake Michigan Ozone Study (LMOS): measurements from an instrumented aircraft, 3265-3277.

D. Grosjean: Formic acid and acetic acid: emissions, atmospheric formation and dry deposition at two southern California locations, 3279-3286.

A. Leonardi, H. Burtscher and *H.C. Siegmann*: Size-dependent measurement of aerosol photoemission from particles in diesel exhaust, 3287-3290.

R.S. Hamilton and *T.A. Mansfield*: The soiling of materials in the ambient atmosphere, 3291-3296.

C. Sabbioni and *G. Zappia*: Characterization of particles emitted by domestic heating units fueled by distilled oil, 3297-3304.

X.Q. Zhang and *P.H. McMurry*: Evaporative losses of fine particulate nitrates during sampling, 3305-3312.

F.O. Hoffman, K.M. Thiessen, M.L. Frank and *B.G. Blaylock*: Quantification of the interception and initial retention of radioactive contaminants deposited on pasture grass by simulated rain, 3313-3321.

T.C. Haas: Redesigning continental-scale monitoring networks, 3323-3333.

J.C. Chow, J.G. Watson, D.H. Lowenthal, P.A. Solomon, K.L. Magliano, S.D. Ziman and *L.W. Richards*: PM10 source apportionment in California's San Joaquin Valley, 3335-3354.

J. Alcamo, J. Bartnicki, K. Olendrzński and *J. Pacyna*: Computing heavy metals in Europe's atmosphere—I. Model development and testing, 3355-3369.

Volume 27A Number 1 1993

D.H.F. Atkins and *D.S. Lee*: Indoor concentrations of ammonia and the potential contribution of humans to atmospheric budgets, 1-7.

A.-L. Pasanen, M. Nikulin, M. Tuomainen, S. Berg, P. Parikka and *E.-L. Hintikka*: Laboratory experiments on membrane filter sampling of airborne mycotoxins produced by *Stachybotrys atra* Corda, 9-13.

Liu Yangang: Statistical theory of the Marshall-Palmer distribution of raindrops, 15-19.

A.P. Altshuller: Production of aldehydes as primary emissions and from secondary atmospheric reactions of alkenes and alkanes during the night and early morning hours, 21-32.

J. Collett Jr, B. Oberholzer and *J. Staehelin*: Cloud chemistry at Mt Rigi, Switzerland: dependence on drop size and relationship to precipitation chemistry, 33-42.

G.P.J. Draaijers and *J.W. Erisman*: Atmosperic sulphur deposition to forest stands: throughfall estimates compared to estimates from inference, 43-55.

K.H. Becker, J. Bechara and *K.J. Brockmann*: Studies on the formation of H_2O_2 in the ozonolysis of alkenes, 57-61.

F. van den Berg: Measured and computed concentrations of methyl isothiocyanate in the air around fumigated fields, 63-71.

D. Weihs and *R.D. Small*: An approximate model of atmospheric plumes produced by large area fires, 73-82.

L. Camarero and *J. Catalan*: Chemistry of bulk precipitation in the central and eastern Pyrenees, northeast Spain, 83-94.

M.S. El-Shobokshy and *Y. G. Al-Saedi*: The impact of the Gulf war on the Arabian environment–I. Particulate pollution and reduction of solar irradiance, 95-108.

Technical Notes

H. Sauren, E. Gerkema, D. Bićanić and *H. Jalink*: Real-time and *in situ* detremination of ammonia

Volume 27A Number 2 1993

Volume 27A Number 3 1993

First Ibero-American Conference on the Atmospheric Environment, CIAMAA91/IACAE91

NOTES TO CONTRIBUTORS

The purpose of *Időjárás* is to publish papers in the field of theoretical and applied meteorology. These may be reports on new results of scientific investigations, critical review articles summarizing current problems in certain subject, or shorter contributions dealing with a specific question. Authors may be of any nationality but papers are published only in English.

Papers will be subjected to constructive criticism by unidentified referees.

* * *

The manuscript should meet the following formal requirements:

Title should contain the title of the paper, the names(s) of the author(s) with indication of the name and address of employment.

The title should be followed by an *abstract* containing the aim, method and conclusions of the scientific investigation. After the abstract, the *key-words* of the content of the paper must be given.

Three copies of the manuscript, typed with double space, should be sent to the Editor-in-Chief: *P.O. Box 39, H-1675 Budapest,* Hungary.

References: The text citation should contain the name(s) of the author(s) in Italic letter or underlined and the year of publication. In case of one author: *Miller* (1989), or if the name of the author cannot be fitted into the text: *(Miller,* 1989); in the case of two authors: *Gamov* and *Cleveland* (1973); if there are more than two authors: *Smith et al.* (1990). When referring to several papers published in the same year by the same author, the year of publication should be followed by letters a,b etc. At the end of the paper the list of references should be arranged alphabetically. For an article: the name(s) of author(s) in Italics or underlined, year, title of article, name of journal, volume number (the latter two in Italics or underlined) and pages. E.g. *Nathan, K. K.,* 1986: A note on the relationship between photosynthetically active radiation and cloud amount. *Időjárás 90,* 10-13. For a book: the name(s) of author(s), year, title of the book (all in Italics or underlined with except of the year), publisher and place of publication. E.g. *Junge, C. E.,* 1963: *Air Chemistry and Radioactivity.* Academic Press, New York and London.

Figures should be prepared entirely in black India ink upon transparent paper or copied by a good quality copier. A series of figures should be attached to each copy of the manuscript. The legends of figures should be given on a separate sheet. Photographs of good quality may be provided in black and white.

Tables should be marked by Arabic numbers and provided on separate sheets together with relevant captions. In one table the column number is maximum 13 if possible. One column should not contain more than five characters.

Mathematical formulas and *symbols:* non-Latin letters and hand-written marks should be explained by making marginal notes in pencil.

The final text should be submitted both in manuscript form and on *diskette.* Use standard 3.5" or 5.25" DOS formatted diskettes for this purpose. The following word processors are supported: WordPerfect 5.1, WordPerfect for Windows 5.1, Microsoft Word 5.5, Microsoft Word for Windows 2.0. In all other cases the preferred text format is ASCII.

* * *

Authors receive 30 *reprints* free of charge. Additional reprints may be ordered at the authors' expense when sending back the proofs to the Editorial Office.

Published by the Hungarian Meteorological Service

Budapest, Hungary

INDEX: 26 361

HU ISSN 0324-6329

IDŐJÁRÁS

QUARTERLY JOURNAL
OF THE HUNGARIAN METEOROLOGICAL SERVICE

CONTENTS

VOL. 97 * NO. 2 * APRIL–JUNE 1993

IDŐJÁRÁS

Quarterly Journal of the Hungarian Meteorological Service

Editor-in-Chief
E. MÉSZÁROS

Editor
T. TÄNCZER

Technical Editor
Mrs. M. ANTAL

Editorial Office: P.O. Box 39, H–1675 Budapest

Subscription from customers in Hungary should be sent to the Financial Department of the Hungarian Meteorological Service Kitaibel Pál u. 1, 1024 Budapest. The subscription rate is HUF 2000.

Abroad the journal can be purchased from the distributor: KULTURA, P.O. Box 149, H–1389 Budapest. The annual subscription rate is USD 56.

IDŐJÁRÁS

Quarterly Journal of the Hungarian Meteorological Service
Vol. 97, No. 2, April–June 1993

The dynamics of a shallow-water flow over topography Part I. Theory

I. Szunyogh

Department of Meteorology, Eötvös Loránd University,
Ludovika tér 2, H-1083 Budapest, Hungary

(Manuscript received 29 April 1993)

Abstract—Conservative quantities play an important role in the long-term behaviour of dynamical systems. This statement is especially valid for the so-called Casimir invariants, since the number of these quantities are infinite for the infinite-dimensional continuous Hamiltonian fluid dynamical systems. The appropriate form of Casimir invariants for motion in a homogeneous fluid with free surface is $C=\int\int hC(q)dxdy$ for any function C, even if the governing differential equations contain the effects of steep topography. Here q is the (absolute) potential vorticity and h is the vertical extent of a fluid column above the bottom surface. According to the above conservation laws, if h is a bounded quantity the statistical mechanics of a shallow-water flow are controlled by the quasi-conservation of $C=\int\int C(\zeta)dxdy$, for any function C of the relative vorticity ζ.

If the applied mathematical approximation conserves the energy, the discretized governing equations define a finite-dimensional quasi-Hamiltonian system which for the conservation laws can be investigated as for a finite-dimensional Hamiltonian system. In this paper using the quasi-Hamiltonian representation it has been shown, that the discretized equations provide the formal invariance only for a finite group of the discretized Casimir invariants (generally for the potential enstrophy and for the circulation), which yield the increasing sensitivity of the discretized equations to the high-frequency perturbations.

Key-words: Casimir invariants, finite-dimensional quasi-Hamiltonian structure, potential vorticity, rotational and divergent kinetic energy spectra.

1. Introduction

The time evolution of a dynamical system is constrained by the invariants of motion. It follows that the stability properties and the statistical mechanics of a fluid system are principally governed by the acting conservation laws.

For a given system of equations the conserved quantities can be classified into two groups. The first one consists of those invariants whose conservation

is formally provided by the governing equations. The other group contains the quasi-conserved quantities which are formally not, but approximately invariant for a given period of time using realistic initial conditions. In this period the stability and the statistical mechanics of the flow are practically controlled by the quasi-conserved quantities, while the time evolution of the meteorological fields is governed by the original system of equations.

It is clear that the quasi-conserved quantities are the formal invariants of the reduced system of equations, which can be derived from the original equations using the method of scale-analysis and the principle of consistency (or, in other words, the simplified system has to preserve all conservation laws of the original system). Accordingly, when examining the statistical mechanics and the stability properties of a given hydrodynamical system, it is necessary to identify the formal invariants for the original system and for its possible simplified versions.

The most efficient way to derive energy consistent reduced systems and examine their conservation laws is using the Hamiltonian formalism in symplectic notation (*Salmon*, 1983, 1988; *Shepherd*, 1990). Therefore, in the latest time the Hamiltonian formalism has an extensive role in the investigation of the stability properties (*Shepherd*, 1992), as well as in studying of statistical mechanical features of fluid mechanical systems.

It must be stated that the role and importance of each conservation law are different. For example, nowadays it is clear that the formal conservation of vorticity-type invariants plays a more important role in the actual conservation of energy (kinetic energy) than the formal conservation of the energy (kinetic energy) itself. Moreover, there are some additional problems in the case of the discretized equations. First of all, the applied discretization techniques can lead to the violation of the formal invariants of the original equations, which follows that these approximations cannot provide the conservation of all quasi-conserved quantities. Strictly speaking, the stability and the statistical mechanics of the discretized equations are principally governed by the conservative properties of the approximating equations. In this way, the identification of conserved quantities for the discretized equations has a great importance in examining the statistical mechanics of the system. An elegant and systematic way to identify these discretized invariants is the use of the quasi-Hamiltonian formalism of the discretized equations (*Szunyogh*, 1993). However, there are two necessary conditions of the applicability of this method. The approximated continuous system has to be a Hamiltonian one and the numerical schemes may not mix the approximations of the time and the spatial derivatives, as, for example, a semi-Lagrangian technique does.

In this paper the shallow-water system of equations containing the effect of bottom topography is considered as an original system of equations. For this system the quasi-conserved quantities are the formal invariants of the two-dimensional vorticity equations, namely the kinetic energy and the enstrophy.

It will be shown very clearly that the conservation of the formal vorticity-type invariants for the shallow-water equations is a necessary condition for the quasi-conservation of the enstrophy which provide the actual conservation of the kinetic energy.

The structure of the paper is as follows: *Section 2* is a short review of the Hamiltonian theory, while in *Section 3* the quasi-Hamiltonian formalism for fluid dynamical equations is described. In *Section 4* the role of the two-dimensional invariants are highlighted. In order to investigate the formal invariants of the shallow-water flow over steep topography, the governing equations are written in Hamiltonian form in *Section 5*. The role of the so-called Casimir invariants are examined in details in *Section 6*. *Section 7* concludes several remarks about the possible extensions. Finally, it should be mentioned that the subsequent part of this paper presents the result of a sequence of numerical experiments which were carried out with a well-known shallow-water model.

2. Hamiltonian structure in continuous model equations

In the symplectic notation the continuous model system can be represented by the equation

$$\boldsymbol{u}_t = J\frac{\delta H}{\delta \boldsymbol{u}}, \tag{1}$$

where $\boldsymbol{u}_t$ is the partial derivative of the prognostical vector variable $\boldsymbol{u}$ with respect to t, $H(\boldsymbol{u}(t))$ is the Hamiltonian function (generally the total energy) and J is a skew-symmetric transformation. In addition, the symplectic operator J satisfies the Jacobi condition (*Shepherd*, 1990). The conservation of energy follows immediately from the skew-symmetry of J, since

$$\frac{dH}{dt} = \left(\frac{\delta H}{\delta \boldsymbol{u}}, \frac{\partial \boldsymbol{u}}{\partial t}\right) = \left(\frac{\delta H}{\delta \boldsymbol{u}}, J\frac{\delta H}{\delta \boldsymbol{u}}\right) = -\left(\frac{\delta H}{\delta \boldsymbol{u}}, J\frac{\delta H}{\delta \boldsymbol{u}}\right), \tag{2}$$

where (,) is the relevant inner product for the function space $\{\boldsymbol{u}\}$. The conservation laws related to explicit symmetries (momentum-type invariants and the energy itself) can be identified by the Noether-theory (*Shepherd*, 1990), but it must be stated that the number of these invariants is finite.

The other group of invariants is associated with the particular form of the operator J. These so-called Casimir invariants are the solutions C of

$$J\frac{\delta C}{\delta \boldsymbol{u}} = 0. \tag{3}$$

Conservation of these quantities follows from

$$\frac{dC}{dt} = \left(\frac{\delta C}{\delta u}, J\frac{\delta H}{\delta u}\right) = -\left(\frac{\delta H}{\delta u}, J\frac{\delta C}{\delta u}\right) = 0, \tag{4}$$

using the skew-symmetry of J and the condition (3).

It can be seen that the Casimir invariants C do not depend on the Hamiltonian itself and they can be isolated by examining the kernel of the operator J. One of the most important features of these quantities is, that their number is infinite and so they can provide a strong control for the infinite-dimensional fluid-dynamical systems.

3. Quasi-Hamiltonian structure in the discretized equations

If the applied mathematical approximation conserves the energy, the model system possesses a quasi-Hamiltonian structure (*Szunyogh*, 1993) and the time evolution of the discretized vector variable x is governed by the equation

$$\frac{dx}{dt} = J\frac{dE}{dx}, \tag{5}$$

where the function $E(x(t))$ defines the total energy of the model and J is a skew-symmetric matrix-operator. The quasi-Hamiltonian denomination of this system is originated in the fact that the operator J does not satisfy the Jacobi condition. As a main advantage of this formalism, the behaviour of the discretized system can be investigated as for a finite dimensional Hamiltonian system.

In this case the Casimir invariants are the solutions C of the equation

$$J\frac{dC}{dx} = 0. \tag{6}$$

Conservation of these quantities follows from

$$\begin{aligned}\frac{dC}{dt} = \frac{dC}{dx}\frac{dx}{dt} &= \sum_{i=1}^{n}\frac{\partial C}{\partial x_i}\frac{\partial x_i}{\partial t} = \sum_{i=1}^{n}\frac{\partial C}{\partial x_i}\sum_{j=1}^{n}J_{ij}\frac{\partial E}{\partial x_j} = \sum_{i=1}^{n}\sum_{j=1}^{n}\frac{\partial C}{\partial x_i}J_{ij}\frac{\partial E}{\partial x_j} \\ &= -\sum_{i=1}^{n}\sum_{j=1}^{n}\frac{\partial E}{\partial x_i}J_{ij}\frac{\partial C}{\partial x_j} = \frac{dE}{dx}J\frac{dC}{dx} = 0.\end{aligned} \tag{7}$$

However, there is an essential difference between the condition (3) and (6),

the Eq. (6) defines only a finite number of independent conserved quantities. In order to see this important property, it has to be taken into consideration that the gradient vector $\partial C/\partial \boldsymbol{x}$ is the solution $\boldsymbol{y}$ of the homogeneous linear system of equations

$$J\boldsymbol{y} = 0. \tag{8}$$

There are nontrivial solutions of Eq. (8) if

$$\det(J) = 0. \tag{9}$$

Since the matrix J is skew-symmetric if the number of rows (columns) of the matrix is odd, the solutions exist independently of the particular value of the matrix elements. On the other hand, if the number of rows (columns) is even, the existence of the solutions depends on the particular value of the elements J_{ij}. It follows that the applied discretizing scheme can provide the conservation of the Casimir invariants only for specially constructed matrix operators. In the case when $\det(J)=0$ the general solution is

$$\boldsymbol{y} = Y_{n-r}\,t, \tag{10}$$

where Y_{n-r} is a matrix containing the n-r particular solutions of the system, while the components of the vector $t=[t_1, t_2,..t_r]$ are arbitrary free parameters. All the other solutions differ from Eq. (10) only in a constant multiplier, thus these solutions do not define new variables in a physical meaning.

4. Role of the two-dimensional invariants

The simplest model equation which has a meteorological meaning is the two-dimensional vorticity equation. In the Hamiltonian formalism it can be written as

$$u = \zeta, \quad J = -\partial(\zeta,.), \quad H(\zeta) = \frac{1}{2}\int\int |\nabla\psi|^2\, dx\,dy, \tag{11}$$

where $\zeta(x,y,t)=\nabla^2\,\psi(x,y,t)$ is the vorticity, $\psi(x,y,t)$ is the stream function and ∂ is the two-dimensional Jacobian (*Shepherd*, 1990). The Hamiltonian function $H(\zeta)$ is equal to the total energy of the fluid which, in this case, is equivalent to the total rotational kinetic energy E_{rot} of the flow.

The Casimir invariants are defined by

$$C = \iint C(\zeta)\, dx dy, \tag{12}$$

for any function C of the vorticity ζ. The most important invariants are associated with $C(\zeta)=\zeta$ and $C(\zeta)=\zeta^2$ which express the conservation of the total circulation and the enstrophy.

Conservation of enstrophy, together with the conservation of kinetic energy, provide the unique phenomenology of a two-dimensional incompressible flow (*Kraichnan*, 1975; *Vallis*, 1992). It means that there is an indirect energy transfer from the small scales, as well as a direct enstrophy cascade to the small scales which leads to the particular stability of the quasi-two-dimensional atmospheric and oceanic structures. This special feature of two-dimensional turbulence follows from the fact that the average wave number

$$k_1^2 = \left(\frac{D}{2\pi}\right)^2 \frac{\iint \zeta^2\, dx dy}{E_{rot}} = \left(\frac{D}{2\pi}\right)^2 \frac{\iint k^2 E(k)\, dp\, dq}{\iint E(k)\, dp\, dq}, \tag{13}$$

is a conserved quantity due to the conservation of the enstrophy, and the rotational kinetic energy E_{rot}, if $\vec{k}=(p,q)$ is the two-dimensional wave number, while the flow is confined in a cyclic box of side D.

Using this fact, following the pioneering works of *Kraichnan* (1967, 1975), many authors investigated the statistical mechanics of two-dimensional turbulence on an energy-enstrophy hypersurface in the phase space. However, as it was pointed out by *Shepherd* (1990), and *Carnevale* and *Fredriksen* (1987) for an infinite-dimensional system, the trajectories of nonlinear stable solutions cannot fill the entire energy-enstrophy hypersurface due to the invariance of higher moments of the vorticity. This means that the necessary condition for the ergodicity does not hold (*Khinchin*, 1949) which restricts the applicability of the *Kraichnan's* classical theory.

Although the enstrophy and the rotational kinetic energy are exact formal invariants only for the two-dimensional incompressible and nondivergent flows, the particular stability of quasi-two-dimensional atmospheric structures shows that for the large scale atmospheric motions in a some days period the rotational kinetic energy and the enstrophy are quasi-conserved quantities.

The situation is fairly different for the model equations which usually do not conserve the higher moments, and so the trajectories may fill the entire energy-enstrophy hypersurface. It means that the parameters of the equilibrium solutions describe the stability properties of the applied mathematical approximation instead of the stability properties of the original system. For instance, the average wave number is a possible index number to measure the inclination of the stability of the truncated models to the nonlinear instability (*Szunyogh*, 1992).

5. *The infinite-dimensional form of the governing equations*

In the symplectic notation the governing equations for quasistatic motion in a homogeneous incompressible fluid over steep topography can be defined by

$$\boldsymbol{u} = (\vec{v},h)^T, \tag{14.a}$$

$$H(\vec{v},h) = \frac{1}{2}\int\int\left[h(|\vec{v}|^2 + \frac{1}{2}gh + 2gh_s)\right]dxdy, \tag{14.b}$$

$$J = \begin{bmatrix} 0 & q & -\partial_x \\ -q & 0 & -\partial_y \\ -\partial_x & -\partial_y & 0 \end{bmatrix}, \tag{14.c}$$

where the potential vorticity q is defined by

$$q = (f+\zeta)h^{-1}, \tag{15}$$

v is the horizontal velocity, f is the Coriolis parameter, $\zeta = \vec{k}\nabla\times\vec{v}$ the vorticity, g the gravitational acceleration, h_s the bottom surface height and h the vertical extent of a fluid column above the bottom surface (for further details see Appendix A).

The Casimir invariants are defined by

$$C = \int\int hC(q)dxdy \tag{16}$$

for some function $C(q)$. It is clear that Eq. (16) defines infinite number of conserved quantities, which provides infinite number of constraints for the shallow-water flows. The most important Casimirs are related to $C=1$, $C=q$ and $C=q$ associated with conservation of mass, conservation of circulation, and conservation of potential enstrophy, respectively.

6. *The role of the Casimir invariants*

For the shallow-water system of Eq. (14) the time evolution of the relative vorticity and the divergence $\delta(x,y,t)$ are governed by the equations

$$\frac{\partial \zeta}{\partial t} = -\nabla(\zeta + f)\vec{v}, \tag{17.a}$$

$$\frac{\partial \delta}{\partial t} = \vec{k}\nabla\times(\zeta + f)\vec{v} - \Delta\left(\Phi + \frac{\vec{v}}{2}\right)^2, \tag{17.b}$$

and

$$\vec{v} = \vec{v}_\psi + \vec{v}_\kappa = \vec{k}\times\nabla\Delta^{-1}\zeta + \nabla\Delta^{-1}\delta, \tag{18}$$

where $\vec{v}_\psi$ is the rotational and $\vec{v}_\kappa$ is the divergent part of the velocity vector. Eq. (18) shows that the kinetic energy (per unit mass) of a shallow-water flow can be separated into two terms,

$$E_{kin} = E_\psi + E_\kappa = \frac{1}{2}(\nabla\Delta^{-1}\zeta)^2 + \frac{1}{2}(\nabla\Delta^{-1}\delta)^2, \tag{19}$$

where E_ψ is the rotational and E_κ is the divergent kinetic energy. In this way, the time evolution of rotational and kinetic energy is governed by the equations

$$\frac{\partial}{\partial t}E_\psi = (\vec{v}_\psi \times \vec{k})\nabla\Delta^{-1}\frac{\partial \zeta}{\partial t} = f(\vec{v}_\psi, \vec{v}_\kappa), \tag{20.a}$$

and

$$\frac{\partial}{\partial t}E_\kappa = \vec{v}_\kappa\nabla\Delta^{-1}\frac{\partial \zeta}{\partial t} = f(\vec{v}_\psi, \vec{v}_\kappa, \Phi). \tag{20.b}$$

As it was pointed out by *Warn* (1986), the divergent part of the kinetic energy evolves toward an equipartition among the wave-modes, while the rotational part of the kinetic energy is constrained by the quasi-conservation of the enstrophy. However, there is an additional transfer between the rotational and the divergent part of the energy, as it can be seen from Eqs. (17) and (20). The numerical experiments indicate that in the final equilibrium most of the kinetic energy is accumulated at the divergent modes, but in the first period there is a fairly stable quasi-two-dimensional equilibrium (*Errico*, 1984).

In this paper only the first period is examined in details. According to Eq. (12) and Eq. (16) the

$$Z^{(n)} = \int\int \zeta^n dx dy, \tag{21.a}$$

$$Q^{(n)} = \iint hq^n dxdy = \frac{1}{2}\int \int h\left[\frac{f+\zeta}{h}\right]^n dxdy, \tag{21.b}$$

($n=1,2,\ldots$) quantities are Casimir invariants for the two-dimensional vorticity equation and the shallow-water equations, respectively. Let

$$h_{\max} = \text{maximum}\,[h(x,y,t)], \tag{22}$$

then

$$|Z^{(1)}| = |Q^{(1)} - fA|, \qquad A = \iint dxdy, \tag{23.a}$$

$$|Z^{(n)}| \le h_{\max}^{n-1} |Q^{(n)}| + \sum_{k=1}^{n} C_k |Z^{(n-k)}|, \tag{23.b}$$

$$C_k = \binom{n}{k} f^k, \quad \text{if } n \ge 2, \tag{23.c}$$

(for further details see Appendix B). It can be seen that the $|Z^{(n)}|$ is a bounded quantity, since the first term on the right-hand side of Eq. (23.b) is constant according to Eq. (16), while the second term is bounded due to the recursion itself. What the most important is, the quasi conservation of $|Z^{(n)}|$ is controlled by the invariants of the original shallow-water system and the time-dependent variable h.

It must be emphasized that the formal conservation of energy has no direct role in the control of the spectral distribution of kinetic energy. It follows that the bottom topography may have an influence only through the parameter h_{max}, since the parameter h_s appears only in the energy function.

It should be mentioned that in the most extreme case $h(x,y,t)$ is a constant function, and the last column and the last row can be eliminated from J in Eq. (14.c) and Eq. (14) is simplified into the two-dimensional vorticity equation, while the quantities $Z^{(n)}$ become exact invariants.

The inequality (23) is valid for the discretized version of the quantity (21.a) and (21.b), too, but the integration in space have to be replaced by summarization for the discretized variables. As a main difference, the discretized equations provide the formal invariance only for a finite group of the $|Q^{(n)}|$ quantities (generally for $n=2$), which yields the increasing sensitivity of the discretized equations to the high-frequency perturbation.

For the sake of deeper understanding of the previous statement, we examine the acting process in details. As a consequence of the orographic effects,

divergent kinetic energy flows into the system. This divergent energy evolves toward an equilibrium among the wave number-modes. This means that, after a given time period, the divergent energy appears at the higher wave numbers, even if it is pumped in at the lowest wave numbers. Simultaneously, there is a continuous energy transfer between the rotational and the divergent part of the kinetic energy. In this way, rotational kinetic energy arises at the higher wave numbers since the numerical model cannot control the higher moments of the vorticity according to Eq. (23). This process leads to the violation of the conservation of lower moments due to the very effective nonlinear interactions. At the end of this process the numerical model becomes unstable and the energy catastrophe is bound to happen.

The process described above in part is the natural behaviour of the shallow-water system, since the conservation of $Z^{(n)}$ can be violated as a consequence of the variation of $h_{\max}$, even if the conservation of $Q^{(n)}$ for any n is preserved. In the nature this process is controlled by the viscosity, which consumes the kinetic energy of the high-frequency velocity perturbations, proportionally to the square of the wave number. However, numerical experiments indicate, that a viscosity coefficient, which is large enough to control the time evolution of the numerical model, after a time period leads to the catastrophic decrease of the kinetic energy (*Sadourny*, 1975).

Summarizing, the quasi-conservation of discretized $| Z^{(n)} |$ depends on two effects. The first of these effects is the time variation of the potential vorticity $| Q^{(n)} |$ due to the numerical approximation of the spatial derivatives, and the other effect is the increase of $h_{\max}$ which is a result of the topography if the flow satisfies the balance condition

$$\operatorname{div} \vec{v} = 0 \quad \text{at} \quad t = 0. \tag{24}$$

7. Concluding remarks

In this paper the influence of the divergent process on the nonlinear instabilities has been investigated. If an additional time dependent variable is introduced a new type of instability occurs and the scheme of the potential vorticity will contain this new variable. However, for all of these systems of equations the enstrophy is a quasi-conserved quantity due to conservation of potential vorticity, which provides the control of the nonlinear instability for a limited time-interval.

Eq. (23) gives a very rough quantitative estimation for the spectral behaviour of the shallow-water models. In order to understand deeper the acting processes involved, a series of numerical experiments were carried out with a well-known quasi-Hamiltonian model which provides the conservation of potential vorticity. The results of these detailed spectral investigations are in a

good accordance with the theoretical considerations presented here and they are demonstrated in the subsequent part of this paper.

References

Carnevale, G.F. and *Frederiksen, J.S.*, 1987: Nonlinear stability and statistical mechanics of flow over topography. *J. Fluid Mech. 175*, 157-181.

Errico, R. M., 1984: The statistical equilibrium solution of a primitive equation model. *Tellus 36A*, 42-51.

Khinchin, A.I., 1949: *Mathematical Foundation of Statistical Mechanics*. Dover, New York.

Kraichnan, R.H., 1967: Inertial ranges in two-dimensional turbulence. *Phys. Fluids 10*, 1417-1423.

Kraichnan, R.H., 1975: Statistical dynamics of two-dimensional flow. *J. Fluid Mech. 67*, 155-175.

Salmon, R., 1983: New equations for nearly geostrophic flow. *J. Fluid Mech. 153*, 133-152.

Salmon, R., 1988: Hamiltonian fluid mechanics. *Ann. Rev. Fluid Mech. 20*, 225-256.

Sadourny, R., 1975: The dynamics of finite-difference models of the shallow-water equations. *J. Atmos. Sci. 32*, 680-689.

Shepherd, T.G., 1990: Symmetries, conservation laws, and Hamiltonian structure in geophysical fluid dynamics. *Adv. Geophys. 32*, 287-338.

Shepherd, T.G., 1992: Arnol'd stability applied to fluid flow: Successes and failures. In *Nonlinear Phenomena in Atmospheric and Oceanic Sciences* (eds.: *G.F. Carnevale* and *R.T. Pierrehumbert*). Springer-Verlag, New-York.

Szunyogh, I., 1992: Statistical mechanics of inviscid truncated models of two-dimensional incompressible flows. *Időjárás 96*, 22-31.

Szunyogh, I., 1993: Finite-dimensional quasi-Hamiltonian structure in simple model equations. *Meteorol. Atmos. Phys. 51* (in press).

Vallis, G.K., 1992: Problems and phenomenology in two-dimensional turbulence. In *Nonlinear Phenomena in Atmospheric and Oceanic Sciences* (eds.: *G.F. Carnevale* and *R.T. Pierrehumbert*). Springer-Verlag, New-York.

Warn, T., 1986: Statistical mechanical equilibria of the shallow water equations. *Tellus 38A*, 1-11.

APPENDIX A

The governing equations in the original Eulerian form can be written as

$$\frac{\partial \vec{v}}{\partial t} + q\vec{k}\times h\vec{v} + \nabla(K + \Phi) = 0, \qquad \text{(A.1)}$$

$$\frac{\partial h}{\partial t} + \nabla(h\vec{v}) = 0, \tag{A.2}$$

where the kinetic energy per unit mass is

$$K = \frac{1}{2}|\vec{v}|^2, \tag{A.3}$$

and the potential energy is

$$\Phi = g(h + h_s), \tag{A.4}$$

and $\vec{k}$ denotes the vertical unit vector. Therefore, the Hamiltonian functional which is equivalent to the total energy of the fluid is

$$H(\vec{v},h) = \frac{1}{2}\int\int(h|\vec{v}|^2 + gh^2 + 2ghh_s)\,dxdy. \tag{A.5}$$

If follows that

$$\frac{\delta H}{\delta \vec{v}} = h\vec{v}, \quad \frac{\delta H}{\delta h} = \frac{1}{2}|\vec{v}|^2 + gh + gh_2, \tag{A.6}$$

and

$$\begin{bmatrix} \frac{\partial u}{\partial t} \\ \frac{\partial v}{\partial t} \\ \frac{\partial h}{\partial t} \end{bmatrix} = \begin{bmatrix} 0 & q & -\partial_x \\ -q & 0 & -\partial_y \\ -\partial_x & -\partial_y & 0 \end{bmatrix} \begin{bmatrix} hu \\ hv \\ \frac{1}{2}|\vec{v}|^2 + g(h+h_s) \end{bmatrix}, \tag{A.7}$$

which is equivalent to Eq. (14).

Shepherd (1990) examined the similar shallow-water system. Although he did not take into account the influence of the bottom surface, the operator J in his paper was the same as (14.c) *Salmon* (1988) pointed out that if the Hamiltonian H has been modified alone, leaving the symplectic operator J undistributed, the energy conservation is satisfied due to the skew symmetry of J, and the Casimirs (which depend on J, not H) do not change. In this way Eq. (14) defines an energy conservative system, and its Casimirs (16) correspond to those which were derived by *Shepherd* (1990).

APPENDIX B

Using (21.a), definition of $Z^{(n)}$ is

$$\begin{aligned} |Z^{(n)}| &= \left|\iint \xi^n dx dy\right| = \left|\iint [(\xi+f)^n - g^{(n)}] dx dy\right| \leq \\ &\leq \left|\iint (\xi+f)^n dx dy\right| + \left|\iint g^{(n)} dx dy\right| \\ &\leq \left|\iint \left(\frac{h_{\max}}{h}\right)^{n-1} (\xi+f)^n dx dy\right| + \left|\iint g^{(n)} dx dy\right| \\ &= h_{\max}^{n-1} |Q^{(n)}| + \left|\iint g^{(n)} dx dy\right| . \end{aligned} \tag{B.1}$$

The $g^{(n)}$ can be derived from the Newtonian binomial form

$$\xi^n = (\xi+f)^n - \sum_{k=1}^{n} C_k \xi^{n-k}, \tag{B.2}$$

from which it follows that

$$g^{(n)} = \sum_{k=1}^{n} C_k \xi^{n-k}. \tag{B.3}$$

Using the (21.a) definition of $Z^{(n)}$ again

$$\begin{aligned} \left|\iint g^{(n)} dx dy\right| &= \left|\iint \left(\sum_{k=1}^{n} C_k \zeta^{n-k}\right) dx dy\right| = \left|\sum_{k=1}^{n} \iint C_k \zeta^{n-k} dx dy\right| \\ &= \left|\sum_{k=1}^{n} C_k Z^{(n-k)}\right| \leq \sum_{k=1}^{n} C_k |Z^{(n-k)}| . \end{aligned} \tag{B.4}$$

The Eq. (B.4), together with Eq. (B.1), gives the inequality (23).

IDŐJÁRÁS
Quarterly Journal of the Hungarian Meteorological Service
Vol. 97, No. 2, April–June 1993

Development of decision method for storm warning at Lake Balaton

I. Bartha

Storm Warning Observatory of Hungarian Meteorological Service
P.O. Box 80, H-8600 Siófok, Hungary

(Manuscript received 4 March 1993; in final form 16 June 1993)

Abstract—Weather warnings are of great importance in respect to protection of life and property. The Storm Warning Observatory at Lake Balaton was founded with the aim of providing warnings 1–2 hours earlier for the holiday-makers on the expected wind gusts exceeding 12 or 17 m/s. As a result of successive investigations an objective decision procedure has been elaborated in which weather radar data are also used. This procedure can be executed interactively on a computer. It combines the method based on conventional data with the approach of using radar information.

As a development, the permanence of wind-hazardous degrees was investigated during frontal and convective weather situations. For the purpose of our investigations, radar and synoptic observational data were used. The determined distribution functions of empirical probability for the permanence of wind-hazardous degrees associated with Cb-clouds can be used for the further optimization of the decision method.

Key-words: Cb-cloud, wind-hazard, wind gust estimation, nowcasting, decision procedure, very short range forecast.

1. Introduction

Stormy wind is one of the most dangerous weather phenomena in the region of Lake Balaton. In respect to protection of life and property the weather warnings are of great importance to the holiday-makers, sailors and surf-riders under severe weather conditions. The Storm Warning Observatory at Lake Balaton was founded with the aim of providing warnings 1–2 hours earlier for the holiday-makers on the expected wind gusts exceeding 12 or 17 m/s.

In wind forecasting, one of the most difficult tasks is to predict the numerical measures in wind strengthening associated with Cb-clouds as they may be related to different synoptic situations. *Fawbush* and *Miller* (1954)

worked out a simple method for the prediction of maximum wind velocities associated with non-frontal thunderstorms. This method is based on the idea of *Brancato* (1942) that there is a close relationship between the temperature decrease induced by thunderstorms and the maximum wind velocity at the surface.

In the 60's, applicable methods for the prediction of maximum wind velocities with Cb-clouds and squall-lines have already been developed in Hungary, too. These methods originating from the era before the establishment of weather radar observations in our service are well-known after *Bodolainé Jakus* and *Götz* (1963), *Götz* (1963), *Ambrózy* and *Tänczer* (1963), *Bodolai et al.*, (1967). From the beginning of the 70's, identification of Cb-clouds and qualitative estimation of wind gusts associated with Cb-clouds have been completed by radar data. In connection with this, new problems have arisen concerning the very short range ($t \leq 2$ hours) forecast of the wind velocity. In particular, following each radar observation, it has been necessary to estimate to which wind category the maximum wind gusts (V_{max}) connected with Cb-echoes belong from the point of view of the storm warnings: no warning (0), alert (1) or storm warning (2). These wind categories are as follows: category 0: $V_{max} < 12$; category 1: $12 \leq V_{max} \leq 17$; category 2: $V_{max} > 17$ m/s. The objective answer was expected from a decision method. For this reason in the 80's, a decision model was developed (*Bartha*, 1987) to estimate the maximum wind gusts associated with Cb-clouds measured by radar. In the everyday practice of storm warning, this procedure can be executed interactively on a computer (*Bartha* and *Zsikla*, 1990). It combines the method based on conventional data with the approach of using weather radar information. This procedure provides an objective foundation for storm warning services at Lake Balaton.

2. *Decision method for prediction of maximum wind gusts associated with Cumulonimbus clouds*

The developed decision method is based on radar, upper-air and synoptic observational data as well as their combinations. The input parameters and data (*Table 1*) used for the decision procedure can be brought into connection with the maximum wind gusts induced by cold air spreading out at the surface under a Cb-cloud. The summary of the decision system is shown in the block diagram in *Fig. 1*:

— It can be seen that the very short range forecast for the region of Lake Balaton serves as basis for the decision-making on storm warning.

— Whenever precipitation systems detectable by satellite and weather radar appear within the closer area of the lake and their vertical development as well as intensity reach or exceed certain threshoulds ($H_{max} \geq 4$ km; $\lg Z_3 > 0$) more frequent radar observations are initiated. In cases when radar

data do not reach the given threshoulds, the warning changes for conventional decision.

— Then input data contained in Table 1 are fed into the decision system, classifying the Cb-echoes on the basis of wind-hazardous degrees.

— It is followed by consideration of the actual weather situation that may have influence on the development of Cb-clouds. The significant weather objects (denoted by letters C, G, H, I, J, MCC and defined later) are analysed one or three hourly on meso-synoptic charts. The surface pressure patterns

Table 1. Input data used for the objective decision procedure

Radar	Upper-air	Surface
measured parameters		
H_{max}, lgZ_3	H_{trop}, $H_{-20°C}$	T_{akt}, V_{max}, p
reduced parameters		
$Y=H_{max}\,lgZ_3$ $\Delta H=H_{trop}-H_{max}$ $\Delta H^*=H_{max}-H_{-20°C}$	Θ_{wo} Θ_k T_{max}^{prog}	$\Delta T=T_{akt}-\Theta_{wo}$ $\Delta T_{max}=T_{max}^{prog}-\Theta_{wo}$ Δp
Weather characteristics		
Marked weather object	Surface pressure pattern	Bagrovian analogy
codes		indices
C, G, H, I, J, MCC	A, E, F, K, L, M, N, O	$\{\rho_\varphi\}$ ground, 500 hPa $\{\rho_\lambda\}$ ground, 500 hPa $\{\rho_\varphi\,\rho_\lambda\}$ ground, 500 hPa

List of symbols

H_{max} – radar echo top
Z_3 – radar reflectivity factor
H_{trop} – height of tropopause
$H_{-20°C}$ – height of -20°C level
Y – criterion of severity
Θ_{wo} – wet-bulb potential temperature of 0°C level
Θ_k – potential temperature of the Cumulus condensation level
T_{akt} – actual temperature
V_{max} – maximum wind gust observed
p – surface pressure
ΔT – cooling rate
ΔT_{max} – maximum cooling rate
Δp – surface pressure gradient
T_{max}^{prog} – maximum temperature predicted

C – convergence zone
G – warm front
H – instability line
I – cold front
J – occluded front
A – no gradient ($\Delta p < 1$ hPa/100 km)
E – divergence
F – prefrontal gradient situation
K – postfrontal gradient situation
L – Genoa-cyclonic situation
M – Azores anticyclonic situation
N – cyclone over the Carpathian-basin
O – anticyclone over the Carpathian-basin
MCC – meso-scale convective complex

(denoted by letters A, F, L, M, N, O and defined in Table 1) are determined by the hourly change of the horizontal pressure gradient (Δp). The decision-making requires the monitoring of changes in the cooling rate (ΔT) as well as in the maximum wind gusts (V_{max}) measured by a telemetry system around Lake Balaton and in the surface pressure gradient (Δp) in the region of West-Hungary.

— Finally, the decision procedure results in one of the decisions: no warning, alert or storm warning.

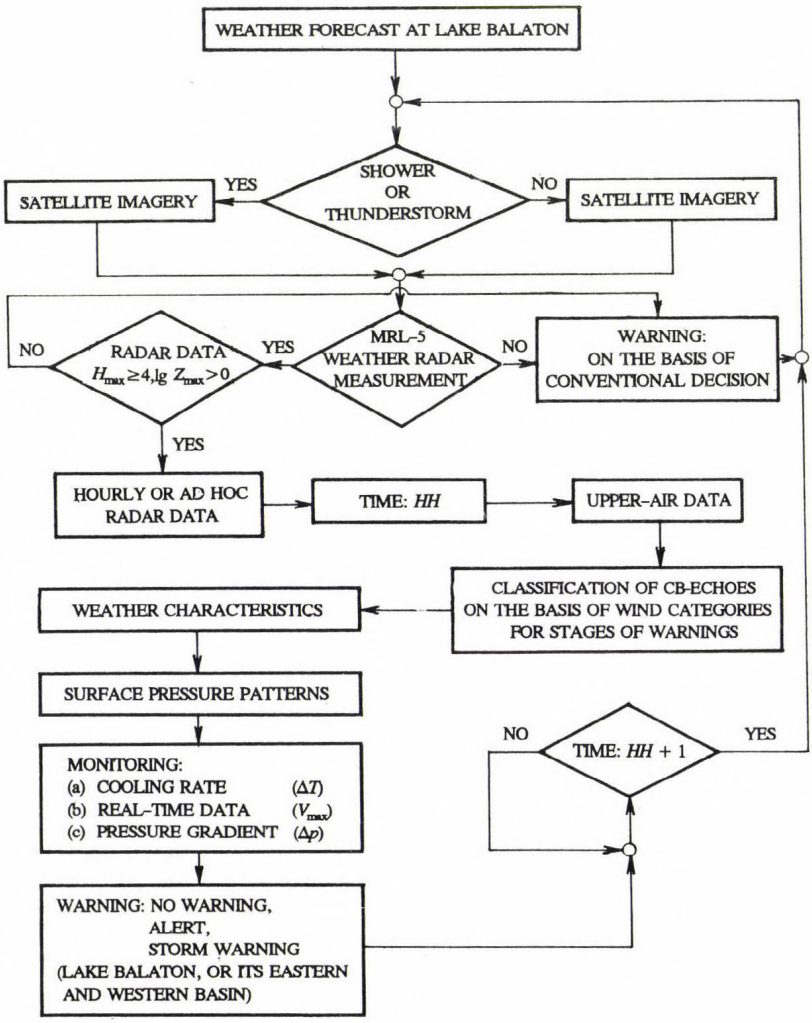

Fig. 1. Block diagram of the objective decision system for forecasting the maximum wind gusts (V_{max}) associated with Cb-echoes.

The programme using the computerized interpretation of manually digitized radar data has been working since 1988. The decision method was tested for the independent decision samples using the observational data of Szentgotthárd/Farkasfa weather radar station in West-Hungary. Warnings issued by the use of computerized decision procedure and those based on conventional method were compared in 548 cases of 1986, 1987, 1989 and the former ones proved to be more reliable by 5% as compared to the conventional ones (the value of accuracy increased from 76% to 81%). At the same time the objective procedure reduced the cases of overestimation by 10% (*Bartha* and *Zsikla*, 1990).

As a development, this decision method used in the storm warning practice also requires the knowledge of permanence for wind-hazards during various weather conditions connected with Cb-clouds (*Bartha et al.*, 1989).

3. Development of decision method

Answers were searched for the following questions from the view-point of wind hazards associated with Cb-clouds:

— Since when has a Cb-cloud become wind-hazardous at the surface?
— Is there difference between the permanence of wind-hazardous degrees associated with Cb-clouds developed during various weather situations?
— How long wind-hazardous periods can be estimated in various weather situations?

3.1 Data used as the starting point for investigation

In order to answer the above-mentioned questions, some active cold fronts (I: cold front or cold front with warm wave) and convective systems (C: convergence zone; H: instability-line; MCC: meso-scale convective complex) were studied. These weather situations (36 frontal and 20 convective storms) were collected in 1986 and 1987 during the periods from May to September. The following data were used for investigation:

— hourly radar observational data (H_{max}; lgZ_3; $Y=H_{max}\ lgZ_3$) from the detection region with a radius of 150 or 200 km of the Szentgotthárd/Farkasfa weather radar station in West-Hungary (the radar is of MRL-5 type and worked on the wavelength of 10 cm, producing information for square elements of 20x20 km^2),
— observational data for the Cb-clouds (SYNOP: $C_L=3$ or 9) and some significant weather phenomena [shower; thunderstorm; hailstorm; wind gusts (V_{max}) associated with Cb-clouds of 7 m/s or stronger] of 13 principal surface synoptic stations in West-Hungary,
— one or three hourly meso-synoptic charts analysing the development and

movement of frontal and convective systems over the region of West-Hungary.

The integration in space and time of radar and surface synoptic observations for the Cb-clouds and their significant weather phenomena was guaranteed by following the considerations of *Brüljov* and *Nizdojminoga* (1977).

The radar and surface observational data connected with Cb-clouds were considered uniform Cb-cloud or significant weather phenomenon in space if one of the principal surface synoptic stations has already observed within a radius of 30 km of maximum reflectivity factor (Z_{3max}) for Cb-echo measured by radar. In consequence of the limited observational area of the principal surface synoptic stations those Cb-clouds and Cb-echoes were considered as simultaneous observational data that were detected by radar within 30 minutes before or after the observation of suitable surface synoptic station(s). In this way, simultaneous data in space and time from the region of West-Hungary were at our disposal in 159 cases.

3.2 Results

It is known that the downdraught within a developed Cb-cloud starts from the height of about 0°C level. The outflowing cold air spreads out at the surface under the Cb-cloud and produces a gust front at its boundary with the ambient air, creating localized, strong, cold winds, squall-lines and large direction changes that are frequently associated with thunderstorms, showers or hailstorms. On that account, the maximum wind gusts connected with Cb-clouds can be expected either simultaneously with the first observation of heavy shower or thunderstorm, or else soon after. As a verification, the frequency distribution of intervals $[\Delta t = t_{V_{max}} - t_{shower;\, thunderstorm}]$ development time ($t_{V_{max}}$) of maximum wind gusts with shower or thunderstorm and the surface observational time $[t_{shower;\, thunderstorm}]$ the same significant phenomena were investigated (*Fig. 2*).

As it follows from Fig. 2, the overwhelming majority (84%) of maximum wind gusts with Cb-clouds developed simultaneously with the first surface observation of heavy shower or thunderstorm and afterwards. The synoptic background of the cases for intervals $\Delta t < 0$ and $\Delta t \geq 2$ hours was also studied. The maximum wind gusts observed with interval $\Delta t < 0$ (in 16% of the cases) were the results of the Cb-clouds with cold front (I) or instability line (H). It is in accordance with the fact that the gust front may propagate in the boundary layer for distance up to 80–100 km away from severe thunderstorm source (*Browning* and *Collier*, 1982). In case of interval $\Delta t \geq 2$ hours, the maximum wind gusts developed in pre- or postfrontal isobaric structures with strong surface pressure gradient (in 9% of the cases) were associated with the Cb-clouds of frontal (I) or convective systems (C or H). On the basis of discussion for Fig. 2, the maximum wind gusts developed either during the first

surface observation for heavy shower and thunderstorm or soon after within 2 hours in 75% of the cases. Consequently it is most likely that the wind-hazardous period of the weaker convective systems developed within the same air mass is equivalent to the interval of $0 \leq \Delta t < 2$ hours.

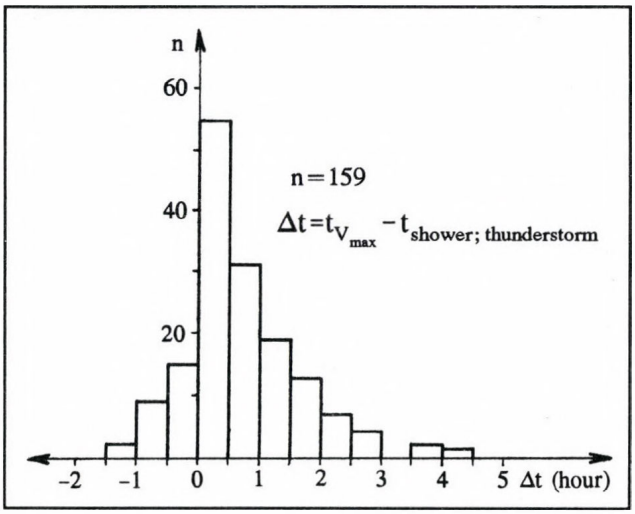

Fig. 2. Frequency distribution of intervals [$\Delta t = t_{V_{max}} - t_{shower;\ thunderstorm}$] between the development time ($t_{V_{max}}$) of maximum wind gusts associated with shower originating from Cb-cloud or thunderstorm and the surface observational time [$t_{shower;\ thunderstorm}$] for the same significant phenomena in case of frontal and convective systems in the region of West-Hungary (1986-1987).

Further investigations were needed to introduce the idea of potential and effective wind-hazardous periods:

— *Potential wind-hazardous period* (Δt_{pot}) is the term when the wind velocity is rapidly and permanently increasing or the gusts are exceeding the value of 7 m/s, associated with Cb-cloud or their significant weather phenomena. These wind gusts develop in the process of downdraught when the outflowing cold air spreads out at the surface under a Cb-cloud.

— *Effective wind-hazardous period* (Δt_{eff}) is the term when the wind velocity is rapidly increasing or the gusts are exceeding the value of 12 m/s, associated with Cb-clouds or their significant weather phenomena. These wind gusts can be expected at the surface whenever the radar detects Cb-echoes with the value of $Y = H_{max} \lg Z_3 \geq 10.9$ (*Bartha*, 1987).

Using these fundamental ideas we investigated the permanence of potential and effective wind-hazardous periods (Δt_{pot} and Δt_{eff}) during different synoptic situations connected with Cb-clouds. The results are shown in *Figs. 3, 4* and *5*. These figures illustrate the empirical probability distribution functions for the

potential and effective hazardous periods of maximum wind gusts associated with frontal (I) and convective systems (C, MCC, H). On the basis of Figs. 3 and 4 it can be seen that the distribution functions for potential and effective

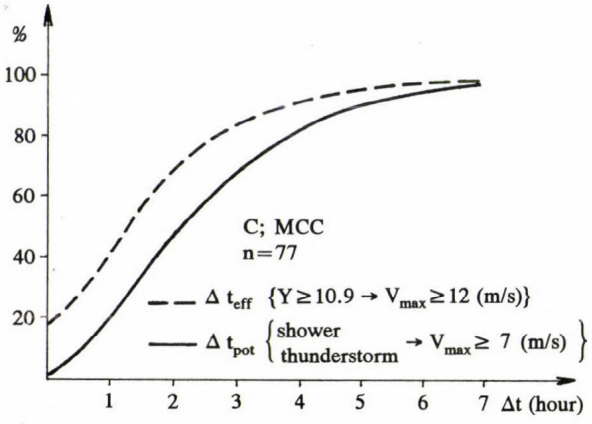

Fig. 3. Empirical probability distribution functions for the potential and effective hazardous periods (Δt_{pot} and Δt_{eff}) of maximum wind gusts (V_{max}) associated with non-frontal thunderstorms in convergence zone (C) or meso-scale convective complex (MCC) in the region of West-Hungary (1986-1987).

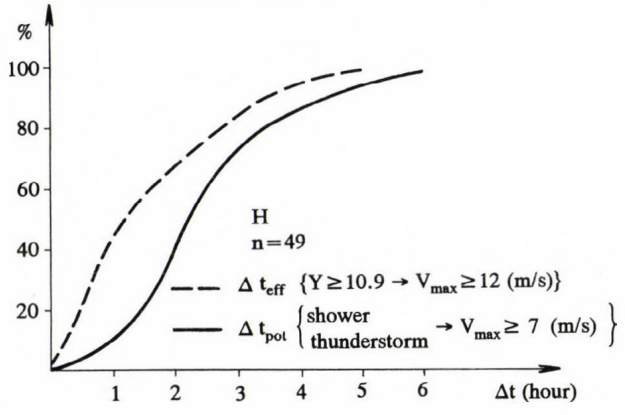

Fig. 4. Empirical probability distribution functions for the potential and effective hazardous periods (Δt_{pot} and Δt_{eff}) of maximum wind gusts (V_{max}) associated with instability lines (H) in the region of West-Hungary (1986-1987).

hazardous periods of maximum wind gusts connected with non-frontal (C, MCC, H) thunderstorms are similar to one another but at the same time they are not similar to the curves for the frontal (I) cases in Fig. 5. Within the convective systems, as it follows from the figures, the empirical probability is nearly zero (2%) when the maximum wind gusts associated with the intensive

radar echoes ($Y \geq 10.9$), belonging to instability lines (H) do not reach the value of 12 m/s. Furthermore, this probability value increases to 17% in case of weaker convective systems (C, MCC).

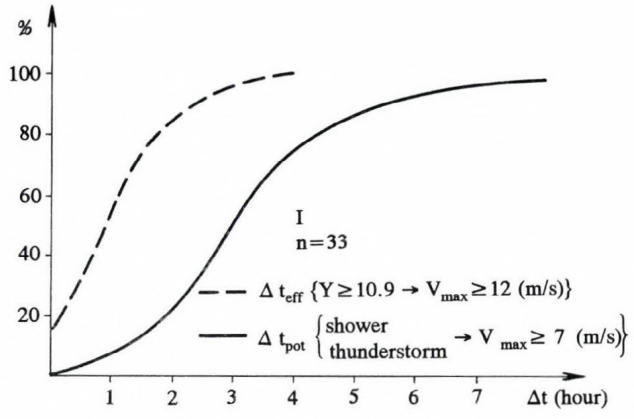

Fig. 5. Empirical probability distribution functions for the potential and effective hazardous periods (Δt_{pot} and Δt_{eff}) of maximum wind gusts (V_{max}) associated with the thunderstorms of cold fronts (I) in the region of West-Hungary (1986-1987).

The results are in accordance with the theoretical and practical results which differentiate between the instability lines and other convective systems from the point of view of wind-hazards (*Götz*, 1965; *Bodolainé Jakus* and *Vissy*, 1990). On the basis of discussions for Figs. 3, 4 and 5, the effective wind-hazardous periods concerning the weaker convective systems (C, MCC) and instability lines (H) proved to be shorter by 0.5–1 hour on the average as compared to the potential ones. Similarly, the same period proved to be shorter by about 2 hours in respect to cold fronts (I). The permanence of potential wind-hazard for the cold fronts (I) with thunderstorms can be increased by the strengthening surface pressure gradient following the fronts. The above-mentioned differences for wind hazards support those theoretical results and practical observations according to which the major part of the instability energy concentrates and gets free in the convective systems (C, MCC, H) developed into line(s) in front of cold fronts (*Horváth* and *Práger*,1985).

4. Conclusions

— Nowadays, additionally to the conventional synoptic data, weather radar and satellite data are also available for the storm forecasters to analyse the weather situation, especially on the meso- and local-scales and to issue warnings as well as to prepare very short range ($t \leq 2$ hours) forecasts. The

success of the so-called NOWCASTING warnings is largely dependent on the integration of non-conventional information into a complex meso-scale analysis (e.g. *Horváth* and *Práger*, 1990) included into the general synoptic framework.

— In case of weaker convective systems developed within the same air mass over West-Hungary, it is most likely that the maximum wind gusts occur either during the first surface observation for heavy shower or thunderstorm, or soon after within 2 hours.
— From the view-point of storm warning the subjective or objective recognition of instability/squall-line must be performed before identifying this weather object by radar, in accordance with the fact that the gust front may propagate in the boundary layer for distance up to 80-100 km away from the thunderstorm source.
— The permanence of wind-hazards associated with Cb-clouds can be increased by the strengthening surface pressure gradient during pre- and postfrontal weather situations.
— The empirical probability distribution functions (Figs. 3, 4 and 5) concerning the permanence of wind-hazard point out the rational periods for practical application. For this reason these results can be used for the further optimization of the nowcasting decision method.

In the near future, one of our tasks is to go on developing this decision method using digitized satellite data (*Horváth et al.*, 1992) as well as digital radar ones.

References

Ambrózy, P. and *Tänczer, T.*, 1963: Prediction of maximum wind velocities connected to thunderstorms (in Hungarian). *Beszámolók 1962*, Orsz. Meteorológiai Szolgálat, Budapest, 84-87.

Bartha, I., 1987: An objective decision procedure for prediction of maximum wind gusts associated with Cumulonimbus clouds. *Időjárás 91*, 330-346.

Bartha, I., Horváth, Á., Kapovits, A. and *Vissy, K.*, 1989: Development of the forecasting methods using radar information for strong and stormy wind associated with convective activity (in Hungarian). *Final Report* on research work, No. 1-3-86-319, sponsored by the Hungarian Academy of Sciences.

Bartha, I. and *Zsikla, Á.*, 1990: Use of radar echoes in storm warning at Lake Balaton (in Hungarian). *Időjárás 94*, 296-307.

Bodolainé Jakus, E. and *Götz, G.*, 1963: Structure and analysis of instability lines (in Hungarian). *OMI Kisebb Kiadványai*, No. 33, Budapest.

Bodolai, I., Bodolainé Jakus, E. and *Böjti, B.*, 1967: Macrosynoptical conditions for the formation of Slovenian squall-lines and some properties of cold fronts with thunderstorm. *Időjárás 71*, 129-143.

Bodolainé Jakus, E. and *Vissy, K.*, 1990: Meso-scale convective systems determined regionally in the Carpathian basin. *Időjárás 94*, 283-295.

Brancato, G.N., 1942: The meteorological behaviour and characteristic of thunderstorms. *U.S. Weather Bureau*, April.

Browning, K.A. and *Collier, C.G.*, 1982: *Nowcasting*. Academic Press, New York, London, 1-42.

Brüljov, G.B. and *Nizdojminoga, G.L.*, 1977: *Use of radar data in synoptic practice* (in Russian). Gidrometeoizdat, Leningrad.

Fawbush, E.J. and *Miller, R.C.*, 1954: A basis for forecasting peak wind gusts in non-frontal thunderstorms. *Bull. Amer. Metorol. Soc. 5*, 1 .

Götz, G., 1963: Prediction of maximum wind velocities connected to non-frontal thunderstorm (in Hungarian). *Beszámolók 1962*, 97-101.

Götz, G. and *Tänczer, T.*, 1965: Wind storms in the region of Lake Balaton in summer half periods (in Hungarian). *Időjárás 69*, 77-86.

Horváth, Á. and *Práger, T.*, 1985: Study of the dynamics and predictability of squall-lines (in Hungarian). *Időjárás 89*, 141-160.

Horváth, Á. and *Práger, T.*, 1990: A meso-β scale objective analysis for meteorological fields (in Hungarian). *Időjárás 94*, 23-38.

Horváth, Á., H.Zsikla, Á. and *Platz, M.*, 1992: Digitized satellite imagery for mesometeorological applications (in Hungarian). *Meteorological Notes of Universities* No. 6, I. 112-123.

IDŐJÁRÁS

Quarterly Journal of the Hungarian Meteorological Service
Vol. 97, No. 2, April–June 1993

Adapted Gaussian plume model characteristics and space-time structure of the estimated SO_2-concentration field due to elevated sources

N. Romanof and **S. Tumanov**

National Institute of Meteorology and Hydrology,
97 Bucureşti-Ploieşti Highway, 71581 Bucharest, Romania

(Manuscript received 8 September 1992; in final form 30 April 1993)

Abstract—The consequences on the air quality of a coal fired power station planned to be located near Turnu Severin, Romania, were assessed using Gaussian plume model estimations along with a significant number of time series of SO_2 hourly concentrations (01, 07, 13 and 19 h) estimated through the same model in the points of a grid around the power station. Beside the "classical" outputs of the model, some upper quantiles and other statistical characteristics of the concentration sets were estimated in each grid-point based on the lognormal and Eggenberger-Polya probability laws.

The time structure of the concentration field has been investigated using a Markov chain for two states: under and over the proper air pollution standard; this allows the calculation of the Besson persistence coefficients which can be useful when air pollution forecasting is attempted.

Correlation coefficients between paired grid-point concentration series were calculated, too, which resulted in areas of representativeness for the main grid-points, defined by equal correlation coefficient (say, 0.75) curves. This can be used in air quality monitoring network planning.

Key-words: Gaussian model, concentration field, Eggenberger-Polya distribution, lognormal distribution, time series model, Markov chain, time-space structure of the field, correlation coefficient, Besson persistence coefficient, area of representativeness.

1. Introduction

As compared to routine air quality studies for planned facilities, this paper was intended to provide more detailed information on the estimated time and spatial characteristics of the concentration field around a point source. The source was a coal fired power station (see the emission characteristics in *Sec-*

tion 3) near Turnu Severin, a medium size town in the south-western part of Romania, on the bank of the Danube. No on-site aerometric measurements were available nor any relief data of the (rather uneven) surroundings were used in the model application, so that the only features characterizing the air flow over the area could be incorporated in the routine meteorological data provided by the near station.

2. *The dispersion model*

The most largely accepted model which is used for the estimation of the air pollutant concentrations due to continuous emission point sources in steady meteorological conditions is the Gaussian plume model (*Hanna*, 1982).

The main problem that arises in applications of the Gaussian model is how to choose the appropriate formulae for the plume rise Δh and dispersion parameters σ_z and σ_y. This choosing must be based upon a preliminary analysis of the experimental data which has generated the relationships for the dispersion parameters and plume rise. For this latter the formulae used in this study were selected on the requirement for the ratio $\Delta h_{\text{observed}}/\Delta h_{\text{calculated}}$ to be as close as possible to the unity. According to *Trampf* (1973), the following expressions seem to be the most suitable and consequently have been selected $\Delta h=(1.5\ WD+9.5\times10^{-6}\ Q_H)/u$ (Holland, for neutral and unstable stratifications), and $\Delta h=(-1.04\ WD+0.6708\ Q_H^{1/2})/u$ (Moses-Carson, for stable stratification); the corresponding $\Delta h_{\text{obs}}/\Delta h_{\text{calc}}$ ratios were 1.00 and 1.05; here D is the stack diameter at the top level (m), W is the exit velocity of the effluent (m s^{-1}), and Q_H is the heat release (W).

There were two stacks in view at Turnu Severin (both are) of 280 m height; this is the reason for which a careful analysis of the dispersion parameters is needed, as these have resulted from various experiments (*IAEA*, 1980; *Briggs* and *Binkowski*, 1985). The relationships for tall stacks were selected and a set of dispersion parameters σ_z and σ_y was derived through statistical treatment as averages over several specific experiments. In the authors' view, such average parameters lead to more realistic estimations than if parameters from single experiments were used.

The dispersion parameters were assumed in the usual form

$$\sigma_z = a\,x^b \quad \text{and} \quad \sigma_y = c\,x^d$$

(x is the downwind source-receptor distance), the coefficients a, b, c and d, and the coefficients of determination r_z and r_y for the exponential curve fit are shown in *Table 1* for each Pasquill stability class. These values were used in the estimations presented in *Section 3*.

Table 1. Coefficients *a, b, c* and *d*, and the coefficients of determination r_z and r_y

Stability class	a	b	r_z	c	d	r_y
A	0.044	1.347	0.999	0.921	0.880	0.999
B	0.136	1.076	0.996	0.530	0.898	0.999
C	0.153	0.960	0.999	0.659	0.827	0.999
D	0.259	0.811	0.999	0.434	0.822	0.999
E	1.124	0.544	0.999	0.685	0.750	0.999
F	0.978	0.516	0.999	0.629	0.769	0.999

2.1 Estimating statistical parameters

Estimation functions for the statistical parameters used herein are presented below; the information content brought about by these is thought to be large enough for decision making.

The relationships for the estimation of the statistical parameters depend upon the way as the concentrations are available throughout the grid. In case when for each meteorological state m (in air pollution studies, m is generally defined by the wind direction D, wind velocity u, and stability class S; but in selected cases, air temperature, mixing height and others are being added) the corresponding concentration $C(x,y,m)$ is known in each grid-point together with the corresponding joint frequencies, then one-point statistical parameters can be estimated in the points (x,y), which characterize the statistical distribution of the concentrations without any space-time statistical correlation between points. In such cases the following estimation functions for the corresponding parameters can be estimated:

Arithmetic mean, $\bar{C}(x,y) = \sum_m C(x,y,m) f(m)$, where m runs the overall set of meteorological states, and $f(m)$ is the frequency of the state m. This frequency can be estimated from a series of meteorological observations (long enough), provided by the meteorological station accepted as representative for the region where the pollutants are dispersed.

Standard deviation, $s(x,y) = \{\sum_m [C(x,y,m) - \bar{C}(x,y)]^2 f(m)\}^{1/2}$.

Cumulative frequency for a given concentration threshold C_p to be exceeded, $G(C_p) = \sum_m f(m)$, *for* $C(m) > C_p$.

Direct use of the Gaussian plume model for the estimation of the expected frequencies for given thresholds C_p to be exceeded is objectionable because uncertainties can occur in the case of extreme weather situations with small frequencies (*Cats*, 1978; *Ludwick et al.*, 1980). This is the reason for which the Gaussian model should be used for its sure estimations, i.e. $\bar{C}$ and s, while for

the cumulative frequencies and quantiles one should resort to selected probability laws, previousely proved to fit frequency distributions of the concentrations. Having this in view, estimations of the expected cumulative frequencies and quantiles based on lognormal and Eggenberger-Polya probability laws are shown below. This latter is more suitable for single sources (*Tumanov*, 1979, 1990).

Statistical distributions used jointly to the Gaussian model.

Beside the main statistical characteristics provided by the Gaussian dispersion model (long term arithmetic mean, mean square deviation and empirical distribution function), some other statistical characteristics were estimated resorting to the two probability laws mentioned above, each of them applicable, as it is known, in specific conditions. The former is the lognormal distribution (*Larsen*, 1971), suitable for urban areas, where there are large numbers of pollution sources spread quite even all over the areas, so that in a given point the concentration does not depend practically on the wind direction. The latter is the Eggenberger-Polya discrete distribution (*Brooks* and *Carruthers*, 1953) which provides right estimations in the case of the concentration series due to single sources (*Tumanov*, 1979, 1990).

Lognormal distribution. The complementary distribution function for the random variable C (the pollutant concentration in a given grid-point), standing for the cumulative probability to equal or exceede a given value c of the concentration C is

$$G(c) = \mathrm{Prob}[C \geq c] = \frac{1}{(2\pi)^{1/2}} \int_c^{\infty} e^{-z^2/2} dz, \tag{1}$$

where $z = \ln(c/m_g)/\ln s_g$, m_g is the geometric mean, and s_g is the geometric deviation of the concentrations, namely (*Larsen*, 1971)

$$s_g = \left[\ln\left(\frac{s}{\overline{C}^2} + 1\right)\right]^{0.5}, \qquad m_g = \frac{\overline{C}}{\exp\left(0.5 \ln^2 s_g\right)}. \tag{2}$$

$\overline{C}$ is the arithmetic mean, and s^2 is the variance of the concentrations.

A C_p-quantile in the case of the lognormal distribution can be expressed as (*Larsen*, 1971)

$$C_p = m_g s_g^{z_p}, \tag{3}$$

where p is the order of the quantile, and the corresponding z_p (see Eq. 1) can be found by solving the equation $G(c)=1-p$.

Different p-order quantiles were calculated up to $p=0.999943$; this latter

corresponds to $p=1-1/17{,}520$, i.e. the cumulative probability of the maximum element out of 17,520 values covering a one year time period of 30-minute average concentrations: this probability has been chosen according to the way as the air quality standards are usually set. The same quantiles were calculated for the Eggenberger-Polya distribution (see below).

It is reminded that a p-order quantile C_p is that value of the distribution for which there is the probability p for the concentration to be less than C_p; that is in $p \cdot 100$ per cent of the time the concentration is expected to be less than C_p in a given point, or, further, C_p is that concentration which will be equalled or exceeded with a probability $1-p$, or in $(1-p)\cdot 100$ per cent of the time. If, for instance, $C_{0.999943} \geq C_{\text{max.permissible}}$ it follows that the air quality standard is violated.

Eggenberger-Polya distribution. The cumulative probability $F(c)$ is given by the expression

$$F(c) = \text{Prob}[C>c] = \sum_{k=0}^{c} p_k . \tag{4}$$

p_k are the Eggenberger-Polya discrete probabilities (*Brooks* and *Carruthers*, 1953):

$$p_0 = \frac{1}{(1+d)^{\bar{C}/d}}$$

$$p_k = \frac{\bar{C}(\bar{C}+d)(\bar{C}+2d)\ \ldots\ (\bar{C}+[k-1]d)}{k!\,(1+d)^{\bar{C}/d+k}} \tag{5}$$

$$k = 1, 2, \ldots$$

where $d = s^2/\bar{C} - 1$.

The complementary distribution function is $G(c)=\text{Prob}[C\geq c]=1-F(c-1)$. Since the Eggenberger-Polya distribution is a discrete one, C is an integer quantity, and it is required for the threshold c to be an integer, too, preferably expressed in $\mu g\ m^{-3}$.

The C_p-quantiles of the distribution are calculated by linear interpolation, in c and p coordinates, between two successive values of the random variable: the first is the greatest integer for which $F(c)\leq p$, and the second is the previous value plus one.

Estimations for the time series case. In case the concentrations in a grid-point are available as time series (one concentration for each observation time), the following relationships are used to calculate the average and variance:

$$\bar{C} = \frac{1}{n}\sum_{i=1}^{n} C_i , \qquad s = \left[\frac{1}{n}\sum_{i=1}^{n}(C_i - \bar{C})^2\right]^{1/2} . \tag{6}$$

One can estimate the empirical distribution function simply by counting the concentrations less than a given threshold and running this latter within the range of the variable.

Time series available in each grid-point can be used to investigate the statistical space and time structure of the concentration field.

2.2. *Time structure investigation based upon a Markov chain model*

A Markov chain model with two states was used: $C \leq 0.75$ mg m^{-3} (the air quality standard for the 30-min SO_2-concentration)–state 1, and $C > 0.75$ mg m^{-3}–state 2. Sequences of random numbers of the form

121122112221211211...

were derived each grid-point. The Markov chain model applied to such sequence allows to find out the type of the statistical (Markov) dependence, i.e. the order of the chain, as well as to estimate the persistence of a given state (for instance, one can estimate the probability to have n times successively the state 2). Such an analysis was first made for SO_2 daily mean concentrations measured at Copşa Mică (*Romanof*, 1982).

We now define a set of statistical quantities and estimation functions for the Markov chains.

Let $p(i)$, $p(i,j)$, $p(i,j,k)$, etc. be the probabilities having the state i, the sequence ij, the sequence ijk, etc. respectively; the indicies ijk assume values 1 and 2. For example, $p(2,2)$ is the probability for the concentration to exceed two times successively the air quality standard.

The statistical dependence is expressed through the so called conditional probabilities: p_{ij} is the probability for the state j provided that at the previous observation time the state i occurred; p_{ijk} is the probability for the state k provided that at the previous observation times the states i and j occurred. If there are four observations a day, p_{22}, for instance, is the probability to exceed the air quality standard at the time h provided that the standard was exceeded at the time h-6.

Denote by $n(i)$, $n(i,j)$, $n(i,j,k)$, etc. the numbers of cases when the states i, ij, ijk, etc. occurred. The probabilities for sequences of states to occur are given by

$$p(i) = \frac{n(i)}{n},$$

$$p(i,j) = \frac{n(i,j)}{n}, \qquad (7)$$

.....

and the conditional probabilities are given by

$$p_{ij} = \frac{n(i,j)}{n(i)},$$

$$p_{ijk} = \frac{n(i,j,k)}{n(i,j)}, \qquad (8)$$

.....

where n is the total number of observations.

The sequence is said to be sequence of independent variables if $p_{...ijk}=p_k$; first order Markov chain if $p_{...ijk}=p_{jk}$; second order Markov chain if $p_{...ijk}=p_{ijk}$, etc. The order of the Markov chain indicates the number of previous states which influences the state at a given moment. Chi-square test can be used as a method to assess the order of a Markov chain (*Mihoc* and *Craiu*, 1972), and this was used herein at a 5% significance level.

The Besson coefficient can be used as a measure of the persistence (*Brooks* and *Carruthers*, 1953):

$$r_B^i = 1 - \left(\frac{1 - p_{ii}}{1 - p_i}\right)^2. \qquad (9)$$

If there is persistence, p_{ii} is greater than p_i. $r_B^i=0$ indicates the absence of the persistence, while $r_B^i=1$ indicates maximum persistence; in certain cases, if p_{ii} is less than p_i, the Besson coefficient can also take negative values, which indicates a tendency for occurrances and non-occurrances to oscillate.

2.3. Spatial structure of the concentration field

The spatial structure was investigated using the coefficient of linear correlation between concentrations estimated in pairs of grid-points:

$$R(x_1,y_1;x_2,y_2) = \frac{\overline{\left[C(x_1,y_1) - \bar{C}_1\right]^2 \left[C(x_2,y_2) - \bar{C}_2\right]^2}}{s_1 s_2}, \qquad (10)$$

where (x_1,y_1) and (x_2,y_2) are the coordinates of the points; $\bar{C}_1$ and $\bar{C}_2$ are the mean concentrations; s_1 and s_2 are the variances. This coefficient is a measure of the degree of statistical dependence between two points, and offers useful information to select measuring points in air pollution monitoring network planning. A line of equal correlation coefficient (e.g. 0.75) around a given

point, say a maximum of a spatial concentration distribution, delimits what could be said to be the area of representativeness of the given point. Dividing a zone of interest into areas of equal correlation is a way to choose measuring points of a monitoring network.

The statistical parameters presented in this section have been estimated and discussed on the base of spatial distribution in *Section 3.*

3. *Results and comments concerning the estimated SO_2-concentration field*

Some input and auxiliary data together with a set of specifications thought to be needed in the discussion are summarized in the beginning of this section.

3.1. Data

Emission data. There were two stacks of 280 m height designed for the power plant; diameter at the top: 8.1 m; exit temperature: 146°C. The emission regime does not depend on the ambient air temperature t_a (emission rate Q=6,193 g s^{-1} SO_2; exit velocity W: 11.53 m s^{-1}), except one of the stacks, for which Q=9,275 g s^{-1}, and W=17.9 m s^{-1} when $t_a \leq 8$°C. It should be mentioned that a set of initially designed emission data are used here, which latter changed but, of course, this fact does not make the procedure proposed less applicable.

The Gaussian model. It was applied in two versions for estimating the statistical parameters of the concentration field: time series version, and frequency based version.

In the time series version, short term (1/2 h) concentrations were generated using 10-year meteorological observations (1971–1980), every 6 hours, provided by the Turnu Severin station: wind velocity and direction, atmospheric stability class, air pressure and temperature. Using these as primary data, 24 h average concentration series were calculated, which allowed Markov type statistical dependence to be studied. As in the primary data the wind direction was reported in sixteen 22.5°-wind sectors, a random direction within each sector was generated based upon the acceptance that all directions are equally probable. In calm conditions, a direction comprised between 0° and 360° was randomly generated, asigning a wind velocity of 1 m s^{-1} to each direction. The Uhlig scheme (*Uhlig*, 1965) was applied to determine the atmospheric stability class.

For the wind velocity vertical profile, a power type law was used for rural areas (*Hanna*, 1982):

$$u(z) = u(10)(z/10)^p \qquad \text{for } z \leq 200 \text{ m};$$
$$u(z) = u(200) \qquad \text{for } z > 200 \text{ m}.$$

$u(10)$ is the wind velocity at 10 m height, and p is an exponent which takes the following values depending upon Pasquill stability classes: 0.07 (A and B), 0.10 (C), 0.15 (D), 0.35 (E), and 0.55 (F/G).

In the frequency based version of the Gaussian model, joint frequencies of the wind direction (2°-wind sectors), wind velocity class (1 m s^{-1} step), and Uhlig stability class (7 classes) were estimated taking into account the slight dependence of some emission characteristics to the ambient air temperature. To preclude underestimations due to calm situations missing from the computations, which is required by the model, the calm case frequencies in the seven stability classes have been asigned to the wind directions proportionally to the first velocity class frequency in each velocity-direction joint frequency matrix.

Computation grid. The grid size was 20 km in the E–W direction by 30 km in the N–S direction; the grid points were 1 km-spaced in the frequency based Gaussian model version (600 grid-points in all); in the time series version, spacing was 1 km in the portions with strong gradients of the estimated fields, and 3 km in the portions away from these (350 grid-points in all).

Computation time. This was 2 min. per grid-point for the frequency based model, and 15 min. per grid-point for the time series based model (FELIX C 512 computer).

3.2. Results: presentation and discussion

Spatial distributions of the statistical parameters estimated using the described procedures are shown in *Figs. 1* to *9* as isolines.

SO_2 annual mean concentrations estimated from ground level wind data can be seen in *Fig.* 1. Three spatial maxima are to be noticed; situated to the NW and SW directions from the source point (marked by dark circle located near Halînga) with concentrations reaching 60 $\mu g\ m^{-3}$, as well as to the E with a maximum of 100 $\mu g\ m^{-3}$ (the 30-min air quality standard for SO_2) are shown in *Fig. 2.*

The frequencies to exceed the 750 $\mu g\ m^{-3}$ threshold, calculated from the Eggenberger-Polya distribution using the estimated long term annual averages and standard deviations (*Tumanov*, 1990) are shown in *Fig. 3.* Although it is known that the lognormal distribution is not suitable for the case of single sources, frequencies were calculated with this distribution, too, as illustrated in *Fig. 4.*

The 0.999943-quantile estimated from the Eggenberger-Polya law (the values on the lines are expected to occur once a year) can be found in *Fig. 5.*

The conditional probability to exceed 750 $\mu g\ m^{-3}$ threshold at the time h if an exceedance occurred at the time h-6 (observations every 6 hours) is presented in *Fig. 6.* The range is seen to be 1 to 10 per cent, indicating a weak statistical time connection in the series. The same effect is shown by the Besson persistence coefficient in *Fig. 7.* Markov chain order can be seen in *Fig. 8,* in

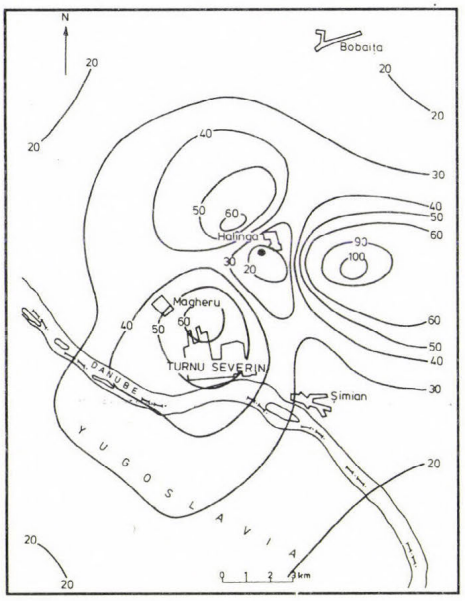

Fig. 1. Annual mean concentration, $\mu g\ m^{-3}$

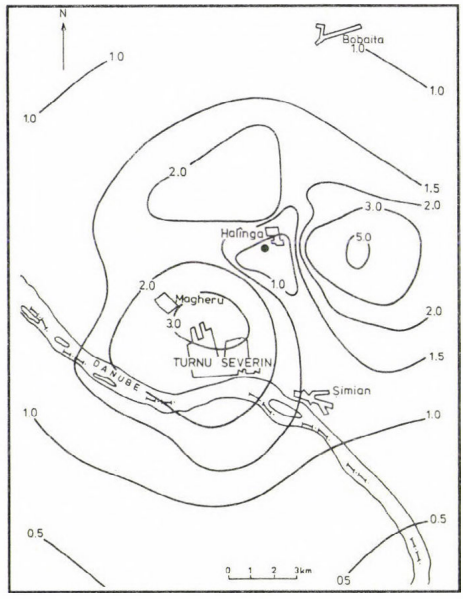

Fig. 2. Frequency to equal or exceed the 750 $\mu g\ m^{-3}$ threshold of the 0.5-h mean concentration, calculated through the Gaussian model.

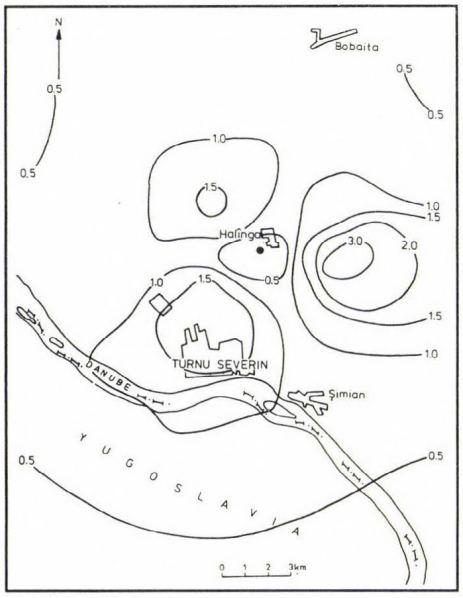

Fig. 3. Frequency to equal or exceed the 750 $\mu g\ m^{-3}$ threshold of the 0.5-h mean concentration, calculated with the Eggenberger-Polya distribution.

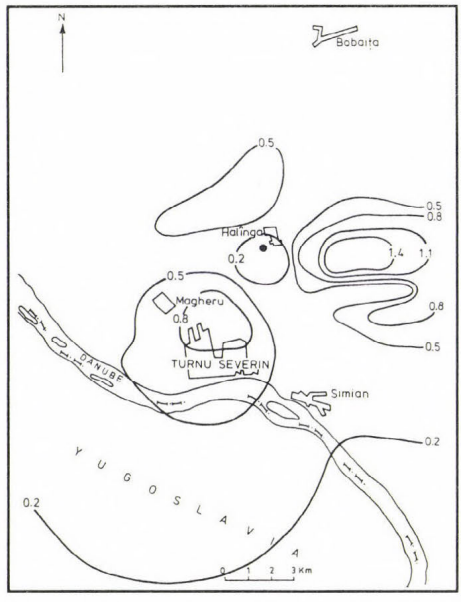

Fig. 4. Frequency to equal or exceed the 750 $\mu g\ m^{-3}$ threshold of the 0.5-h mean concentration, calculated with the lognormal distribution.

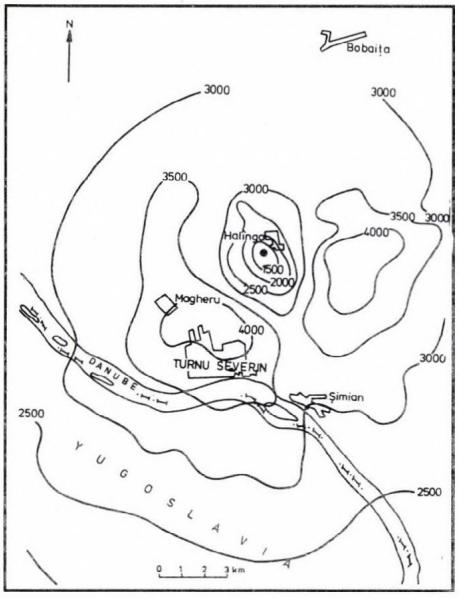

Fig. 5. 0.999943-quantile ($\mu g\ m^{-3}$) calculated from the Eggenberg-Polya distribution.

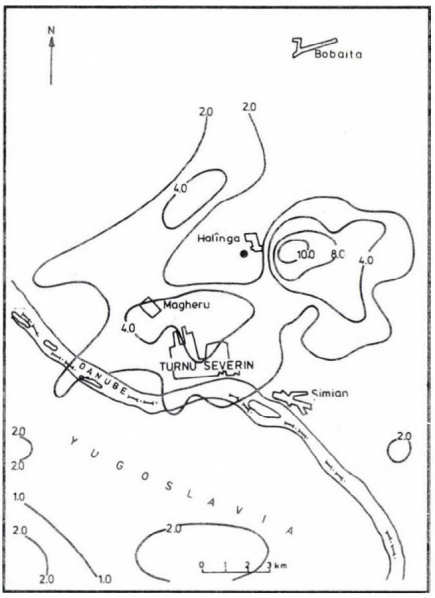

Fig. 6. Conditional probability p_{22}, per cent.

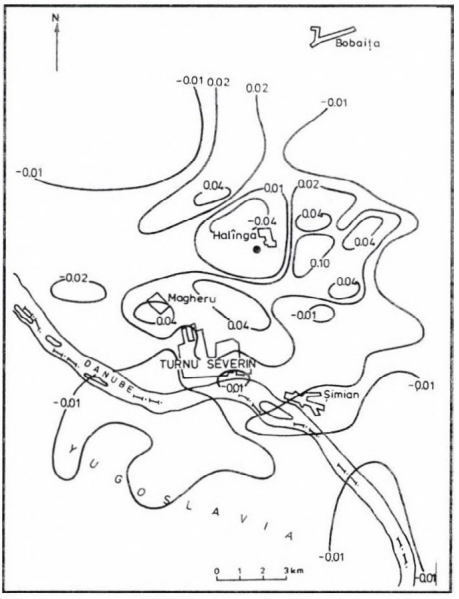

Fig. 7. Besson persitence coefficient r_B^2.

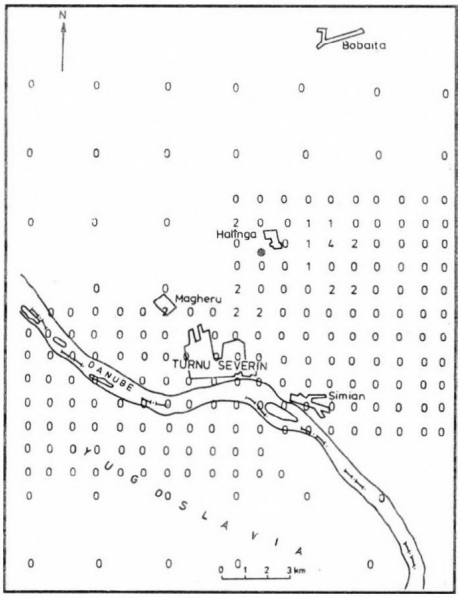

Fig. 8. Markov chain order.

which 0 means that the 6-h spaced concentrations are independent, whereas 1 indicates first order Markov chain, etc. Sparcely, statistical dependence as first to fourth order Markov chains occur in the centres of the maximum mean concentration areas. One could conclude that stochastic methods would hardly be successful in similar cases.

Curves of equal correlation coefficient (0.75) between maximum (M) and neighbouring points are presented in *Fig. 9.* Areas enclosed by such isolines, said areas of representativeness (see *Section 2.3*), could be used to place monitoring points inside them and thereby be sure that in a given grid the number of points would be reduced inside the areas of representativeness. But on the other hand, the areas of representativeness in this case are rather small, and a quite dense monitoring network is required to get reliable data.

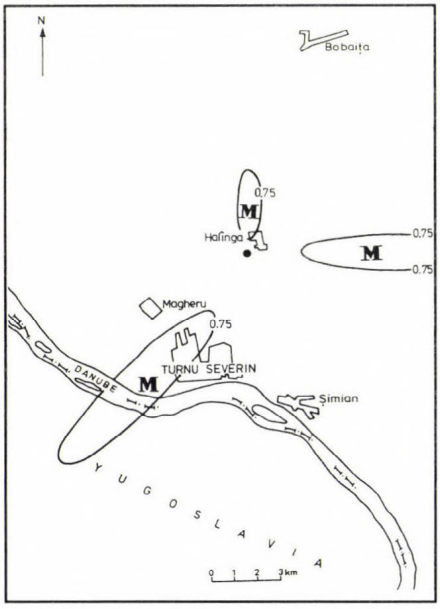

Fig. 9. Areas of representativeness (M) for three monitoring points corresponding to the 0.75 correlation coefficient.

Acknowledgements—The authors would like to thank *Mr. Ion Sandu* for running the computation programme of the Gaussian model. We are particularly grateful to our former colleague *István Elekes* for his valuable programming work aimed at estimating such a great deal of new and "unusual" statistical characteristics of the air pollutant concentration fields.

References

Briggs, G.A. and *Binkowski, F.S.*, 1985: *Research on Diffusion in Atmospheric Boundary Layers: A Position Paper on Status and Needs*. EPA Publication No. 600/3-85/072.

Brooks, C.E.P. and *Carruthers, N.*,1953: *Handbook of Statistical Methods in Meteorology*. Her Majesty's Stationary Office, London, 315-318.

Cats, G.J., 1978: A simple method for quick estimates of frequency distributions of air pollution concentrations from long-term average concentrations. *Proc. WMO Symp. on Boundary Layer Phys. Applied to Specific Problems of Air Pollution*, 19-23 June, Norrköping, WMO No. 510, 157-162.

Hanna, S.R., 1982: Review of atmospheric diffusion models for regulatory applications. *WMO Technical Note* No. 177.

IAEA, 1980: *Atmospheric Dispersion in Nuclear Power Plant Siting*. A Safety Guide, Vienna.

Larsen, R.I., 1971: *A Mathematical Model for Relating Air Quality Measurements to Air Quality Standards*. Env. Prot. Agency, Triangle Park, N. Carolina, Publication No. AP-89.

Ludwick, J.D., Weber, D.B., Olsen, K.B. and *Garcia, S.R.*, 1980: Air quality measurements in the coal fired power plant environment of Colstrip, Montana. *Atmos. Environ. 14*, 523-532.

Mihoc, G. and *Craiu, M.*, 1972: *Statistical Inference for Dependent Variables*. Ed.: Academiei Române (in Romanian).

Romanof, N., 1982: A Markov chain model for the mean daily SO_2 concentrations. *Atmos. Environ. 16*, 1895-1897.

Trampf, W., 1973: *Formeln zur Berechnung der Schornsteinüberhöhung. Speziell für grossemittenten und für kalte Quellen*. Institut für theoretische Meteorologie der Freien Universität Berlin.

Tumanov, S., 1979: Frequency distributions of gas pollutant concentrations measured in the neighbourhood of a high single source. *Meteorology and Hydrology 2*, 11-16.

Tumanov, S., 1990: Statistics of concentrations due to single air pollution sources to be applied in numerical modelling of pollutant dispersion. *Atmos. Environ. 24A*, 1029-1035.

Uhlig, S., 1965: *Bestimmung der Stabilitätsgrade der Luft an Hand von Wettermeldungen*. Mitt. des Deutsches Wetterdienst, Offenbach.

IDŐJÁRÁS

Quarterly Journal of the Hungarian Meteorological Service
Vol. 97, No. 2, April–June 1993

The effects of winter temperature on the migration of insects

A. Stollár*, Z. Dunkel[1], F. Kozár and Diaa A.F. Sheble****

** Hungarian Meteorological Service,*
P.O. Box 38, H-1525 Budapest, Hungary
*** Plant Protection Institute, Hungarian Academy of Sciences,*
Hermann Ottó út 15, H-1022 Budapest, Hungary

(Manuscript received 5 June 1992; in final form 17 May 1993)

Abstract—On the basis of climatological studies it is generally accepted that the increase of the amount of greenhouse gases in the atmosphere can lead to a global warming. However, the degree and impact of warming are not entirely clear. In this paper we study the possible effects of changing climatic conditions on the migration of insect pests. The results of our studies show that during the period of 1881–1990 when the winter temperature increased significantly in Hungary a northward migration of some termophilous pest insects was observed. The decreasing number of short cold periods during the milder winters in the last decades could not stop this northward movement of the insects.

Key-words: migration of insects, winter temperature, changing climatic conditions, regional warming.

1. Introduction

Different living organisms like insect pests require special climatic conditions which are essential for their survival, spreading and migration. Generally, the expansion of the living-environment is possible in two ways. First, during the evolution such species develop which are resistant to a given climate. On the other hand, living-species can migrate to other regions where climate is favourable for their existence. If new species appear in a certain region, both possibilities should be studied to clarify more exactly whether the climatic or the biological factors are more significant for this phenomenon.

As a matter of fact, some new insect pests have appeared in Hungary during this century. Our study focuses on the variation of the winter temperature

[1] Corresponding author address: Z. Dunkel, Institute for Atmospheric Physics, P.O. Box 39, H-1675 Budapest, Hungary.

during the last 110 years which has had considerable impact on the above mentioned process. Due to human activity, the concentration of CO_2 and some other greenhouse gases has increased significantly during the last decades (*Mészáros* and *Götz*, 1988; *Götz*, 1988, 1990; *Mika*, 1987, 1988; *Faragó et al.* 1991). The increasing amount of these gases can lead to global warming, which will affect the climate of Hungary, too. According to studies the warming may reach 1.5–4.0°C by the middle of the next century, however, the exact rate and its regional climatic effects are uncertain. Subsequently, the biological and other consequences of the anticipated climate change can not be clearly determined.

The problems related to new insect pests in Hungary were analysed earlier by *Kozár* and *Dávid* (1986), *Kozár* and *Stollár* (1990) and *Kozár* (1991a, 1991b). The varying climatic conditions have significant implications for other groups of living organisms, as well. *Németh* (1990) and *Solymosi* (1992) have analysed the effect of the climate-variations during this century on some Mediterranean weed species appearing around Eger. In this paper the relationship between the variability of the winter temperature and the spatial distribution of new pests in Hungary is analysed. More concretely, the migration and regional distribution of the *Mediterranean Pseudaulacaspis Pentagona* is studied. This species first appeared around Pécs in 1923 then slowly spread northward, and in 1929 it was already found all over the county Baranya and in some parts of Somogy and Zala (*Fig. 1*). After this initial phase the migration stopped for a long period. In 1976 this pest was found in the southern part of the Hungarian Great Plain moreover in the surroundings of Budapest, too. The migration continued and this species was already found in several places of the county Pest in 1983 and, shortly after in other parts of the country. Similar expansion has been observed for other insects. For example, the *Corytuca ciliata* has spread all over the country in only 15 years (*Fig. 2*). The aim of this study is to find an explanation for the rapid northward movement of different insects.

2. Data and methods

In this study, we used the long-term representative temperature observations from nine stations of the Hungarian Meteorological Service. These continuous observations and the derived data series started in 1881. Thus, we can make our analyses of data on the basis of 110 years of meteorological observations. The location and spatial distribution of these stations are suitable for the determination of the regional differences in the climatic characteristics of our country.

The winter temperature is a determinative factor in the life cycles of the insects, because their resistance is very low in the cold periods with critical temperature minima. Therefore the insects hardly survive the intensive cooling

of the winter. For this reason, the winter (December-January-February) mean temperature was selected as the principal meteorological factor.

In the first phase of our work, we analysed the winter temperatures. We calculated annually the mean temperature of winters from 1881 to 1990 years. After this we calculated the average temperature for the decades 1881–1890, 1891–1900, ..., 1981–1990 for each station, then we represented the draft country-wide regional distribution of this parameter in Hungary. The temperature data were also graphically represented and analysed for the existence of long-term tendencies by linear trend analyses. The spatial distribution and temporal migration of the insects were taken from the surveys made by the Plant Protection Institute, Budapest.

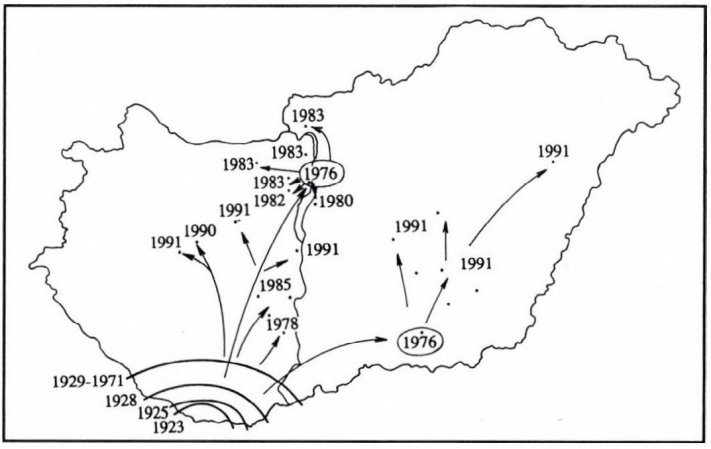

Fig. 1. Migration of *Pseudaulacaspis pentagona* in Hungary.

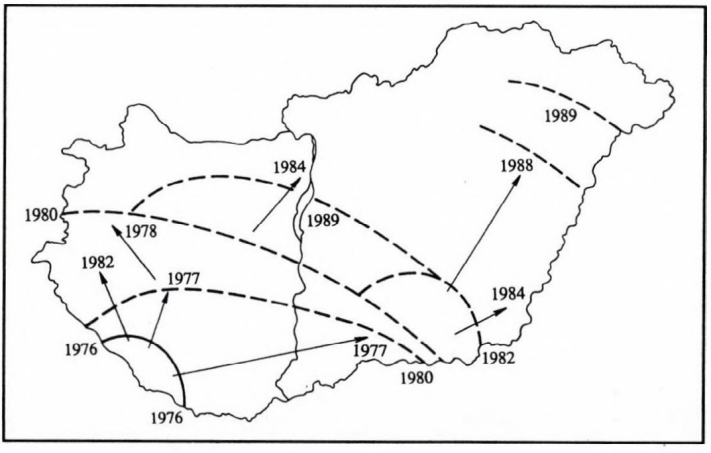

Fig. 2. Migration of *Corytuca ciliata* in Hungary.

3. Results

As it is well known, one of the most important limiting factors in the insect migration is the occasionally low or critical winter temperature. Cold winters decrease the density of the insects because of the high mortality, and in this case the migration will be very slow, or it will stop. After extreme winter situations some insect species can totally disappear from certain regions. On the contrary, the mild winters can result in a rapid increase in the local density of the insects and subsequently an intense migration and extensive distribution of the insects can start to other and new regions.

Analysing the winter temperature for the last 110 years for different parts of the country, considerable fluctuations were revealed everywhere. The maximum amplitude range reaches 8–9°C. The interannual fluctuations are also large in time scale. Very cold winters appeared after mild winters in the last decades. Now there is a question: how did our climate change during last century and there is another question: are 110 years enough to verify it? The trend analysis of winter temperature data shows a slow increase in this parameter for most stations. Analysing the data from 9 stations, we found that this increase of warming tendency was the highest for Budapest (0.016°C per year that can be partly mainly explained by the increasing heat-island effect of the capital. The increase was true also for the coldest eastern regions for instance, around Nyiregyháza the increase was also very high (0.014°C per year). In the southern regions, the estimated increase was not statistically significant much lower, for example in Pécs only 0.005°C per year. The mean trend calculated from the data of the 9 stations, shows an average increase

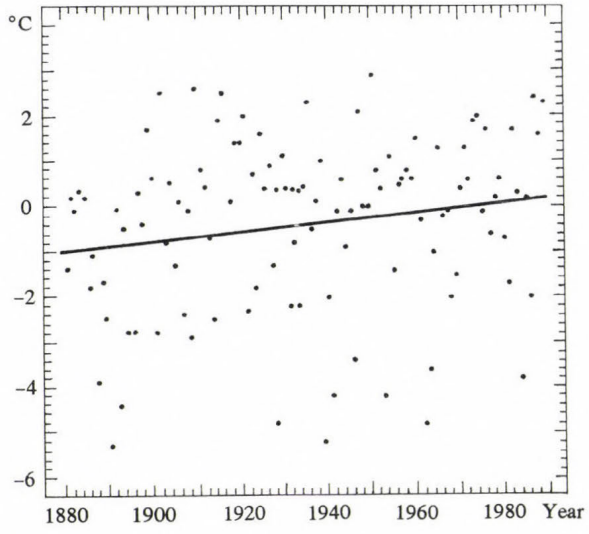

Fig. 3. The averages and trend of winter temperature in Hungary from 1881.

0.011°C per year (*Fig. 3*), and the correlation coefficient of the linear regression is significant at $P=5\%$ level.

In this study we calculated the averages of winter temperature for every decade (*Table 1*). It is also obvious from the above analysis that after the very cold decades at the end of the last century, a slow warming appeared which was followed by a smaller variation of temperature for a long period. The decade of 1961–1970 was again cold, which was followed by warmer periods during the last two decades. The average winter temperature in Hungary, based on the data of nine stations for 110 years was –0.40°C. The regional distribution of winter averages for ten years is shown in *Fig. 4*. The darker places were colder and the lighter were warmer places and periods. The various hatching of the maps shows the fluctuation of winter average temperatures. In Hungary, the decade 1901–1910 was the first one when the winter average above 0°C appeared over the territories of the country and in the next decade this average value continued to increase. It is possible that several termophilous insect species appeared in this period in Hungary, such as the *Pseudaulacaspis Pentagona* also and they could spread to some other regions under warm conditions. The mild winters in area of Pécs and Budapest with an average above 0°C lasted for a long time, could stimulate the survival of the above-mentioned insect species after their first appearance (in 1923). For several decades, these species have occurred only in the southern counties, but after the cold decade of 1961–1970, those appeared in other regions, e.g., in the southern part of the Great Plain and in Budapest where it was found that they appeared in 1976. After 1980 this species continued its spreading into the counties Pest, Komárom, Nógrád and this process continues nowadays. If the mild winters will recur in the future, this species or these species can occupy additional regions of the country.

Table 1. Winter temperature averages (°C) for ten years in different parts of Hungary

Stations	1881-1890	1891-1900	1901-1910	1911-1920	1921-1930	1931-1940	1941-1950	1951-1960	1961-1970	1971-1980	1981-1990	Mean 1881-1991
Pécs	-0.77	-0.27	0.64	1.37	0.36	0.65	0.06	0.71	-0.90	1.06	0.51	0.29
Budapest	-0.69	-0.45	0.68	1.43	0.34	0.01	0.48	0.85	-0.05	2.06	1.26	0.53
Keszthely	-1.21	-0.60	0.44	0.94	-0.20	-0.44	0.15	0.49	-0.18	0.89	0.39	0.05
Szombathely	-1.77	-1.21	-0.22	0.22	-1.02	-1.55	-0.58	-0.60	-1.73	0.60	-0.21	-0.74
Mosonmagyaróvár	-1.53	-1.08	0.09	0.51	-0.64	-0.93	-0.53	-0.17	-1.28	0.83	0.05	-0.45
Kalocsa	-1.40	-0.90	0.07	0.94	-0.28	-0.67	-0.03	0.62	-0.95	0.76	0.33	-0.14
Szeged	-1.73	-1.27	-0.15	0.65	-0.26	-0.99	-0.22	0.14	-1.23	0.71	0.07	-0.40
Debrecen	-2.14	-1.91	-0.78	-0.02	-1.07	-1.69	-1.12	-0.48	-1.83	-0.13	-0.75	-1.10
Nyíregyháza	-2.69	-2.40	-1.67	-0.85	-1.69	-2.11	-1.01	-1.04	-2.30	-0.45	-1.13	-1.63
Country mean	-1.52	-1.21	-0.10	0.58	-0.50	-0.86	-0.41	0.06	-1.16	0.70	0.06	-0.40

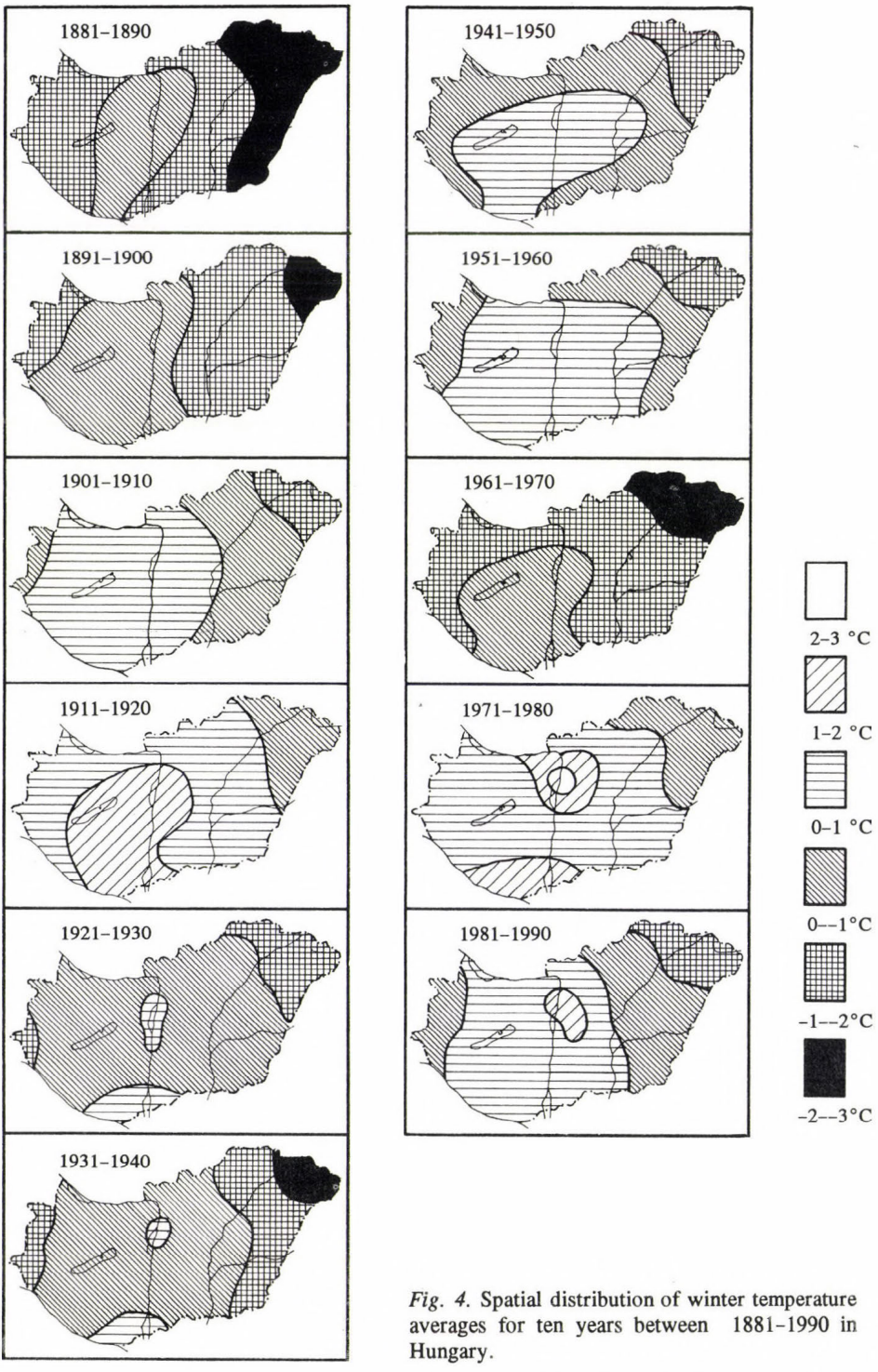

Fig. 4. Spatial distribution of winter temperature averages for ten years between 1881–1990 in Hungary.

4. Conclusions

Analysing the averages of winter in Hungary from the beginning of the systematic meteorological observations (1881), we found a great fluctuation in the annual data. Using the temperature averages of decades instead of the annual average, we can see cold decades in 1931–1940 and 1961–1970 followed the previous warmer periods. The linear trends of the winter averages for different stations show a slow increase. The country-wide average of winter temperature indicates a significant increase of 0.01 °C per year and it means an 1 °C increase per 100 years. The changing temperature will affect animal and plant communities. New species appear, which could alter the species composition. The new pest and weed species can cause serious problems in agriculture.

The higher averages of the winter temperature in the southern and middle parts of Hungary and surroundings of Budapest compared with the migration process of insects in time show good correlation. In the future the study of the appearance, migration and distribution of termophilous insect and weed species require more attention. The winter mortality data would help to clarify the impact of an expected global warming on the life of insects.

References

Faragó, T., Iványi, Zs. and *Szalai, S.*, 1991: *Climate variability and change II.* OMSZ, Budapest, 1-218.

Götz, G., 1988: Climatic variations and predictability (in Hungarian). *Időjárás 92*, 140-152.

Götz, G., 1990: Century of the effect of greenhouse gases (in Hungarian). *Tudomány 6*, No. 9, 16-22.

Kozár, F., 1991a: Global warming and the living nature in Hungary (in Hungarian). *Természet Világa 122*, 515-517.

Kozár, F., 1991b: Recent changes in the distribution of insects and the global warming. *Proceedings of European Congress of Etymology*. Budapest, 1-10 (in print).

Kozár, F. and *Dávid, A.*, 1986: The unexpected northward migration of some species of insects in Central Europe and climatic changes. *Anz. Schadlinskunde, Pflanzenschutz und Umweltschutz 59*, 90-94.

Kozár, F. and *Stollár, A.*, 1990: Do the insects predict climate change (in Hungarian)? *Élet és Tudomány 30*, 939-940.

Mészáros, E. and *Götz, G.*, 1988: The future of our climate (in Hungarian). *Magyar Tudomány 95*, 562-570.

Mika, J., 1987: Application of the annual cycle of meteorological elements to estimate the regional properties of global climate change (in Hungarian). *Időjárás 91*, 34-42.

Mika, J., 1988: Regional features of a global warming in the Carpathian Basin (in Hungarian). *Időjárás 92*, 178-180.

Németh, I., 1990: Appearence of Mediterranean weed species in the region of Eger (in Hungarian) (ed.: I. Seprős). Növény-

védelmi Tudományos Napok 1990. Összefoglalók. Budapest, 127.

Solymosi, P., 1992: Indigeneous and adventive vegetation in Hungary (in Hungarian). *Növényvédelem 28*, 1-15.

IDŐJÁRÁS

Quarterly Journal of the Hungarian Meteorological Service
Vol. 97, No. 2, April–June 1993

The flying activity of turnip moth (Scotia segetum Schiff.) in different Hess-Brezowsky's macrosynoptic situations

L. Nowinszky*, Cs. Károssy* and Gy. Tóth**

* *Teacher's Training College "Berzsenyi Dániel", P.O. Box 170, H-9701 Szombathely, Hungary*
** *Gothard Astrophysical Observatory of Roland Eötvös University, H-9707 Szombathely, Hungary*

(Manuscript received 15 October 1992; in final form 8 June 1993)

Abstract—The collection of insects by light-trap is a wide-spread sampling method of plant-protection, but its efficency is influenced by many environmental factors especially the weather. Knowing these influencing parameters, one can elaborate more reliable prognoses.

The authors pointed out in their earlier paper that the macrosynoptic weather types of *Péczely* are very useful for investigation of insect ecology in territory of Carpathian-Basin.

The present paper deals with macrosynoptic situations of *Hess-Brezowsky* extended for the whole Europe in connection with the flying activity of a harmful insect, the turnip moth (Scotia segetum Schiff.) being represented by the number of collected individuals.

The authors have established that from the various 29 types of macrosynoptic weather situations, if they are continuous, which are favourable or unfavourable from the point of view of collecting the moths, moreover how the species investigated react to the change of the weather situations.

Key-words: Hess-Brezowsky's macrosynoptic situations, turnip moth, light trap.

1. Introduction

The principal condition of effective and economical plant-protection taking care of the environment is the reliable prognosis of harmful insects. In order to elaborate a suitable prognosis it is necessary to make simultaneous observations of the time of appearence and the number of individuals, using adequate methods and sampling devices. The light-trap is a wide-spread tool for catch of insects flying at night which kills the insects flown to the artifical light source.

There has been a uniform light-trap network of *Jermy* type in Hungary for

about thirty years which has collected a great amount of valuable data for scientific research. The data representing the activity of insects are influenced by several factors, including the weather. It is easy, therefore, to understand that many entomologists deal with the investigations of the effect of meteorological parameters all over the world. Unfortunately, most of the Hungarian light-trap stations did not observe the meteorological elements. These stations were in general situated remote from meteorological observing stations. We published the effectiveness of catching the most harmful insects by light-traps in earlier papers (*Károssy* and *Nowinszky*, 1987a; *Nowinszky* and *Károssy*, 1986) associated with the *Péczely*'s macrosynoptic weather situations existing in the Carpathian Basin.

In some papers the results of light-trap catches were demonstrated at the time of change of *Péczely*'s type (*Nowinszky* and *Károssy*, 1988; *Károssy* and *Nowinszky*, 1987b). In these publications we searched for the connection between the catching data and the change of 13 types of *Péczely*. The types which seldom occured were eliminated. This method gave much information, but its application was complicated for plant-protecting forecast. In the recent paper a simple method is presented which is easily applicable for plant-protecting forecast. Based on the air flow the 13 situations had been contracted into 6 types and after that the time of their change was investigated (*Károssy et al.*, 1990, 1992).

In the present paper the authors analyse the light-trap catches of turnip moth (*Scotia segetum Schiff.*) in connection with the macrosynoptic weather types of *Hess-Brezowsky* (1977) extended to whole Europe.

2. Material

The determination of macrosynoptic types of *Hess-Brezowsky* had been similarly and subjectively worked out as *Péczely*'s ones, taking into account the circulation conditions of the continent (Europe). The catalogue of *Hess-Brezowsky* (1977) based on baric circumstances of Central Europe, distinguishes 4 zonal, 18 meridional and 7 mixed types of weather situations, maintaining one type for unclassified baric areas. *Bartholy* and *Kaba* (1987) interpreted the *Hess-Brezowsky*'s situations for the whole Atlantic-European area. They analysed a great amount of data processed from 8 Hungarian meteorological stations of 60 years and 18 daily values and determined the *Hess-Brezowsky*'s weather picture for Hungary. The characteristics of these types can be found in literature cited. The codes which were necessary for this investigation, are similarly taken from publication of *Hess-Brezowsky* (1977).

The Hungarian light-trap network is supported by the Forestry Research Institute, the plant-protecting stations and other research organisations. The

uniform light-trap device consists of a 100 W incandescent lamp situated at 2 m above the ground surface and the killing material is chloroform.

During the interval between 1957 and 1976, i.e. through 20 years, 32,100 individuals of turnip moth (*Scotia segetum Schiff.*) were caught by the 61 traps of the network from 20,508 observations and 249 swarmings at 2,647 nights. In our terms, swarming is the time-span of one generation and an observational datum is denoted as the result collected at a single station during one night.

The turnip moth (*Scotia segetum Schiff.*) has two generations yearly and is characterized as a polyphag harmful insect. The first generation in most cases occurs from the beginning of May to the middle of June, while the second one from middle of July to September. This moth is equally dangerous for vegetables, root crops, industrial plants, cereals, leguminouses and ornamental plants.

3. Method

We calculated relative catches (RC) from the obtained data belonging to each collecting stations and generations. This procedure gives us a possibility to compare the results taken at various light-trap stations to each other. The RC is defined as a quotient of the number of individuals caught during a sampling time (a night) and the mean number of a given generation.

The catching data belonging to the same *Hess-Brezowsky*'s 29 types in the evening and morning, have been averaged. After this the significance levels have been computed between them using the *Welch*-test (i.e. an approximate t-test). In cases, if we did not take the macrosynoptic types into account, we applied 1 (the unity) as relative catch value (RC).

In so far as during a two days period the weather types changed, the original 29 situations were sorted into zonal, mixed, meridional, cyclonic or anticyclonic groups on the basis of their circulation characteristics. On this basis we accepted 6 groups, containing the original situations too, as follows:

- Zonal anticyclone: Wa (1), Ws (3), and Ww (4),
- Zonal cyclone: Wz (2),
- Mixed anticyclone: SWa (7), NWa (13), HM (17) and BM (30),
- Mixed cyclone: SWz (8), NWz (14) and TM (25),
- Meridional anticyclone: Sa (5), SEa (9), Na (11), NEa (15), HB (18), HNa (19), HFa (21) and HNFa (23),
- Meridional cyclone: Sz (6), SEz (10), Nz (12), NEz (16), HNz (20), HFz (22), HNFz (24), TB (26), TRM (27) and TRW (28).

The above listed 6 groups can change into 36 possible categories. Continuing the procedure, we have averaged the RC belonging to each variable situation and after this the confidence level was calculated related to the expected value, using the *Welch*-test.

4. Results and discussion

Table 1 contains the averages of RC of the turnip moth (*Scotia segetum Schiff.*) with the number of observations, the confidence levels of the *Hess-Brezowsky* situations which have the same characters in the evening and morning. *Table 2* shows the same data of the changing situations.

The data of Table 1 show that in most case of northern, northwestern and western situations, when the macrosynoptic situations remained unchanged in the evening and in the morning, the number of moths significantly decreased. This phenomenon may be explained by windy and cool weather, which characterizes the night hours generally in these cases. It is conspicuous that high catch can be associated only with four situations, of which three belong to southern or southwestern types. It seems that the continuously existing weather situations are unfavourable for the activity of insects. We obtained similar results earlier in connection with *Péczely*'s situations. From the varying situations in general, the anticyclones are unfavourable, because the character of circulation changes, moreover an anticyclone is followed by a cyclone or a cyclone by anticyclone, respectively.

We have high catch, if a cyclone is succeeded by a cyclone and if a meridional anticyclone is followed by an other one or a meridional cyclone.

The low values of RC are referring in all cases to such a weather situation which cause decresed flying activity of insects. The high values cannot be interpreted unambiguously. The significant changes in environment induce some physiological variations in organism of insects. The life of an imago is short, therefore the unfavourable weather is dangerous as well for individuals as for remaining of whole species. We suggest that an individual, in order to avoid the bad circumstances hindering his normal life, can apply two strategies. The insect shows increased activity which consists of expanded flying, copulation and laying eggs, or passively, hide themself through the unfavourable times. Based on facts discussed above, high RC belongs both to good and bad weather situations.

The present paper is a first one of those investigations, which are associated with the connection between the macrosynoptic situations of *Hess-Brezowsky* and the life circumstances of insects. To the further work, we think it necessary to reveal the characteristics of the behaviours connected with the times of variations of the weather situations. We hope, based on our new results, that a reliable forecast can be established using *Hess-Brezowsky*'s classification all over Europe. In Hungary the *Péczely*'s situations give also good approximation to plant-protection service.

Acknowledgements–The insects caught by light-traps were identified by a team at the Hungarian Museum for Natural Science under the direction of *Lajos Kovács*. The note-books were kindly disposed to us by *András Vojnits*, to whom we express our sincere acknowledgements hereby.

Table 1. The RC of turnip moth (*Scotia segetum Schiff.*) in situations when the *Hess-Brezowsky's* macrosynoptic type has the same character both in the evening and in the morning

Code	H-B situations	Mean of RC	Number of data	Confidence level
	Northern macrosynoptic types			
11	Na	0.757	97	94.45
12	Nz	0.922	463	91.68
19	HNa	0.930	248	-
20	HNz	0.772	376	99.84
18	HB	0.861	384	97.16
	Northwestern macrosynoptic types			
13	NWa	0.972	123	-
14	NWz	0.938	1139	92.68
27	TRM	0.733	240	99.25
	Western macrosynoptic types			
1	Wa	0.948	869	90.05
2	Wz	0.945	2512	96.16
3	Ws	1.020	483	-
	Southwestern macrosynoptic types			
7	SWa	1.295	661	99.90
8	SWz	0.960	471	-
28	TRW	1.210	1084	99.83
4	Ww	1.127	274	-
	Southern macrosynoptic types			
5	Sa	0.746	49	92.70
6	Sz	1.321	18	-
26	TB	1.200	446	96.30
	Southeastern macrosynoptic types			
9	SEa	0.775	66	-
10	SEz	0.812	6	-
	Eastern macrosynoptic types			
21	HFa	0.868	758	98.98
22	HFz	0.969	409	-
23	HNFa	0.895	249	-
24	HNFz	1.061	505	-
	Northeastern macrosynoptic types			
15	NEa	0.999	430	-
16	NEz	1.328	274	98.90
	Types with its center situated above Central-Europe			
17	HM	1.001	1032	-
30	BM	1.104	1055	90.34
25	TM	0.734	142	96.75

Note: The codes are obtained from the paper of *Bartholy* and *Kaba* (1987).

Table 2. The RC of turnip moth (*Scotia segetum Schiff.*) when the *Hess-Brezowsky*'s macrosynoptic types has been changed

Variable situations	RC	Number of data	Confidence level
FROM ZONAL ANTICYCLONE TO			
-zonal anticyclone	-	-	-
-zonal cyclone	0.757	123	97.71
-mixed anticyclone	0.892	188	-
-mixed cyclone	0.813	71	-
-meridional anticyclone	0.714	105	98.67
-meridional cyclone	1.231	103	-
FROM ZONAL CYCLONE TO			
-zonal anticyclone	0.567	106	99.99
-zonal cyclone	-	-	-
-mixed anticyclone	1.031	208	-
-mixed cyclone	1.240	122	90.57
-meridional anticyclone	1.126	24	-
-meridional cyclone	0.916	201	-
FROM MIXED ANTICYCLONE TO			
-zonal anticyclone	1.054	102	-
-zonal cyclone	1.359	276	99.34
-mixed anticyclone	1.058	124	-
-mixed cyclone	1.254	113	-
-meridional anticyclone	0.844	164	93.28
-meridional cyclone	0.976	326	-
FROM MIXED CYCLONE TO			
-zonal anticyclone	1.015	178	-
-zonal cyclone	1.450	72	90.54
-mixed anticyclone	1.073	171	-
-mixed cyclone	1.440	122	-
-meridional anticyclone	1.030	241	-
-meridional cyclone	0.783	120	97.36
FROM MERIDIONAL ANTICYCLONE TO			
-zonal anticyclone	0.543	72	99.75
-zonal cyclone	0.666	12	-
-mixed anticyclone	0.745	179	99.69
-mixed cyclone	1.132	53	-
-meridional anticyclone	1.245	225	94.38
-meridional cyclone	1.267	222	95.70
FROM MERIDIONAL CYCLONE TO			
-zonal anticyclone	1.102	115	-
-zonal cyclone	0.912	219	-
-mixed anticyclone	0.901	222	-
-mixed cyclone	1.182	176	-
-meridional anticyclone	0.833	247	96.59
-meridional cyclone	1.112	491	-

References

Bartholy, J. and *Kaba, M.*, 1987: Statistical analysis and correction of *Hess-Brezowsky*'s macrosynoptic types (in Hungarian). *Meteorológiai Tanulmányok* 57, OMSZ, Budapest.

Hess, P. and *Brezowsky, H.*, 1977: *Katalog der Grosswetterlagen Europas*. Berichte des Deutschen Wetterdienst, 113, 15. Offenbach am Main.

Károssy, Cs. and *Nowinszky, L.*, 1987a: The flying activity of harmful insects at various macrosynoptic situations (in Hungarian). *Légkör 32*, No. 2, 33-35.

Károssy, Cs. and *Nowinszky, L.*, 1987b: Relationship between the amount of turnip moth caught by light-traps and the different macrosynoptic situations (in Hungarian). *Időjárás 91*, 246-252.

Károssy, Cs., *Nowinszky, L.* and *Tóth, Gy.*, 1990: Die Flugaktivität der Saateule (Scotia segetum Schiff.) während des Wechsels von Grosswetterlagen. *Wetter und Leben*, 42, 189-194.

Károssy, Cs., *Nowinszky, L.*, *Tóth, Gy.* and *Puskás, J.*, 1992: Flying activity of the agricultural harmful insects and the connection of macrosynoptic weather types. *Boletin de la Sociedad Geografica de Lima 105*, 57-58.

Nowinszky, L. and *Károssy, Cs.*, 1986: Results of catching of the winter moth (Operophtera brumata L.) by light-traps in different macrosynoptic climatic conditions (in Hungarian). *Kertgazdaság 18*, No. 6, 31-38.

Nowinszky, L. and *Károssy, Cs.*, 1988: The result of light-trapping in connection with macrosynoptic weather situations (in Hungarian). *Növényvédelem 24*, No. 1, 10-17.

INFORMATION

GEDEX: a comprehensive data set on global and regional change

T. Pálvölgyi

Institute for Atmospheric Physics, P.O. Box 39, H-1675 Budapest, Hungary

(Manuscript received 4 March 1993)

Abstract—The primary aim of this paper is to outline the GEDEX (*Greenhouse Effect Detection Experiment*) data set developed for global change analysis. This first issue includes surface, upper air, and/or satellite-derived measurements of temperature, solar irradiance, clouds, greenhouse gases, fluxes, albedo, aerosols, ozone, and water vapour, along with Southern Oscillation Indices and Quasi-Biennial Oscillation statistics. Additionally, the documentation of individual climatic records is discussed briefly and some technical details of handling the data set are also presented. All data incorporated into the GEDEX data set are available on CD-ROMs at the Hungarian Meteorological Service.

Key-words: global change, climate variables monitoring, digital data base.

1. Introduction

During the past 20 years, much attention has been devoted to the potential climatic effects of increasing concentrations of atmospheric greenhouse gases. There are growing evidences that these potential climatic effects could have far-reaching environmental, economic and social consequences, as well. Much of recent study (*IPCC,* 1992) has involved

— climate modelling or empirical analyses attempting to attribute climate change to various atmospheric and astronomical forcing, and
— assemblage and examination of new geological, historical and instrumental data.

From these studies, researchers have gained important new insights into the possible climatic response to the growing level of atmospheric CO_2 and other trace gases, together with a better understanding of the sensitivity of the overall climate system to both human and natural perturbations.

In order to detect the "greenhouse signal" that is indicative of increased concentrations of greenhouse gases, it is imperative to collect observational records that can be used to identify the climate change. For the past century, many climate variables have been measured at a large number of meteorological

stations, mostly at land locations in the Northern Hemisphere. One of the goals of NASA's Climate Data System (NCDS) staff at Goddard Space Flight Center is to provide ready access data and information pertinent to global and regional changes. NCDS has attempted to achieve this goal by providing reports, numerical data packages and other information center products and services.

2. Overview

The *Greenhouse Effect Detection Experiment* (GEDEX) program takes a major step in providing timely data to a multidisciplinary audience of researches, policy-makers, energy and environmental professionals and educators (*GEDEX,* 1992). The GEDEX program is a part of NASA's involvement in the International Space Year (ISY) activities. In preparation for the International Space Year, the *Greenhouse Effect Detection Experiment* organized a workshop to bring together a core group of scientists to share their research and ideas in the area of global climate change. Participants in this workshop, which was designated GEDEX Atmospheric Temperature Workshop, met in Columbia, Maryland, in July 1991 for the purpose of obtaining a measure of progress and recommending actions required to better understand the global atmospheric temperature record and its relationship with climate forcings and feedbacks (*NASA,* 1992).

One of the primary objectives of the workshop was to assemble and document existing data (focusing on temperature) for the analysis of global and regional climate change and to consolidate these selected data sets onto CD-ROMs for distribution nationally and internationally to promote further research. With climate at the focus, NASA's Climate Data System (NCDS) participates and prepares for the acquisition, archiving, implementation, and documentation of data recommended for distribution. NCDS has been designated as the core system for the Goddard Space Flight Center's Distributed Active Archive Center (DAAC) of the Earth Observing System Data and Information System (EOSDIS), and in this role will continue to update GEDEX-relevant data sets. All data will remain in the Goddard DAAC (NCDS) and will be updated whenever new releases are made available. Subsequent updates will therefore be made available in an ongoing manner to the climate user community. More than 60 data sets were identified by workshop participants for inclusion, yielding nearly 1 gigabyte of data for this first 2-disk set of CD-ROMs. Most participants contributed data and helped in the preparation of the standard documentation for each data set proposed for CD-ROM. Each data set was verified by the NCDS after it was transformed into a standard format (the Common Data Format [CDF] to allow for the use of a single set of software tools to access the data on disks). Iterations of the detailed documentation and extensive verification with data producers ensure that the data are reproduced

as received from data producers. The data producers cooperated fully with this essential effort.

3. *Contents*

Although the focus of the first GEDEX workshop was on temperature, other parameters such as solar irradiance, atmospheric constituents, cloud, and radiation budget data, which affect the temperature record, were considered essential components of the data base. The GEDEX data sets include surface, upper air, and/or satellite-derived measurements of temperature, solar irradiance, clouds, greenhouse gases, fluxes, albedo, aerosols, ozone, and water vapour, along with Southern Oscillation Indices and Quasi-Biennial Oscillation statistics. Many of the data sets provide global coverage. The spatial resolutions vary from zonal to 2.5 degree grids. Temporal coverage also varies. Some surface station data sets cover more than 100 years, while most of the satellite-derived data sets cover only the most recent 12 years. Temporal resolution, for most data sets, is monthly (*Table 1*).

Table 1. Basic characteristics of some selected GEDEX data sets

	Spatial coverage	Spatial resolution	Temporal coverage	Temporal resolution
Surface temperature	global	2.5° grid	> 100 years	monthly
Upper air temperature	Northern Hemisphere	zonal	35 years	monthly
Cloudiness	global	2.5° grid	5 years	monthly
Radiation budget	global	5° grid	9 years	monthly
Solar irradiance	single site (Mauna Loa)	-	32 years	daily
CO_2 concentration	certain sites (32 stations)	-	10-25 years	monthly
CH_4 concentration	certain sites (21 stations)	-	9-13 years	monthly
N_2O concentration	Northern Hemisphere	zonal	7 years	seasonal
Total ozone	certain sites (85 stations)	-	22 years	monthly

3.1 Surface temperature

The basic surface station temperature data set from NCDC/NCAR contains monthly temperature and precipitation values and is subdivided by continent. A few records dated from as early as 1738, and modern station data extend

through 1989. Other surface temperature anomaly data sets containing monthly gridded values were provided by the University of East Anglia Climate Research Unit (*Jones et al.*, 1991), and by the Goddard Institute for Space Studies (*Hansen* and *Lebedeff*, 1988). Zonal and station temperature data are included from the Russia's State Hydrologic Institute (*Vinnikov et al.*, 1990). These data sets extend over 100 years of record. Gridded 2.5 degree monthly sea-surface temperature data and anomalies as calculated by NOAA's Climate Analysis Center also reside on this disk. These SST values are from AVHRR sensors on NOAA polar orbiters and are blended with ship and buoy data. Investigating the effect of the El Niño/Southern Oscillation (ENSO) on the temperature anomaly record, may be done with the data set provided by the University of East Anglia's Climate Research Unit containing the Southern Oscillation Index calculations, along with the Tahiti and Darwin mean sea level pressures from which they are derived.

3.2 Upper air temperature

NCDC/NCAR contributed comprehensive monthly station rawinsonde data (*Spangler* and *Jenne*, 1990). Both temperature and humidity profiles are included in this data set. Another upper air temperature data set was produced by NOAA ARL (*Angell*, 1988). It contains seasonal zonal temperature deviations from rawinsonde data around the world. *Angell* also provided Quasi-Biennial Oscillation temperature and zonal wind data at 50, 30, and 10 hPa. Marshall Space Flight Center provided more than 12 years of mid-tropospheric temperature and anomaly data from the TIROS Operational Vertical Sounder Microwave Sounding Unit (TOVS-MSU), flown on NOAA polar orbiters (*Spencer* and *Christy*, 1992). Stratospheric temperature data were provided by NCAR (*Labitzke* and *van Loon*, 1991). Although these data are only available for the Northern Hemisphere, they provide a valuable monthly zonal product for the years 1957 to 1991. In addition, profiles of meteorological data from NMC were provided at 1 km intervals for the Stratospheric Aerosol and Gas Experiment (SAGE II) time period .

3.3 Solar irradiance and transmission

Solar transmission and surface-measured irradiance data were compiled by NOAA Climate Monitoring and Diagnostics Laboratory (CMDL). The daily solar transmission indices, given from the Mauna Loa Observatory, begin in 1958 and continue through 1990 (*Reid*, 1991). The hourly solar irradiance data make up a rare collection of solar data collected at the surface from 1976 to 1989 at selected sites. NASA Goddard Space Flight Center provided solar irradiance data from the Nimbus-7 Earth Radiation Budget (ERB) instrument, and Langley Research Center offered the solar irradiance data from NOAA-9,

NOAA-10, and ERBS. Jet Propulsion Laboratory has collaborated with the NCDS staff over the years in making 9 years of solar irradiance data from the Solar Maximum Mission's ACRIM sensor available to users online (*Willson* and *Hudson,* 1991). From the Dominion Radio Astrophysical Observatory (DRAO) (formerly Ottawa) 2800 MHz radio flux data are also available on the disk with observed, absolute, and adjusted variables from 1947 to the present.

3.4 Radiation budget and clouds

Langley Research Center provided the combined Earth Radiation Budget Experiment's (ERBE S4) satellite gridded products, including the scanner data at 2.5 degree resolution and the wide-field-of-view monthly averages. NASA GISS suggested and subsequently provided a comprehensive subset of the *International Satellite Cloud Climatology Project's* (ISCCP) monthly cloud products at 2.5 degree resolution. ISCCP also assisted in the review and verification of those data worked closely with the staff in the validation of data on the disk from the Earth Radiation Budget instrument on board Nimbus-7. Data from the wide-field-of-view sensor span the period 1978 to 1987 and are monthly in temporal resolution and approximately 4.5 by 5 degrees in spatial resolution. Data are derived from NOAA Polar Orbiting satellites using TOVS-HIRS and TOVS-MSU sensors.

3.5 Atmospheric constituents

The Carbon Dioxide Information Analysis Center (CDIAC), Department of Energy, is the source providing carbon dioxide and methane values spanning the geological record (through ice core techniques) and more recent values collected by NOAA from flask sampling and continuous monitoring techniques (*TRENDS*, 1990). NOAA ARL also contributed seasonal layer ozone data from Umkehr sounding and ozonesondes from 1957 to 1990, and total ozone from Dobson spectrophotometers for the period 1967 to 1989 (*Stolarski et al.*, 1991). NASA's Langley Research Center worked closely with NCDS in providing ozone, nitrogen dioxide, and aerosol data from the Atmospheric Explorer Mission's SAGE I instrument, and aerosol, ozone, water vapor, and nitrogen dioxide data from the Earth Radiation Budget Satellite's (ERBS) SAGE II instrument beginning with data from the November 1984 launch through 1991 (*McCormick et al.*, 1992).

3.6 Satellite-based data

The satellite-based data sets are those from Solar Maximum Mission's ACRIM instrument, the Nimbus-7 Earth Radiation Budget instrument, the Atmospheric Explorer Mission's SAGE I sensor, the Earth Radiation Budget

Satellite's SAGE II sensor, the NOAA polar orbiter TOVS-HIRS and TOVS-MSU instruments, the Earth Radiation Budget Experiment (NOAA-9, NOAA-10, and ERBS sensors), and AVHRR, MIR and VAS sensors on NOAA Polar Orbiters, GOES, METEOSAT, and GMS satellites.

4. Documentation

Each record of the data set is supplied by detailed catalogues containing fourteen items (with standardized subheadings). These give information on the type of the data, spatial and temporal characteristics, instrument description, data processing sequence, quality assessment, contacts for data production, output products and availability, data access, archive information, references, related data sets, summary/sample, and a final item for notes (*Appendix A*). Much of the information was provided by the data producers, however NCDS staff members supplemented this information and standardized presentation. As a result, specific details can be readily located through the table of contents. In addition to the detailed catalogues directly linked with the data sets held on the CD-ROM, ancillary catalogues that are closely related to the resulting products are included. These catalogues give descriptions of the products from which many of the data sets are derived and include:

ERB:	Nimbus-7 Earth Radiations Budget
ERBE	Earth Radiation Budget Experiment
AVHRR	Advanced Very High Resolution Radiometer
SAGE I	Stratospheric Aerosol and Gas Experiment I
SAGE II	Stratospheric Aerosol and Gas Experiment II
TOVS HIRS	TIROS Operational Vertical Sounder High-resolution. Infrared Radiometer
TOVS MSU	TIROS Operational Vertical Sounder Microwave Sounding Unit
TOVS SSU	TIROS Operational Vertical Sounder Stratospheric Sounding Unit
VISSR	Visible and Infrared Spin Scan Radiometer
VAS	VISSR Atmospheric Sounder

In addition, the detailed documentation also contains descriptions of satellite sensors and the products from which the geophysical parameters of this data base are derived. Among these are AVHRR, TOVS, VAS, VISSR, ERB, ERBE, SAGE I, and SAGE II.

5. Technical background

All of the data incorporated into GEDEX are stored in binary files, written in the NASA/GSFC Common Data Format (CDF). Common Data Format is a

conceptual data abstraction for storing multi-dimensional data sets widely used in the climate research community. The CDF program allows direct access to related variable data values. The data values of up to 27 variables may be displayed at once (the CDF can have more variables but only 27 may be viewed at any one time). The data value for each variable at a given record/index location within the CDF conceptual view is displayed. The user can "walk" from one record/index location to another sequentially (in any "direction") or a particular record/index location can be "jumped" to directly. Variable values may also be used to directly "jump" to a record/index location. They are network-encoded for portability and are written with the single file option for simplicity.

The directory hierarchy is the same for both CD-ROMs. There are five major subdirectories on the discs, as given below:

[DATA] The data sets (in Common Data Format) containing the actual data sets (with file name extension CDF). A separate file CDF.DOC in the DOCUMENT subdirectory serves as references to the format of the data and supporting software.

[DETAILED] Detailed catalogues for the individual data sets and sensors describing comprehensive information about the data sets on the disk. Files are in ASCII: each line of text delimited by a carriage return (ASCII 13) and a line feed (ASCII 10).

[DOCUMENT] Overall documentation for the CD-ROM (ASCII text files of documentation about the disk structure, data formats and accompanying software).

[INDEX] Various tables of data describing the data sets that are suitable for import into a database management system. This contains comma-delimited index files which may be imported into a database program, in order to facilitate searches of the data present on the disk.

[SOFTWARE] Utility programs for manipulating data in CDF under MS-DOS, DEC VAX or UNIX operating systems, along with the portable CDF software library for working with the data sets on the disk. There are separate directories for MS-DOS, HP-UX, SunOS, IRIX and VMS utilities, as well as a CDF subdirectory which contains the complete CDF distribution set of files.

[SUMMARY] Summary documentation required by the access software to provide standard information for each individual data set.

There are several files associated with each data set. The kind of information stored in a file can be inferred from the extension on the file name:

[CDF] The data, formatted to CDF v2.1 as network-encoded, single

file data sets. These are all located in the DATA subdirectory.

[DET] A text file, containing the NCDS Detailed Catalogue associated with the data set. All of these files are located in the DETAILED subdirectory.

[SUM] A text file, containing summary information about the data set. All of these files are located in the SUMMARY subdirectory.

Since several data sets may share a single detailed catalogue, the file PRODUCTS.LIS (in the SUMMARY subdirectory) gives a tabular listing of the name of the data file, a brief description of the data set and the name of the associated detailed catalogue, as well.

6. Conclusions

Activities in the scientific and policy-making communities have been stimulate by public concerns related to global environmental issues. Recognition is growing that it is increasingly important to have valid and reliable data at hand to develop effective policies related to these issues. The most promising potential key research areas for the application of GEDEX data sets are

- detection of enhanced greenhouse effect based on evaluation and prediction of climate variability and trends on various space and time scale,
- parameterization of climate processes, validation and verification of climate models,
- investigation of spatial distribution and life cycle of climatic fluctuations and teleconnections arising on decadal time scale,
- assessment of global and regional climate scenarios based on analogue method,
- renewed climatological database into a limited area model,
- various applications in the satellite climatology

It can be concluded that such data sets are essential to analyse and evaluate the magnitude of environmental problems that have global or regional implications.

References

Angell, J.K, 1988: Variations and trends in tropospheric and stratospheric global temperatures, 1958-1987. *J. Clim. 1*, 1296-1313.

GEDEX, 1992: *Booklet on the greenhouse effect detection experiment* (eds.: L.M. Olsen and A. Warnock), NASA Goddars Space Flight Center, Greenbelt, U.S.A.

Hansen, J. and *Lebedeff, S.*, 1988: Global surface air temperatures: update through 1987. *Geophys. Res. Lett. 15*, 323-326.

IPCC, 1992. *Climate Change: The Supplementary Report to the IPCC Scientific Assessment* (eds.: J.T. Houghton, B.A. Callander and S.K. Varney). Cambridge University Press, Cambridge, 192 pp.

Jones, P.D., Wigley, T.M.L. and *Farmer, G.*, 1991: Marine and land temperature data sets: a comparison and a look at recent trends. In *Greenhouse Gas Induced Climate Change: a Critical Appraisal of Simulations and Observations* (ed.: M.E. Schlesinger). Elsevier, Amsterdam, pp. 153-172.

Labitzke, K. and *van Loon, H.*, 1991: Some complications in determining trends in the stratosphere. *Adv. Space Res. 11*, (3)21-(3)30.

McCormick, M.P., Veiga, R.E. and *Chu, W.P.*, 1992: Stratospheric ozone profile and total ozone trends derived from the SAGE I and SAGE II data. *Geophys. Res. Lett. 19*, 269-272.

NASA, 1992: *The Detection of Climate Change due to the Enhanced Greenhouse Effect* (A synthesis of findings based on the GEDEX atmospheric temperature workshop, ed.: R.A. Schiffer). NASA Goddard Space Flight Center, Greenbelt, U.S.A.

Reid, G.C., 1991: Solar total irradiance variations and the global sea surface temperature record. *J. Geophys. Res. 96*, 2835-2844.

Spangler, W.M. and *Jenne, R.L.*, 1990: *World Monthly Station Climatology*. CDT documentation, NCAR, Boulder, U.S.A.,

Spencer, R.W. and *Christy, J.R.*, 1992: Precision and radiosonde validation of satellite gridpoint temperature anomalies. *J. Clim.* (in press).

Stolarski, R.S., Bloomfield, P., McPeters, R.D. and *Herman, J.R.*, 1991: Total ozone trends deduced from NIMBUS 7 TOMS data. *Geophys. Res. Lett. 18*, 1015-1018.

TRENDS, 1990: *A Compendium of Data on Global Change*. Oak Ridge National Laboratory, Oak Ridge, U.S.A.

Vinnikov, K.Ya., Groisman, P.Ya. and *Lugina, K.M.*, 1990: Empirical data on contemporary global climate changes (temperature and precipitation). *J. Clim. 3*, 662-677.

Willson, R.C. and *Hudson, H.S.*, 1991: The Sun's luminosity over a complete solar cycle. *Nature 351*, 547-560.

APPENDIX A Detailed documentation of GEDEX data sets

1. TYPE OF DATA
   - 1.1 Parameter/Measurement
   - 1.2 Unit of Measurement
   - 1.3 Data Source
   - 1.4 Data Set Identification

2. SPATIAL CHARACTERISTICS
   - 2.1 Spatial Coverage
   - 2.2 Spatial Resolution

3. TEMPORAL CHARACTERISTICS
   3.1 Temporal Coverage
   3.2 Temporal Resolution

4. INSTRUMENT DESCRIPTION
   4.1 Mission Objectives
   4.2 Key Satellite Flight Parameters
   4.3 Principles of Operation
   4.4 Instrument Measurement Geometry

5. DATA PROCESSING SEQUENCE
   5.1 Processing Steps and Data Sets
   5.2 Derivation Techniques/Algorithms
   5.3 Special Corrections/Adjustments
   5.4 Processing Changes

6. QUALITY ASSESSMENT
   6.1 Data Validation by Producer
   6.2 Confidence Level/Accuracy Judgement
   6.3 Usage Guidance

7. CONTACTS FOR DATA PRODUCTION INFORMATION

8. OUTPUT PRODUCTS AND AVAILABILITY
   8.1 Tape Products
   8.2 Film Products
   8.3 Other Products

9. DATA ACCESS
   9.1 Archive Identification
   9.2 Procedures for Obtaining Data
   9.3 NCDS Status/Plans

10. CONTACTS FOR ARCHIVE/DATA ACCESS INFORMATION

11. REFERENCES
   11.1 Satellite/Instrument/Data Processing Documentation
   11.2 Journal Articles and Study Reports
   11.3 Archive/DBMS Usage Documentation

12. RELATED DATA SETS

13. SUMMARY/SAMPLE

14. NOTES

BOOK REVIEW

Atlas of Paleoclimates and Paleoenvironments of the Northern Hemisphere. Late Pleistocene–Holocene (published by the Geographical Research Institute, Hungarian Academy of Sciences, Budapest, on behalf of the International Union for Quaternary Research; edited by *Frenzel, B., M. Pécsi* and *A.A. Velichko*; explanatory text edited by *L. Bassa* and *O. Soffer*; Published by Fisher Verlag, Stuttgart–Jena–New York, Geographical Res. Inst., Hung. Acad. Sci., Budapest, 1992; 153 pages, 35 large size color maps.)

The production of this important publication was sponsored by the Executive Committee of the International Union for Quaternary Research (INQUA), the Hungarian Academy of Sciences, the Academy of Sciences and Literature (Mainz), the Federal Ministry of Research and Technology (Bonn) and the Enkidu Foundation (Berne–Tübingen). The contributing institutions were: the Geographical Research Institute of the Hungarian Academy of Sciences, the Research Project Group "Terrestrial Paleoclimatology" of the Academy of Sciences and Literature (Mainz) and the Laboratory of Paleogeography of the Academy of Sciences of the USSR. Contributions from 62 authors (mainly from Germany and the USSR) were compiled and carefully edited. In addition to the contributors, 16 more scientists were involved in the revision of the maps. The number of references (353) also gives an idea of the magnitude of the undertaking. The cartography and printing was done by the Geographical Research Institute of the Hungarian Academy of Sciences.

In the atlas altogether 9 maps deal with the *Last Interglacial* (about 120,000 yr B.P.), 5 maps with the *interstadial of the last glaciation* (about 35,000 to 25,000 yr B.P.), 11 maps with the *maximum cooling period* of the last glaciation (about 20,000 to 18,000 yr B.P.), 2 maps with the *upper pleniglacial* of the last glaciation (about 24,000 to 12,000 yr B.P.), and finally 8 maps with the *Holocene* (between 7,000 and 5,500 yr B.P.).

The *Quaternary* period (Pleistocene and Holocene) comprises the last 2 million years of the history of the Earth. This was the time span of the emergence of early man, whose evolution was greatly influenced by climatic changes. The *International Union for Quaternary Research* (INQUA) was established in the early thirties in recognition of the particular importance of this period.

Some 14 years ago INQUA has established its *Commission on Paleogeographic Atlas of the Quaternary* in order to compile and publish the results of the wide ranging research works on the spatial and temporal paleogeographical changes on the Northern Hemisphere during the *last climatic macrocycle* (last 130,000 years).

It is generally assumed that the above mentioned last climatic macrocycle is a typical example of the climatic cycles which followed each-other during the 2 million years of the Quaternary. A detailed analysis of the last climatic macrocycle is considered, therefore, a relevant contribution to the deeper understanding of the climatic history of the whole period.

The *climatic reconstructions* contained in the atlas are based on different approaches and methods, consequently they are not always in full agreement. Nevertheless, these reconstructions allow some conclusions about the hydrothermal regime of the Northern Hemisphere and provide an idea about various environmental responses, such as conditions and distribution of vegetation, permafrost and hydrology.

During the last 130,000 years the Earth experienced at least twice periods of pronounced warmer climates (during the Last Interglacial and during the Holocene climatic optimum), and two phases of cold climates (the interstadial complex and the pleniglacial phase).

In connection with paleoclimatic reconstructions and mapping two major types of difficulties are usually encountered: (*a*) *the difficulties in establishing correlations (synchronism) between events occurring in different regions of the globe, and (b) the synthesis of reconstructions obtained by different methods.*

As regards the Holocene, dating is easy by radiocarbon analysis, or by dendrochronology. Thus, for the Holocene climatic optimum no major problems were encountered in correlating the events that occurred in various parts of the globe. It seems, it was a bit tricky to deal with the Last Interglacial, and it was quite difficult to analyse the two cold periods mentioned above. Because of such difficulties it was decided in some cases to show different reconstructions rather than trying to give preference to a single one.

The climatic reconstructions in the atlas are often based on comparing former vegetation communities and soil types to their nearest modern equivalents. This approach, however, is sometime complicated by the fact that neither during the Last Interglacial, nor during the Holocene had all plant and animal taxa (categories of species) sufficient time to occupy their climate-controlled optimal distribution areas.

Nevertheless, it was possible to focus on those phases which could be shown to be synchronous directly by biostratigraphical methods. To mention some examples: the *Eem* epoch of Western Europe could be correlated with the *Mikulino Interglacial* of Eastern Europe, and with marine sequences of the North Sea, Baltic Sea, and Norwegian Sea. Also some episodes of the Eemian pollen sequence are recorded in the Oxygen Isotope Substage 5e, which is also the case for the *Sangamon Interglacial* of Western North America.

One of the very interesting points in these reconstructions is the finding that during the *Last Interglacial* an apparently *warmer climate* (2 to 3°C warmer than today) was accompanied—almost everywhere—by an *increased humidity*. This conclusion *contradicts current GCM model-predictions* which mostly

suggest a greenhouse induced climatic warming accompanied by increasing aridity in presently dry regions (and also in that part of Europe which extends between 35 and 50°N). This point is mentioned just as an example of the kind of intriguing questions which may provide ample food for speculations in connection with the 35 maps of the atlas and the findings of the climatic reconstructions which are described in the text.

In conclusion I would like to stress the importance of this publication. As we can see, nowadays an increasing number of textbooks and publications deal with climatic change, and they usually contain at least brief summaries of paleoclimatic information. Probably I'm not the only one who used to be confused and frustrated by such summaries, which try to provide a simplified picture of a rather chaotic subject. Isolated and sporadic reconstructions of past climates make seldom sense in explaining global climate change chronologies. The only way to somewhat ease this problem is to go meticulously through the hard work of establishing correlations between paleoclimatic events that occurred in different parts of the globe and to produce maps like the ones presented in this atlas.

R. Czelnai

A. Carbonneau, C. Riou, D. Guyon, J. Riom and *C. Schneider*: **Agrometeorology of the Vine Crop** (in French). Centre Commune de Recherche, Commission des Communautés Européennes, 1992, pp. 1–165.

This publication of the *Commission of the European Communities* (CEC) provides an inventory of available information on the agrometeorology of vine, based on a review of literature and experts' opinions. It contains two main parts: the first (and main) part, dealing with the *agrometeorology of vine*, and the second part, containing a preliminary study on *monitoring of vine-lands by remote sensing techniques*.

The flow of accurate and timely information on the state of crop cultures is a vital component in market economies. The Commission of the European Communities, considering the necessity of obtaining such early information, established a *pilot project* for the introduction of remote sensing in the agricultural statistical information system of the Community. It was also a requirement that the whole methodology should be developed in a way suitable for generating a meteorological input in a compatible form for the standard Geographical Information System of CEC.

Although, it was fully recognized that for an adequate early (or advance) information system primarily remote sensing techniques would be required, it was also clear that such techniques were not yet sufficiently developed for the

monitoring of the vine crop. Therefore, it was concluded that remote sensing techniques will have to be applied in combination with quite sophisticated agrometeorological modelling techniques.

Thus the first part of the work done under the project aimed at the development of *agrometeorological models* appropriate for a regional monitoring of the state of the cultures and for the quantitative prediction of crops. The sub-titles in this first part of the publication are: The biological cycle of vine and the climatic parameters; Mesoclimate and microclimate of vine; Climate and growth; The climatic influences on the photosynthesis; Climatic interactions with the organism of the entire plant and its productivity; Methods of viticultural harvest-prediction. These chapters together provide a concise package of very useful information.

The second part of the publication, as already indicated above, contains a *preliminary study on the application of remote sensing techniques* for the monitoring of vine-lands. This is a very sobering report, from which we can see how little has been done so far in the area of remote sensing studies of the vine crop.

The main reason is that the vineyards do not behave well on LANDSAT or even SPOT images. A relatively large percentage of the surface "seen" by a satellite is the bare soil between the rows of vines. The spatial resolution of even the HRV sensor of the SPOT satellite (which is the best at the moment) is quite insufficient to tackle this problem and to provide useful information in a direct fashion.

Two ways were, however, considered for the possible enhancement of such satellite information: the use of multi-temporal series of images, and the application of stereo-radiometric methods (which provide a chance for evaluating the differences between the images taken under different angles relating to the rows of the vine plants). The report only gives us a hint on the possible future direction of research into these possibilities.

R. Czelnai

ATMOSPHERIC ENVIRONMENT

an international journal

To promote the distribution of Atmospheric Environment *Időjárás* publishes regularly the *contents* of this important journal. For further information the interested reader is asked to contact *Dr. P. Brimblecombe,* School for Environmental Sciences, University of East Anglia, Norwich NR 7TJ, U.K.

Volume 27A Number 4 1993

Volume 27A Number 5 1993

D. Grosjean, E. Grosjean and *E.L. Williams II*: Fading of artists' colorants by a mixture of photochemical oxidants, 765-772.

E.Yu. Bezuglaya, A.B. Shchutskaya and *I.V. Smirnova*: Air pollution index and interpretation of measurements of toxic pollutant concentrations, 773-779.

R. Bianconi and *M. Tamponi*: A mathematical model of diffusion from a steady of short duration in a finite mixing layer, 781-792.

Technical Note

M.T. Odman and *A.G. Russell*: A nonlinear filtering algorithm for multidimensional finite element pollutant advection schemes, 794-799.

Volume 27A Number 6 1993

European Monitoring and Evaluation Program Workshop on the Combined Analysis of Measurements and Model Results with Special Emphasis on NO_x/VOC/Oxidants

D.M. Whelpdale: Foreword, 805.

J. Padro: Seasonal contrasts in modelled and observed dry deposition velocities of O_3, SO_2 and NO_2 over three surfaces, 807-814.

N.Z. Heidam: Nitrogen deposition to the Baltic Sea: experimental and model estimates, 815-822.

K. Kemp: A multi-point receptor model for long-range transport over southern Scandinavia, 823-830.

J. Schaug, T. Iversen and *U. Pedersen*: Comparison of measurements and model results for airborne sulphur and nitrogen components with kriging, 831-844.

Z. Zlatev, J. Christensen and *A. Eliassen*: Studying high ozone concentrations by using the Danish Eulerian model, 845-865.

H. Hass, A. Ebel, H. Feldmann, H.J. Jakobs and *M. Memmesheimer*: Evaluation studies with a regional chemical transport model (EURAD) using air quality data from the EMEP monitoring network, 867-887.

T. Iversen: Modelled and measured transboundary acidifying pollution in Europe–verification and trends, 889-920.

D. Simpson: Photochemical model calculations over Europe for two extended summer periods: 1985 and1989. Model results and comparison with observations, 921-943.

A. Sirois: Temporal variation of sulphate and nitrate concentration in precipitation in eastern North America: 1979-1990, 945-963.

N.C. Treloar: Source types in Canadian precipitation chemistry, 965-974.

R.L. Dennis, J.N. McHenry, W.R. Barchet, F.S. Binkowski and *D.W. Byun*: Correcting RADM's sulfate underprediction: discovery and correction of model errors and testing the corrections through comparisons against field data, 975-997.

J.E. Pleim and *J.K.S. Ching*: Interpretive analysis of observed and modeled mesoscale ozone photochemistry in areas with numerous point sources, 999-1017.

A.M. Macdonald, C.M. Banic, W.R. Leaitch and *K.J. Puckett*: Evaluation of the Eulerian Acid Deposition and Oxidant Model (ADOM) witn summer 1988 aircraft data, 1019-1034.

C.S. Davis: Wet deposition monitoring and modelling in New Brunswick–an area dominated by wet deposition due to long-range transport, 1035-1049.

Volume 27A Number 7 1993

S.E. Pitovranov, V.V. Fedorov and *L.L. Edwards*: Optimal sampler siting for atmospheric tracer experiments taking into account uncertainties in the wind field, 1053-1059.

T. Kitada, P.C.S. Lee and *H. Ueda*: Numerical modeling of long-range transport of acidic species in association with meso-β-convective-clouds across the Japan Sea resulting in acid snow over coastal Japan–I. Model description and qualitative verifications, 1061-1076.

T. Kitada and *P.C.S. Lee*: Numerical modeling of long-range transport of acidic species in association with meso-β-convectice-clouds across the Japan Sea resulting in acid snow over coastal Japan–II. Results and discussion.

J.A. Adedokun and *B. Holmgren*: Acoustic sounder Doppler measurement of the wind fields associated with a mountain stratus transformed into a valley fog: a case study.

K.E. Fekete and *L. Gyenes*: Regional scale transport model for ammonia and ammonium, 1099-1104.

M. Schatzmann, W.H. Snyder and *R.E. Lawson Jr.*: Experiments with heavy gas jets in laminar and turbulent cross-flows, 1105-1116.

G. Zappia, C. Sabbioni and *G. Gobbi*: Non-carbonate carbon content on black and white areas of damaged stone monuments, 1117-1121.

R. Sequeira: On the mass-transfer of major salt constituents from sea water to atmospheric precipitation, 1123-1129.

J.-M. Lin, G.-C. Fang, T.M. Holsen and *K.E. Noll*: A comparison of dry deposition modeled from size distribution data and measured with a smooth surface for total particle mass, lead and calcium in Chicago, 1131-1138.

J.F. Pankow: A simple box model for the annual cycle of partitioning of semi-volatile organic compounds between the atmosphere and the Earth's surface, 1139-1152.

J.W. Erisman, A.H. Versluis, T.A.J.W. Verplanke, D. de Haan, D. Anink, B.G. van Elzakker, M.G. Mennen and *R.M. van Aalst*: Monitoring the dry deposition of SO_2 in the Netherlands: results for grassland and heather vegetation, 1153-1161.

NOTES TO CONTRIBUTORS

The purpose of *Időjárás* is to publish papers in the field of theoretical and applied meteorology. These may be reports on new results of scientific investigations, critical review articles summarizing current problems in certain subject, or shorter contributions dealing with a specific question. Authors may be of any nationality but papers are published only in English.

Papers will be subjected to constructive criticism by unidentified referees.

* * *

The manuscript should meet the following formal requirements:

Title should contain the title of the paper, the names(s) of the author(s) with indication of the name and address of employment.

The title should be followed by an *abstract* containing the aim, method and conclusions of the scientific investigation. After the abstract, the *key-words* of the content of the paper must be given.

Three copies of the manuscript, typed with double space, should be sent to the Editor-in-Chief: *P.O. Box 39, H-1675 Budapest,* Hungary.

References: The text citation should contain the name(s) of the author(s) in Italic letter or underlined and the year of publication. In case of one author: *Miller* (1989), or if the name of the author cannot be fitted into the text: *(Miller,* 1989); in the case of two authors: *Gamov* and *Cleveland* (1973); if there are more than two authors: *Smith et al.* (1990). When referring to several papers published in the same year by the same author, the year of publication should be followed by letters a,b etc. At the end of the paper the list of references should be arranged alphabetically. For an article: the name(s) of author(s) in Italics or underlined, year, title of article, name of journal, volume number (the latter two in Italics or underlined) and pages. E.g. *Nathan, K. K.,* 1986: A note on the relationship between photosynthetically active radiation and cloud amount. *Időjárás 90,* 10-13. For a book: the name(s) of author(s), year, title of the book (all in Italics or underlined with except of the year), publisher and place of publication. E.g. *Junge, C. E.,* 1963: *Air Chemistry and Radioactivity.* Academic Press, New York and London.

Figures should be prepared entirely in black India ink upon transparent paper or copied by a good quality copier. A series of figures should be attached to each copy of the manuscript. The legends of figures should be given on a separate sheet. Photographs of good quality may be provided in black and white.

Tables should be marked by Arabic numbers and provided on separate sheets together with relevant captions. In one table the column number is maximum 13 if possible. One column should not contain more than five characters.

Mathematical formulas and *symbols:* non-Latin letters and hand-written marks should be explained by making marginal notes in pencil.

The final text should be submitted both in manuscript form and on *diskette.* Use standard 3.5" or 5.25" DOS formatted diskettes for this purpose. The following word processors are supported: WordPerfect 5.1, WordPerfect for Windows 5.1, Microsoft Word 5.5, Microsoft Word for Windows 2.0. In all other cases the preferred text format is ASCII.

* * *

Authors receive 30 *reprints* free of charge. Additional reprints may be ordered at the authors' expense when sending back the proofs to the Editorial Office.

Published by the Hungarian Meteorological Service

Budapest, Hungary

INDEX: 26 361

HU ISSN 0324-6329

IDŐJÁRÁS

QUARTERLY JOURNAL
OF THE HUNGARIAN METEOROLOGICAL SERVICE

CONTENTS

VOL. 97 * NO. 3 * JULY–SEPTEMBER 1993

IDŐJÁRÁS

Quarterly Journal of the Hungarian Meteorological Service

Editorial Office: P.O. Box 39, H–1675 Budapest

Subscription from customers in Hungary should be sent to the Financial Department of the Hungarian Meteorological Service Kitaibel Pál u. 1, 1024 Budapest. The subscription rate is HUF 2000.

Abroad the journal can be purchased from the distributor: KULTURA, P.O. Box 149, H–1389 Budapest. The annual subscription rate is USD 56.

IDŐJÁRÁS

Quarterly Journal of the Hungarian Meteorological Service
Vol. 97, No. 3, July–September 1993

The dynamics of a shallow-water flow over topography Part II. Numerical experiments

I. Szunyogh

Department of Meteorology, Eötvös Loránd University,
Ludovika tér 2, H-1083 Budapest, Hungary

Abstract—If a numerical approximation to the shallow-water system of equations conserves the total energy and the potential enstrophy, the purely rotational interactions will satisfy the Liouville theory of statistical physics. It means that in the absence of divergent vorticity forcing (energy flow from the divergent part to the rotational part of the kinetic energy), the rotational kinetic energy evolves toward a two-dimensional equilibrium. The divergent forcing is controlled by the conservation of potential enstrophy, thus the two-dimensional approximation well describes the temporary spectral distribution of the rotational kinetic energy. In order to examine the acting processes, numerical experiments were carried out by a well-known kinetic energy and potential enstrophy conserving scheme, which takes into consideration the effect of the bottom topography. The numerical model was integrated for sinusoidal-shaped, but different maximum-height topographies until the "energy catastrophe".

In the presented experiments, the quasi-two-dimensional constraints cannot control the rotational kinetic energy of the wavenumbers higher than five. This fact leads to the "energy catastrophe", which occurs when the divergent kinetic energy approaches an equipartition among the higher wavenumbers, and in this way, the time of the "energy catastrophe" is approximately independent of the height of the topography. These results show that the main cause of the energy catastrophe in a discretized Eulerian model is the restricted number of the potential vorticity type invariants in addition to the absence of the parametrization of the subgrid processes.

Key-words: Liouville theory, quasi-two-dimensional equilibrium of the rotational kinetic energy, equipartition of the divergent kinetic energy, energy catastrophe.

1. Introduction

In the first part of this paper (*Szunyogh*, 1993b, hereafter referred to as Part I) the quasi-two-dimensional behavior of the shallow-water flows has been examined from a theoretical point of view. It has been shown that the conservation of potential vorticity type invariants plays a principal role in the control of the vorticity type quantities. The most important invariant of this type

is the potential enstrophy, which provides the quasi-conservation of the enstrophy for properly chosen initial conditions. For these initial conditions in a given period of time the shallow-water flows possess quasi-two-dimensional features.

In Part I, it was supposed that the rotational kinetic energy evolves toward a two-dimensional equilibrium, which is determined by the temporary value of the rotational kinetic energy and the enstrophy. However, this consideration is valid only in the case when the purely rotational interactions satisfy the Liouville theory of statistical physics. It is well-known that the necessary condition in Liouville theory is satisfied in the continuous case (*Kraichnan,* 1975), but it is not straightforward in the case of the finite-difference equations. In *Section 2,* it will be shown that if a numerical scheme conserves the total energy and the potential enstrophy for a nondivergent shallow-water flow, the above condition is satisfied and considerations of Part I can be applied to numerical models. For the sake of more detailed examination of the acting processes, numerical experiments are carried out by a numerical scheme suggested by *Arakawa* and *Lamb* (1981). This scheme conserves the total energy and the potential enstrophy even if the effects of the mass-divergence and the bottom topography are taken into account. The only problem is that higher moments of the potential vorticity are not conserved, or, in other words, the individual conservation of the potential vorticity is violated, but this is an avoidable error of Eulerian numerical schemes (*Szunyogh,* 1993a). The general description of the experiments is presented in *Section 3,* and the results are demonstrated in *Section 4.* Finally, *Section 5* summarizes the main conclusions of both parts of this paper.

2. How to choose the numerical scheme?

Eq. (Part I. 17.a) can be rewritten in the form

$$\frac{\partial \zeta}{\partial t} = \partial(\zeta + f, \Delta^{-1}\zeta) + DF, \tag{1}$$

where the term

$$DF = -(\zeta + f)\delta \tag{2}$$

is the divergent vorticity forcing. According to Eq. (1), in the absence of forcing ($DF=0$) the time evolution of the rotational kinetic energy is governed by the equation

$$\frac{\partial \zeta}{\partial t} = \partial(\zeta + f, \Delta^{-1}\zeta). \tag{3}$$

In the continuous case the spectral form of Eq. (3) satisfies the Liouville theory via the satisfaction of the necessary condition

$$\frac{\partial}{\partial \zeta_k}\left(\frac{\partial \zeta_k}{\partial t}\right) = 0, \tag{4}$$

for all k, where ζ_k denotes the components of the prognostical vector variable in the spectrally transformed Eq. (3) (for the exact definition of ζ_k see *Kraichnan,* 1975; *Basdevant* and *Sadourny*, 1975), and the rotational kinetic energy evolves toward a two-dimensional equilibrium. However, for discretized model equations the condition (4) is not satisfied automatically, and the important question arises whether it is possible to find a numerical scheme which satisfies the Liouville theory.

In the following, it is shown that the condition (4) is held if the applied finite-difference scheme conserves the rotational kinetic energy and the enstrophy for flows satisfying the condition $DF(t)=0$. Discretizing the Eq. (3) by a finite-difference scheme in the the first step, and transforming the discretized system of equations by a discrete Fourier transformation in the second step, the system of governing equations takes the form

$$\frac{\partial \zeta_i}{\partial t} = \sum_j \sum_k c_{i,j,k} K_j^{-2} \zeta_j \zeta_k, \quad i,j,k = 1,...,N^2 + 2N, \tag{5}$$

where the wavenumbers (sometimes referred to as pseudo-wavenumbers) K_j (j=1,..,N^2+2N) are defined by the eigenvalues K_j^2 of the finite-difference Laplacian, which is used for the approximation to term $\Delta^{-1}\zeta$, while the coefficients $c_{i,j,k}$, (i,j,k=1,..,N^2+2N) are depending on the numerical approximation applied to the two-dimensional Jacobian $\partial(.,.)$ (for further details see Appendix). In this way, the Liouville theory is satisfied if

$$\forall\ i,k\ (i,k = 1,...,N^2+2N): c_{i,i,k} = 0, \tag{6.a}$$

$$\forall\ i,j\ (i,j = 1,...,N^2+2N): c_{i,j,i} = 0. \tag{6.b}$$

Under the conditions

$$E_{rot} = \sum_{m=-N/2}^{N/2} \sum_{l=-N/2}^{N/2} (\nabla \Delta^{-1})^2_{m,l} = const, \tag{7.a}$$

$$Z = \sum_{m=-N/2}^{N/2} \sum_{l=-N/2}^{N/2} \zeta^2_{m,l} = const, \tag{7.b}$$

if $DF(t)=0$, the system of spectral Eq. (5) conserves both the rotational kinetic

energy and the enstrophy, since the quadratic quantities satisfy the following equalities:

$$\sum_{m=-N/2}^{N/2}\sum_{l=-N/2}^{N/2}(\nabla\Delta^{-1}\zeta)_{m,l}^2 = 2\sum_{i=0}^{N^2+2N}(\nabla\Delta^{-1}\zeta)_i^2, \tag{8.a}$$

$$\sum_{m=-N/2}^{N/2}\sum_{l=-N/2}^{N/2}\zeta_{m,l}^2 = 2\sum_{i=0}^{N^2+2N}\zeta_i^2, \tag{8.b}$$

where the rotational kinetic energy and enstrophy of the system of Eq. (5) are defined by the right-hand side of Eq. (8.a) and Eq. (8.b), respectively. However, the conditions (7.a) and (7.b) are held for a given system of discretized equations if and only if

$$\forall\ i,j,k\ (i,j,k = 1,..,N^2+2N):\ c_{i,j,k} = -c_{k,j,i}, \tag{9.a}$$

$$\forall\ i,j,k\ (i,j,k = 1,...,N^2+2N):\ c_{i,j,k} = -c_{i,k,j}, \tag{9.b}$$

respectively (*Szunyogh,* 1993a). From (9.a)

$$\forall\ i,j\ (i,j = 1,..,N^2+2N):\ c_{i,j,i} = -c_{i,j,i} = 0, \tag{10.a}$$

while from Eq. (9.b) and (10.a)

$$\forall\ i,k\ (i,k = 1,..,N^2+2N):\ c_{i,i,k} = -c_{i,k,i} = 0, \tag{10.b}$$

which implies that the condition (4) is satisfied according to (6.a) and (6.b).

When the numerical scheme conserves the total energy and the potential enstrophy for the whole system of shallow-water equations, the rotational kinetic energy and the enstrophy are conserved quantities for flows satisfying the condition $DF(t)=0$. Therefore, for these schemes the purely rotational interactions satisfy the Liouville theory and the rotational kinetic energy spectrum can change only as a result of the divergent vorticity forcing. However, it is worth to mention that the condition in the above presented statement is valid even for a much wider group of the numerical schemes than the group of the potential enstrophy and the total energy conserving schemes. On the other hand, the conservation of the potential enstrophy together with the conservation of the total circulation provide a realistic (continuous-type) control for the enstrophy via Eq. (Part I. 23).

Summarizing, a total circulation, potential enstrophy, and total energy conserving scheme is an optimal model to investigate the spectral energetics of

a shallow-water flow in the sense that it provides the quasi-conservation of enstrophy in addition to the satisfaction of the Liouville theory for the purely rotational interactions.

3. Numerical experiments

Numerical experiments were carried out by a finite-difference scheme which conserves the total energy, the circulation and the potential enstrophy (*Arakawa* and *Lamb*, 1981); therefore this model satisfies the optimum condition which was derived in the previous section. The domain used in numerical experiments is bounded by $x,y=0$ km, and $x,y=1920$ km, where cyclic boundary conditions are applied in both directions. The Coriolis parameter f is $10^{-4}\,s^{-1}$, and the acceleration of gravity g is $9.8\ ms^{-2}$. The bottom topography is sinusoidal-shaped and generates divergent kinetic energy only at the wavenumber $K=1$. Experiments were carried out with three different maximum-height bottom topographies: $h_{smax}=1$ km, 2 km, 3 km. The grid size in every experiments is $d=60$ km. The time derivative is approximated by leap-frog differencing and Heun scheme in the first and once in every 50 time steps, while the time interval is $\Delta t=1$min. The initial condition is a uniform zonal current of 10 m/s with $h(x,y,t_0)=5$ km height of the free surface. It should be mentioned that for these initial conditions $DF(t_0)=0$, but $\partial DF/\partial t(t_0)\neq 0$.

In both three experiments, the governing equations were integrated until the "energy catastrophe", when the numerical invariance of the total energy and the potential enstrophy is violated. The computation has broken down after 6200, 6100, and 5700 steps for $h_{smax}=1$ km, 2 km, and 3 km, respectively, as a consequence of overflow errors.

In order to compute the detailed spectral distribution of kinetic energy, the velocity field was splitting into its rotational and divergent parts $\vec{v}_r$, and $\vec{v}_d$. Computing double discrete Fourier transforms of $\vec{v}_r$, and $\vec{v}_d$, the rotational and divergent kinetic energy spectra may be evaluated by

$$E_{rot}(K) = \vec{v}_r^{\,2}(K), \tag{11.a}$$

$$E_{div}(K) = \vec{v}_d^{\,2}(K), \tag{11.b}$$

respectively, where the wavenumber K is defined by the eigenvalues of the finite-difference central Laplacian as

$$K^2(p,q) = (N/\pi)^2\,(\sin^2[\,p\,\pi/N\,] + \sin^2[\,q\pi/N\,]). \tag{12}$$

In order to describe phase errors associated with Eq. (12), the number of modes in wavenumber bands of unit width related to Eq. (12) may be computed and

the result of this computation can be found elsewhere (*Bennett* and *Middleton*, 1983; *Szunyogh*, 1992).

On purpose to describe more accurately the spectral changes of energy, the energy of individual modes were summed in each wavenumber bands of unit width, thus figures of this paper show the so-called band-summed energy spectra. However, in the case of the spectral computations the time evolution of the energy is presented only for h_{smax}=3 km, because of the strong similarity to the other cases.

4. Results and discussion

The time evolution of kinetic energy (*Fig. 1*) shows periodic changes in the first 5000 timesteps, but, as it can be seen, the amplitude of the changes is a function of the maximum height of topography. However, in this first period, the frequency and the amplitude of the energy oscillation do not change for a given experiment and the numerical instability occurs accidentally in the model in all three cases. Control computations have shown that in the first period of the sudden energy increase the model could allow the conservation of total energy and potential enstrophy, thus these conservation laws were violated only in the last few timesteps as a result of the numerical instabilities.

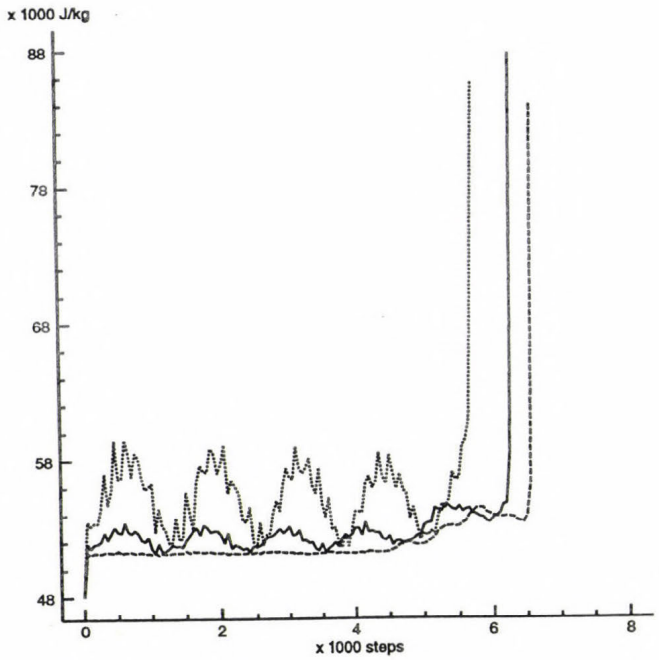

Fig. 1. Time evolution of the total kinetic energy for the different maximum height topographies (·····: h_{smax}=3 km, ———: h_{smax}=2 km, -------: h_{smax}=1 km).

Examination of the time evolution of kinetic energy is a proper way to detect main energetical changes in the model, but in this way we cannot obtain information about the causes leading to the sudden increase of the kinetic energy. Therefore, for the sake of deeper understanding of acting processes, time evolution of the rotational and divergent parts of kinetic energy (*Fig. 2*, and *Fig. 3*) have been computed. It can be seen that the rotational kinetic energy shows the same periodic changes as the total kinetic energy, which is not surprising if we take into consideration that the rotational part of the kinetic energy is at least three orders of magnitude higher than the divergent part of the kinetic energy. On the other hand, the divergent part of the kinetic energy shows higher frequency changes and the strong increase is started about after 5000 timesteps. In addition, it can be stated that the time evolution of the different types of energy is very similar for the different height topographies. More accurately, although there are considerable differences between the amplitudes of changes, there are no significant differences between the frequencies and the times of the energy catastrophe.

According to the earlier theoretical considerations (Part I) it can be expected that the sudden rotational kinetic energy increase is started when the quasi-two-dimensionality of the flow is violated. Taking into account the above mentioned theoretical considerations, the best index parameter of the quasi-two-dimension-

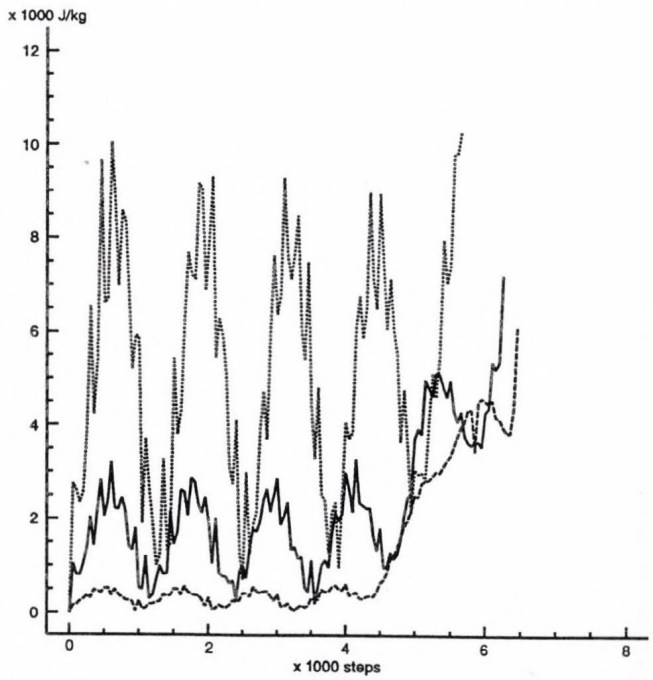

Fig. 2. Time evolution of the rotational part of the kinetic energy for different maximum height topographies. The meaning of the lines is the same as in Fig. 1.

ality is the average wavenumber whose time evolution is presented in *Fig. 4*. The model shows two-dimensional time evolution until the "energy catastrophe" since the average wavenumber remains under the value $K_1=2$, which defines an extremely stable "negative temperature" equilibrium for the spectral distribution of the rotational kinetic energy (*Szunyogh,* 1992). This means that the statistical mechanics of shallow-water flows are controlled by two-dimensional constraints, which provides extreme stability of the model in a statistical mechanical sense.

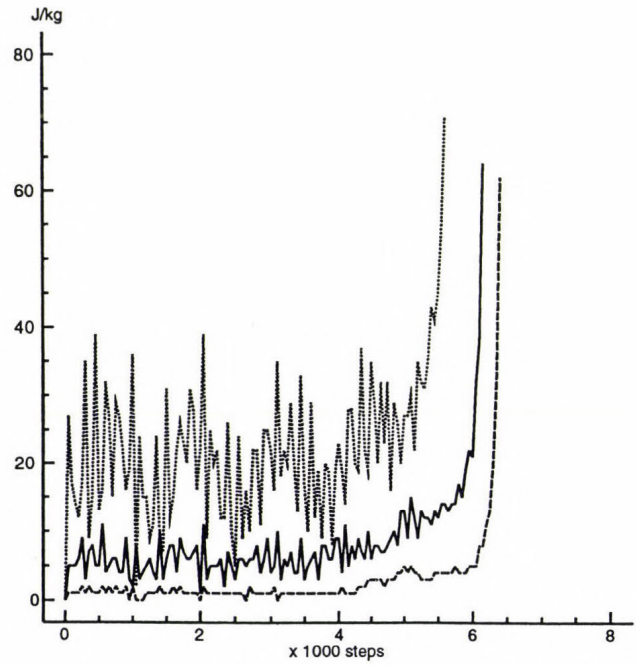

Fig. 3. Time evolution of the divergent part of the kinetic energy for the different maximum height topographies. The meaning of the lines is the same as in Fig. 1.

Since the applied numerical scheme provides the conservation of the the enstrophy and rotational kinetic energy in the absence of the divergent processes, purely rotational interactions cannot change the average wavenumber. In other words, the only effect which can produce an increase of the average wavenumber is the divergent vorticity forcing. More accurately, this forcing can increase the average wavenumber if it produces rotational kinetic energy at wavenumbers higher than the temporal average wavenumber of the flow. More specifically, average wavenumber changes are governed by spectral characteristics of the term $DF(t)$. In the presented experiments, at the first step the term $DF(t)$ is zero due to the initial conditions, thus there is no rotational

kinetic energy forcing. However, beginning with the next step the forcing term differs from zero since the topography necessarily produces divergence according to Eq. (Part I.17.b). The term $DF(t)$ is nonlinear as it can be seen from Eq. (2), therefore it can exchange the rotational and the divergent kinetic energy between different scales of rotational and divergent motions. It means that the divergent motion of a given wavenumber can produce rotational motions which is related to a higher wavenumber than the divergent process itself. This statement is valid only in the presence of rotational motions in the flow which can be described by wavenumbers higher than zero. In the presented

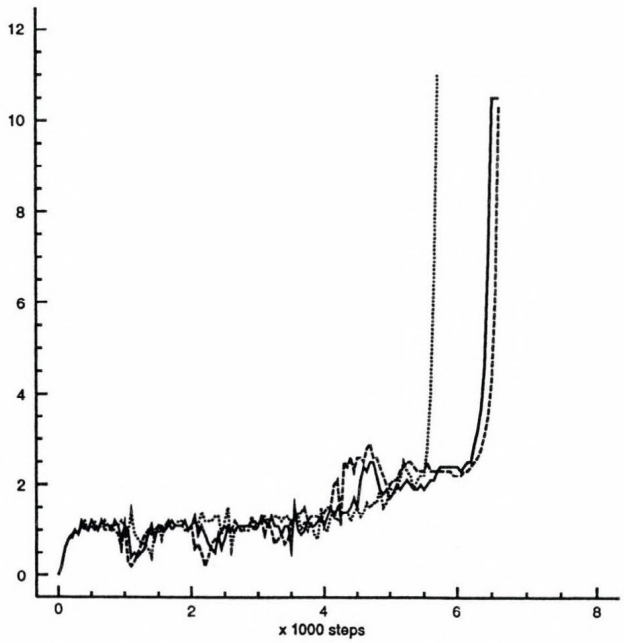

Fig. 4. Time evolution of the average wavenumber for the different height topographies. The meaning of the lines is the same as in Fig. 1.

experiments, the initial forcing occurs at the wavenumber $K=1$ (due to the spectral characteristics of the topography), while there are no rotational motions associated with wavenumbers higher than zero (due to the initial conditions for the velocity components). In this way, the rotational energy is forced under the wavenumber two. Unfortunately, this is true only in the first few steps since, as it was stated in Part I, the divergent kinetic energy evolves toward an equipartition among the wavenumber modes. It follows that the divergent kinetic energy flows to the higher wavenumbers independently of the wavenumber, where the divergent energy is fed into the model. The validity of

these ideas has been verified for our experiments (*Fig. 5*). In the first period, the divergent kinetic energy has only one spectral maximum near the wavenumber $K=1$, which is the scale of the orographical forcing. The divergent kinetic energy flows to the higher wavenumbers and a secondary spectral maximum is built up at the ninth wavenumber band. It indicates that the divergent kinetic energy is approaching to the equipartition at the higher wavenumbers since, as a consequence of the phase errors, the number of wavenumber modes is the highest in the ninth wavenumber band (*Szunyogh*, 1992). After 5700 timesteps (in the immediate vicinity of the energy catastrophe) the divergent kinetic energy is distributed equipartitionally at the wavenumbers higher than $K=5$, and the secondary maximum appears at the scale of the orographical forcing.

As a result of the above described process, rotational kinetic energy is forced at the higher wavenumbers. In order to investigate this process quantitatively, time evolution of the rotational kinetic energy has been computed

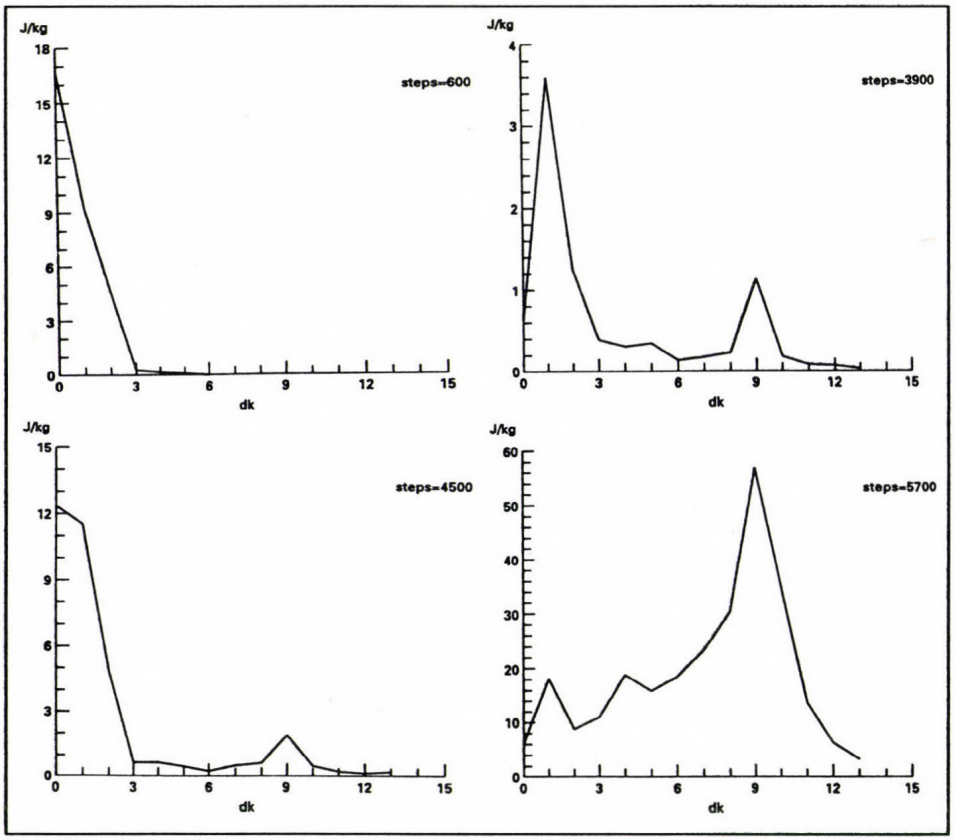

Fig. 5. Spectral distribution of the divergent kinetic energy for timesteps, when the kinetic energy is extremely high. The parameter $h_{smax}=3$ km.

for each wavenumber band and the results are presented in *Fig. 6* for some selected wavenumber bands. Since the magnitude of the divergence (or divergent energy) is much less than the magnitude of the rotational kinetic energy, rotational kinetic energy of the higher wavenumbers is very low and practically negligible in the first period but, as it can be seen, the invariance of the average wavenumber (which is the strongest two-dimensional constraint) has no influence on the rotational kinetic energy of the wavenumbers higher than $K=5$. After the well-balanced first period the rotational kinetic energy of the higher wavenumbers starts to increase suddenly as a consequence of the strongly nonlocal (and so extremely effective) two-dimensional rotational interactions. At the end, the sudden rotational kinetic energy increase leads to the "energy catastrophe". It should be mentioned that the fastest kinetic energy increase can be observed in the ninth wavenumber band due to the highest number of the wavenumber modes. This fact confirms the statement that phase errors and alised interactions (which amplify the effects of the phase errors) play an important role in statistical mechanics (or, in other words, in the spectral energetics) of the finite-difference models of the atmosphere.

5. Conclusions

It has been shown that the Eulerian shallow-water system of equations shows quasi-two-dimensional behavior as a consequence of the conservation of potential enstrophy and total circulation. Validity of the theoretical considerations has been verified by numerical experiments. The applied numerical scheme is optimal for investigating the spectral energetics of the shallow-water system in the sense that it provides the conservation of the potential enstrophy, the total circulation and satisfies the Liouville theory for purely rotational interactions. The experiments have revealed that the time of the "energy catastrophe" is closely independent of the maximum height of the topography. This fact indicates that the principal cause of the energy catastrophe is the developement of the unstable energy distribution, while the amplitude of the energy oscillation plays only a secondary role. This means that the shape of the topography plays a more important role in the development of the numerical instabilities than the height of the topography. In the first period of the model integration the spectral characteristics of the topography play a predominant role in the spectral distribution of divergent kinetic energy. However, after this first period (in the presented experiments after 5000 timesteps) the shape of the divergent kinetic energy spectrum becomes independent of the spectral characteristics of the initial conditions and this fact necessarily leads to "energy catastrophe".

The presented results are in a good accordance with the well-known fact that long-term numerical integrations of the shallow-water equations require the control of the high-frequency divergent perturbations (by normal-mode initial-

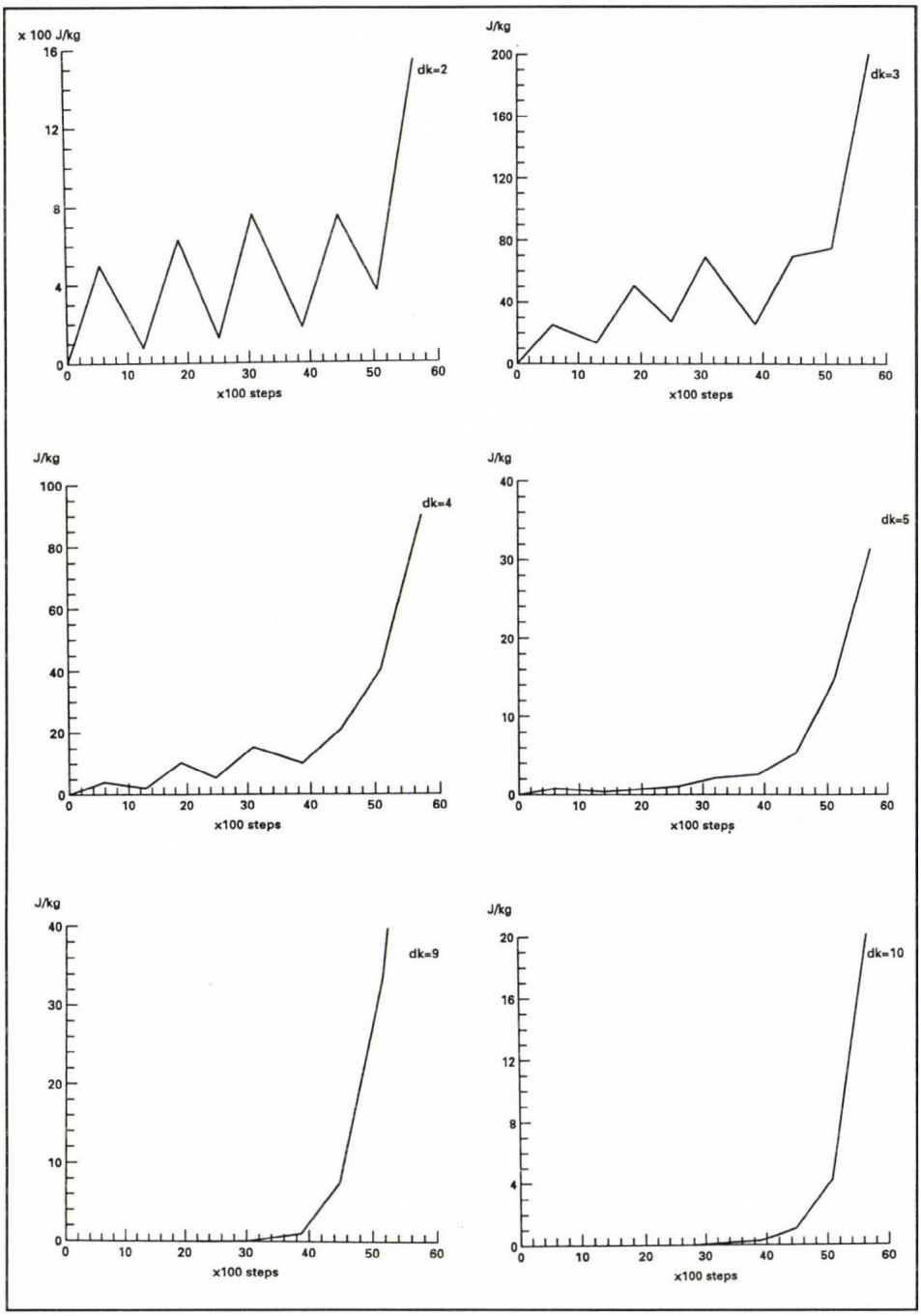

Fig. 6. Time evolution of the rotational kinetic energy for some selected wavenumber bands *dk*. The parameter h_{smax}=3 km.

ization or with the introduction of artificial viscosity). However, it must be stated that the absence of realistic parametrization of the subgrid physical processes is not the only cause of the existence of uncontrolled high-frequency perturbations as it is considered in many papers. Namely, discretization of the Eulerian fluid dynamical equations necessarily restricts the infinite number of the independent potential vorticity type invariants (the infinite number of the independent constraints) to one or two invariants. In other words, taking into consideration the relation between the vorticity-type integral (Casimir) invariants in the Eulerian form of the equations and the individual invariants in the Lagrangian form of the equations (*Shepherd*, 1990), discretizations of the Eulerian equations necessarily violate the individual conservation laws. For instance, in the presented experiments the conservation of total circulation and potential enstrophy could not control the disturbances whose spatial frequency was higher than $K=5$.

Finally, the above considerations call the attention to danger of the method trying to describe the long-term behavior of the atmosphere on the basis of numerical experiments, which are carried out by extremely low-resolution numerical models. These models are discretized, strongly truncated Eulerian models which are really far from the simulated continuous physics with individual conservation laws. In addition, the spectral energetics of these models cannot be controlled by two-dimensional constraints since do not possess statistical mechanical equilibrium states because of the strongly limited number of interactions.

References

Arakawa, A. and *Lamb, R.V.*, 1981: A potential enstrophy and energy conserving scheme for the shallow water equations. *Mon. Wea. Rev. 109*, 18-36.

Basdevant, C. and *Sadourny, R.*, 1975: Ergodic properties of inviscid truncated models of two-dimensional incompressible flows. *J. Fluid Mech. 69*, 673-688.

Bennett, A.F. and *Middleton, J.F.*, 1983: Statistical mechanics of a finite-difference approximation to the barotropic vorticity equation. *Quart. J. Roy. Meteorol. Soc. 109*, 795-808.

Kraichnan, R.H., 1975: Statistical dynamics of two-dimensional flow. *J. Fluid Mech. 67*, 155-175.

Shepherd, T.G., 1990: Symmetries, conservation laws, and Hamiltonian structure in geophysical fluid dynamics. *Adv. Geophys. 32*, 287-338.

Szunyogh, I., 1992: Statistical mechanics of inviscid truncated models of two-dimensional incompressible flows. *Időjárás 96*, 22-31.

Szunyogh, I., 1993a: Finite-dimensional quasi-Hamiltonian structure in simple model equations. *Meteorol. Atmos. Phys.* 52, 49-57.

Szunyogh, I., 1993b: The dynamics of a shallow-water flow over topography. Part I. Theory. *Időjárás 97*, 73-85.

APPENDIX

Using an arbitrary finite-difference scheme to discretize Eq. (3) the model equations can be written as

$$\frac{\partial \zeta_{l,m}}{\partial t} = \partial_{l,m}(\zeta + f, \Delta^{-1}\zeta), \; -N/2 \le l,m \le N/2, \tag{A.1}$$

where l and m denote the position of the gridpoints in each direction, and $\partial_{l,m}(.,.)$ is the finite-difference approximation to the two-dimensional Jacobian. On the finite-difference grid the two-dimensional discrete Fourier transformation is defined by

$$\zeta_{p,q} = \frac{1}{(N+1)^2} \sum_{m=-N/2}^{N/2} \sum_{l=-N/2}^{N/2} \zeta_{m,l} e^{i(pm+ql)}, \tag{A.2}$$

where the spectral coefficients $\zeta_{p,q}$ satisfy the following relation:

$$\zeta_{m,l} = \sum_{p=-N/2}^{N/2} \sum_{q=-N/2}^{N/2} \zeta_{p,q} e^{-i(pm+ql)}. \tag{A.3}$$

Taking into account Eq. (A.2) and Eq. (A.3), the system of complex spectral equation is

$$\frac{\partial \zeta_{p,q}}{\partial t} = \partial_{p,q}(\zeta + f, \Delta^{-1}\zeta), \tag{A.4}$$

where $\partial_{p,q}(.,.)$ is the spectrally transformed form of the finite-difference Laplacian $\partial_{l,m}(.,.)$. Using the conservation of total circulation and the assumption $f=const$, the variable $\zeta_{0,0}$ becomes independent of time, thus it can be removed from the prognostical vector variable. Moreover, since the grid values are real, the spectral coefficients satisfy the relation

$$\zeta_{p,q} = \zeta^*_{-p,-q}, \tag{A.5}$$

where the star denotes the complex conjugate. It means that only N^2+2N variables are independent of the $2(N+1)^2$ prognostical variables in Eq. (4). According to this fact a new vector variable can be introduced, whose components are defined by the following index transformation:

$$\zeta_{P,Q} := Re(\zeta_{p,q}) = Re(\zeta_{-p,-q}),$$

$$\zeta_{P',Q'} := Im(\zeta_{p,q}) = -Im(\zeta_{-p,-q}),$$

$$-N/2 \le P \le N/2; \;\; 0 \le Q \le N/2.$$

$$(\zeta_1, \zeta_2, \ldots, \zeta_{N^2+2N}) = (\zeta_{-N/2,0}, \ldots \zeta_{N/2,N/2}, \; \zeta_{-N/2',0'}, \ldots \zeta_{N/2,N/2'}). \tag{A.6}$$

Using this notation, Eq. (A.4) takes the form

$$\frac{\partial \zeta_i}{\partial t} = \sum_{j=1} \sum_{k=1} c_{i,j,k} K_j^{-2} \zeta_j \zeta_k, \quad i,j,k = 1,..,N^2+2N, \tag{A.7}$$

where $K_j^2 = K^2(p,q)$ are the eigenvalues of the finite difference Laplacian $\Delta_{m,l}^2$ and the coefficients $c_{i,j,k}$ are defined by $\partial_{p,q}(.,.)$.

***

Errata—In Part I (*Szunyogh, 1993b*) of this work equations (17.b) and (20.b) were incorrectly given by the author. In a correct way they are

$$\frac{\partial \delta}{\partial t} = \vec{k} \nabla \times (\zeta + f) \vec{v} - \Delta \left(\Phi + \frac{\vec{v}^2}{2} \right), \tag{17.b}$$

and

$$\frac{\partial}{\partial t} E_\kappa = \vec{v}_\kappa \nabla \Delta^{-1} \frac{\partial \delta}{\partial t} = f(\vec{v}_\psi, \vec{v}_\kappa, \Phi). \tag{20.b}$$

IDŐJÁRÁS

Quarterly Journal of the Hungarian Meteorological Service
Vol. 97, No. 3, July–September 1993

An application of multiregression model for evaluation of precipitation chemistry

S. F. Rajšić and **Z. B. Vukmirović**

Institute of Physics,
Pregrevica 118, 11080 Belgrade-Zemun, Yugoslavia

(Manuscript received 7 May 1993; in final form 13 September 1993)

Abstract—Using the five-year data sets for stations from EMEP network of the former Yugoslavia, the multiregression model is successfully applied for evaluation of basic relations relevant for precipitation chemistry. Such type of supervising pollutant transmission in the lower troposphere is appropriate for national monitoring and should be recommended to non-developed countries. A meritorious estimate of exported and imported amounts of pollutants, as well as regional and local contributions, could be established in the episodes with precipitation by applications of the proposed multiregression model with stepwise variable selection.

Key-words: precipitation chemistry, multi-variable regression, EMEP network.

1. Introduction

On the basis of detailed analysis of multi-year data sets for precipitation using a multiregression model (*Prat et al.*, 1983), the authors of this work have applied successfully this method to available data sets from the sites in Yugoslavia (*Vukmirović*, 1983; *Rajšić*, 1991) and Belgium (*Rajšić et al.*, 1991). In the last attempt (*Rajšić*, 1991) a more sophisticated model has been used in which a stepwise variable selection is provided. Besides, an original method for "missing values" is developed and applied, thus improving available data base.

A measuring project according to the Cooperative Programme for the Monitoring and Evaluation of the Long-Range Transmission of Air Pollutants in Europe (EMEP) was implemented on Puntijarka station in 1977 (*Table* 1). In the following years other stations also began to operate. The last station included in EMEP network was Kamenički Vis (1983). Being in Serbia, this station is of particular interest for this work, so that first complete five-year

data sets in the period of 1984−1988 are chosen for analysis. 24-h precipitation samples were taken at the indicated stations (Table 1) and transported to the Central Laboratory of the Federal Hydrometeorological Institute in Belgrade. Sampling and chemical analysis were in accordance with the methodology established by EMEP (*EMEP*, 1977).

Table 1. Basic data for EMEP stations of the former Yugoslavia

Station	Coordinates		Altitude
	λ	φ	amsl (m)
Mašun (Slovenia)	14°22'	45°39'	1026
Puntijarka (Croatia)	15°58'	45°54'	988
Zavižan (Croatia)	14°59'	44°49'	1599
Kamenički V. (Serbia)	21°57'	43°24'	813
Ivan Sedlo (Bosnia-Herzegovina)	18°02'	43°46'	970
Lazaropolje (Macedonia)	20°42'	41°32'	1332

The aim of this work is to evaluate basic relations of microconstituents in precipitation and therefore to determine the common issues of the network. Also, it is important to point out the diversity of each station located in areas with different natural and anthropogenic precursor sources of microconstituents in precipitations.

2. Experimental procedure

Sampling was organized in non-automated devices in the intervals of 24 hours by 07 to 07 of next day. Only at Ivan Sedlo station in the last year (1988) an automated sampler "ERNI" (Swiss) was applied. Every day samplers were cleaned by rinsing with distilled water.

Precipitation samples collected are filtered into polyethylene bottles and maintained at cold dark place prior to the transport to the Central Laboratory.

A brief listing of analytical methods applied for measuring microconstituents is given as follows. Acidity of precipitations is measured by a pH-meter named "Radiometer", which is calibrated by buffers from the manufacturer in the range from 4.01 to 7.00 at temperature of 25°C. The accuracy is

$\pm 1\%$. Sulphate ions are determined by turbidimetric method on 400 nm. The sensitivity is 0.05 mg S l^{-1}. Nitrate ions are analyzed by spectrophotometric n-(1-naphthyl)ethylenediamine method (Griess's method) on 520 nm. The sensitivity threshold is 0.02 mg N l^{-1}. Spectrophotometric mercury thiocyanate method is used for chloride determination. The sensitivity threshold is 0.05 mg Cl l^{-1}. For ammonia, spectrophotometric indophenol method is applied with sensitivity threshold of 0.04 mg N l^{-1}.

Alkaline metals (Na and K) as well as alkaline-earth metals (Ca and Mg) are determined by atomic absorption method. The sensitivity threshold for all microconstituents was approximately 0.02 mg l^{-1}.

Obtained weighted average concentrations, expressed as amount of relevant microconstituent in mg l^{-1}, as well as a number of samples, in the period 1984–1988, are presented in *Table* 2.

Data sets are very representative for detailed statistical analysis. The most mineralized precipitations are those of Kamenički Vis. Of particular concern is high concentration of sulphates and nitrates. At the same station maximum number of days (67) with precipitations of $pH \leq 4.5$ has been found in the observed period. Then, Zavižan and Puntijarka follow and at the end Lazaropolje with only 6 days.

Table 2. Weighted average concentrations in mg l^{-1} (1984–1988)

Station	No. of samples	SO_4-S	NO_3-N	Cl	NH_4-N	Ca	Mg	Na	K
Mašun	511	0.88	0.39	1.47	0.27	1.03	0.30	0.59	0.25
Puntijarka	631	1.63	0.45	1.38	0.45	1.25	0.45	0.60	0.54
Zavižan	736	1.47	0.75	2.02	0.43	1.84	0.49	1.04	0.45
Kam. Vis	546	3.47	1.50	1.46	0.71	2.08	0.48	1.87	0.51
Ivan Sedlo	537	1.40	0.30	1.80	0.19	0.65	1.11	2.34	0.17
Lazaropolje	570	1.68	0.34	2.00	0.46	1.43	0.49	1.17	0.57

Statistical analysis is performed on AMSTRAD PC with 8087 coprocessor. The standard programmes: STATGRAF, QUATRO and STEPFOR for regression analysis are used. In addition to algorithm in procedure of regression, an original algorithm for iterative calculation of "missing values" is developed for the purposes of this work. Sometimes, the quantity of collected precipitation is not satisfactory for complete analysis or may be the analysis is unsuccessful, so that the calculation of "missing values" by model improves data bases (*Rajšić*, 1991). Using this model data base for all stations increased, approximately, from 10% to 30%.

The principal characteristic of chosen multiregression model is the stepwise variable selection which provides test of significancy of involved variables in each step. The procedure runs from zero independent variable and in every next step one variable is added. Previously tested variable may be insignificant in any next step. In this case it is automatically rejected from further study.

3. Results and discussion

The simplest multiregression model is that with one dependent variable (X_1) and two independent variables (X_2 and X_3):

$$X_1 = a_1 + a_2X_2 + a_3X_3,$$

for which the correlation coefficient, R, can be expressed as:

$$R_{1.23} = \sqrt{\frac{r_{12}^2 + r_{13}^2 - 2\,r_{12}\,r_{13}\,r_{23}}{1 - r_{23}^2}},$$

where r represents the coefficients of linear correlation and indices show corresponding pairs of variables.

The correlation matrices of linear correlation coefficients are presented in *Table 3*. The relations selected by proposed model are given in *Table 4*. Besides, the principal microconstituents significancy test is performed for correlation with precipitation height (mm). Poor negative correlation is found mostly for dilution effect, except at Kamenički Vis, where precipitations were the most mineralized. No good correlation of H^+-ion with other ions is found, while the situation becomes better when pH has been introduced. The similar conclusion concerning H^+ has been found for Hungary (*Horváth* and *Mészáros*, 1984). Nevertheless, correlations for both forms are presented in Table 4.

As can be seen, better correlations are found for Cl (Table 3 and 4), then for SO_4-S and NO_3-N. Chloride ions might be of natural origin (NaCl), but SO_4^{2-} and NO_3^- are the indicators of strong acid presence in the lower troposphere.

Taking into consideration the continental background concentrations (*Szepesi* and *Fekete*, 1987) and the results of the analysis of meteorological factors influence (*Rajšić*, 1991), one may conclude that acid precipitations at Kamenički Vis are not only transported from Western Europe, but that a contribution from short-regional scale is also significant. Probably, industrial sources in Kosovo as well as Bor mining and smeltering basin influence the elevated acidity and relatively higher concentrations of sulphate and nitrate

Table 3. Correlation matrices for EMEP network of the former Yugoslavia in the period 1984 – 1988

	mm	pH	SO_4–S	NO_3–N	NH_4–N	Na	Mg	Ca	Cl	K	H^+
Mašun											
mm	1.00	–0.09	–0.31	–0.18	–0.26	–0.17	–0.21	–0.23	–0.18	–0.17	–0.04
pH	–0.09	1.00	0.20	0.16	0.08	0.20	0.25	0.34	0.15	0.18	–0.66
SO_4–S	–0.31	0.20	1.00	0.45	0.50	0.21	0.36	0.39	0.36	0.21	0.01
NO_3–N	–0.18	0.16	0.45	1.00	0.23	0.22	0.34	0.33	0.26	0.31	–0.03
NH_4–N	–0.26	0.08	0.50	0.23	1.00	0.16	0.13	0.21	0.17	0.24	0.05
Na	–0.17	0.20	0.21	0.22	0.16	1.00	0.22	0.25	0.67	0.77	–0.07
Mg	–0.21	0.25	0.36	0.34	0.13	0.22	1.00	0.62	0.21	0.24	–0.13
Ca	–0.23	0.34	0.39	0.33	0.21	0.25	0.62	1.00	0.25	0.32	–0.12
Cl	–0.18	0.15	0.36	0.26	0.17	0.67	0.21	0.25	1.00	0.42	–0.01
K	–0.17	0.18	0.21	0.31	0.24	0.77	0.24	0.32	0.42	1.00	–0.05
H^+	–0.04	–0.66	0.01	–0.03	0.05	–0.07	–0.13	–0.12	–0.01	–0.05	1.00
Puntijarka											
mm	1.00	–0.14	–0.24	–0.19	–0.24	–0.22	–0.19	–0.26	–0.30	–0.23	–0.00
pH	–0.14	1.00	0.19	0.04	0.26	0.05	0.30	0.36	0.28	0.36	–0.66
SO_4–S	–0.24	0.19	1.00	0.44	0.52	0.25	0.34	0.49	0.52	0.46	0.03
NO_3–N	–0.19	0.04	0.44	1.00	0.17	0.39	0.28	0.30	0.31	0.22	0.04
NH_4–N	–0.24	0.26	0.52	0.17	1.00	0.20	0.23	0.36	0.49	0.45	0.00
Na	–0.22	0.05	0.25	0.39	0.20	1.00	0.29	0.28	0.39	0.25	0.01
Mg	–0.19	0.30	0.34	0.28	0.23	0.29	1.00	0.55	0.28	0.41	–0.09
Ca	–0.26	0.36	0.49	0.30	0.36	0.28	0.55	1.00	0.46	0.41	–0.09
Cl	–0.30	0.28	0.52	0.31	0.49	0.39	0.28	0.46	1.00	0.65	–0.09
K	–0.23	0.36	0.46	0.22	0.45	0.25	0.41	0.41	0.65	1.00	–0.12
H^+	–0.00	–0.66	0.03	0.04	0.00	0.01	–0.09	–0.09	–0.09	–0.12	1.00
Zavižan											
mm	1.00	0.01	–0.25	–0.18	–0.19	–0.19	–0.21	–0.20	–0.22	–0.21	–0.07
pH	0.01	1.00	–0.07	–0.07	–0.18	0.13	0.22	0.31	0.12	0.13	–0.64
SO_4–S	–0.25	–0.07	1.00	0.47	0.64	0.34	0.31	0.57	0.42	0.49	0.26
NO_3–N	–0.18	–0.07	0.47	1.00	0.27	0.37	0.20	0.41	0.29	0.32	0.23
NH_4–N	–0.19	–0.18	0.64	0.27	1.00	0.18	0.14	0.21	0.21	0.32	0.31
Na	–0.19	0.13	0.34	0.37	0.18	1.00	0.15	0.33	0.67	0.31	0.01
Mg	–0.21	0.22	0.31	0.20	0.14	0.15	1.00	0.47	0.19	0.23	–0.08
Ca	–0.20	0.31	0.57	0.41	0.21	0.33	0.47	1.00	0.40	0.46	–0.06
Cl	–0.22	0.12	0.42	0.29	0.21	0.67	0.19	0.40	1.00	0.45	0.05
K	–0.21	0.13	0.49	0.32	0.32	0.31	0.23	0.46	0.45	1.00	0.01
H^+	–0.07	–0.64	0.26	0.23	0.31	0.01	–0.08	–0.06	0.05	0.01	1.00

Continued Table 3

	mm	pH	SO_4–S	NO_3–N	NH_4–N	Na	Mg	Ca	Cl	K	H^+
Kamenički Vis											
mm	1.00	–0.10	–0.41	–0.29	–0.29	–0.13	–0.26	–0.39	–0.33	–0.35	–0.06
pH	–0.10	1.00	0.13	–0.02	0.11	–0.13	0.17	0.24	0.07	0.28	–0.56
SO_4–S	–0.41	0.13	1.00	0.37	0.42	0.09	0.37	0.55	0.50	0.57	0.08
NO_3–N	–0.29	–0.02	0.37	1.00	0.06	0.01	0.36	0.61	0.14	0.25	0.10
NH_4–N	–0.29	0.11	0.42	0.06	1.00	–0.04	0.20	0.09	0.17	0.23	0.12
Na	–0.13	–0.13	0.09	0.01	–0.04	1.00	0.00	0.13	0.57	0.23	0.05
Mg	–0.26	0.17	0.37	0.36	0.20	0.00	1.00	0.38	0.14	0.30	–0.02
Ca	–0.39	0.24	0.55	0.61	0.09	0.13	0.38	1.00	0.32	0.45	–0.02
Cl	–0.33	0.07	0.50	0.14	0.17	0.59	0.14	0.32	1.00	0.70	0.05
K	–0.35	0.28	0.57	0.25	0.23	0.23	0.30	0.45	0.70	1.00	–0.03
H^+	–0.06	–0.56	0.08	0.10	0.12	0.05	–0.02	–0.02	0.05	–0.03	1.00
Ivan Sedlo											
mm	1.00	0.03	–0.03	–0.07	–0.03	–0.01	–0.05	–0.07	–0.01	–0.06	–0.03
pH	0.03	1.00	–0.02	0.01	0.15	–0.08	–0.10	0.33	0.03	0.17	–0.71
SO_4–S	–0.03	–0.02	1.00	0.10	0.37	0.07	0.18	0.18	0.03	0.09	0.11
NO_3–N	–0.07	0.01	0.10	1.00	–0.01	–0.03	–0.03	0.66	0.13	0.27	0.01
NH_4–N	–0.03	0.15	0.37	–0.01	1.00	–0.05	–0.07	0.01	0.04	0.09	–0.06
Na	–0.01	–0.08	0.07	–0.03	–0.05	1.00	–0.10	0.00	0.43	0.06	–0.00
Mg	–0.05	–0.10	0.18	–0.03	–0.07	–0.10	1.00	0.12	–0.13	0.16	0.20
Ca	–0.07	0.33	0.18	0.66	0.01	0.00	0.12	1.00	0.29	0.64	–0.12
Cl	–0.01	0.03	0.03	0.13	0.04	0.43	–0.13	0.29	1.00	0.30	–0.04
K	–0.06	0.17	0.09	0.27	0.09	0.06	0.16	0.64	0.30	1.00	–0.07
H^+	–0.03	–0.71	0.11	0.01	–0.06	–0.00	0.20	–0.12	–0.04	–0.07	1.00
Lazaropolje											
mm	1.00	–0.09	–0.24	–0.12	–0.17	–0.06	–0.14	–0.25	–0.16	–0.21	–0.06
pH	–0.09	1.00	0.14	0.00	0.32	–0.04	–0.06	0.25	0.17	0.24	–0.65
SO_4–S	–0.24	0.14	1.00	0.39	0.46	0.06	0.37	0.68	0.49	0.77	0.10
NO_3–N	–0.12	0.00	0.39	1.00	0.04	–0.01	0.09	0.29	0.09	0.37	0.09
NH_4–N	–0.17	0.32	0.46	0.04	1.00	0.02	0.02	0.30	0.35	0.49	–0.06
Na	–0.06	–0.04	0.06	–0.01	0.02	1.00	0.01	0.05	0.59	0.20	0.02
Mg	–0.14	–0.06	0.37	0.09	0.02	0.01	1.00	0.51	0.12	0.22	0.16
Ca	–0.25	0.25	0.68	0.29	0.30	0.05	0.51	1.00	0.37	0.58	0.01
Cl	–0.16	0.17	0.49	0.09	0.35	0.59	0.12	0.37	1.00	0.55	–0.10
K	–0.21	0.24	0.77	0.37	0.49	0.20	0.22	0.58	0.55	1.00	–0.02
H^+	–0.06	–0.65	0.10	0.09	–0.06	0.02	0.16	0.01	–0.10	–0.02	1.00

Table 4. Relations of microconstituents in precipitations from EMEP network of the former Yugoslavia in the period 1984–1988

Station	Principal relation	Correlation coefficient
Mašun		
	$pH = 5.57 + 0.08Na + O.11Ca$	R=0.36
	$H^+ = 9.18 - 3.69Mg$	R=0.13
	$SO_4^{2-} = 0.32 + 1.75NH_4 + 0.56Mg + 0.15Ca$	R=0.60
	$NO_3^- = 0.01 + 0.47NH_4 + 0.55Mg + 0.09Ca + 0.31K$	R=0.44
	$Cl^- = 0.86 + 0.28NH_4 + 1.07Na + 0.08Ca - 0.43K$	R=0.70
Puntijarka		
	$pH = 5.62 + 0.10Mg + 0.09Ca + 0.17K - 0.05NO_3$	R=0.46
	$H+ = 7.60 - 0.93Ca - 2.25K + 1.19SO_4$	R=0.18
	$SO_4^{2-} = 0.47 + 1.12NH_4 + 0.35Ca + 0.44K + 0.01H$	R=0.66
	$NO_3^- = 0.02 + 0.49Na + 0.28Mg + 0.16Ca$	R=0.47
	$Cl^- = 0.82 + 0.38NH_4 + 0.21Na - 0.17Mg + 0.13Ca + 0.54K$	R=0.75
Zavižan		
	$pH = 5.85 - 0.10SO_4 - 0.05NO_3 - 0.16NH_4 + 0.05Na + 0.09Mg + 0.11Ca + 0.09K$	R=0.50
	$H^+ = 4.48 + 2.98SO_4 + 1.90NO_3 + 7.76NH_4 - 1.04Na - 2.21Mg - 1.82Ca - 0.55K$	R=0.45
	$SO_4^{2-} = -0.09 + 1.82NH_4 + 0.10Na + 0.29Ca + 0.33K + 0.01H$	R=0.80
	$NO_3^- = -0.43 + 0.36NH_4 + 0.34Na + 0.27Ca + 0.27K + 0.03H$	R=0.55
	$Cl^- = 1.20 + 0.54Na + 0.07Ca + 0.47K$	R=0.72
Kamenički Vis		
	$pH = 5.56 - 0.04Na + 0.09Mg + 0.09Ca + 0.22K - 0.04SO_4 - 0.07NO_3$	R=0.47
	$H^+ = 10.50 + 8.57NH_4 - 1.91Ca + 2.20NO_3$	R=0.19
	$SO_4^{2-} = 0.96 + 1.42NH_4 + 0.29Mg + 0.32Ca + 0.90K + 0.01H$	R=0.74
	$NO_3^- = -0.65 + 0.53Mg + 0.61Ca + 0.01H$	R=0.65
	$Cl^- = 0.83 + 0.18NH_4 + 0.18Na + 0.86K$	R=0.83
Ivan Sedlo		
	$pH = 5.64 - 0.10SO_4 - 0.44NO_3 + 0.36NH_4 - 0.18Mg + 0.36Ca - 0.08Cl - 0.14K$	R=0.52
	$H^+ = 6.51 + 1.87SO_4 + 3.45NO_3 - 3.07NH_4 + 4.32Mg - 2.38Ca$	R=0.32
	$SO_4^{2-} = 0.68 + 0.01H + 1.01NH_4 + 0.02Na + 0.29Mg + 0.16Ca - 0.16K$	R=0.49
	$NO_3^- = -0.12 + 0.01H - 0.13Mg + 0.39Ca - 0.21K$	R=0.71
	$Cl^- = 1.47 + 0.07Na - 0.24Mg + 0.12Ca + 0.23K$	R=0.55
Lazaropolje		
	$pH = 5.96 + 0.24NH_4 - 0.03Na - 0.10Mg + 0.13Ca + 0.09K - 8SO_4 + 0.05Cl$	R=0.45
	$H^+ = 2.88 + 0.31Na + 1.00Mg - 0.64Ca + 0.63SO_4 - 0.96Cl$	R=0.29
	$SO_4^{2-} = -0.08 + 0.51NH_4 - 0.05Na + 0.22Mg + 0.49Ca + 1.34K + 0.04H$	R=0.84
	$NO_3^- = 0.20 - 0.34NH_4 - 0.03Na + 0.07Ca + 0.46K + 0.02H$	R=0.44
	$Cl^- = 1.08 + 0.43NH_4 + 0.27Na + 0.13Ca + 0.50K - 0.03H$	R=0.77

ions at this site. This is very important for the estimate of transboundary pollutant transport in the lower troposphere. The more complex analysis has shown that only 34% of SO_4^{2}-S at Kamenički Vis is originated from the import (*Rajšić*, 1991), the rest is from emitters in Serbia. A more detailed analysis will be published.

Very good correlations are found between anions observed and some cations like Na^+ and K^+. The best correlation with the highest contents is at Mašun and Zavižan (close to the seaside) indicating thus the influence of sea spray on NaCl and KCl contents in precipitations.

However, the best correlation for both linear and multi-regressions is found for SO_4^{2-} and NH_4^+ ions at all stations. The presence of $(NH_4)HSO_4$ or $(NH_4)_2SO_4$ confirms the intensive processes of transformation of SO_2 into H_2SO_4 and partially or completely neutralization of sulphuric acid with ammonia. Ammonia could be released by natural and anthropogenic sources. These results indicate the territory of the former Yugoslavia as a field of strong SO_2 emission originating from foreign and own sources.

The model is very appropriate for describing precipitation chemistry. In a situation without communication with other countries, precipitations reflect both behavior of neighbors and ourselves.

Finally, one network for precipitation chemistry under high-professional control is not so expensive, but offers very useful information for strategies of sustainable development and participation in the international activities for abatements of SO_2 and NO_x emissions.

4. Conclusion

On the basis of the obtained results, the following conclusions may be underlined:

- Multiregression with stepwise variable selection is recommended for describing diversity of sites included in one network with the same purpose.
- Application of the proposed multiregression model for precipitation chemistry provides very useful information on transformation and transport of atmospheric microconstituents relevant for environmental protection.
- This type of analysis is necessary in the network of a non-developed country for which an organization of automated monitoring of gaseous pollutants-precursors of acid rains, is too expensive.

Acknowledgements—The authors are very grateful to the *Federal Hydrometeorological Institute* for providing data bases from EMEP network of the former Yugoslavia. Also, the authors appreciate financial support received from the *Ministry of Science and Technology of the Republic of Serbia*. The particular acknowledgements of valuable help in development of the programme for "missing values" is given to *Ljubomir Rajšić*.

References

EMEP, 1977: *Manual for Sampling and Chemical Analysis*. EMEP/CHEM. 3.77, NILU, Lillestrøm.

Horváth, L. and *Mészáros, E.*, 1984: The composition and acidity of precipitation in Hungary. *Atmos. Environ. 18*, 1843-1847.

Prat, G.C., Coscio, M., Gardner, D.W., Chenone, B.I. and *Krupa, S.V.*, 1983: An analysis of the chemical properties of rain in Minnesota. *Atmos. Environ. 17*, 347-355.

Rajšić, S., 1991: *Consistency of Physico-Chemical Parameters for Transmission of Pollutant in the Troposphere*. Doc. Dissert., University of Belgrade, Faculty of Science, Belgrade.

Rajšić, S., Otten, P. and *Van Grieken, R.*, 1991: Chemical composition of rain water in Antwerp, Belgium. *Environ. Techn. 12*, 257-261.

Szepesi, D.J. and *Fekete, K.E.*, 1987: Background levels of air and precipitation quality for Europe. *Atmos. Environ. 21*, 1623-1630.

Vukmirović, Z.B., 1983: An application of regression model for determination of the precipitation acidity origin (Serbian). *Zaštita atmosfere 11*, 1-5.

IDŐJÁRÁS

Quarterly Journal of the Hungarian Meteorological Service
Vol. 97, No. 3, July–September 1993

Some data on the elemental composition of atmospheric aerosol particles in Xinjiang, NW China

A. Molnár[1], **L. Makra**[2], **Chen Yaning**[3] and **I. Borbély-Kiss**[4]

[1] *Department of Analytical Chemistry, University of Veszprém, P.O. Box 158, H-8201 Veszprém, Hungary*
[2] *Department of Climatology, University of Szeged, Egyetem u. 2, H-6722 Szeged, Hungary*
[3] *Xinjiang Institute of Geography, Chinese Academy of Sciences, Urumqi, Xinjiang, China*
[4] *Institute of Nuclear Research, P.O. Box 51, H-4001 Debrecen, Hungary*

(Manuscript received 1 July 1993; in final form 31 August 1993)

Abstract—Six aerosol samples were collected in the air over arid areas of NW China during a Hungarian expedition in 1990. The samples collected were analyzed by the PIXE method. The results of the analyses are presented and discussed.

Key-words: elemental composition of aerosol particles, PIXE, China.

1. Introduction

The elemental composition of atmospheric aerosol particles has been studied widely during the last two decades (e.g. *Mészáros*, 1991). This is due to the importance of such measurements for estimating the environmental impact of the particles on local, regional and global scales. Among other things, samplings in the atmosphere far from human influences were carried out under oceanic and continental conditions to investigate the global cycle of aerosols. In spite of these efforts (e.g. *Penkett et al.*, 1979; *Adams et al.*, 1983; *Morales et al.*, 1990; *Winchester et al.*, 1981) the chemical composition of aerosol particles over continents like Africa, South America and Asia is not well understood.

Thus, few information are available from the aerosol in the air over the vast inner regions of China (*Winchester* and *Wang*, 1989). Further, concentration data from an area near the Great Wall (*Winchester et al.*, 1981) and from

Huangshan mountain (Eastern China, *Xu et al.*, 1991) can also be found in the open literature.

The aim of this paper is to present the results of the analysis of aerosol samples collected in the air over Xinjiang, NW area of China (Central Asia).

2. *Sampling*

Aerosol samples were collected by means of Nuclepore polycarbonate filters with 0.4 μm pore size. The sampling time was 4–6 hours in the afternoon, during which 3–4 m^3 of air were sampled. The geographical position and characteristics of the sampling sites are given in *Table 1*. Generally speaking,

Table 1. Date of sampling and geographical position and description of sampling sites

Sample No.	Date	H (m)	φ (°N)	λ (°E)	Site description
1	17 June	1290	44°20'	84°50'	N slope of Tiensan (steppe)
2	18 June	420	44°50'	86°10'	Dzungaria (steppe)
3	19 June	0	42°30'	88°45'	Turfani basin (desert)
4	20 June	865	40°55'	86°20'	Takla-Makan (desert)
5	21 June	1255	42°20'	83°00'	Tiensan (mountain desert)
6	22 June	1950	43°50'	88°07'	E Tiensan (semi-arid)

each site was far from located areas, the distance from the nearest large city (Urumqi, with population of 1 million) varied between 100–400 km. The electric current necessary for the function of the pump was supplied by an electric generator. The exhaust gases from the generator were conducted downwind with a tube. After sampling the filters were placed in small plexiglass boxes sealed carefully. The filters remained in these boxes until their analysis by PIXE in Hungary.

3. *Results and discussion*

The results of the analyses of samples are summarized in *Table 2*, where the absolute concentrations as well as the enrichment factors are given. These latter data were calculated relative to aluminum by using average crustal fractions reported by *Mason* (1966).

One can see from the numbers listed that elements like silicon, sulfur, calcium and iron were found in a relatively high concentration. While silicon, calcium and iron have enrichment factors below about 10 proving their soil origin, sulfur is enriched considerably at all sites indicating its formation either by gas-to-particle conversion or by the disintegration of the surface, the sulfur

Table 2. Concentration (x: ngm^{-3}) and enrichment factor (EF) of different elements in the atmospheric aerosol over the regions of NW China

Element	Sample 1		Sample 2		Sample 3		Sample 4		Sample 5		Sample 6	
	x	EF	x	EF	x	EF	x	EF	x	EF	x	EF
Al	66.8	1	82.7	1	195.5	1	991.6	1	152.9	1	162.2	1
Si	222.9	0.79	259.3	0.74	711.8	0.86	4752	1.1	656.4	1.0	851.2	1.2
P	<6.3		<5.1		<5.9		<9.6		<5.9		<5.1	
S	115.5	824	120.5	694	163.6	398	619.6	298	123.0	383	177.5	521
Cl	76.5	954	50.9	513	77.1	329	666.2	560	56.2	306	58.7	276
K	69.5	4.7	54.1	3.0	173.9	4.0	1326	6.0	139.2	4.1	164.6	4.6
Ca	133.1	6.0	186.6	6.7	473.6	7.3	5231	15.8	668.5	13.1	478.8	8.8
Ti	7.65	2.8	6.37	1.9	21.1	2.6	150.0	3.7	24.0	3.8	28.7	4.3
V	<1.2		<1.0		<1.3		4.24	5.5	<1.3		1.3	10.3
Cr	7.31	177	5.40	105	8.18	67.5	24.4	39.6	6.89	72.7	7.99	79.5
Mn	1.19	2.1	1.44	2.1	5.65	3.5	25.2	3.1	3.23	2.5	4.44	3.3
Fe	126.3	3.7	113.5	2.7	348.4	3.5	1884	3.7	315.5	4.0	374.9	4.5
Co	<2.1		<1.8		<3.2		33.6	106.6	3.85	79.2	<3.1	
Ni	<0.9		0.68	15.1	1.86	17.6	19.1	35.6	1.12	13.5	0.99	11.2
Cu	<0.7		0.89	21.7	0.98	10.1	7.78	15.6	1.38	18.2	1.35	16.7
Zn	<0.9		1.65	40.2	3.52	36.3	25.9	52.6	2.49	32.8	2.17	27.0
As	<3.2		<1.7		<2.0		13.5	1099	2.66	1400	1.32	656
Pb	9.49	1478	<5.9		<5.5				<7.6		<5.7	

content of which is very different in this area from the average crustal composition reported by *Mason* (1966). Besides, the concentration of aluminum and potassium is also high. They also originate from the Earth crust. The concentration of the elements of soil origin is important in particular for sample of number 4. This is understandable since sampling was carried out in this case under desertic conditions when the air was very dusty.

The case of chlorine should be mentioned separately. Its concentration level is very significant in spite of the fact that oceanic influences can practically be excluded. In addition, the Cl enrichment factor is between 300 and 900 similar to that of sulfur. It is proposed with caution that this is due to the fact that soils are rather salty and several lakes contain a lot of sodium chloride in the regions considered. Anyway, similar results were obtained in Sudan, Africa (*Penkett et al.*, 1979). Penkett and his coworkers attributed this finding to the disintegration of salt flats and to the evaporation of rainwater leaving a salt rich layer.

The concentration of some notorious pollutants like lead, zinc, copper and vanadium is generally low. Even, the enrichment factor of zinc, copper and vanadium has a magnitude of ten which indicates that they are at least partly of crustal origin. On the other hand, chromium was found in a concentration similar to that measured over Hungary (*Molnár et al.*, 1993). Also, this element was enriched like in the air over industrial areas. Thus, it cannot be ruled out that Cr level reflects the effect of the city Urumqi, where iron smelting is an important human activity. It is also possible, however, that chromium is of crustal origin (*Nriagu,* 1989) and its concentration in soils of this area is higher than the average (see *Mason,* 1966). This latter hypothesis is supported by the fact that the highest chromium concentration was found over the Takla-Makan desert.

It should be also noted that no clear changes in concentration are found if we consider our data as a function of the altitude above the sea level. This seems to indicate that the effects of the underlying surface are practically independent of the height for a vast region. However, much more measurements would be necessary to obtain a clear vertical pattern.

4. Comparison with other data

It is attempted to compare our data with those of *Penkett et al.* (1979) and *Annegarn et al.* (1983) gained in China, Sudan and Namibia, respectively. These results are of great value since they are based on samplings done *in situ* under desertic conditions. Data tabulated indicate (see *Table 3*) that in Sudan, when winds blow from the Sahara, the concentrations of different elements are very high and they are in general agreement with our results for Takla-Makan (sample No. 4, see Table 2). On the other hand, data published for Namibia agree rather well with our other results. This obviously means that aerosol composition is a function of the extension of the desertic area as well as of the

Table 3. Concentration of different elements in atmospheric aerosol particles in Sudan during Sahara wind (*Penkett et al.*, 1979) and in the Namib desert (*Annegarn et al.*, 1983). The values are expressed in ngm^{-3}

Element	Al	Fe	Ca	K	S	Cl	Cu	V	Ti	Mn	Zn	Cr
Sudan	3030	2996	< 1000	-	767	970	49	9	-	35	31	1
Namibia	-	246	425	94	264	616	< 0.8	3	22	4	~ 1	2

meteorological conditions during sampling. We emphasize again that at each desertic site chlorine in the aerosol particles has a higher level than sulfur. Finally, chromium concentrations over NW China are surprisingly high, mainly over the Takla-Makan desert.

References

Adams, F., Van Espen, P. and *Maenhaut, W.*, 1983: Aerosol composition at Chacaltaya, Bolivia, as determined by size-fractionated sampling. *Atmos. Environ. 17*, 1521-1536.

Annegarn, H.J., Van Grieken, R.E., Bibby, D.M. and *Von Blottnitz, F.*, 1983: Background aerosol composition in the Namib desert, South West Africa (Namibia). *Atmos. Environ. 17*, 2045-2053.

Mason, B., 1966: *Principles of Geochemistry*. Wiley, New York.

Mészáros, E., 1991: The atmospheric aerosol. In *Atmospheric Particles and Nuclei* (G. Götz, E. Mészáros and G. Vali). Akadémiai Kiadó, Budapest, 17-84.

Molnár, A., Mészáros, E., Bozó, L., Borbély-Kiss, I., Koltay, E. and *Szabó, Gy.*, 1993: Elemental composition of atmospheric aerosol particles under different conditions in Hungary. *Atmos. Environ.* (accepted for publication).

Morales, J.A., Hermoso, M., Serrano, J. and *Sanhueza E.*, 1990: Trace elements in the Venezuelan savannah atmosphere during dry and wet periods, with and without vegetation burning. *Atmos. Environ. 24A*, 407-414.

Nriagu, J.O., 1989: A global assessment of natural sources of atmospheric trace metals. *Nature 338*, 47-49.

Penkett, S.A., Atkins, D.H.F. and *Unsworth, M.H.*, 1979: Chemical composition of the ambient aerosol in the Sudan Gezira. *Tellus 31*, 295-307.

Xu, J., Hu, H. and *Zhou, J.*, 1991: Model study of atmospheric aerosols in some typical places of China. *J. Aerosol Sci. 22*, S625-S628.

Winchester, J.W., Lü Weixiu, Ren Lixin and *Wang Mingxing*, 1981: Fine and coarse aerosol composition from a rural area in North China. *Atmos. Environ. 15*, 933-937.

Winchester, J.W. and *Wang, M.-X.*, 1989: Acid-base balance in aerosol components of the Asia-Pacific region. *Tellus 41B*, 323-337.

IDŐJÁRÁS

Quarterly Journal of the Hungarian Meteorological Service
Vol. 97, No. 3, July–September 1993

Decreasing concentration of air pollutants and the rate of dry and wet acidic deposition at the three forestry monitoring stations in Hungary

L. Horváth[1], **Gy. Baranka**[1] and **E. Gy. Führer**[2]

[1] *Institute for Atmospheric Physics,*
P.O. Box 39, H-1675 Budapest, Hungary
[2] *Forest Research Institute,*
Frankel Leó u. 44, H-1023 Budapest, Hungary

(Manuscript received 29 March 1993; in final form 23 August 1993)

Abstract—Concentration and dry+wet deposition of acidic atmospheric pollutants were determined in three Hungarian forestry monitoring stations between 1988 and 1992. Concentration of most important acidic compounds (sulfur and nitrogen dioxide) does not reach the critical level therefore forest decline as consequence of direct effects (foliar uptake through stomata) may be excluded. Total (dry+wet) deposition of acidic pollutants are 187 mg H^+ m^{-2} yr^{-1} as an average of 3 stations. The acidic load at Hungarian forestry stations frequently exceeds the critical value recommended by international organizations. Though concentration and deposition of atmospheric acidic compounds has considerably decreased in the recent years, further monitoring of acid deposition in forests is necessary because the accumulation effects of acid load to forest soil.

Key-words: forest decline, acid deposition, critical load.

1. Introduction

Forest decline occurring in some North American and Central European forests during the recent decades is attributed to anthropogenic air pollution and acidic deposition according to some authors.

Harmful effect of air pollution on forest health may be direct and/or indirect. In the case of direct impact, air pollutants through stomata initiate biochemical processes resulting in toxic effects, e.g. radical pathology. Deposition can affect the leaves directly, mostly if the leaves are destructed by some oxidants (O_3, H_2O_2).

Indirect effect of acidic substances appears in the long term acidification of forest soil. In Hungary the opinions differ concerning the primary cause of forest decline. *Stefanovits* (1986) pointed out that the pH of some Hungarian forest soil has decreased by 0.4–1.9 unit during 20–30 years as a consequence of deposition and accumulation of acidic pollutants.

In the country serious problems in sessile oak forests mostly in the northern area of Hungary have been observed. According to *Jakucs* (1986) mostly the indirect effect of acidic deposition is responsible for decline of sessile oaks. On the other hand the majority of foresters and ecologists believes that forest damages are as the consequence of different biotic and abiotic effects.

Phenomena above mentioned, i.e. acidification of forest soils, forest decline, furthermore the fact that Hungary belongs to moderately polluted countries in Europe (*Horváth*, 1989a) support the need for continuous monitoring of the rate and trend of atmospheric acidic deposition in Hungarian forests.

For these reasons Forest Research Institute and Institute for Atmospheric Physics of Hungarian Meteorological Service have started a monitoring program in 1988 at three forestry monitoring stations. Preliminary results for the stations has been reported elsewhere (e.g. *Horváth* and *Führer*, 1991; *Führer* and *Horváth*, 1992). The aim of this paper is to summarize the results of the first five years of the monitoring program (1988–1992).

It should be mentioned here that beside acidic compounds there is an other important group of compounds which can be responsible for forest damages, namely the photooxidants (ozone) and free radicals generating by the reaction between ozone and alkenes (*Möller*, 1988). Modeling and monitoring the effect of photooxidants on forest are the subject of one of our research projects.

The aims of this paper are to calculate the concentration and deposition of acidic compounds for forests and compare them with standards and recommendations. By this comparison we can make an attempt to decide, if the acidic components may influence the forest health in Hungary.

2. Measuring program of the monitoring stations

The three forestry monitoring stations are located in pine forests at the west and the middle of Hungary (Farkasfa: $\varphi = 45°55'$, $\lambda = 16°18'$, $H = 312$ m and K-puszta: $\varphi = 46°58'$, $\lambda = 19°33'$, $H = 126$ m, respectively) as well as in the Mátra-Mountains, north-east of Hungary (Nyírjes: $\varphi = 47°54'$, $\lambda = 19°58'$, $H = 560$ m).

Forestry stations were located on openings in the forest. The generally recommended siting criteria (approximately 50 m distance from forest edge)

are fulfilled at Nyírjes and Farkasfa stations. At K-puszta station the 10 m height sampling tube is located above the canopy so the canopy influences can be practically neglected.

Sampling and measuring program of the three stations involves the determination of the daily 24h average of the most important acidic gaseous pollutants including sulfur dioxide, nitrogen dioxide, nitric acid and ammonia and chemical composition of aerosol particles (ammonium, sulfate and nitrate). Chemical composition of precipitation is also measured on the basis of monthly wet-only sampling. In this paper concentrations of ammonium, sulfate and nitrate measured in the program are reported. Dry and wet deposition rates has been calculated by use of concentrations measured in the air or in the precipitation water and of the dry deposition velocity (cm s^{-1}) or the precipitation rate (L m^{-2} mo^{-1}). Detailed description of sampling and analytical methods including the estimated average dry deposition velocities can be found e.g. in *Horváth* (1989a) or *Pais* and *Horváth* (1990). From practical point of view concentration of nitric acid gas and the chemical composition of aerosol particles have been determined only at two stations (K-puszta, Nyírjes). Concentration of ammonia gas is measured only at the K-puszta station.

In this paper only the acidic deposition is discussed. Acid deposition rate was calculated as described in *Horváth* (1989a) and *MSZ* (1988). It can be respected as the upper limit of acidity. Basic compounds (mainly soil-derived HCO_3^- ions in the large aerosol fraction) due to their short lifetime have great spatial concentration variability (*Horváth*, 1981). Therefore, instead of uncertain net (acidic and alkalinic) deposition we prefer to use the term of possible highest rate of acid deposition.

Beside chemical measurements main meteorological parameters including air temperature and humidity, wind direction and velocity have also been continuously monitored.

It should be noted that Nyírjes station was burnt down in July, 1992 because of a forest fire. For this reason only the first half year of 1992 was taken into account during the calculation.

3. Results

3.1 Concentration of air pollutants

As it was mentioned above direct effects of acidic air pollutants are related to their high atmospheric concentrations. The exact determination of the "dangerous" level of pollutants is impossible. There are different approaches to estimate the air quality standards for forest ecological systems. According to *WHO* (1985) the harmful level of sulfur dioxide and nitrogen

dioxide for forests (for the two most important air pollutants from the point of view of acidification) is 30 $\mu g\ m^{-3}$ as a yearly average. These figures correspond to Hungarian standards determined for "particularly protected" areas (*MSZ*, 1990). Proposed critical loads for forests are 20 and 30 $\mu g\ m^{-3}$ as a yearly average for sulfur dioxide and nitrogen dioxide, respectively (*Várallyay et al.*, 1992).

Yearly averages for sulfur dioxide and nitrogen dioxide as well as the variation of mean monthly values can be seen in *Fig. 1*. According to Fig. 1

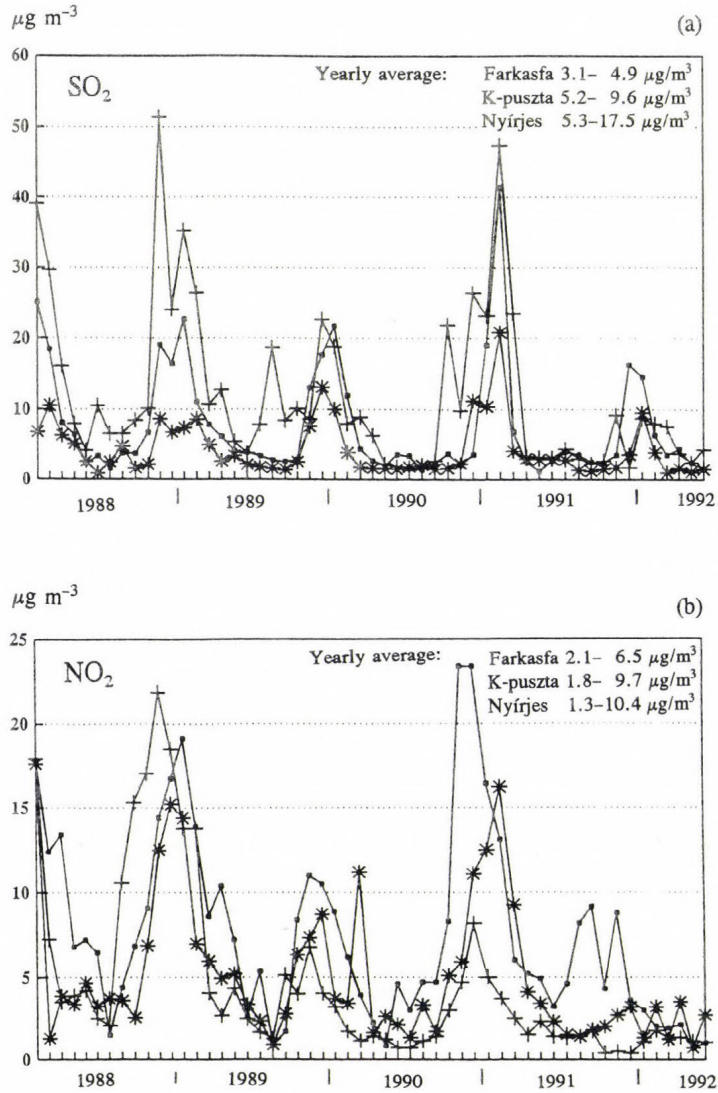

Fig. 1. Variation of the mean monthly concentration of sulfur dioxide (a) and nitrogen dioxide (b) (K-puszta ——, Nyírjes +, Farkasfa ∗).

yearly mean values of pollutants do not reach the harmful level. A west-east increase can be observed in the concentration of sulfur and nitrogen dioxides. Further important information is that higher sulfur dioxide and nitrogen dioxide levels occur during the winter half-year, out of the vegetation period. For deciduous forests the foliar uptake of gases is possible only during the vegetation period (practically during summer half-year, April–November). In the case of coniferous forest the uptake of sulfur and nitrogen dioxide is minimized in the winter half-year because of the closed stage of the stomata. It means that direct effect of acidic air pollution can be probably excluded.

Concentration of other acidic pollutants does not comparable to that of sulfur and nitrogen dioxide. The level of nitric acid which is the third most important pollutant beside sulfur and nitrogen dioxide does not reach the 2.0 $\mu g\ m^{-3}$ as an average.

3.2 Deposition of air pollutants

In contrast with high atmospheric level of pollutants dry and wet deposition of acidic substances (sulfur and nitrogen compounds) may affect the forest health by indirect processes through accumulation in the forest soil. The rate of dry, wet and total (dry+wet) acidic deposition was determined by the method described in *MSZ* (1988) and *Horváth* (1989b) (*Table 1*). Deposition of sulfur and nitrogen compounds was expressed in hydrogen ion equivalents. The average rate of total deposition (for the period of 1988–92 as an average of 3 station) is 187 mg $H^+\ m^{-2}\ yr^{-1}$. The share of dry and wet deposition is approximately the same. However, in the summer half-year the

Table 1. Dry (d), wet (w) and total (t) acidic deposition at forestry monitoring stations expressed in mg $H^+\ m^{-2}$ ½ yr^{-1} and mg $H^+\ m^{-2}\ yr^{-1}$ units

Name of station	Period	1988			1989			1990			1991			1992			Mean		
		d	w	t	d	w	t	d	w	t	d	w	t	d	w	t	d	w	t
K-puszta	Year	111	85	196	107	99	206	88	73	161	99	85	184	67	49	116	94	78	172
	Winter	81	35	116	76	28	104	64	34	98	67	32	99	43	16	59	66	29	95
	Summer	30	50	80	31	71	102	24	39	63	32	53	85	24	33	57	28	49	77
Nyírjes	Year	165	163	328	129	141	270	90	125	215	86	105	191	57	60	117	105	119	224
	Winter	81	35	116	76	28	104	64	34	98	64	32	96	34	31	65	64	32	96
	Summer	84	128	212	53	113	166	26	91	117	22	73	95	23	29	52	41	87	129
Farkasfa	Year	72	93	165	78	107	185	66	124	190	67	81	148	55	75	130	68	96	164
	Winter	47	39	86	55	14	69	46	56	102	43	30	73	32	26	58	45	33	78
	Summer	25	54	79	23	93	116	20	68	88	24	51	75	23	49	72	23	63	86
Mean of stations	Year	116	114	230	104	116	220	81	107	188	84	90	174	60	61	121	89	98	187
	Winter	70	36	106	69	23	92	58	41	99	58	31	89	37	24	61	58	32	90
	Summer	46	78	124	36	92	128	23	66	89	26	59	85	23	37	60	31	66	97

wet, in winter half-year the dry deposition dominates (*Fig. 2*). While dry deposition has a winter, wet deposition has a summer peak. Consequently, there is no expressed annual variation in the total deposition.

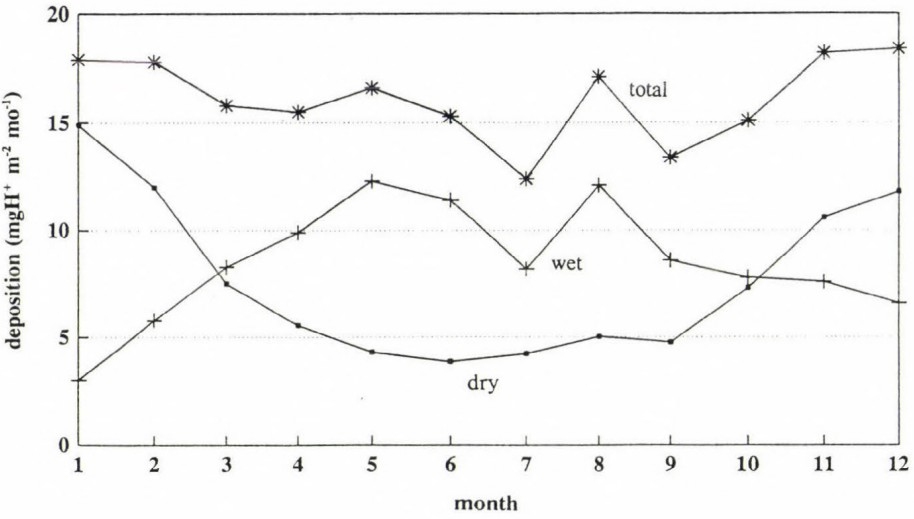

Fig. 2. Annual variation of dry, wet and total acidic deposition as an average measured at the three forestry monitoring stations (1988–1992).

The ratio of sulfur to nitrogen compounds in the total deposition is 42 and 58%. The relative importance of sulfur compounds is continuously decreased from 46% to 36% during the 5 years. It is in agreement with our earlier results (*Horváth*, 1989a) suggesting that N/S ratio is increasing in the acidic deposition.

The average yearly acidic depositions of Farkasfa and K-puszta stations are similar, 164 and 172 mg H^+ m^{-2} yr^{-1}, which can be regarded as a "background" acid deposition for Hungary. For Nyírjes station the acidic deposition is higher, 224 mg H^+ m^{-2} yr^{-1} indicating local pollution effect.

The yearly deposition figures for the 3 stations generally do not exceed the proposed critical load for Hungary. It is established total acid deposition is 280 mg H^+m^2 yr^1 (*Várallyay et al.*, 1992). It can be seen from Table 1 that exceedance of the critical load occurred only in 1988 at Nyírjes station.

According to the recommendation of UN and ECE (*RIVM*, 1991), Hungary is divided into different grids according to sensibility of the given area. The critical loads for the 4 different areas for Hungary are 20–50; 50–100; 100–200 and >200 mg H^+ m^{-2} yr^{-1}. Lowest figures are generally determined for western and northern part of Hungary. Taking into consideration these recommendations we can see that in the majority of the cases the critical load is exceeded.

3.3 Trends in concentration and deposition

As Fig. 1 and Table 1 suggest, concentration of the most important acidic compounds (sulfur and nitrogen dioxide) as well as total (dry+wet) deposition of pollutants have decreased during the 5 years of investigation. It is probably due to reduced sulfur and nitrogen emission in Hungary and in the neighbouring countries as a consequence of change in economical structure of East European region. Roughly, the atmospheric level of pollutants and the rate of acidic deposition have reached to the half of the value measured in 1988 as *Fig. 3* illustrates.

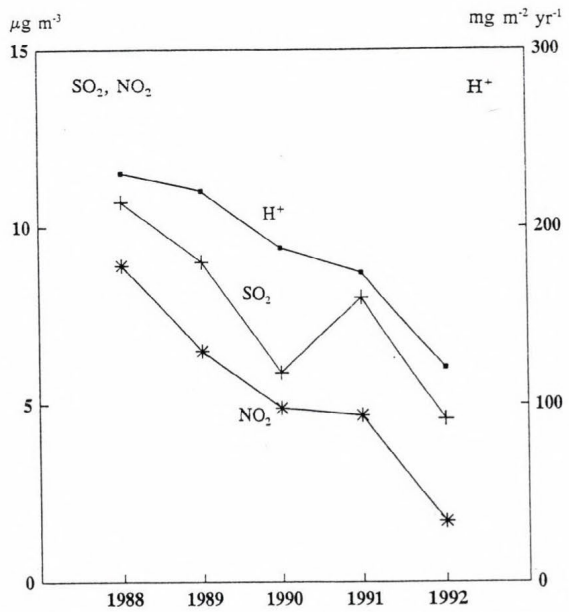

Fig. 3. Variation of the concentration of sulfur dioxide and the nitrogen dioxide and the rate of total acidic deposition at forestry stations.

This fortunate tendency suggests that we can not probably face the danger of direct forest decline in the near future caused by increased level of pollutants. In spite of the decreasing deposition rate the critical loads recommended by international organizations are frequently exceeded. For this reason the continuous monitoring of acid deposition is needed for the effects of pollution may accumulate in the forest soil (e.g. accumulation of nitrogen loading, mobilization of heavy metals, decrease of buffer capacity against acid stress) causing long term indirect damages in forests.

Furthermore, other types of pollution (e.g. high level of photochemical oxidants, including ozone), also responsible for forest decline, should be included into the study.

Acknowledgements—This work has been supported by *Hungarian Academy of Sciences* as an OTKA project, contract number: 341.

References

Führer, E.Gy. und *Horváth, L.*, 1992: Saure deposition in Ungarn. *Agrokémia és Talajtan 41*, 90-101.

Horváth, L., 1981: Chemical composition of precipitation water in Hungary (in Hungarian). *Időjárás 85*, 201-212.

Horváth, L., 1989a: Measurement of atmospheric acid deposition in Hungary (in Hungarian). *OMSZ Kisebb Kiadványai*, No. 65, Budapest.

Horváth, L., 1989b: Measurement of acid deposition in Hungary. In *Acid Deposition, Sources, Effects and Controls* (ed.: J.W.S. Longhurst). British Library Technical Communications, Letchworth.

Horváth, L. and *Führer, E.Gy.*, 1991: Acid deposition in forest ecosystems. In *Proceedings "Expertentagung Waldschadenforschung im östlichen Mitteleuropa und in Bayern"*, GSF-Bericht 24/91.

Jakucs, P., 1986: The impact of atmospheric acidification on living organisms (in Hungarian). *Időjárás 90*, 150-158.

Möller, D., 1988: Production of free radicals by an ozone-alkene reaction-A possible factor in the new-type forest decline? *Atmos. Environ. 22*, 2607-2611.

MSZ, 1988: Determination of atmospheric acid deposition (Hungarian Standard). MSZ 21860.

MSZ, 1990: Requirements of cleanness of ambient air (Hungarian Standard). MSZ 21854.

Pais, I. and *Horváth, L.*, 1990: Atmospheric acidic deposition and its environmental effect in Hungary. In *Advances in Environmental Science* (ed.: D.C. Adriano). University of Georgia, USA.

Stefanovits, P., 1986: A few new data on soil acidification (in Hungarian). *Magyar Tudomány 93*, 339-341.

Várallyay, Gy., Fekete-Nárai, K., Führer, E., Gopcsa, E., Haszpra, L. and *Várkonyi, T.*, 1992: *System for Rural Air Quality Standards*. Proposal for provision of law. Institute for Environmental Management, Budapest, Hungary, (manuscript).

RIVM, 1991: Mapping critical loads for Europe. *CCE Technical Report* No. 1. National Institute of Public Health and Environmental Protection, Bilthoven, The Netherlands.

WHO, 1985: *Air Quality Guidelines-Ecological Effects of Air Pollutants*. World Health Organization ICP/CEH 902/m 71 (S), 29 July, 1985.

IDŐJÁRÁS

Quarterly Journal of the Hungarian Meteorological Service
Vol. 97, No. 3, July–September 1993

An advanced traffic accident forecasting technique based on weather sensitivity of drivers

I. Örményi

National Institute for Rheumatics and Physiotherapy,
Laboratory for Electrobiometeorology,
Frankel Leó u. 25/27, H-1023 Budapest, Hungary

(Manuscript received 5 May 1993; in final form 2 August 1993)

Abstract—Data of 2130 accidents made by the drivers of Budapest Post Office between 1978 and 1983 are studied based on weather and geophysical factors. The weather sensitivity of individuals who caused the accidents was classified into 7 subtypes. Provable significant differences were found between the accidents made by warm and cold front sensitive on 24 hour, monthly and seasonal basis. Significantly higher number of accidents was made by weather sensitive car drivers during stationary fronts. Among air masses in the higher level of the troposphere the subtropical and the arctic air masses affect mostly the warm and cold front sensitive drivers. The effect of the variations in the geomagnetic activity with different types of weather sensitivity can also be proved. In geomagnetic storms the warm front sensitive and in severe geomagnetic storms the mixed front sensitive make more accidents. The above findings are very useful for medical meterological and accident forecast provided that the weather sensitivity of individuals is known.

Key-words: traffic accidents effects of fronts and air masses, geomagnetic activity, individual weather sensitivity.

1. Introduction

The meteorological and cosmic effects on traffic and industrial accidents have been investigated since 1965 in Budapest. The influence of fronts, air masses near to the ground and in the higher level of the troposphere, solar flares and variations in the geometric activity were examinated (*Örményi*, 1972a, 1977, 1978). There seems to be no relation (at last in Budapest) between the ordinary meteorological elements (phenomen such as fog) like humidity, barometric tendency, temperature and the accidents. The start of precipitation involves risk of accident, especially in winter time in view of the icy conditions (*Örményi*, 1970). The efficiency of meteorological elements on traffic acting in

a metropolitan area versus the road transport in country may be entirely different because of the variation infrastucture (*WMO*, 1990).

Experiences obtained in the road accidents' forecast show that the type of weather sensitivty of car drivers in the accident should also be taken into account (*Örményi*, 1972b, 1990).

2. *Material and method*

The accidents made by the car drivers of the Budapest Post Office between 1978 and 1983 were used to the statistical data processing. 2130 accidents made by 2011 male and 119 female car drivers of age between 18 and 60 were registered. The type of weather sensitivity was established by means of a questionnaire (*Örményi*, 1972c, 1990) prepared by the collaborators of the Psychological Laboratory of the Hungarian Post. The questionnaire was compiled based on the work of *Curry* (1948) and standardised on a Hungarian population of more than 26,000 (see Appendix). The answers to questions on the ergotropic working phase (E) are divided by the values of trophotropic working phase (T) of the human organism. On the basis of these quotients in *Table 1*, three types of warm front sensivitity, two types of mixed front sensitivity and three types of cold front sensitivity are differentiated. In this paper all mixed sensitive car drivers are considered as one group. On the other hand, this typology is, at the same time, suitable for the establishment of the sensitivity to geophysical factors, among others the solar activity. The role of geophysical factors was proved at accidents occurred in chemical industry in Nyergesújfalu and Budapest between 1969 and 1973 (*Örményi*, 1986).

Different types of front and air masses were used in the investigation based on *Berkes*' classification (1961) as well as macrosynoptic types determinated by *Péczely* (1957) for the Carpathian Basin. The list of meteorological elements

Table 1. Distribution of various geophysical biotypes (GBT), according to E/T quotients

Geophysical biotypes		Intervallum E/T quotients	Frequency distribution %
Cold front type sensitive 3	C_3	0.01 - 0.43	1.3
Cold front type sensitive 2	C_2	0.44 - 0.68	9.7
Cold front type sensitive 1	C_1	0.69 - 0.88	22.4
Mixed cold front type sensitive	M_c	0.89 - 0.99	13.1
Mixed warm front type sensitive	M_w	1.00 - 1.08	15.5
Warm front type sensitive 1	W_1	1.09 - 1.28	17.8
Warm front type sensitive 2	W_2	1.29 - 1.88	17.2
Warm front type sensitive 3	W_3	1.89 -49.00	3.0

were compiled in the Laboratory for Electrobiometeorology of the National Institute of Rheumatics and Physiotherapy using the data of the National Meteorological Service. The influence of the solar activity was related to the variations in the geomagnetic activity by means of the *Bartha-Berkes* classification (*Berkes*, 1970) so as it is shown in *Table 2*. The daily elongation of the horizontal component of geomagnetic activity (characteristic number) was taken into account in the classification. The data were obtained from the Geomagnetic Observatory Tihany. *Bernoulli*'s method (*Jessel*, 1954) and *Schelling*'s (1937, 1940) "n" and "T" tests were used in the data processing. Significant values were considered at least P=0.05.

Table 2. Corresponding values of geomagnetic variations according to *Bartha'* and *Berkes'* classifications and K_p values

Characteristic number	Range of daily elongation in H-component, expressed in nT	Corresponding limit value of K_p max during a day
0	0 - 30	$0 - 2^o$
1	30 - 60	$2^+ - 3^+$
2	60 - 100	$4^- - 5^o$
3	100 - 160	$5^+ - 6^+$
4	160 - 210	$7^- - 8^-$
5	210 -	$8^o - 9^o$

Periodical effects such as 24 hours rhythms as well as the weekly and annual effects all were taken into account. The distribution of types of weather sensitivity (geophysical biotypes=GBT) in the accidents was the following: 132 of W_3 type (6.2%); 314 of W_2 type (14.7%); 301 type of W_1 type (14.1%); 503 of M type (23.6%); 478 of C_1 type (22.4%); 353 of C_2 type (16.6) and 49 of C_3 type (2.4%). Consequently, in the accidents 35% of the drivers belonged to warm front sensitive, 23.6% to mixed front sensitive and 41.4% to cold front sensitive.

3. Results

3.1 Distributions of the accidents with respect to types of weather sensitivity

Fig. 1 shows 24 hours rhythms of accidents made by individuals of different weather sensitivity. In the lower part of the figure all cases are specified. The peak in accidents was at 11.00 a.m. and the second peak at 2.00 p.m., a minimum at 10.00 p.m. and a second minimum at 4.00 a.m. As there was less accidents with sub-types, therefore, instead of seven only the three main types of weather sensitivity were used. In the upper part of Fig. 1. 24 hour rhythms of the accidents of warm front sensitive (W), in the middle part those of mixed front sensitive (M) and in the lower part those of cold front (C) are given. The

number of accidents caused by warm front sensitive usually has opposite trend against those done by cold front sensitive (correlation coefficient $r=-0.68\pm 0.11$).

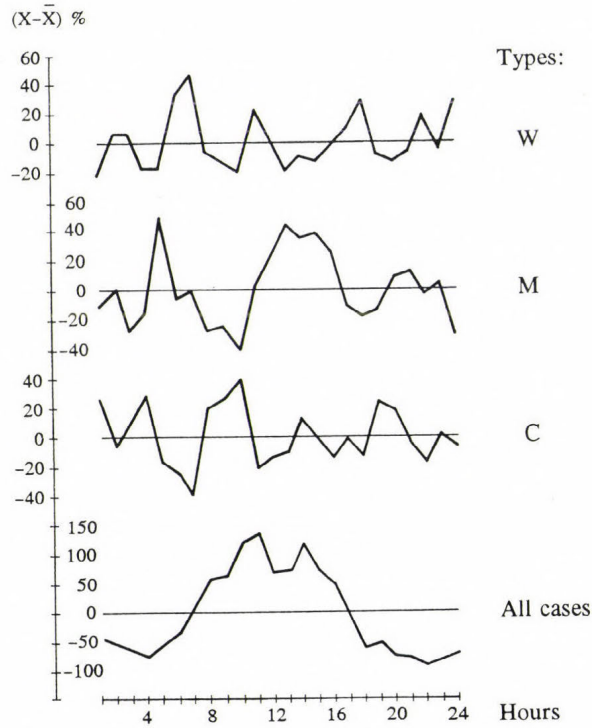

Fig. 1. Daily rhythm of traffic accidents made by various GBT. On the vertical axis deviations from the mean of cases are presented in percentage.

The weekly rhythm was also monitored which is illustrated in *Table 3*. The decrease on weekend may be explained by the reduced traffic in Budapest. On the other hand, there is no significant difference in the distribution of the accidents caused by the three types of weather sensitivity (warm, cold, mixed).

Table 3. The number of accidents on each day of the week and their deviation from the mean $(X-\bar{X})$

	Mon	Tue	Wed	Thur	Fri	Sat	Sun
Number of cases	329	388	365	352	405	191	100
$(X-\bar{X})$ %	8	28	20	16	33	-37	-68

The study of distribution was also performed on monthly scale (*Table 4*). The high number of accidents in tht first three months of the year is related to winter weather conditions (icy roads, weak visibility etc.).

Table 4. The monthly distribution of accidents and the deviations from the average $(X-\bar{X})$

	Jan	Feb	Mar	Apr	May	Jun	Jul	Aug	Sep	Okt	Nov	Dec
Number of cases	230	198	213	173	172	175	168	150	178	186	142	145
$(X-\bar{X})$ %	30	12	20	-3	-3	-1	-6	-16	0	5	-20	-18

Fig. 2 shows the annual rhythms of accidents (deviations from the mean) for the three types of weather sensitivity in percentage. The compilation of the figure is similar to that of Fig. 1. The values of smoothed curves are plotted by dotted lines. The number of accidents caused of warm front sensitive also shows a trend opposite to that of accidents done by cold front sensitive. The correlation coefficient between the two series is $r=-0.70\pm0.14$. The same correlation is $r=-0.84\pm0.085$ for smoothed values, indicating a close but opposite relation between the two curves.

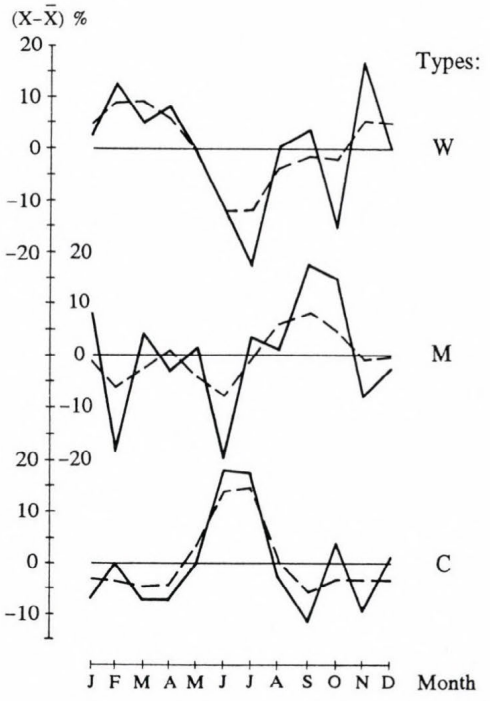

Fig. 2. Annual variations of traffic accidents made by various GBT.

Fig. 3 shows the seasonal distribution of accidents made by different types of weather sensitivity. Data of warm front sensitive are displayed in the upper part, of mixed front sensitive in the middle and cold front sensitive in the lower

part of the figure. The figure also verifies that accidents caused by warm front sensitive (W) and cold front sensitive (C) show an opposite trend and the correlation coefficient is very high, $r = -0.95 \pm 0.048$.

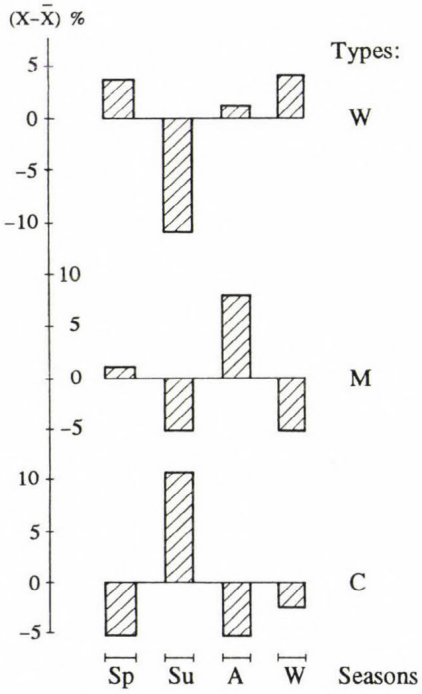

Fig. 3. Seasonal variations of traffic accidents made by various GBT (3 types).

Warm front sensitive make the highest number of accidents in winter and spring, mixed front sensitive in autumn and cold front sensitive in summer. Result of the seasonal statistics of accidents are shown in *Table 5*.

Table 5. The seasonal distribution of all accidents (No.) and their deviations from the mean (X-X̄)

Season	No.	(X-X̄) %
Spring	558	5
Summer	493	-8
Autumn	506	-5
Winter	573	8

3.2 *The effect of different weather types*

Result of significancy test based on the correlation between prevailing weather conditions in the time of car accidents and types weather sensitivity are found in *Table 6*. In compilation of this table all the seven subtypes of weather sensitivity are used.

Table 6. Results of significancy test based on the correlation between prevailing weather conditions in the time of car accidents and types of weather sensitivity. The underlined numbers indicate the significant results on the level of p=0.05

Types of fronts	Types of weather sensitivity													
	W_3		W_2		W_1		M		C_1		C_2		C_3	
	d/s	N	d/s	N	d/s	N	d/s	N	d/s	N	d/s	N	d/s	N
W	-1.13	2	2.69	16	1.16	13	4.06	31	1.89	21	0.19	11	-0.19	2
W_h	1.49	8	1.38	18	2.21	18	1.52	24	1.43	22	1.45	17	-1.67	0
O_w	1.23	4	1.87	4	0.09	2	-0.02	3	1.99	6	1.41	4	2.37	2
W_u	1.25	4	2.27	9	1.42	8	4.53	8	2.55	14	1.16	8	0.16	1
C	-0.92	4	-1.26	8	-2.74	4	-1.38	16	-1.71	13	-0.28	14	0.37	4
C_h	0.08	8	-1.48	10	-1.12	13	-1.26	22	-2.68	13	-0.75	16	-1.14	2
O_c	-1.18	0	0.7	4	0.5	4	-0.48	4	0.13	5	-1.35	1	0.31	1
I	-1.21	4	-1.14	10	-1.05	12	-0.40	24	-0.31	22	2.21	26	-1.53	1
O_{or}	4.11	3	1.49	2	5.68	6	-0.31	1	4.35	6	2.22	3	1.71	1
S_{ww}	1.85	4	4.79	12	5.89	15	3.66	15	4.47	16	0.94	6	-0.96	0
S_{cc}	6.31	12	1.49	8	3.34	13	2.83	17	1.81	13	6.75	22	5.09	7
S_{wc}	2.49	6	0.23	5	3.55	13	3.06	17	0.54	22	2.36	11	4.37	6
S_{cw}	3.05	5	1.44	5	5.03	16	1.69	8	1.69	8	1.51	6	0.29	1
D	-0.76	2	-1.06	4	-1.67	3	-2.39	4	-0.67	9	-1.87	3	0.9	3
S	-1.43	1	2.24	13	0.67	10	0.21	14	2.04	14	-0.29	8	0.02	22
D_c	-1.35	0	-1.91	0	-2.03	0	-1.01	4	-1.63	2	-1.15	2	0.06	1
Front nil	-3.41	2	-4.53	5	-4.55	7	-5.38	14	-5.23	12	-5.26	5	-2.08	2

The upper part of the table shows the statistical analysis of accidents made by individuals of different weather sensitivity during warm front situations: in the first line during surface warm front (W), in the second line during upper warm front (W_h), in the third line during a warm occluded front (O_w) and in the fourth line during unstable warm front (W_u). Types of weather sensitivity are indicated in columns of the table. The ratio Δ/σ is the difference between the expected mean and the actual number of accidents divided by the standard deviation. The number of accidents (N) is also given. The numbers of accidents made by various subtypes of warm front sensitive are different. The number of accidents made by subtypes C_2 and C_3 of cold front sensitive is very low. The ratio for accidents made by C_3 during an occluded warm front is high, but

the number of cases is low. It is typical that W_2, M and C_1 react strongly to different warm fronts passage.

The second part of the table shows accidents made during different cold fronts. Statistical analysis for surface cold fronts (C) is given in the first line, for upper cold fronts (C_h) in the second line, for cold occluded fronts in the third line (O_c), for line of instability in the fourth line (I), and for orographic occlusion fronts (O_{or}), typical to the Carpathian Basin, in the fifth line. The most efficient situation is the orographic occlusion front since four types of weather sensitivity react strongly to it. The speed of the frontal passage is usually so that their biological effects are felt for three or four hours, except for the case of orographic occlusion.

The third part of the table shows the effects of stationary fronts. The effect of a stationary front that arrives and leaves as warm front (S_{ww}) is given in the first line, if it arrives and leaves as a cold front (S_{cc}) in the second line, if it arrives as a warm front and leaves as a cold front (S_{wc}) in the third line, if it arrives as a cold front and leaves as a warm front (S_{cw}) in the fourth line. In these weather conditions different types of weather sensitivity make significantly more accidents than under other situations. S_{cc} situation the W_3 types made much more accidents than expected. But, as it turned out latter it was a consequence of common effect of several factors (like air masses in the higher level of the troposphere, geomagnetic activity). After eliminating extremes the number of accidents is not significantly higher.

The last part of the table shows four situations: subsidence (D) in general in the upper first line, destroying high pressure system (S) accompanied by following falling barometric tendency in the second line, descending motion between two cold front (D_c) in the third line and non frontal conditions (Front Nil) in the fourth line. The table shows that in nil frontal conditions none of the types of weather sensitivity are inclined to make accidents. But during destroying high pressure system the risk of accidents is obviously high for W_2 and C_1.

3.3 The effect of the air masses

Hereafter the influence of biologically efficient air masses near to the ground and in the higher level of the troposphere is outlined.

Fig. 4 shows the effect of maritime arctic air masses (mA) and continental arctic air masses (cA) near the ground (subscript GL) and in the higher level of the troposphere (subscript H). The effect of maritime and continental air masses near to the ground are given in the upper two graphs and the influence of the maritime and continental air masses in the higher level of the troposphere in the lower two graphs. The probable error ($P=0.05$) is also plotted. Air masses near the ground have no particular influence except for W_3, when the air is coming from the higher level of the troposphere. Contrary to these in the

case of air masses in the higher layer of the troposphere the mixed and some cold front sensitive are inclined to make accidents.

Fig. 5 shows the influence of subtropical air masses coming into the Carpathian Basin. mT is the abbreviation of subtropical air masses from the Azores and m'T the subtropical air masses from the Mediterranean. The sudden arrival of subtropical air masses in the higher level of the troposphere is indexed by 1 (mT_1 and $m'T_1$, respectively). From Fig. 5 follows that the number of accidents and the level of significance are much lower for cold front sensitive than expected. However, a sudden subtropical air flow from the Azores mT_1 is most reacted by W_3 then W_2 and W_1 and finally by M. The

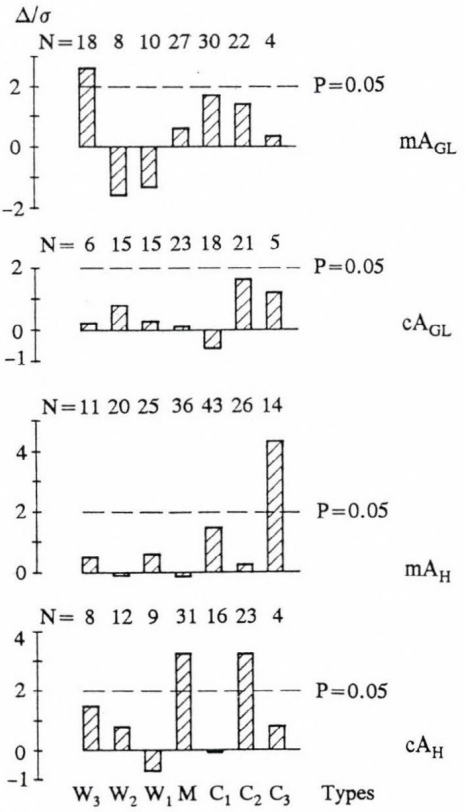

Fig. 4. Influence of arctic air masses near the ground (subscript GL) and higher level of the troposphere (subscript H) on road accidents made by various GBT. On the vertical axis the difference between the expected mean and actual number of accidents divided by standard deviation is depicted. N is the number of accidents.

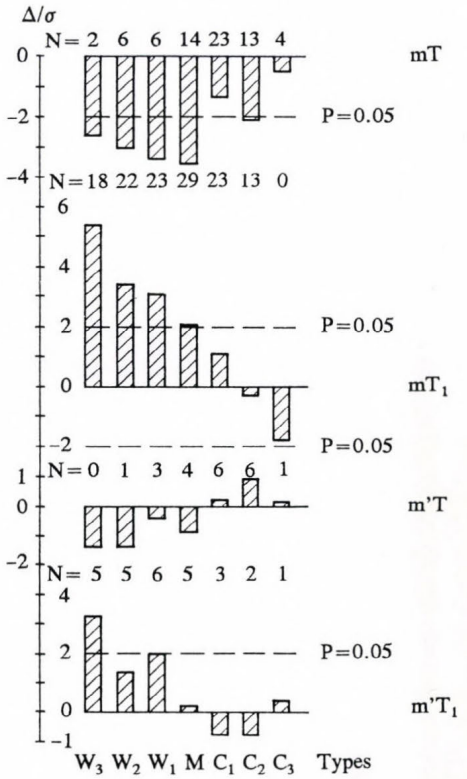

Fig. 5. Road accidents made by various GBT in the case of intrusion of subtropical air masses in the higher levels of the troposphere. The meaning of the vertical axis agrees with that of Fig. 4. Subscript 1 refers to arrival to sudden arrival of air masses. N is the number of accidents.

influence of a sudden m'T_1 air flow is not as significant although W_3 and W_1 make sensibly more accidents.

The influence of macrosynoptical types are not dealt with here because they are peculiar to the Carpathian area. Neverthless, there are such types of weather sensitivity who are liable to make accident in significantly higher number even in high pressure system and it confirms the findings with the destroying high pressure system.

3.4 Influence of solar activity

The influence of solar activity was related to the variation of the geomagnetic activity (*Örményi* and *Majer-Hock*, 1991). The key day ("0" day) is the day of the geomagnetic activity. In *Fig. 6a* accident for characteristic numbers Ch=2 and Ch=3 and in *Fig. 6b* those for characteristic numbers Ch=4 and Ch=5 are shown within ± 3 days of the geomagnetic activity in question. In this case three types of weather sensitivity together were taken into account. From the figure it is concluded that the number of accidents made by warm front sensitive decreased significantly on the key day (Ch=2) just like the total number of accidents. In the lower part of the figure it can be seen that the number of accidents increased significantly on the key day (Ch=3). There is a remarkable increase in the accidents made by warm front sensitive as well. The number is accidents also increases two days after the storm.

In the cases of Ch=4 there is a significant increase in the accidents caused warm sensitive one day after storm (left side of Fig. 6b). The number of accidents made by mixed front sensitive increases significantly two days before storm, probably because a severe geomagnetic storm is usually preceded by an increased geomagnetic activity. Finally, in a very severe geomagnetic storm (Ch=5), there is a nearly significant increase in the accidents made by mixed front sensitive whereas the total number of accidents made by cold front sensitive decreased on the key day (right side of Fig. 6b).

4. Conclusions

From the investigations it is concluded that the number of industrial and traffic accidents increases during front passages. According to our experiences in many cases as a result of correct weather forecast, the number of accidents could be decreased by 25 to 35%. To improve the method the type of weather sensitivity (geophysical biotypes) has to be determined. A study was made on car drivers if the Budapest Post Office in which circumstances of 2130 accidents were examined.

There was sensible differences among the 24 hours, monthly and seasonal distributions of effects especially for warm and cold front sensitive. There is an opposite relationship between the accidents made by warm and cold front sensi-

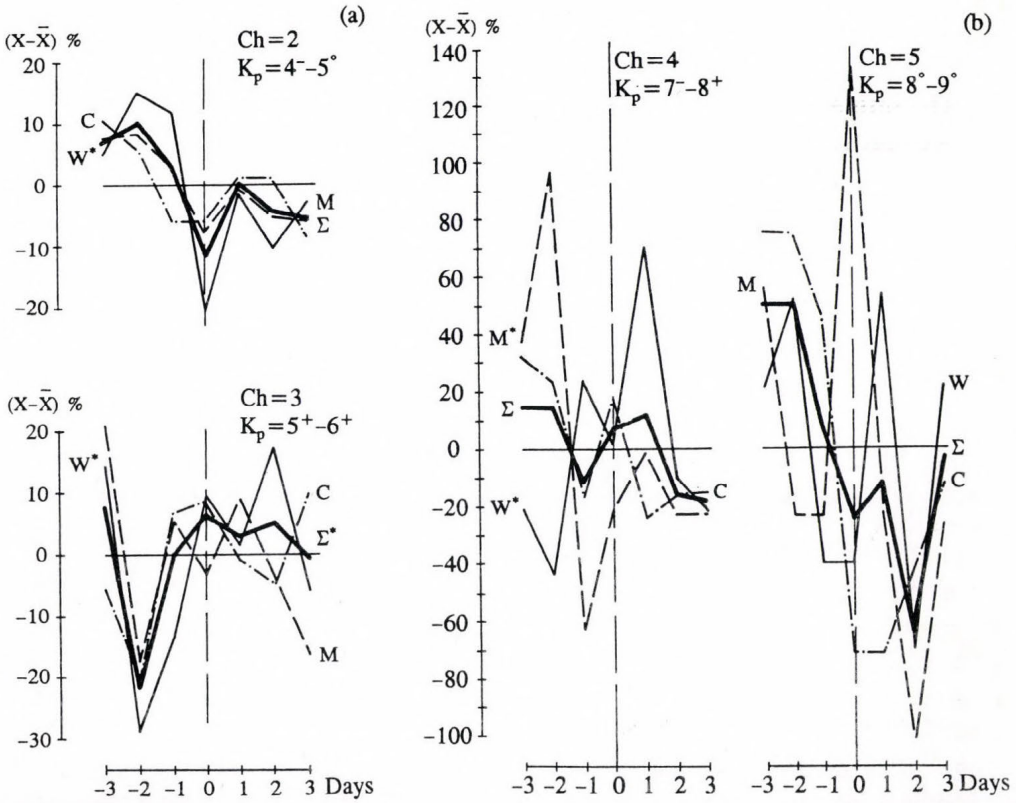

Fig. 6. Road accidents of various GBT as a function of geomagnetic characteristic numbers (Ch) in cases of Ch=2 and 3 (a) and in cases of Ch=4 and 5 (b). The curves show deviations from the mean of accidents in percentage. *Denotations:* W (solid line)–warm front sensitive, C (dashed line)–cold front sensitive, M (dot-dash line)–mixed front sensitive, Σ (bold line)–all data; asterisks denote significant variations.

tive in the monthly and seasonal distribution. The highest number of accidents are made by weather sensitive individuals during stationary fronts and not in short time front passages. It is remarkable that different subtypes of warm front sensitive react significantly but not in the same way to subtropical air masses coming in the higher level of troposphere, when the actual temperature is by 6 or 8 degrees higher than the average temperature calculated for the suitable period. In the case of cold front sensitive the average temperature is by 6 or 8 degrees lower than the average for arctic air masses in the higher level of troposphere. In these case the number of accidents is significantly higher.

The effect of solar activity can be proved by numerous accidents made in disturbed geomagnetic activity (Ch=2) and in geomagnetic storms (Ch=3). Individuals of different weather sensitivity do not react to them in same way. Warm front sensitive make more accidents in storms Ch=3, 4. Mixed front sensitive react to most severe geomagnetic storms (Ch=5).

The above findings help to make the accident more efficient and lead to a lower number of accidents. *The types of weather sensitivity can be determined in a couple of minutes and as a result an individual weather forecast valid to specific types of weather sensitivity may be issued.*

Acknowledgements – The author wishes to express his thanks to *Mrs. Jolan Majer-Hock* for her technical assistance.

References

Berkes, Z., 1961: Luftmassen und Fronttypen im Karpatenbecken. *Időjárás 65*, 289-293.

Berkes, Z., 1970: Cosmic effects in the lower atmosphere (in Hungarian). *Publications of the 10th Section of the Hungarian Academy of Sciences 3*, 131-157, Budapest.

Curry, M., 1948: *Bioklimatik*. American Research Institute, Riederau, Ammersee.

Jessel, U., 1954: Bemerkung zur medizin-meteorologischen Statistik. *Med. Med. Hefte 9*, 7-20.

Örményi, I., 1970: Influence of weather and solar activity on the insurance of the traffic (in Hungarian). *Review of Home Affaires 8*, 61-72.

Örményi, I., 1972a: Possible effect of ELF Atmospherics of 3 cps range on traffic accidents in a metropolitan area in Hungary. *Biometeorology 5*, 93-94.

Örményi, I., 1972b: A random sample test to determine the possible distribution of weather sensitive human subjects in Hungary. *Biometeorology 5*, 94-95.

Örményi, I., 1972c: Questionary method for determintaion of weather sensitivity (in Hungarian). *Ergonomia 5*, 156-165.

Örményi, I., 1977: Bases of medical-meteorological forecast of industrial and traffic accidents in Budapest. *Cahiers de Medicine du Travail XIV*, 243-246.

Örményi, I., 1978: Modification effect of solaractivity on reliability of the forecasts of traffic accidents. *Cycles 29*, 37-41.

Örményi, I., 1986: The needs and applications of forecasting of geoactive solar activity for human reactions. Solar terrestrial prediction. *Proc. of a Workshop of Meudon*, France, Publ. of Air Force Geophys. Lab. 601-605.

Örményi, I., 1990: Variation of weather sensitivity (Geophysical Biotypology) over 40 years among representative population of Budapest. *Proc. Symposium of Human Biometeorology*, Stribské Pleso, 288-296.

Örményi, I. and *Majer-Hock, J.*, 1991: Alteration of geomagnetic activity during traffic accidents caused by car drivers of various geophysical biotypes. *Proc. of IAGA, XX. Assembly*, Wien, p. 632.

Péczely, G., 1957: Grosswetterlagen in Ungarn. *Kleinere Veröffentlichungen der Zentralanstalt für Meteorologie*. No. 30, Budapest.

Schelling, H., 1937: Zur statistischen Beurteilung des Erfolges von Schutzimpfung. *Klin. Wschr. 16*, 1691-1692.

Schelling, H., 1940: *Arbeiten aus dem Staatlichen Institut für experimentelle Therapie u. dem Forschungsinstitut für Chemoterapie*. Frankfurt, No. 39.

WMO, 1990: *Economic and social benefits of meteorological and hydrological services*. No. 733, Geneva.

APPENDIX

Questionnaire to the determination of the weather sensitivity

Name.....Birth'splace.....
Date of birth.....Month.....Day.....Hours.....
Note! It is in your interest, that on the basis of this questionnaire we should get a correct reference. Please answer to it candidly. There are four possibilities to your reply. Kindly fill out the squares on the right with one of the 4 following numbers corresponding to your preference

1 if you prefer the question of group 1
2 if you prefer the question of group 2
3 if both of them seem not to apply to you
4 if you prefer both of them

Group 1 of questions (E)	Group 2 of questions (T)
1. Are you of a hot temper?	Are you of a quiet temper?
2. Are you exhausted by excitements?	Can you easily tolerate excitements?
3. Can you take quickly decisions?	Are you cool in your decisions?
4. Do you easily blush?	Do you blush rarely?
5. Are you sociable?	Are you not sociable?
6. Are you vivid, irritated?	Are you slow to rouse?
7. Are you talkative?	Are you tongue-tied?
8. Are you often in high spirits?	Are you often moody?
9. Can you learn easily by heart?	Do you slowly learn by memory?
10. Do you feel yourself well in a cool (Northern) wind?	Do you feel yourself uncomfortable in a cool (Northern) wind?
11. Do you feel yourself uncomfortable in a warm (Southern) wind?	Do you feel yourself well in a warm (Southern) wind?
12. Do you suffer from warm air?	Do you tolerate well warm air?
13. Do you tolerate well cold air?	Do you suffer from cold air?
14. Don't you like to take a sunbath?	Do you like to take a sunbath?
15. Are you not disturbed by draught?	Do you suffer from aerophobia?
16. Do you tolerate a hot day badly?	Do you tolerate a hot day well?
17. Do you prefer a coll sleeping room in winter?	Do you prefere a heated sleeping room in winter?
18. Do you feel low before a thunderstorm?	Do you feel low during or after a thunderstorm?
19. Do you sweat to much?	Do you sweat little?
20. Do you like to make excursions or to cultivate some sport?	Do you not like to make excursion or to cultivate some sport?
21. Can you stand for a long time?	You can't stand for a long time?
22. Are you in a better general condition after taking a rest?	Are you in a better general condition after moving?

23.	Do you like to swing?	You don't endure swinging?
24.	Do you prefer to sleep on a high pillow?	Do you prefer to sleep on a low pillow?
25.	Are you disturbed by noise during sleep?	You are not disturbed by noise during sleep?
26.	Do you dream little?	Do you dream frequently?
27.	Do you wake up frequently in the night?	You do not often wake up in the night?
28.	Do you need little sleep? (less than 8 hours)	Do you need much sleep? (more than 8 hours)
29.	Are you fit immediately after waking up?	You are still tired after waking up?
30.	Do you feel better in the morning?	Do you feel better in the evening?
31.	Do you prefer to wear an open suit or shirt?	You prefer to wear a closed suit or shirt?
32.	Do you wake up early in the morning?	Do you wake up later on?
33.	Do you have sensitive eyes against light?	Your eyes are not sensitive against light?
34.	Do you have short sighted eyes?	Do you have long sighted eyes?
35.	Are your arms and legs generally warm?	Are your arms and legs generally cold?
36.	Do you have your illness with a high fever (over 38°C)?	Do you have your illness with a low fever (below 38°C)?
37.	Do you have a quick recovery after an illness?	Do you have a slow recovery after an illness?
38.	Are you susceptible to an acute disease with fever?	You are susceptible to an acute disease without fever?
39.	Do you tolerate pains badly?	Do you tolerate pains easily?
40.	Do you have a strong menstruation?	Do you have a weak menses?
41.	Do you have pains during menses?	Do you have pains after menses?
42.	Do you prefer heavy work for a short time?	Do you prefer easier work for a long time?
43.	Do you have a good appetite?	Do you have a bad appetite?
44.	Are you not festidious about your food?	You are not festidious about your food?
45.	Do you prefer meat?	Do you prefer fruit or vegetables?
46.	Do you like your food salted and spiced?	You don't like your food salted and spiced?
47.	Are you sensitive to smells?	You are not sensitive to smells?
48.	Can you hardly fall asleep after taking coffee in the evening?	You are able to sleep easily after having had coffee in the evening?
49.	Do you tolerate alcohol well?	Do you tolerate alcohol badly?
50.	Do you prefer milk or tea?	Do you prefer tea or milk?

Date.....

1. Number of the answers in group 1.....

2. Number of the answers in group 2.....

$\frac{E}{T}$:..... Type:.....

BOOK REVIEWS

J.R. Holton: **An Introduction to Dynamic Meteorology**. Third Edition. International Geophysics Series, Vol. 23. Academic Press, San Diego, 1992, 511 pages.

First two editions of *An Introduction to Dynamic Meteorology* have served as a standard basic textbook of dynamic meteorology for generations of meteorologists. The classical work of *Professor Holton* provided a bridge to the pioneers of the dynamic meteorological research in the fifties and the sixties. First edition was published in 1972 and 7 years later, it was followed by the second, revised version.

About 13 years have been elapsed since second edition of the widely respected textbook was published. During that period, a number of significant advances have been made in our understanding of a variety of atmospheric phenomena, ranging from the introduction of the so-called Q-vector formalism for diagnosing vertical motion in extratropical weather systems to the role of sea surface temperature anomalies in low-frequency variability. The new edition reflects the advances made in these fields and others, while providing a systematic treatment of the fundamental laws governing the atmospheric motion.

The third edition contains about fifty percent new material, including many new figures, while much of the previous materials has been revised and reorganized.

In Chapters 1–4, the author provides a systematic development of the basic conservation laws. Except for a short section on surface pressure tendency in Chapter 3 and a section on the baroclinic potential vorticity in Chapter 4, the first four chapters remain the same as in the second edition.

Chapter 5 about the planetary boundary layer (PBL) has been rewritten in order to incorporate sections on the boundary layer turbulent kinetic energy budget and the mixed layer model of the PBL.

In Chapter 6 the quasi-geostrophic system of equations is developed and it is demonstrated how they can be used to diagnose synoptic-scale motions at middle latitudes. Excellent physical interpretation of quasi-geostrophic potential vorticity and its relation to Ertel's potential vorticity are given. The mechanisms responsible for vertical motion in quasi-geostrophic systems are examined using two approaches: the classical omega equation, which was discussed in the second edition, and the Q-vector form of the omega equation, which represents an important new addition to this chapter. A brief new section on the ageostrophic circulation in synoptic systems is also presented.

An introduction to the linear wave theory is given in Chapter 7. Chapter 8 is devoted to the formulation and solution of the baroclinic instability problem. A new section includes a derivation of the Rayleigh necessary condition for instability. The basic kinematics and dynamics of mesoscale circulation systems are presented in Chapter 9. This material is a new addition to the book with topics in the kinematics of frontogenesis, semi-geostrophic theory, symmetric instability, mountain waves, cumulus convection, convective storms and dynamics of hurricanes.

An introduction to the theory of the general circulation of the atmosphere is given in Chapter 10. The following chapter is addressed to the structure and dynamics of equatorial circulations. A linear, inviscid shallow-water model on an equatorial plane is used to derive the dispersion relations and structures of equatorial Kelvin, Rossby-gravity and Rossby waves.

The dynamics of vertically propagating planetary waves are treated and their importance in sudden stratospheric warmings is discussed in Chapter 12. Discussion of the quasi-biennial oscillation and several aspects of the ozone layer are given in the last sections of the chapter. The final chapter contains new material on numerical modelling and weather prediction.

Holton's *An Introduction to Dynamic Meteorology* will continue to serve as the cornerstone for education at undergraduate and graduate levels and also provides references for researchers in the atmospheric sciences.

Gy. Gyuró

T.E. Graedel and *P.J. Crutzen*: **Atmospheric Change; An Earth System Perspective**. W.H. Freeman and Company, New York, 1993. 446 pages, hardback with tables, figures and coloured pictures and illustration. Price: 48,22 U.S. dollars.

It is now well documented that human activities modify the Earth environment on different scales. The modifications are serious in particular in the case of the atmosphere which plays an essential role in the control of biogeochemical cycles and climate. One can speculate that atmospheric changes will lead to important alteration of the Earth system.

In spite of the importance of the problem relatively few books are devoted to the subject. Thus, the present book of the two famous atmospheric scientists has been really badly-needed. Briefly speaking, their volume is an excellent and very clear summary of this field, in spite of the fact that it is a bit difficult to decide whether the authors aim was to write about atmospheric changes or the entire Earth system. This is not an important question, however, since the atmosphere is in a close relationship with other media of our planet.

It is a great advantage of the book that each chapter is completed with exercises and a list for further reading, which makes it very useful for beginners and students. In addition to this, a glossary of the most important expressions and an index can be found at the end of the volume.

As the writers inform the readers in the preface and introduction, five chapters (2–6) at their book discuss generally the basic topics in Earth system science. These chapters include the brief description of the driving forces of the planet, the dynamics and radiation balance of the atmosphere as well as our principal ideas about aerosols, hydrosols and water cycle. This first part is followed by the description of chemical principles applied in Earth system science (Chapter 7), while the next two chapters are devoted to the chemistry of the atmosphere and aquatic systems. Then, four chapters (10-13) describe our knowledge of the histories of climate and chemistry on the basis of up-to-date information gained by different techniques including the ice core record. Chapters 14 and 15 present in a didactic way the budgets and cycles of different constituents as well as the numerical models used in environmental chemistry; Chapters 16-18 discuss possible future climates on different time scale. Finally, the book is closed by a chapter on change and sustainability. In this last chapter, among other things it is concluded that "On very long time scales, the planet will surely become incapable of sustaining life as a consequence of the increasing solar radiation. Whether that time scale is of any interest, however, may or may not turn out to be under humanity's control. As a people, we are causing stresses to the biospheric system beyond all previous experience, and hoping that a surprise that cannot be managed is not waiting in the wings."

In summary, the reviewers believes that this thoughtful book should be used in each schools and at all universities, where the aim is to explain to students, the future generation, what to do "to minimize in every way possible the stresses on our planet".

E. Mészáros

NEWS

"Harmony with Nature"
ISES Solar World Congress

The International Solar Energy Society (ISES) is a worldwide nonprofit organization dedicated to the advancement of the utilization of solar energy. Founded in 1954, the Society has members in more than 90 of the world's countries. In each second year, some part of the Society's members and non-member experts meet regularly on the Solar World Congresses. In 1993 the host of this congress was the Hungarian Section of the ISES, the congress took place in Budapest, between August 23–27. The next meeting will be in Harare, Zimbabwe in September of 1995.

"Harmony with Nature" has been selected as general title of the recent congress, to emphasize the fact, that the solar energy as renewable energy does not pollute the environment. In the distant future, its role will be deterministic in the sustainable development of the humankind.

The Budapest congress was organised in co-operation with the following International Organizations:

Comission of European Communities
European Parliament
EUROSOLAR
International Energy Agency
International Energy Foundation
International Atomic Energy Agency
World Bank
World Resources Institute and
several United Nations Organizations.

World Meteorological Organization was represented by a Hungarian expert.

The sponsors of the meeting were several Hungarian ministries, as well several foreign ministries and agencies.

The program of the congress was composed from exhibitions and several types of meeting as plenary sessions, committee meetings, board meeting, working group meetings, seminars, forums, workshops, honour and special sessions and technical sessions. The topics connected to the meteorology were presented on oral and poster technical sessions. Contrary to the previous congresses, where 15–20 meteorological papers were presented, in this year more than 60 abstracts have been accepted in the field of meteorology and

radiation measurements. (The full number of the abstract accepted for all of the technical sessions exceeded 1200.)

The overwhelming part of the meteorology related papers dealt with the utilization of meteorological solar radiation measurements for the purposes of solar energy users. Several statistical and theoretical models were presented to drive radiation parameters for those places where radiation measurements do not exist or the time series are not long enough to calculate climatological characteristics. Interesting instrument developments might result in more precise or less expensive radiation data. This way this meeting is the largest regular scientific meeting of the solar radiation measuring experts. The meteorologists must pay more attention to the ISES meetings.

The scientific proceedings of the Budapest Solar World Congress will be published in eight volumes, namely:

I. Energy Policy, Environment, Education
II. Radiation, Meteorology, Fundamentals
III. Photovoltaics
IV. Solar Thermal
V. Active Systems
VI. Passive Systems
VII. Solar Architecture
VIII. Biomass, Agriculture, Wind Energy.

As it is seen from the above list, the ISES congresses are mainly technical in their nature, but the meteorology (including solar radiation data and instruments) plays a founding role in the solar energy utilization activity.

G. Major

ATMOSPHERIC ENVIRONMENT

an international journal

To promote the distribution of Atmospheric Environment *Időjárás* publishes regularly the *contents* of this important journal. For further information the interested reader is asked to contact *Dr. P. Brimblecombe,* School for Environmental Sciences, University of East Anglia, Norwich NR 7TJ, U.K.

Volume 27A Number 8 1993

Fourth International Conference on Carbonaceous Particles in the Atmosphere

Volume 27A Number 9 1993

D. Anfossi, E. Ferrero, G. Brusasca, A. Marzorati and *G. Tinarelli*: A simple way of computing buoyant plume rise in Lagrangian stochastic dispersion models, 1443-1451.

C.K. Laird and *S.A. Sloan*: Nitrous oxide emissions from U.K. power stations, 1453-1457.

S. Grinshpun, K. Willeke and *S. Kalatoor*: A general equation for aerosol aspiration by thin-walled sampling probes in calm and moving air, 1459-1470.

E.J. Palen, D.T. Allen, S.N. Pandis, S. Paulson, J.H. Seinfeld and *R.C. Flagan*: Fourier Transform Infrared analysis of aerosol formed in the photooxidation of 1-octene, 1471-1477.

P. Zannetti, I. Tombach, S. Cvencek and *W. Balson*: Calculation of visual range improvements from SO_2 emission controls—II. An application to the eastern United States, 1479-1490.

S.R. Hanna and *J.C. Chang*: Hybrid plume dispersion model (HPDM) improvements and testing at three field sites, 1491-1508.

H. Sakugawa and *I.R. Kaplan*: Comparison of H_2O_2 and O_3 content in atmospheric samples in the San Bernardino Mountains, southern California, 1509-1515.

Volume 27A Number 10 1993

G. Christakos and *G.A. Thesing*: The intrinsic random field model in the study of sulfate deposition processes, 1521-1540.

S.A. Young, D.R. Cutten, M.J. Lynch and *J.E. Davies*: Lidar-derived variations in the backscatter-to -extinction ratio in Southern Hemisphere coastal maritime aerosols, 1541-1551.

R. Sequeira: On the large-scale impact of arid dust on precipitation chemistry of the continental Northern Hemisphere, 1553-1565.

L. Giusti, Y.-L. Yang, C.N. Hewitt, J. Hamilton-Taylor and *W. Davison*: The solubility and partitoning of atmospherically derived trace metals in artificals and natural waters: a review, 1567-1578.

P. Hurley and *W. Physick*: Lagrangian particle modelling of buoyant point sources: plume rise and entrapment under convective conditions, 1579-1584.

V.E. Cachorro, A.M. De Frutos and *M.J. Gonzalez*: Analysis of the relationships between Junge size distribution and Ångström α turbidity parameters from spectral measurement of atmospheric aerosol extinction, 1585-1591.

X.Q. Zhang, P.H. McMurry, S.V. Hering and *G.S. Casuccio*: Mixing characteristics and water content of submicron aerosols measured in Los Angels and at the Grand Canyon, 1593-1607.

A. Greenburg, J.-H. Lwo, T.B. Atherholt, R. Rosen, T. Hartman, J. Butler and *J. Louis*: Bioassay-directed fractionation of organic compounds associated with airborne particulate matter: an interseasonal study, 1609-1626.

Volume 27A Number 11 1993

Volume 27A Number 12 1993

NOTES TO CONTRIBUTORS

The purpose of *Időjárás* is to publish papers in the field of theoretical and applied meteorology. These may be reports on new results of scientific investigations, critical review articles summarizing current problems in certain subject, or shorter contributions dealing with a specific question. Authors may be of any nationality but papers are published only in English.

Papers will be subjected to constructive criticism by unidentified referees.

* * *

The manuscript should meet the following formal requirements:

Title should contain the title of the paper, the names(s) of the author(s) with indication of the name and address of employment.

The title should be followed by an *abstract* containing the aim, method and conclusions of the scientific investigation. After the abstract, the *key-words* of the content of the paper must be given.

Three copies of the manuscript, typed with double space, should be sent to the Editor-in-Chief: *P.O. Box 39, H-1675 Budapest,* Hungary.

References: The text citation should contain the name(s) of the author(s) in Italic letter or underlined and the year of publication. In case of one author: *Miller* (1989), or if the name of the author cannot be fitted into the text: *(Miller,* 1989); in the case of two authors: *Gamov* and *Cleveland* (1973); if there are more than two authors: *Smith et al.* (1990). When referring to several papers published in the same year by the same author, the year of publication should be followed by letters a,b etc. At the end of the paper the list of references should be arranged alphabetically. For an article: the name(s) of author(s) in Italics or underlined, year, title of article, name of journal, volume number (the latter two in Italics or underlined) and pages. E.g. *Nathan, K. K.,* 1986: A note on the relationship between photosynthetically active radiation and cloud amount. *Időjárás 90,* 10-13. For a book: the name(s) of author(s), year, title of the book (all in Italics or underlined with except of the year), publisher and place of publication. E.g. *Junge, C. E.,* 1963: *Air Chemistry and Radioactivity.* Academic Press, New York and London.

Figures should be prepared entirely in black India ink upon transparent paper or copied by a good quality copier. A series of figures should be attached to each copy of the manuscript. The legends of figures should be given on a separate sheet. Photographs of good quality may be provided in black and white.

Tables should be marked by Arabic numbers and provided on separate sheets together with relevant captions. In one table the column number is maximum 13 if possible. One column should not contain more than five characters.

Mathematical formulas and *symbols:* non-Latin letters and hand-written marks should be explained by making marginal notes in pencil.

The final text should be submitted both in manuscript form and on *diskette.* Use standard 3.5" or 5.25" DOS formatted diskettes for this purpose. The following word processors are supported: WordPerfect 5.1, WordPerfect for Windows 5.1, Microsoft Word 5.5, Microsoft Word for Windows 2.0. In all other cases the preferred text format is ASCII.

* * *

Authors receive 30 *reprints* free of charge. Additional reprints may be ordered at the authors' expense when sending back the proofs to the Editorial Office.

Published by the Hungarian Meteorological Service

Budapest, Hungary

INDEX: 26 361

HU ISSN 0324-6329

IDŐJÁRÁS

QUARTERLY JOURNAL
OF THE HUNGARIAN METEOROLOGICAL SERVICE

CONTENTS

VOL. 97 * NO. 4 * OCTOBER–DECEMBER 1993

IDŐJÁRÁS

Quarterly Journal of the Hungarian Meteorological Service

Editorial Office: P.O. Box 39, H–1675 Budapest

Subscription from customers in Hungary should be sent to the Financial Department of the Hungarian Meteorological Service Kitaibel Pál u. 1, 1024 Budapest. The subscription rate is HUF 2000.

Abroad the journal can be purchased from the distributor: KULTURA, P.O. Box 149, H–1389 Budapest. The annual subscription rate is USD 56.

IDŐJÁRÁS

Quarterly Journal of the Hungarian Meteorological Service
Vol. 97, No. 4, October–December 1993

Forward trajectory calculation program system for the Central European region

Z. Ferenczi and **K. Labancz**

Institute for Atmospheric Physics,
P.O. Box 39, H-1675 Budapest, Hungary

(Manuscript received 4 October 1993; in final form 22 November 1993)

Abstract – A program system for predicting wind fields and air parcel trajectories at the 850 hPa pressure level is described. The computer model calculates the possible path of a radioactively polluted air parcel started in any accidental event at a nuclear power station in the Central European region. A case study for Paks, Hungary on 26 August 1993 is presented.

Key-words: transport of air pollutants, wind field calculation, air trajectories.

1. Introduction

The environmental impact of the transport of atmospheric pollutants such as chemical components as well as radioactive elements from an isolated source has become increasingly important in recent years. The claim to predict the trajectories of air masses transporting radioactive or chemical pollutants came to the front after several accidents in nuclear power plants.

A forward trajectory calculation program system is being developed at the Hungarian Meteorological Service for predicting wind at the 850 hPa pressure level and air parcel trajectories for one day over the Central European region.

The program system consists of two main parts: the first part produces a mesoscale wind field, the other calculates trajectories over this field. Because we have limited computer resources and sparse spatial resolution of measured input data, only a simplified model for diagnosing and forecasting the wind field could be chosen. We examined three kind of simplified models: a mass conversation model (*Dickerson*, 1978) which was not expected to function well in a region with sparse data, a one-layer vertically integrated primitive equation model introduced by *Lavoie* (1974) which was suspectible to numerical instability, and a one-level version of the primitive equations in sigma-coordinates

first developed by *Danard* (1977). This model integrates tendency equations for pressure, potential temperature and wind only at the surface and does not demand mass conservation. A version of the Danard model—called MESMOD model—was refined and further developed by *Mass* and *Dempsey* (1985) at the University of Washington. The qualitative stability investigation of their model was done by *Barát* (1990) at the Eötvös Loránd University, Budapest. In according to this investigation the MESMOD model has the potential for diagnosing the important details of the low level wind field and it is computationally stable and efficient.

For computing the air parcel trajectories the kinematic method of *Petterssen* (1956) has been chosen. As a widely used transport level, the 850 hPa pressure level was selected for the calculations. At this pressure level we forecast the wind field for one day by the modified MESMOD model and then we calculate the trajectories.

2. *Calculation of the wind field*

2.1 MESMOD—the mesoscale model for diagnosing surface winds

The original model (MESMOD—*Mass* and *Dempsey*, 1985) is suitable for diagnosing surface winds. The model has been modified for predicting winds at the 850 hPa pressure level for one day.

The original MESMOD is a single-layer, sigma-coordinate, mesoscale model. The basic equations of the model are the horizontal momentum equations and the first law of thermodynamics; these are given in sigma-coordinates at the surface

$$\frac{\partial \vec{v}_s}{\partial t} = -\vec{v}_s \nabla_\sigma \vec{v}_s - f\vec{k} \times \vec{v}_s - (g\nabla_\sigma z_s + RT_s \nabla_\sigma \ln p_s) + \vec{F} + K_M \nabla_\sigma^2 \vec{v}_s, \quad (1)$$

$$\frac{\partial T_s}{\partial t} = -\vec{v}_s \nabla_\sigma T_s + \frac{RT_s}{c_p}\left(\frac{\partial \ln p_s}{\partial t} + \vec{v}_s \nabla_\sigma \ln p_s\right) + \frac{Q}{c_p} + K_T \nabla_H^2 T, \quad (2)$$

where $\vec{v}_s$, T_s, p_s are wind vector, temperature and pressure, respectively, at the surface, z_s is the height of the surface. f denotes the Coriolis parameter, g the gravitational acceleration, c_p the specific heat capacity, and $\vec{F}$ is the frictional force. K_M and K_T represent the momentum and the temperature horizontal diffusion, and finally Q is the diabatic heating. For the deduction of equations $\dot{\sigma}=0$ at surface level was applied.

The third unknown variable in the equations is the surface pressure. This variable is a diagnostic one, because it does not have tendency in Eqs. (1) and (2).

p_s can be determined by integrating the hydrostatic equation between the surface and the 850 hPa pressure level. To this end we suppose that the pollution processes are taking place between the surface and the 850 hPa pressure level, at which the geopotential height and temperature fields are known. Furthermore, we assume that the topographically caused orographic flow occurs within a 2 km layer above the surface.

The prognostic variables of the model are $\vec{v}_s$ and T_s. T_s refers to the surface layer. The values of the wind speed calculated by the model are related to the upper boundary of the friction layer, 50–100 m height. In vertical direction linear thermal stratification is assumed in the model.

The diabatic effect depends on the daily variation of the radiant exposure, the frictional force can be expressed as the vertical divergence of the stress, the horizontal diffusion of the momentum and the temperature are parameterized in the model.

2.2 The wind field at the 850 hPa pressure level

For calculating the path of radioactive elements over a region, the 850 hPa pressure level is widely used. Therefore the previously described model has been re-written for predicting winds at the 850 hPa pressure level.

The coordinate system used is a σ-system

$$\sigma = \frac{p - 850}{p_s - 850}.$$

The choice of the σ-system is reasonable because at the surface $\sigma = 1$ and at the 850 hPa pressure level $\sigma = 0$, hence $\dot{\sigma} = 0$ (*Práger*, 1982). Substituting this expression into the momentum and temperature tendency equations we obtain the following equations

$$\frac{\partial \vec{v}_{850}}{\partial t} = -\vec{v}_{850} \nabla_\sigma \vec{v}_{850} - f\vec{k} \times \vec{v}_{850} - g \nabla_\sigma z_{850} + \vec{F} + K_M \nabla_\sigma^2 \vec{v}_{850}, \qquad (3)$$

$$\frac{\partial T_{850}}{\partial t} = -\vec{v}_{850} \nabla_\sigma T_{850} + \frac{R T_{850}}{c_p} \left(\frac{\partial u_{850}}{\partial x} + \frac{\partial v_{850}}{\partial y} \right) + \frac{Q}{c_p} + K_T \nabla_\sigma^2 T_{850}. \qquad (4)$$

In these equations we apply the earlier notations, $\vec{v}_{850}$ and T_{850} denote the 850 hPa pressure level wind vector and temperature, respectively. By the production of this motion field we parameterize the diabatic warming and cooling, the horizontal diffusion as well as the frictional force.

3. *Calculating kinematic trajectories*

It is well known that the trajectories indicate the actual path which an air parcel travels along. *Ihász* (1992) investigated the different trajectory calculation methods used in meteorological practice. In our program system we use an isobaric method for the 850 hPa level.

If the $\vec{v}(x,y,z,t)$ wind field and its temporal variation are known, the trajectory of a parcel situated at the point $\vec{r}_o(x_o,y_o,z_o)$ and at the moment $t=t_o$ can be determined as the solution of the initial value problem referring to the differential equation defining the wind field

$$\vec{r}(t) = \vec{r}_o(t_o) + \int_{t_o}^{t} \vec{v}(\vec{r}(\tau))d\tau . \tag{5}$$

As an approach of this integration formula we use the kinematic iterative method suggested by *Petterssen* (1956). The $\vec{v}(\vec{r}(t))$ wind field at the 850 hPa pressure level in the form of successive wind charts for 24 hours is available as the result of the MESMOD model. After a given Δt time step, the new position of an air parcel started from $\vec{r}_o$ point is calculated by means of the following iterational steps:

(1) We draw the $\delta\vec{r}_1=\vec{v}(\vec{r}_o(t_o))\Delta t$ displacement vector. Thus on the next map the parcel would arrive at the point Q_1 (see *Fig. 1*).

(2) In the meantime the pressure distribution has changed so we have to draw the $\delta\vec{r}_2=\vec{v}(\vec{r}_o+\delta\vec{r}_1(t_o+\Delta t))\Delta t$ displacement vector.

(3) As a second approximation of the new position of the air parcel we draw the displacement vector $\delta\vec{r}_1=\frac{1}{2}(\delta\vec{r}_1+\delta\vec{r}_2)$ and the point Q_2.

(4) The operation described in the 2nd and 3rd steps should be repeated until the difference between $\delta\vec{r}^{(n-1)}$ and $\delta\vec{r}^{(n)}$ will be small enough. Δt and n were set to 1 hour and 2, respectively. This method is shown in Fig. 1.

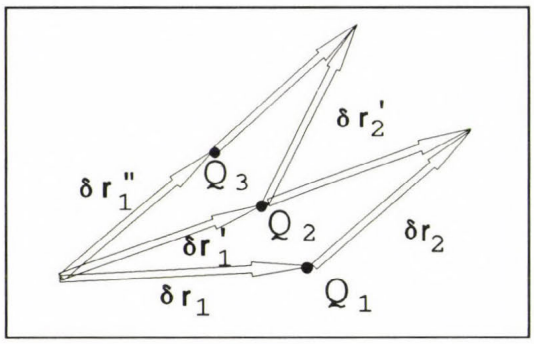

Fig. 1. Scheme for the use of the trajectory method.

4. The data base used

The area to be investigated is located between 12.5°E–25°E and 40°N–50°N. The grid resolution of the used terrain field is 1/3° along both longitude and latitude, which gives 30×38 grid points over the area.

As initial conditions the program needs temperature and geopotential height at the 850 hPa level at the initial moment of the model integration. The so called GRID data from the British Meteorological Office (Bracknell) have been used for this purpose. The resolution of the GRID information is 2.5°×2.5°, so there are 5×6 GRID points in the domain of the MESMOD model. For interpolating the GRID data over the model area the formula

$$\varphi = \frac{\sum_i \left(\frac{\varphi_i}{r_i^2} \right)}{\sum_i \left(\frac{1}{r_i^2} \right)} \tag{6}$$

is used, where φ is any variable in the grid point of MESMOD, r_i is the distance between the grid point of MESMOD and the grid point of GRID, and φ_i is the given variable in the GRID.

5. Practical realization and results

First we have to produce the wind field over the area of our examination for calculating the trajectory with the required temporal resolution. The investigated area is Central Europe in the operational application. In this area we have to determine the wind field with hourly resolution in the next 24 hours.

After initialization, the model is integrated without diabatic heating to steady-state. After that the calculation of the wind field begins. The model makes an output at every Δt time step (in our examination Δt is equal to 1 hour). After producing the successive wind fields, the model starts to calculate the trajectories of the pollutants originating from a given point of the region.

The mesoscale model we use to calculate the wind field gives different results in different synoptic situations. In their paper the authors (*Mass* and *Dempsey*, 1985) mention that "There are situations in which this simple model is not suitable for diagnosing the low level wind field such as for high Froude number cases, ... e.g. during a frontal passage.". After some model runs for real cases we realised that except the above mentioned situations the model calculates the mesoscale wind field suitably but it gives only small changes in the predicted field, therefore it does not follow the quick meteorological changes such as frontal passages.

As an example we have chosen a calm meteorological situation on 26 August 1993 when a slowly moving cold front situated south of Hungary. To the north of the front there was a cold air mass over Europe and this situation had not considerably changed during that day. We calculated a trajectory of an imagined radioactively polluted air parcel started from the nuclear power station at Paks at 00 UTC on 26 August 1993. *Fig. 2* shows the wind field at the 850 hPa pressure level after one-hour integrating.

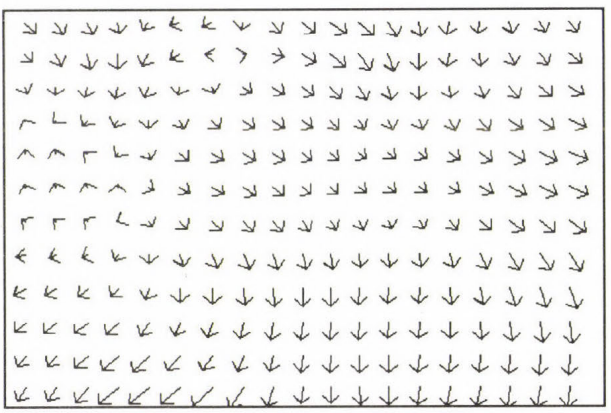

Fig. 2. The calculated wind field at the 850 hPa pressure level at 01 UTC on 26 August 1993 over the examined region.

The wind field had not changed on that day thus after 24 hours we could draw a trajectory started from Paks shown by *Fig.3.*

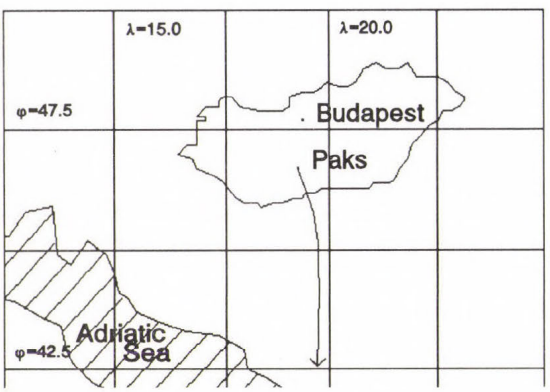

Fig. 3. Trajectory starting from Paks on 26 August 1993.

In the future we want to use this technique for forecasting the path of the air masses containing radioactive or chemical pollutants released in any

accident. For this purpose we intend to develop the capability of the mesoscale model to give better predictions of changing meteorological situations.

Acknowledgements—The authors are much indebted to *Dr. Tamás Práger* for valuable suggestions and comments.

References

Barát, I., 1990: *Qualitative Investigation of a Mesoscale Model Predicting Surface Air Flow* (in Hungarian). Master's Thesis.

Danard, M., 1977: A simple model for mesoscale effects of topography on surface winds. *Mon. Wea. Rev. 105*, 572-581.

Dickerson, M.H., 1978: MASCON–A mass consistent atmospheric flux model for regions with complex terrain. *J. Appl. Meteor. 17*, 241-253.

Ihász, I., 1992: Isobaric and isentropic objective analysis of meteorological fields for regional and continental scale trajectories. *Időjárás 96*, 81-92.

Lavoie, R.L., 1974: A numerical model of trade wind weather on Oahu. *Mon. Wea. Rev. 102*, 630-637.

Mass, C.F. and *Dempsey, D.P.*, 1985: A one-level, mesoscale model for diagnosing surface winds in mountains and coastal region. *Mon. Wea. Rev. 113*, 1211-1227.

Petterssen, S., 1956: *Weather Analyses and Forecasting*. Vol. I. McGraw-Hill, New York, Toronto, London.

Práger, T., 1982: *Numerical Prediction*. Part I. Lecture Notes (in Hungarian). Eötvös Loránd University, Budapest.

IDŐJÁRÁS

Quarterly Journal of the Hungarian Meteorological Service
Vol. 97, No. 4, October–December 1993

Comprehensive hydrostatic quality control of radiosonde height and temperature data

É. Borbás

Satellite Research Laboratory, Hungarian Meteorological Service,
P.O. Box 32, H-1675 Budapest, Hungary

(Manuscript received 13 August 1993; in final form 10 November 1993)

Abstract—The errors in observational data can damage analysis and forecast fields, so any control procedure of radiosonde data of height and temperature at the mandatory isobaric surfaces plays an important role in *numerical weather prediction* (NWP). We have created a hydrostatic quality control for the Hungarian NWP model. To this end we have chosen a *comprehensive hydrostatic quality control* (CHQC) method. The introduction gives a brief description of the history of *quality controls* (QC) and an experiment is presented to illustrate the effect of the erroneous data on the objective analysis. In the next two sections the method of CHQC is described. In the fourth section, a few examples show the efficiency of the method for different error types. At the end of the paper, we refer to statistical results, and conclusions and plans for the future are given.

Key-words: complex quality control, comprehensive hydrostatic quality control, decision-making algorithm.

1. Introduction

Meteorological observational data contain errors in a smaller or higher degree. These errors can be divided into two categories: the first one contains errors which have no large absolute values and they are inherent in all data. The second category of errors—*gross errors*—is the one which is important for us in this paper. They are caused by the failure of measuring instruments and/or by mistakes during data processing, transmission and reception. Gross errors can be very large, though they occur rarely. These errors are important because they can highly damage the analysis and forecast fields. In order to avoid them, it is necessary to control the meteorological information.

The Hungarian NWP model uses SYNOP and TEMP data over the European area. We have controlled the data of mandatory pressure levels of TEMP reports with the method which was designed and implemented at the

National Meteorological Center (NMC) in Washington, D. C. (*Gandin* and *Collins*, 1990). Two sets of observational data are available for our model: measured data at 00 and 12 UTC.

We have carried out an experiment in order to investigate the effect of the wrong data on analysis fields. First of all we have created a correct set of reports (12 UTC, 18th May 1993.). In *Fig. 1a* the objective analysis for these data can be seen. Afterwards we have artificially introduced stations with erroneous reports: we have damaged the height data of some selected stations [Bodø (01152), Vienna (11052), Budapest (12843) and Szeged (12982)] at 500 hPa with about 150–200 m. *Fig. 1b* shows the modified objective analysis field. The effect of these artificially introduced gross errors is significant, as it can be seen from the difference field of the two analyses for two damaged areas (*Fig. 1c, d*). Finally, we have corrected the wrong data with our method. The correction perfectly reproduced the original field. This experiment also proved the necessity of checking the observational data.

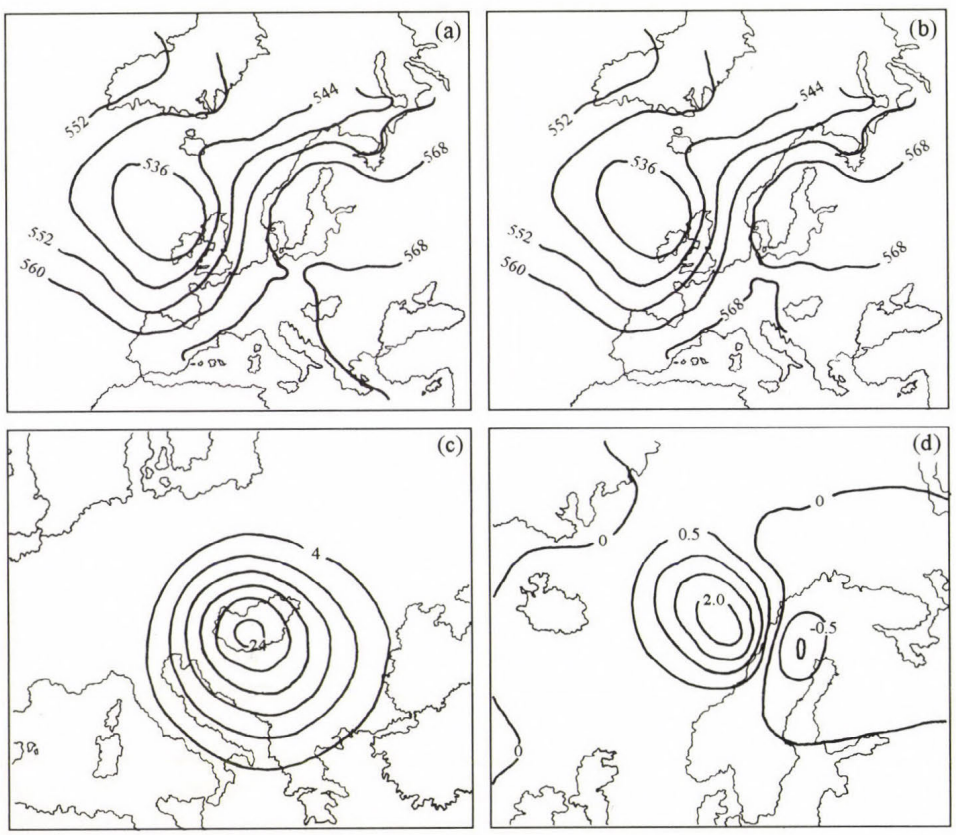

Fig. 1. 00 UTC 18th May 1993 analysis of 500 hPa geopotential height with correct data (*a*), and with erroneous data in some places (*b*) (values are given in dkm), difference fields for two erroneous areas (*c, d*).

The development of quality control (QC) of meteorological data is a sequence of actions directed against gross errors. The presence and danger of gross errors in meteorological data had been recognized before NWP activity was started. Visual examination of weather charts and other graphical representations were the only ways to detect these errors, so correction or rejection of erroneous data was done on the basis of subjective decisions. This manual QC was applied at the very beginning of the NWP era. At the dawn of NWP, the QC of meteorological information became much more important and its importance has permanently grown together with the improvement of analysis and NWP models. In this respect, we have to underline that the more improved a NWP model is, the more sensitive it is to the errors of initial data. Simultaneously, the problem of automatic QC has become much more complicated because of two factors: dramatic increase of the number of available meteorological data, and development and application of new meteorological observations. QC could not be accomplished manually because of the increasing number of meteorological data.

Several QC methods have been developed parallelly. The first objective analysis system was developed by *Gilchrist* and *Cressman* (1954) which contained an automatic QC. *Bergthorson* and *Döös* (1955) suggested the application of the first guess fields in objective analysis in order to check the observation data. The first version of hydrostatic check was suggested at the same time. *Belousov et al.* (1968) proposed the first version of the spatial continuity check in his three-level quasi-geostrophic NWP model. The next very important step in the QC development was the introduction of methods based on optimum interpolation. These were first developed in the USSR in the sixties. The multivariate three dimensional version of these methods was applied in 1977 (*Lorenc et al.*, 1977).

For a long time, however, QC was considered as a purely technical task. Fortunately, the situation has changed recently. Several QC methods are now being used sequentially and each of these made the decisions independently (*ECMWF*, 1985). The idea of *complex quality control* (CQC) was formulated by *Gandin* (1969). CQC is able to do more than horizontal and hydrostatical checks, as two QC methods are used sequentially: CQC is a more complex approach. The first *decision-making algorithm* (DMA) was developed by *Parfiniewicz* (1976). Three components were applied in his method: the horizontal check of height and temperature, and the hydrostatical check.

All the existing versions of CQC consist of at least these three components. The most advanced CQC contains two additional components: vertical check of height and temperature.

Many specialists still consider the quality control as a secondary task. This is the reason why CQC algorithms of other radiosonde data (wind, humidity) have not been developed yet. Therefore, CQC of height and temperature data remained the only operationally functioning CQC (see further details in *Gandin*, 1988).

Instead of developing the existing system, the design of a new quality control system was started at NMC, Washington, D. C. in 1988. NMC decided to design and implement a comprehensive hydrostatic quality control (CHQC) which uses only hydrostatic check, but it still contains an advanced DMA. This DMA is capable of detecting and correcting the gross hydrostatic errors. This is the first step to design a complex multicomponent quality control, which still has to include horizontal and vertical check of height and temperature without the hydrostatic check. The CHQC was put into operation at the end of 1988. The experiments showed that the data corrected by CHQC were never rejected by subsequent checks.

There exists a kind of man-machine interaction in the process of CHQC. It appears in all cases when CHQC cannot correct the data alone, and specialists make the final decisions. Using this procedure, there is a possibility to correct more erroneous data. There is no doubt that in the future, when the hydrostatic check is used together with statistical interpolation checking, still more wrong data can be corrected automatically.

In Hungary, *Ozorai* (1972) and *Dévényi* (1983) have made attempts at automatic hydrostatic quality control so far. Though our method in its present form, which is described in the next section, is based on hydrostatic control only, a complex quality control method must contain both horizontal and vertical check. Data check in the horizontal direction can be realized, e.g., by using Bayesian quality control methods (*Lorenc* and *Hammon*, 1988). The Bayesian method assumes that observation errors can be described by a probability distribution, which is a combination of a Gaussian white noise and the uniform distribution, the latter representing gross errors.

2. *The method*

Let us apply the hydrostatic equation to a layer between two adjacent mandatory surfaces, and let us compose the difference between the two sides of the equation. Furthermore, let us define this difference as a hydrostatic residual. The CHQC is based on the examination of these residuals.

Integrating the hydrostatic equation through a layer between the isobaric surfaces (p_i, p_{i+1}), and applying the following formulas

$$A_{i,\,i+1} = (RT_0/g)\ln(p_i/p_{i+1}), \tag{1}$$

$$B_{i,\,i+1} = (R/2g)\ln(p_i/p_{i+1}), \tag{2}$$

where T_0=213.15 K, g is the acceleration of gravity, R is the gas constant for dry air, and p_i, p_{i+1} are pressure of the ith and $i+1$th surfaces, then the hydrostatic equation can be written in the following form

$$z_{i+1} - z_i = A_{i,i+1} + B_{i,i+1}[(T_i + T_{i+1}) + 2t_{i,i+1}], \tag{3}$$

where z is height (dkm) and T is temperature (°C).

The term $t_{i,i+1}$ consists of three factors: neglect of humidity and roundoff errors, and the use of mandatory levels only (this results from allowing the nonlinearity of temperature with the logarithm of pressure).

The hydrostatic residual in terms of height and temperature is defined as

$$S_{i,i+1} = z_{i,i+1} - z_i - A_{i,i+1} - B_{i,i+1}(T_i + T_{i+1}) \tag{4}$$

and

$$X_{i,i+1} = (z_{i+1} - z_i)D_{i,i+1} - (T_i + T_{i+1}) - 2T_0, \tag{5}$$

where $D_{i,i+1} = 1/B_{i,i+1}$ ($X_{i,i+1}$ stems from dividing $S_{i,i+1}$ by $B_{i,i+1}$).

If height and temperature data contain gross errors,

$$z_i = \hat{z}_i + z_i' \qquad T_i = \hat{T}_i + T_i', \tag{6}$$

$$Z_{i+1} = \hat{Z}_{i+1} + Z_{i+1}' \qquad T_{i+1} = \hat{T}_{i+1} + T_{i+1}', \tag{7}$$

where $\hat{z}_i$, $\hat{z}_{i+1}$, $\hat{T}_i$, $\hat{T}_{i+1}$ are values, which exactly satisfy the hydrostatic balance (primed values are gross errors), then residuals in terms of gross errors are

$$S_{i,i+1} = z_{i+1}' - z_i' - B_{i,i+1}(T_i' + T_{i+1}' - 2t_{i,i+1}), \tag{8}$$

$$X_{i,i+1} = (z_{i+1}' - z_i')D_{i,i+1} - (T_i' + T_{i+1}' - 2t_{i,i+1}). \tag{9}$$

To detect the errors and error types, a "backward" problem has to be solved, because it is an easier task to approximately determine what the residuals should be for a particular error or several errors. The actual problem is to find the errors which are obtained by a particular pattern of residuals.

The DMA of CHQC examines four levels (three layers) at the same time (*Fig. 2.*). This "template" progressively moves upward along the profile, while looking for errors on the basis of a definite pattern of residuals. After reaching the top of the profile, a second pass is made through the data in order to examine them more precisely. To find an error which has to be corrected, existence and magnitude conditions have to be satisfied. The DMA can separate errors of different types by existence conditions, while magnitude conditions assure that any suspected error has a sufficient size (not the result of the $t_{i,i+1}$s).

Formulas for provisional correction (*Table 1*) in terms of temperature have been derived by minimizing the sum of the squares of the resulting residuals.

We have checked the accuracy of the equation with disturbing some data and deducing the equations. We can get the formulas for existence conditions (*Table 2*): by writing Eqs. (8) or (9) for the layer which contained an erroneous level,

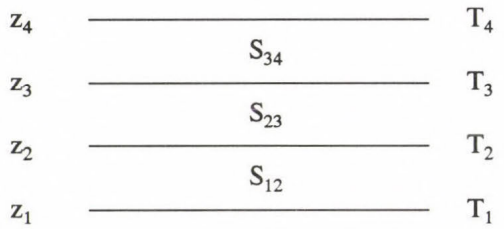

Fig. 2. The template.

eliminating the errors (e.g. by Gaussian elimination), then squaring the obtained equations and averaging over many realizations. We have deduced these formulas, too. The magnitude conditions can be seen in *Table 3*.

Table 1. Formulas for provisional corrections

Type	Formulas for provisional corrections
1	$z_3' = (D_{34}X_{34} - D_{23}X_{23})/(D_{34}^2 + D_{23}^2)$
2	$T_3' = (X_{23} + X_{34})/2$
3	$z_3' = (B_{23}S_{34} - B_{34}S_{23})/(B_{23} + B_{34})$ $T_3' = (S_{23} + S_{34})/(B_{23} + B_{34})$
7	$z_2' = (-D_{12}(D_{23}^2 + D_{34}^2)X_{12} + D_{23}D_{34}^2X_{23} + D_{23}^2D_{34}X_{34})/$ $((D_{12}^2 + D_{34}^2)D_{23}^2 + D_{12}^2D_{34}^2)$ $z_3' = (-D_{12}D_{23}^2X_{12} - D_{23}D_{12}^2X_{23} + (D_{12}^2 + D_{23}^2)D_{34}X_{34})/$ $((D_{12}^2 + D_{34}^2)D_{23}^2 + D_{12}^2D_{34}^2)$
8	$T_2' = (2X_{12} + X_{23} - X_{34})/3$ $T_3' = (2X_{34} + X_{23} - X_{12})/3$
9	$z_2' = (D_{23}X_{23} - 2D_{12}X_{12} - D_{23}X_{34})/(2D_{12}^2 + D_{23}^2)$ $T_3' = (D_{12}^2X_{23} + D_{12}D_{23}X_{12} + (D_{12}^2 + D_{23}^2)X_{34})/(2D_{12}^2 + D_{23}^2)$
10	$T_2' = ((D_{23}^2 + D_{34}^2)X_{12} + D_{34}^2X_{23} + D_{23}D_{34}X_{34})/(D_{23}^2 + 2D_{34}^2)$ $z_3' = (D_{23}X_{12} + 2D_{34}X_{34} - D_{23}X_{23})/(D_{23}^2 + 2D_{34}^2)$

We can get a huge residual if one of the four values in question for the hydrostatic residual (two heights and two temperatures) is distorted by a gross

communication-related error. Accordingly, if the erroneous level is not the highest or the lowest reported one, then a large hydrostatic residual for the two adjacent layers contained this level will be involved by an error in either height

Table 2. Existence conditions

Type	Existence conditions
1	$\lvert S_{23} + S_{34} \rvert < 2\bar{t}_{all}(B_{23}^2 + B_{34}^2)^{1/2}$
2	$\lvert X_{23} + X_{34} \rvert < 2\bar{t}_{all}$
7	$\lvert S_{12} + S_{23} + S_{34} \rvert < 2\bar{t}_{all}(B_{12}^2 + B_{23}^2 + B_{34}^2)^{1/2}$
8	$\lvert X_{12} - X_{23} + X_{34} \rvert < 2\bar{t}_{all}3^{1/2}$
9	$\lvert S_{12} + S_{23} - (B_{23}/B_{34})S_{34} \rvert < 2\bar{t}_{all}(B_{12}^2 + 2B_{23}^2)^{1/2}$
10	$\lvert S_{23} + S_{34} - (B_{23}/B_{12})S_{12} \rvert < 2\bar{t}_{all}(B_{34}^2 + 2B_{23}^2)^{1/2}$

or temperature at this level. Examining these residuals, DMA has to decide whether height or temperature or both are wrong in the level.

Table 3. Magnitude conditions

Type	Magnitude conditions
1	$\lvert z_3' \rvert > 2\bar{t}_{all}(B_{23}^2 + B_{34}^2)^{1/2}$
2	$\lvert T_3' \rvert > 2\bar{t}_{all}$
7	$\lvert S_{12} \rvert > S_{12}^{thres}$ and $\lvert S_{34} \rvert > S_{34}^{thres}$
8	$\lvert X_{12} \rvert > 2\bar{t}_{all}$ and $\lvert X_{34} \rvert > 2\bar{t}_{all}$
9	$\lvert S_{12} \rvert > S_{12}^{thres}$ and $\lvert X_{34} \rvert > 2\bar{t}_{all}$
10	$\lvert X_{12} \rvert > 2\bar{t}_{all}$ and $\lvert S_{34} \rvert > S_{34}^{thres}$

If so, *Type 1* is an error at a single, isolated height, resulting in huge hydrostatic residuals of opposite sign in the adjacent layers.

In the same way, let us define *Type 2*, as an error in a single, isolated

temperature, but this type of error results in large hydrostatic residuals of the same sign in the adjacent layers. If both height and temperature are wrong, then we can consider it as a *Type 3* error.

The CHQC developed by *Gandin* and *Collins* (1990) analyses four levels (template) at the same time, and DMA defines the error types in the third level of the template. However, it is not possible to detect isolated errors of the second level of the profile. In order to avoid this problem, *Gandin* and *Collins* introduced an additional test of the profile by scanning it downwards, starting from the top level. Instead of this, we have introduced additional error types to examine the second level of the template by the same method as analysing the third one. Consequently, *Types 11, 12* and *13* were introduced similarly to *Types 1, 2* and *3*. We have decided to follow this way, because it is simpler than Gandin's and Collins' method, and introducing the new types was more advantageous for our purposes.

A gross error in either height or temperature at the lowest level leads to a large hydrostatic residual. This is the *Type 4* error. The CHQC DMA is unable to decide which of the two values is wrong (maybe both of them). Unique decision for this is a much more complex procedure of correction, which must be combined with other checking residuals. Since it has not been implemented, our DMA rejects the lowest level in this case.

The analogy of *Type 4* error is a single large residual for the highest layer, when either temperature or height of the highest level (or both of them) is wrong (*Type 5* error).

A gross error in the computation (or documenting) of the layer's thickness may result in a large hydrostatic residual for only one layer. Let us define this as *Type 6* error. If this kind of error occurs, the height of all surfaces above this layer should be corrected. To make any correction automatically based on only one residual, is risky, so this case was not investigated. We can neglect it because the statistical calculation demonstrates (*Gandin*, 1991) that *Type 6* of errors happens relatively seldom. One can say that the computational errors represent a small part of hydrostatic errors. In the future, if a hydrostatic QC is completed with other checking systems, for example in case of Type 6 errors with height increments and horizontal statistical interpolation residuals at several levels (*Collins*, 1991), more corrections can be checked.

Experiment shows that most of the hydrostatic errors are telecommunication related. A part of these belongs to the category called "simple" errors. It appears during processing the data at the station or in the course of communicating them. Simple error is (1) an error of a single digit, (2) interchange of digits and (3) sign error of temperature or any combinations of these.

Both height and temperature at a level have to exist in the report to be controlled hydrostatically. If any of them (or both of them) is missing and both neighbours below and above are not empty, that level is called a missing level. One or several of missing levels in a report does not prevent the DMA from

performing the QC of existing levels. However, it may happen that a report contains the same parameter of several missing levels, then the report contains a "data-hole". We do not examine this case. Nevertheless, a lack of temperature or height of one level is defined as a *Type 14* error.

Two or more hydrostatic errors seldom occur in a report, and if at least one error-free level exists between those containing errors, then DMA can detect it successively and, if possible, DMA can correct them. It is different from the case when two adjacent mandatory levels contain gross errors. In this case DMA has to analyze three adjacent layers (4 levels) simultaneously, instead of two adjacent layers (for this reason the template consists of 4 levels). If gross errors were found independently of each other, these cases occur much more often than they would. The NMC's CHQC (and also our method) is able to deal with the next four types: two adjacent height errors (*Type 7*), two adjacent temperature errors (*Type 8*), adjacent errors in height below and temperature above (*Type 9*), and *vice versa* (*Type 10*). Every type of errors is summarized in *Table 4*.

What happens if there are three or more hydrostatic errors at adjacent levels? These situations are more complicated cases, so CHQC is unable to treat them because too many branches of the DMA would have to be added in order

Table 4. Error types

Type	Description
1	Large isolated height error
2	Large isolated temperature error
3	Error in height and temperature of the same level
4	Error in height or temperature or both of the highest level
5	Error in height or temperature or both of the lowest level
6	Computational error in a layer thickness (not detected)
7	Errors in heights of two adjacent levels
8	Errors in temperatures of two adjacent levels
9	Adjacent errors in height below and temperature above
10	Adjacent errors in temperature below and height above
11	Type 1 error in the second reported level
12	Type 2 error in the second reported level
13	Type 13 error in the second reported level
14	Lack of temperature or height in one level

to achieve this aim, and still there would remain more complicated combinations of errors not treatable by the DMA. Such combinations happen very seldom. In the present stage of DMA, in these most complicated cases human help is necessary .

3. *The decision-making algorithm*

The reason of describing the DMA in more detail is that a very specialized logic is necessary for hydrostatic error correction. In spite of the fact that DMA is relatively complicated, the required computer time is minimal since only suspected reports are examined.

First of all, error determination begins with computing residuals for each profile of heights and temperatures, and looking for large residuals. If DMA finds a large residual in a profile, it is examined further. The selection of suspicious, erroneous profiles is done by using empirical thresholds. These thresholds are derived from a residual of about seven times the standard deviation of error-free data published by *Gandin* and *Collins* (1990). We need the threshold values when the profile contains isolated missing levels. In this case, we had to derive these values from thresholds of available two adjacent layers. Thus, we had to determine a residual of about seven times the standard deviation of the values in the absence of gross errors for sum of these adjacent layers. If these residuals can be considered as independent random variables then a threshold value for a sum of two adjacent layers is the sum of the two threshold values. On the other hand, these residuals are not independent in general, so the required values have to be smaller than the sum of the two threshold values. Our experiments have shown that the mean of the maximum and sum of these two threshold values is an appropriate choice as a threshold value of the missing layer. These values for each mandatory layer (and also for isolated missing layers) can be found in *Table 5*.

Table 5. Threshold residuals (also for layers containing one missing level)

Pressure layers hPa	Threshold residuals m	Pressure layers hPa	Threshold residuals m
1000–925	40	1000–850	65
925–850	30	925–700	50
850–700	35	850–500	70
700–500	50	700–400	70
500–400	35	500–300	60
400–300	40	400–250	60
300–250	35	300–200	60
250–200	40	250–150	70
200–150	50	200–100	110
150–100	85		

Errors of *Types 1, 2* and *7* to *10* must satisfy existence and magnitude conditions. It also occurs that both height and temperature are erroneous at the same level. Investigations (*Gandin* and *Collins*, 1990) show that two adjacent residuals containing this level are large, but the existence conditions are not satisfied for a height or temperature correction (*Type 3* error). In this case there is a pair of height and temperature that will make the residuals zero. This pair is suggested as height and temperature corrections (Table 1).

We have already mentioned that a radiosonde profile is examined by progressively moving the template upward from the lowest existing level. First, our DMA computes hydrostatic residuals with omitting missing levels (if any). If a large residual is found in a report, it begins to examine errors (*Types 4, 5* and *14* errors) which cannot be corrected. In this case the DMA rejects the erroneous level. In the case of *Type 3* error (and *Type 13* error) the operator decides to accept or to reject the suggested correction. After the detection of the errors that cannot be corrected, correctable ones are searched on the bases of existence and magnitude conditions.

It also happens that more than one error type satisfies both conditions. In this case the DMA calculates the ratio of two sides of the existence condition for every satisfied type and then accepts the correction which has given the largest value of ratio (fulfils existence condition most strongly).

Sometimes Arctic stations report 700 hPa heights less than 2400 m in winter, but the thousand's digit of the 700 hPa height is not included in the coded message. Therefore, in general, 3 is added during the decoding process. Then the DMA can correct safely these heights by 1000 m.

Finally, our algorithm accepts the proposed corrections only if the temperature correction is at least 10°*C* in magnitude, and height correction is at least 30 m at 1000–700 hPa, and at least 90 m at the other levels. Multiple corrections (*7–10 types*) are not made if both are small, as defined above.

In some rare cases, residuals of *7* and *8 types* or *9* and *10 types* are the same. This case occurs when the median of the three residuals is small. Then DMA is unable to distinguish between these two types.

4. Examples for the different error types

In this section we show the possibilities and limitation of the method. The examples are partly derived from real cases. On the other hand, we have also artificially introduced errors for some error types. Information in the examples includes the date and time; station identification number, pressure p (hPa); height z (m); temperature T (°C); residual S (decameter); height correction *ZCOR* (m) (if any); temperature correction *TCOR* (°C) (if any); and error type. First examples show the most frequent errors, while rarely occurring errors are introduced by ourselves.

Accordingly, variable forms of *Type 1* (or *Type 11*) can be seen in examples 1–4 and then 2 error types follow.

Example 1: *Type 1* error; single digit error. Operator makes "simple" correction (it is clear from roundoff correction); height at 500 hPa is corrected with 2000 m.

10.11.1992		00 UTC		Barencburg (20 107)		
p	z	T	S	ZCOR	TCOR	Type
850	1250	-9.4				0
			0.12			
700	2740	-13.4				0
			-199.85			
500	3230	-28.0		2000		1
			200.53			
400	6800	-39.6				0
			-0.02			

Example 2: *Type 1* error; general error type. This correction can be executed.

10.11.1992		00 UTC		Rjazan' (27 731)		
p	z	T	S	ZCOR	TCOR	Type
400	6940	-40.6				0
			-1.11			
300	9840	-52.2				0
			18.25			
250	10200	-53.2		-180		1
			-17.92			
200	11460	-52.8				0
			0.79			

Example 3: *Type 1* error; small height correction. The height correction is 40 m at 400 hPa, so it is smaller than 90 m (limited correction). No correction is made by our program in this case.

29.09.1992		00 UTC		Barencburg (20 107)		
p	z	T	S	ZCOR	TCOR	Type
700	2940	-12.4				0
			-0.33			
500	5440	-26.0				0
			4.44			
400	7070	-35.2		-40		0
			-3.41			
300	8990	-47.4				0
			-			

Example 4: *Type 11* error; the second level of report contains height error (this type was introduced by us). Operator corrects the height at 700 hPa with -100 m.

29.09.1992	00 UTC		Simferopol' (33 946)			
p	z	T	S	ZCOR	TCOR	Type
1000	–	–				0
925	–	–				0
850	1514	11.3				0
			10.31			
700	3206	1.1		-100		11
			-7.9			
500	5750	-15.2				0
			0.23			

Example 5: *Type 2* error; sign correction. -52°C correction is proposed at 400 hPa instead of 25.9°C. Obviously this is a "simple" error.

30.09.1992	12 UTC		Constanta (15 480)			
p	z	T	S	ZCOR	TCOR	Type
700	3159	1.3				0
			-0.01			0
500	5780	-15.8				0
			-16.87			
400	7430	25.9			-52	2
			-22.43			
300	9440	-42.4				0
			0.42			

As already mentioned, DMA can correct the 7–10 error types, too. The next two examples show *Types 7* and *8* errors of them.

Example 6: *Type 7* error; height of two adjacent levels are erroneous.

29.09.1992	00 UTC		Bucuresti (15 420)			
p	z	T	S	ZCOR	TCOR	Type
			-0.38			
700	3130	0.7				0
			-399.5			
500	1760	-14.4		4000		7
			200.29			
400	5410	-28.0		2000		7
			200.13			
300	9410	-44.0				0
			0.06			

Example 7: We have added 20°C at 300 hPa and -30°C at 400 hPa to the temperature. Then the template contained two error types: *Type 1* and *Type 8*, but our program suggested *Type 8*, because this type satisfies rather the existence condition.

29.10.1992	12 UTC			Bjornoya (01 028)		
p	z	T	S	ZCOR	TCOR	Type
			-0.34			
500	5140	-40.2				0
			-9.65			
400	6300	-79.8			30	8
			-4.42			
300	9480	-38.0		-50	-20	1, 8
			-5.69			
250	9630	-56.4				0
			0.86			

Hereafter we show examples for the correction, which cannot be made by DMA. Example 8: *Type 7* and *Type 8* errors. In this example both types satisfy both conditions, because hydrostatic control is unable to distinguish whether height errors of two adjacent levels have the same value and same sign, or temperature errors of two adjacent levels have the same value but opposite sign. In this case the medium residual will be small, while the other two residuals will have the same values and sign. Then our method does not correct them. (The situation is similar for the *Type 9* and *Type 10* errors.)

27.10.1992	12 UTC			Isparta (17 240)		
p	z	T	S	ZCOR	TCOR	Type
			-0.38			
400	7330	-27.8				0
			-7.97			
300	9260	-41.6		80	-19	7, 8
			-0.67			
250	10480	-50.4		70	21	7, 8
			6.84			
200	11970	-61.0				0
			2.36			

Example 9: *Type 5* error. The highest level is wrong. Operator deleted this level from the report. Similar to *Type 4* error.

30.09.1992	12 UTC			Simferopol' (33 946)		
p	z	T	S	ZCOR	TCOR	Type
850	1367	-4.0				0
			-2.64			
700	2871	-4.2				0
			-5.91			
500	5330	-31.2				5
400	-	-				

Example 10: We damaged the temperature by 20°C at 850 hPa and the height by 1000 m at 500 hPa. The proposed corrections can be seen in the example. Operator will correct the temperature at 850 hPa and the height at 500 hPa, because *Type 1* satisfies rather the existence condition. Therefore correction of *Type 7* error at 700 hPa is not performed.

17.11.1992	00 UTC			Vienna (11 035)		
p	z	T	S	ZCOR	TCOR	Type
925	636	4.3				0
			-2.36			
850	1320	20.7			-18	12
			-5.06			
700	2868	-7.0		44		7
			101.15			
500	6430	-20.6		-1000		1, 7
			-99.24			
400	7050	-32.4				0
			0.34			

Example 11: *Type 3* error; height was changed by 1000 m and the temperature by 20°C at 500 hPa. This type of error seldom occurs and the proposed corrections are not reliable, so operator has to decide to correct them or not. In the example the corrections are good.

17.11.1992	00 UTC			Bjornoya (01 028)		
p	z	T	S	ZCOR	TCOR	Type
850	1386	-5.6				0
			0.51			
700	2897	-11.2				0
			92.77			
500	6430	-20.6		-1000	-14	3
			-104.2			
400	6980	-37.4				0
			0.21			

Example 12: *Type 6* error (computation error of layer thickness). Every height at 500–250 hPa was damaged by 100 m. Our method does not make correction, as explained above. A typical large residual can be seen in the example.

30.09.1992	12 UTC			Simferopol' (33 946)		
p	z	T	S	ZCOR	TCOR	Type
1000	-	-				
925	-	-				
850	1321	2.5				
			0.01			
700	2858	-8.4				
			9.81			
500	5490	-23.8				
			0.45			
400	7090	-34.4				
			-0.31			
300	9030	-50.8				
			-0.33			
250	10200	-56.2				
			-11.55			
200	11510	-54.0				
			0.7			

5. Results and conclusions

The information on the CHQC at NMC was produced automatically from the monthly summaries by CHQC Performance Statistics Code between May 1989 and April 1991 (*Gandin*, 1991). These summaries contain not only information about all suspected and corrected data, but also some statistics about errors of different types. These statistics were made over different regions of the globe, and at different elevations. The main purpose of the monthly summaries is to create error statistics in operationally received radiosonde reports on mandatory level heights and temperatures, and of the CHQC performance in correcting these errors. On the basis of some globally averaged CHQC statistics, about 7% of radiosonde reports are suspected by the CHQC and about half of these can be corrected by CHQC alone. In details: ratio of reports with *Type 1* errors is about 26.9%, with *Type 2* errors is about 23.1%, and with errors at two adjacent mandatory levels (*Types 7–10*) is about 4%.

These statistics are made over the globe, so there is a strong geographical inhomogeneity in the occurrence of hydrostatic errors. The reason of this inhomogeneity is the overwhelming majority of "hydrostatic" errors originating from countries where communication processes are not, or incompletely, computerized. In these regions of the globe, the rate of gross hydrostatic errors is higher than in the regions where the processing of radiosonde measurement is entirely automatized.

We are particularly interested in the statistics for Eastern European and Western European regions because our operational NWP model makes forecasts over these regions. Reports from European regions contain 4.7% of hydrostatic error (*Gandin*, 1991). We have obtained smaller values by running our operational model, but we have to take into account that the hydrostatic control is preceeded by a "formal" control, which checks decoding errors.

We are also interested in the information about errors in operationally received radiosonde reports for our model. So we made statistics for the period between June 1992 and May 1993. Two aspects were examined: (1) missing of radiosonde reports of every single station and every part (A, B, C, D) of the reports, and (2) erroneous radiosonde reports of every single station by error types and mandatory levels. We have divided the area used by our model into three regions: Western Europe (I), Central Europe (II) and Eastern Europe (III) (*Fig. 3*). We received most of the reports from region I and these reports contained the least errors in contrast with region III (*Table 6*). Average over the whole area showed that 102 reports were complete (received and included part (*a*) from the available 124 reports, and 3 of them were erroneous. It can be seen in *Table 6b* that the number of presence of *Types 1* and *2* errors and other types altogether is nearly the same, and missing level occurred in a significant

number. The main reason of this is the lack of 925 hPa level (as it can also be seen from the error statistics in *Table 6c* and *Table 7*). The results of the latter

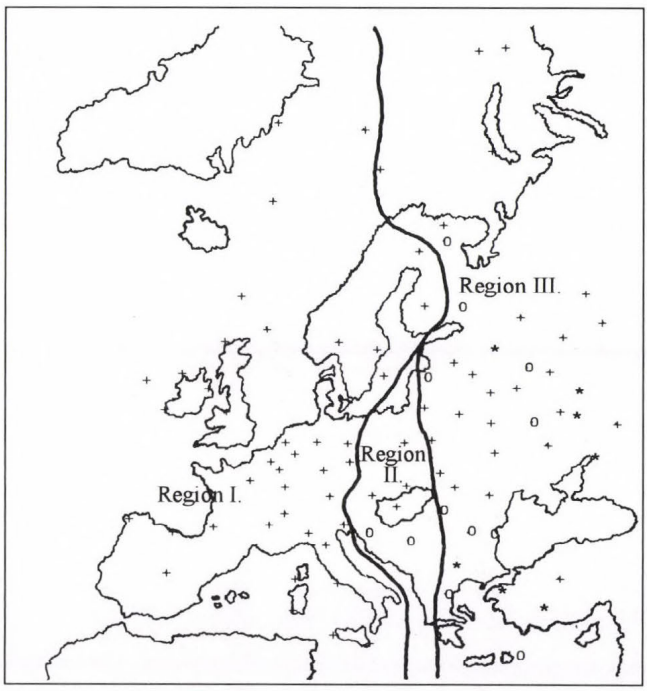

Fig. 3. Summary of statistics for stations in Europe: o stations, not disseminated reports in most cases; * stations, disseminated erroneous data in most cases.

Table 6. Some avareged CHQC statistics (every value is given in percent)

	Region I (61)	Region II (9)	Region III (60)	Whole area
(a)				
Available reports	90	80	73	82
Missing reports	8	19	23	15
Missing part A	2	1	4	3
Error contained reports	1.4	1.3	3.4	2.2
(b)				
Distribution of errors by types	Region I	Region II	Region III	Whole area
Type 1 and 2	34	25	41	38
(Type 1, Type 2)	(28, 5)	(16, 8)	(28, 13)	(27, 8)
Other types	24	30	31	33
Missing level	42	45	28	27

Continued Table 6

(c)

Distribution of errors by level (hPa)	Region I	Region II	Region III	Whole area
1000	0	0	0	0
925	28	39	44	39
850	2	2	5	4
700	14	2	7	9
500	10	13	11	10
400	8	12	7	8
300	11	10	9	9
250	8	8	6	7
200	9	8	4	6
150	8	4	4	5
100	2	2	3	3

two tables justify a systematic 1000 m decoding error of 700 hPa level, so *Type 1* error often occurred in this level (mainly in winter). This table shows that 500 hPa level often was the highest reported level and it was at the same time frequently erroneous.

Our plans for the future are supplementing the procedure with a horizontal check and further development of this method.

Table 7. Distribution of errors by types and levels (every value is given in percent).

Level (hPA)	Type 1	2	3	4	5	6	7	8	9	10	14
1000	0	0	0	0.3	0	0	0	0	0	0	0
925	3.9	0	0	3.6	0	0	0	0	0	0	21.7
850	1.3	0.8	0.1	1.8	0	0	0.1	0	0	0.1	0.2
700	9.0	1.2	0	0.1	0	0	0.3	0.1	0.2	0.1	0.5
500	2.6	1.9	0	0	7.6	0	0.3	0.1	0.3	0.2	0.4
400	2.3	1.9	0	0	0.5	0	0.5	0.6	0.3	0.3	1.9
300	2.6	2.0	0	0	0.3	0	0.8	1.2	0.2	0.1	2.3
250	2.1	1.3	0.1	0	0.2	0	0.5	0.9	0.1	0	2.1
200	2.2	1.0	0	0	0.5	0	0.3	0.3	0.1	0	1.9
150	1.7	0.8	0	0	0.4	0	0.2	0.1	0.1	0	1.9
100	0	0	0	0	4.0	0	0	0	0	0	0

Acknowledgements—I would like to thank, first of all, to *István Ihász* and *Gábor Radnóti* for their help during my work. Also, I would like to thank to *Dr. Dezső Dévényi* for his suggestions and *Prof. György Major* for his support.

References

Belousov, S.L., Gandin, L.S. and *Mashkovich, S.A.*, 1968: *Computer Processing of Current Meteorological Data* (in Russian). Gidrometeoizdat (Meteor. Trans. No. 18, 1972. Canada Dept. of the Enviroment, Atmospheric Enviroment Service, Downsview, Ontario).

Bergthorson, P. and *Döös, B.R.*, 1955: Numerical weather map analysis. *Tellus 7*, 367-374.

Collins, W.G., 1991: Complex quality control of rawinsonde heights and temperatures at the National Meteorological Center. *Preprints, 9th Conference on Numerical Weather Prediction*, Denver, Colorado, 14-18 October, 15-18.

Dévényi, D., 1983: Methods of automatic control of operative meteorological information (in Hungarian). *Meteorológiai Tanulmányok* No. 45, OMSZ, Budapest.

ECMWF, 1985: *Workshop on the Use and Quality Control of Meteorological Observation.* Readings, U. K., European Centre for Medium Range Weather Forecast.

Gandin, L.S., 1988: Complex quality control of meteorological observations. *Mon. Wea. Rev. 116*, 1138-1156.

Gandin, L.S. and *Collins, W. G.*, 1990: Comprehensive hydrostatic quality control at the National Meteorological Center. *Mon. Wea. Rev. 118*, 2752-2767.

Gandin, L.S., 1991: Two years of operational comprehensive quality control at the National Meteorological Center. *Preprints, 9th Conference on Numerical Weather Prediction*, Denver, Colorado, 14-18 October, 11-14.

Gilchrist, B. and *Cressman, G.P.*, 1954: An experiment in objective analyses. *Tellus 6*, 309-318.

Lorenc, A.C., Rutherford, I. and *Larsen, G.*, 1977: The ECMWF analysis and data assimilation scheme—Analysis of mass and wind fields. European Centre for Medium Range Weather Forecasts, Reading, Berkshire, U.K., *Tech. Rep.* No. 6.

Lorenc, A.C. and *Hammon, O.*, 1988: Objective quality control of observations using Bayesian methods. Theory, and a practical implementation. *Quart. J. Roy. Meteorol. Soc. 114*, 515-543.

Ozorai, Z., 1972: Control of the calculation of the attitudes included in TEMP messages (in Hungarian). *Időjárás 76*, 326-333.

Parfiniewicz, J., 1976: *Complex Quality Control of Upper Air Information* (in Russian). Methodical guidelines. Hidrometeorological Center. Gidrometeoizdat, Leningrad.

IDŐJÁRÁS

Quarterly Journal of the Hungarian Meteorological Service
Vol. 97, No. 4, October–December 1993

Application of satellite digital images in the investigation of the daily temperature amplitude of the surface

I. Csiszár, E. Fejes, J. Kerényi and **A. Rimóczi-Paál**

Satellite Research Laboratory, Hungarian Meteorological Service,
P.O. Box 32, H-1675 Budapest, Hungary

(Manuscript received 14 January 1993; in final form 10 November 1993)

Abstract—Digital data of the meteorological satellites give new opportunities to investigate the heat and radiation budget of the Earth-atmosphere system. The good spatial resolution of AVHRR (*Advanced Very High Resolution Radiometer*) on board the polar orbiting NOAA satellites makes it possible to construct detailed temperature, vegetation and radiation maps of Hungary and to search for statistical connections between them. A new project sponsored by the *Hungarian Scientific Found* started to determine the relationship between the daily changes of surface temperature and other meteorological parameters. In this paper the methods of the calculation of temperature, vegetation index and radiation balance components and the first results are presented.

Key-words: daily temperature amplitude, NOAA and METEOSAT digital images, radiation balance, vegetation index.

1. Introduction

The exact knowledge of the heat budget of the surface is very important in both climatology and agriculture. Variation of the temperature of the surface in different areas of Hungary on cloudless days can give important information about the heat capacity and characteristics of different soil types or vegetation. Last year a four-year investigation sponsored by the Hungarian Scientific Found (Project OTKA No. 2024) started to determine the relationship between temperature variation and other meteorological parameters. Digital images of the meteorological satellites give a new opportunity to construct maps of the temperature distribution and variability for the whole country. In this investigation Hungary and its surroundings are covered by squares of 20 by 20 kilometers and each area can be studied separately using digital METEOSAT and NOAA/AVHRR images. Without applying satellite images a large series of local measurements would be necessary to obtain good spatial resolution. All

the satellite images were acquired at the digital receiving station of the Hungarian Meteorological Service.

In this paper the method, the data basis and the first results are presented.

2. *Determination of the data basis*

2.1 Vegetation index

The NOAA/AVHRR measurements are suitable to give objective information about the development and the geographical distribution of the vegetation due to their good spatial resolution. From the five channels the visible (VIS) and the near infrared (NIR) bands give the opportunity to calculate the vegetation index. The first spectral channel is in that part of the spectrum where chlorophyll causes considerable absorption of incoming radiation, whereas the second one is in a spectral region where spongy mesophyll leaf structure leads to significant reflectance (*Justice et al.*, 1985). This contrast between the two channel responses can be conveniently shown by a ratio transform, i.e. dividing one channel by the other. Several ratio transforms have been proposed for the study of different land surfaces (*Tucker*, 1979). The normalized difference vegetation index (*NDVI*) is one of such ratios, which has been shown to be highly correlated with vegetation parameters such as biomass and green-leaf area and hence it is of considerable value for the investigation of the vegetation (*Jackson et al.* 1983)

$$NDVI = (X_{NIR} - X_{VIS})/(X_{NIR} + X_{VIS}), \tag{1}$$

here *NDVI* is the normalized differential vegetation index, X_{NIR} is the brightness value (count) in the near-infrared spectral band, X_{VIS} is the brightness value (count) in the visible spectral band.

The value of the vegetation index is between -1 and $+1$. Clouds, water and snow have larger reflectances in the visible than in the near infrared, so for these features *NDVI* is negative. Rock and bare soil have similar reflectances in these two bands and the vegetation index is near zero (*Yates et al.*, 1984). In scenes with vegetation, *NDVI* ranges from 0.1 to 0.6; the higher values are associated with greater density and greenness of the plant canopy. The vegetation index has large values when the vegetation is well developed. The largest values indicate forests and the 0 values are water surfaces or clouds.

2.2 Radiation balance components

The radiation balance at the surface is calculated from the global radiation,

reflected solar radiation, longwave radiation reaching the surface and emission of the surface

$$R = G(1 - RS) + (LD - LU), \tag{2}$$

where R is the radiation balance of the surface, G is the global radiation, RS is the surface albedo, LD is the longwave radiation reaching the surface, LU is the longwave radiation emitted by the surface.

The solar radiation reaching the surface is calculated by the empirical multilinear equation (*Rimóczi-Paál,* 1989)

$$G = 49.5 - 4.65B + 32.5 \cos h. \tag{3}$$

Here G is the global radiation given in percents of the solar radiation at the top of the atmosphere, B is the relative brightness characterizing the cloud coverage and transmittance and h is the solar zenith angle.

The definition of the relative brightness is (*Rimóczi-Paál,* 1985)

$$B = (F - F_{\min})/(F_{\max} - F_{\min})10, \tag{4}$$

where F is the outgoing flux over the investigated area, $F_{\min}$ is the outgoing flux over a cloudless area (near the investigated area), $F_{\max}$ is the outgoing flux over a totally cloudy area (near the investigated area).

The empirical constants in Eq. (3) were determined from a data set of two years from surface measurements and from redigitized analogue data of METEOSAT 2 satellite. Using Eq. (4) the relative brightness values are calculated from digital visible images of METEOSAT 4 satellite.

The surface albedo is determined from the minimum brightness values of an extended area in the southern part of Central Europe. The brightness of the cloudfree surface is chosen by using histograms in the range of 16–48 counts. In most cases the first peak is the sea surface and the second one is the brightness of the land surface.

The surface albedo (RS) is approximated by Eq. (5)

$$RS = 1.25\, CC + 0.07, \tag{5}$$

$$CC = (B_{\min} - C_0)/(I_0 \cos h \sin Z\, RF), \tag{6}$$

where $B_{\min}$ is the minimum surface brightness, C_0 is the count of the space, I_0 is the solar constant, h is the solar zenith angle, RF is the normalized Sun-Earth distance, Z is the satellite zenith angle.

The constants are determined from case-studies by comparing the estimated values to the measurements.

The longwave radiation reaching the surface is calculated by a radiative transfer model adapted from the University of St. Petersburg (*Práger* and *Kovács*, 1988), which applies broad band approximation with 17 spectral intervals. The humidity and temperature profiles are taken from radiosonde observations of Budapest. The effects of CO_2, O_3, CH_4, NO_2, Freon11, Freon12 and the aerosols are taken into account. The profiles of the trace gases are considered as climatological averages. The effect of the clouds is approximated by a simple cloud parameterization. The cloud parameter *BC* is calculated by Eq. (7)

$$BC = 0.05\, B\,(B_{\min}/B_{\max}) + RS, \tag{7}$$

where $B_{\min}$ is the minimum brightness, $B_{\max}$ is the maximum brightness, B is the relative brightness like in Eq. (4), *RS* is the surface albedo.

The cloud amounts and the cloud levels are taken from *Table 1*. For example if the *BC* is 0.35, then a cloud amount of *B/2* is considered in the middle level. This simple cloud parameterization based only on cloud albedo is subjective. Our purpose is to construct an objective cloud-parameterization using both albedo and cloud temperature.

Table 1. Cloud amount and level from the BC cloud parameter

BC	>0.50	0.40–0.50	0.30–0.40	0.24–0.30	<0.24
Low	B/2	B/3	–	–	–
Middle	B/2	B/3	B/2	–	–
High	–	B/3	–	B/2	–

The values of the longwave radiation reaching the surface estimated by the radiative transfer model in the grid point containing Budapest were significantly lower than the measured values. Thus a magnification factor of 1.2 had to be applied.

In *Table 2* our results are compared with model calculations of *Schmetz* (1984) in the case of mid-latitude summer model atmosphere for extended area around the Carpathian Basin. The radiation balance values calculated by our method are grouped with respect to different cloud conditions on warm days in September 1991, when the atmospheric conditions were similar to the summer model atmosphere. Homogeneous areas were chosen where the sea and the land surfaces were totally cloudless or covered by extended stratus clouds. From Table 2 it can be seen that there is a good agreement between our results and the model calculated radiation balance values.

Table 2. Surface radiation balance from model calculations and our method

	Clear sky and sea surface	Clear sky and land surface	Cloud of medium thick
Schmetz (1991)	320	290	230
Our method mean values	333	291	226
Variance	4.0	17.6	13.4
N	5	20	26

2.3 Surface temperature

For the determination of the land surface temperature (*LST*) we applied the method of *Prata* (1991):

$$LST = 40 \left[\frac{1-\epsilon}{\epsilon}\right] + \frac{1+\beta}{\epsilon} T_4 - \frac{\beta}{\epsilon} T_5, \tag{8}$$

where

$$\beta = \frac{1-\tau_4}{\tau_4-\tau_5} \tag{9}$$

and all temperature values are in °C.

The channel 4 and 5 transmittances τ_4 and τ_5 were calculated by the radiative transfer model LOWTRAN-7 using TOVS (*TIROS-N Operational Vertical Sounder*) temperature and humidity profiles derived by the *International TOVS Processing Package* (ITPP). ϵ is the average value of the channel 4 and 5 spectral emissivities, which were determined from the 8–14 μm values by the formulae (*Sobrino* and *Caselles*, 1991)

$$\begin{aligned} \epsilon_4 &= \epsilon_{8-14} - 0.003, \\ \epsilon_5 &= \epsilon_{8-14} - 0.001, \end{aligned} \tag{10}$$

whereas the ϵ_{8-14} values were assumed to be linearly related to the vegetation index

$$\epsilon_{8-14} = 0.98 - 0.085 * NDVI. \tag{11}$$

The coefficients for Eq. (11) were determined on the basis of the emissivity data given by *Salisbury* and *Milton* (1988) and from daytime *NDVI* values of agricultural and forested areas in Hungary.

3. *First results*

The accurate knowledge and predictability of the daily amplitude of the active surface temperature (δT) is of primary importance in agriculture. On days without major weather events its magnitude is dependent on the thermophysical properties of the active surface and the daily variation of its energy budget. The total gain of radiant energy during the warming period can well be characterized by the 09 GMT surface radiation balance (R_{09}). On the other hand, investigations (see, for example *Hope* and *McDowell*, 1992) have revealed that there is a linear decrease in the active surface temperature with increasing value of *NDVI*, indicating the relationship between the amount of transpirationally active vegetation and the thermal inertia of the active surface. Hence, these satellite-derived parameters can be good indicators of the daily variation of the active surface temperature. Here the relationship between δT, R_{09} and *NDVI* is investigated over mainly agricultural areas of the Carpathian Basin.

We chose situations when major part of both the afternoon and the previous or following night 1024×1024 pixel NOAA-11 AVHRR images of the Carpathian Basin were found cloud-free by visual interpretation and assumed to be least affected by the disturbing atmospheric effects. At nighttime the cloudy pixels were removed by a thresholding technique using a histogram constructed from the brightness values of channel 4. In the case of the afternoon images the pixels with zero *NDVI* were omitted. Then the brightness temperature and *NDVI* values were averaged over a 16×12 grid with an approximately 20 km spatial resolution.

The investigated area is located in the Great Hungarian Plain (*Fig. 1*), mainly covered with winter and summer crops and forage. We used data of six days from early spring to late autumn representing the whole vegetation period

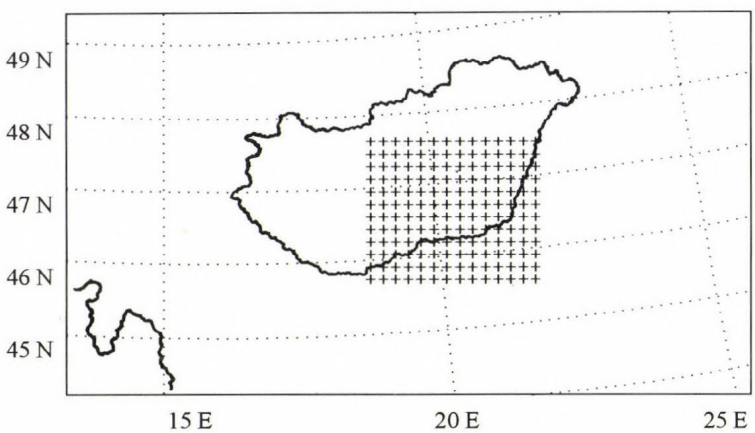

Fig. 1. The geographical area studied.

(*Table 3*). Unfortunately, the years 1992 and early 1993 have been dry and hence are characterized by low *NDVI* values.

Table 3. Dates and case numbers

Date	1992.	20.09	07.11	1993.	10.03	21.04	12.05	02.06
Number		123	18		130	130	115	126

The morning net radiation balance values were calculated from 09 UTC METEOSAT 4 data as described in 2.3. The fields were filtered by spatial coherence calculations. The daily amplitude of the active surface was derived as the difference of the skin temperatures calculated from AVHRR channel 4 and 5 data of the night and afternoon overpasses of the NOAA-11 satellite.

The net radiation at clear sky conditions has small spatial variability over the investigated area. On *Fig. 2* δT data corresponding to separate days form column-like clusters over narrow intervals of net radiation values. This enabled us to investigate the partial effect of the vegetation index. *Fig. 3* illustrates average values of δT corresponding to narrow intervals of *NDVI* on two late spring days. An increasing trend of the temperature amplitude can be observed until the *NDVI* value of 0.25 followed by a decrease due to the evapotranspirational effect of the dense vegetation.

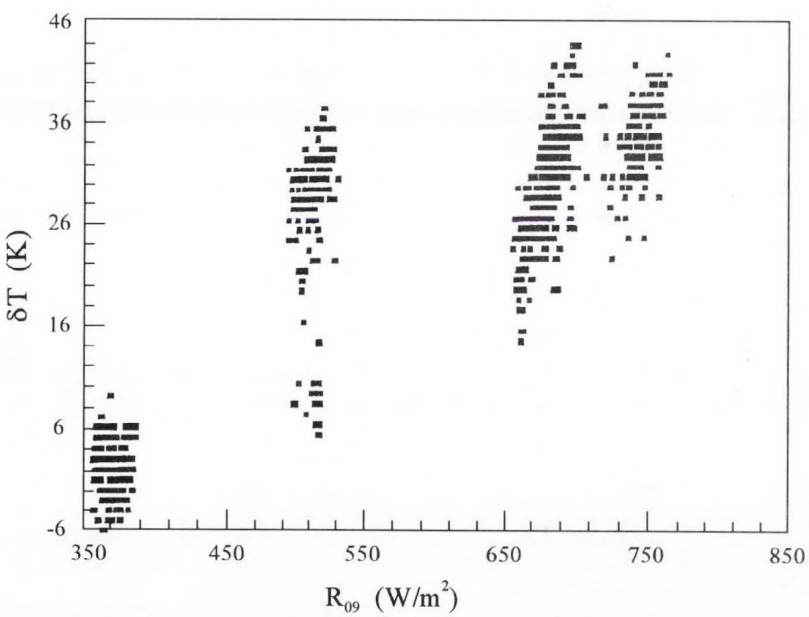

Fig. 2. Variation of δT with R_{09} on the six days studied.

The same phenomenon is shown in *Fig. 4* where data of all the six days have been displayed. It should be noted, however, that in this case the observed

feature is a combined effect of both the *NDVI* itself and the net radiation which has a good correlation with the vegetation index.

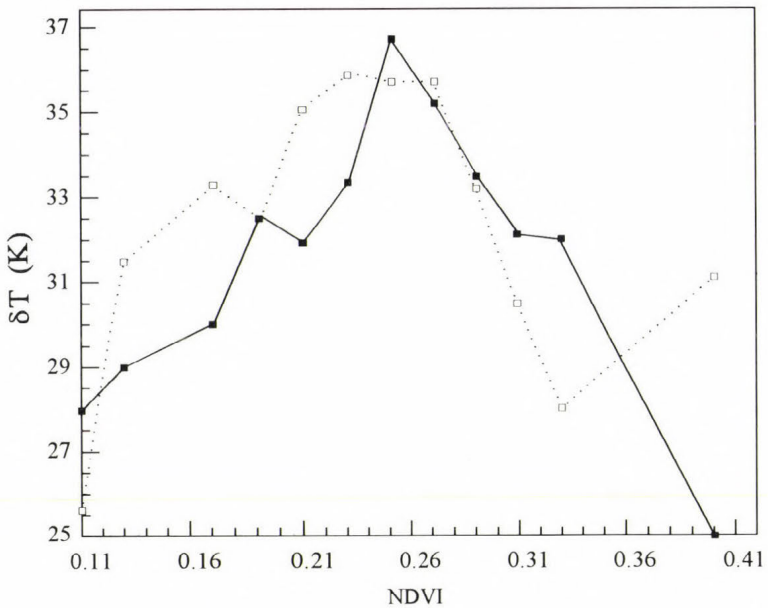

Fig. 3. δT versus *NDVI* on May 12 (solid) and June 2 (dotted).

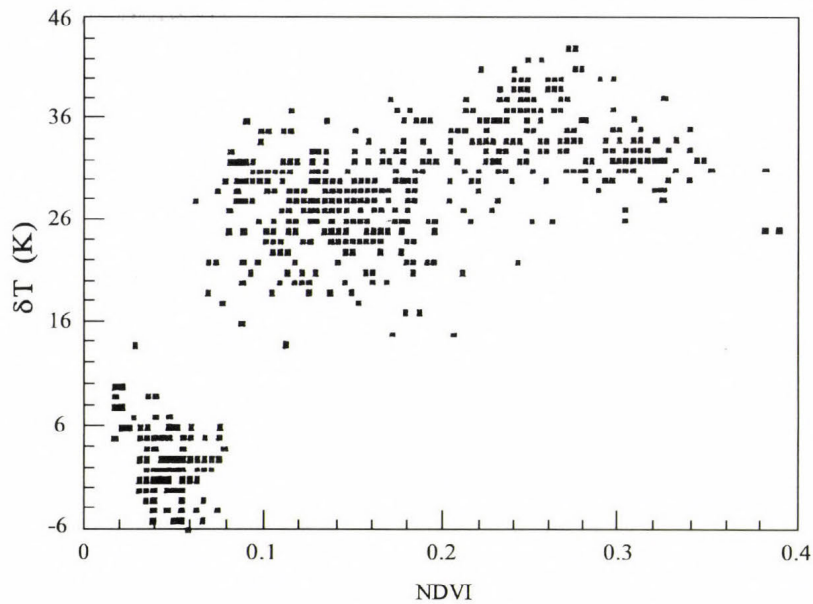

Fig. 4. Variation of δT with *NDVI* on the six days studied.

The partial effect of the net radiation is illustrated in *Fig. 5*. It shows interval-averaged δT as a function of T_{09} corresponding to two intervals of *NDVI*

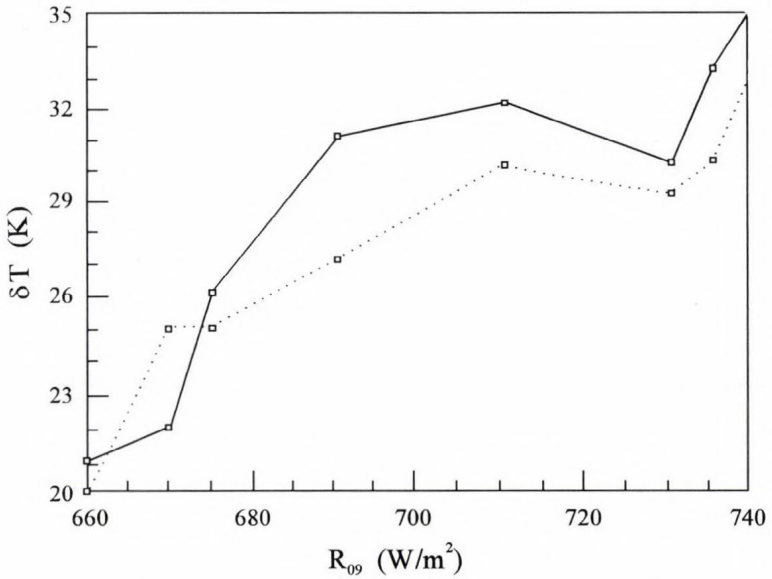

Fig. 5. δT versus R_{09} at $NDVI = 0.20$ (solid) and 0.16 (dotted).

taken from April 21, May 12 and June 2. There is an increase in δT with increasing R_{09}, although this effect on a particular day is small because of the homogeneity of the radiation data.

On *Fig. 6* daily average values of δT, R_{09} and *NDVI* are plotted against the day of the year. The net radiation shows a feature that is determined by the change of the solar height. The annual variation of *NDVI* is characterized by a maximum in late spring and a relatively sharp decrease toward the end of the summer, as it was found by *Derrien et al.* (1992) for agricultural areas simular to the investigated one. On the curve representing δT it can also be seen that the average vegetation index, hardly exceeding the critical value of 0.25 on 12 May could not counteract the increasing effect of the net radiation on the average temperature amplitude.

The above figures indicate that the net radiation is mainly responsable for the annual trend of the daily amplitude of the active surface temperature on which superimposed is a smaller variation caused by the territorial differences of the vegetation index. Thus, to make a quantitative prediction the two parameters have to be taken into account simultaneously.

Therefore, we carried out multiple linear regression calculations. The equation to estimate δT with R_{09} and *NDVI* as independent variables is as follows

$$\delta T = 38.257 * NDVI + 0.05438 * R_{09} - 13.92 . \quad (12)$$

The accuracy of the equation is characterized by a correlation of 0.84 between the observed and predicted δT values.

4. Conclusion and plans

This investigation has shown that the morning net radiation and the vegetation index can be used for the prediction of the daily amplitude of the active surface temperature with an acceptable accuracy. Its annual variation is governed by the net radiation, whereas the territorial differences on a given day are mainly due to the spatial distribution of the vegetation index. The latter has a critical value beyond which the temperature amplitude decreases, indicating the effect of the evapotranspiration of the vegetation.

With the continuous extension of our archive we plan to repeat this study with more data, eliminating the particularities of the chosen days and the dry weather of the investigated period. We plan to use also AVHRR images of the morning NOAA satellites to calculate the net radiation.

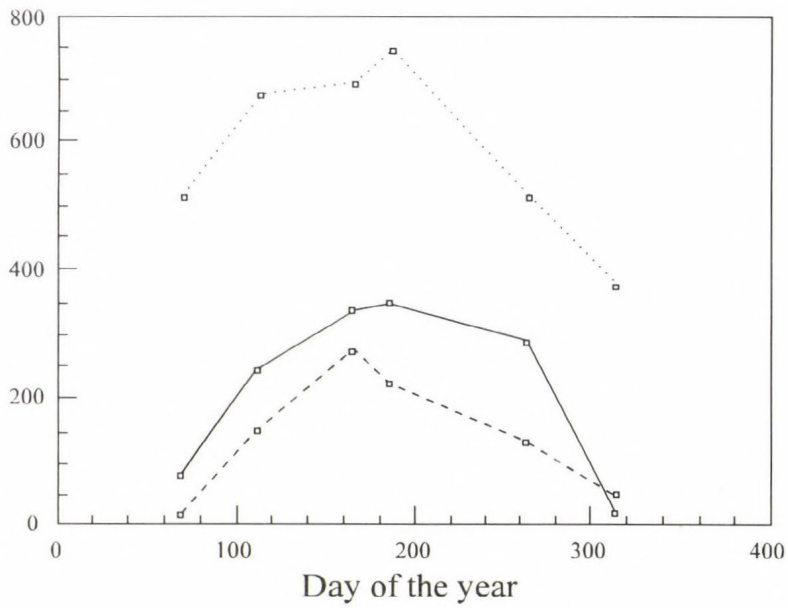

Fig. 6. Annual variation of R_{09} (dotted, W/m^2), δT *10 (solid, K*10) and *NDVI**1000 (dashed).

References

Derrien, M., Farki, B., Le Gléau, H. and *Sairouni, A.*, 1992: Vegetation mapping in 1990 over France using NOAA-11/-AVHRR. *Veille Climatique Satellitaire*, No. 42, 59-67.

Hope, A.S. and *McDowell, T.P.*, 1992: The relationship between surface temperature and a spectral vegetation index of a tall-grass prairie: effects of burning and other landscape controls. *Int. J. Remote Sensing 13*, 2849-2863.

Jackson, R.D., Slater, P.N. and *Pinter, P.J.*, 1983: Discrimination of growth and water stress in wheat by various vegetation indices through clear and turbid atmospheres. *Remote Sensing Environ. 15*, 187-195.

Justice, C.O., Townshend, J.R.G., Holben, B.N. and *Tucker, C.J.*, 1985: Analysis of the phenology of global vegetation using meteorological satellite data. *Int. J. Remote Sensing 6*, 1271-1318.

Kidwell, K. B., 1991: NOAA polar orbiter data users guide. *NOAA National Environmental Satellite, Data and Information Service, National Climatic Data Center Satellite Data Services Division*, Washington, D.C.

Práger, T. and *Kovács, E.*, 1988: Investigation of the climate modifying effects of atmospheric trace gases and aerosol particles by a radiative-convective model. *Időjárás 92*, 153-162.

Prata, F., 1991: Land surface temperature derivation using AVHRR/TOVS. *Technical Proceedings of the Sixth International TOVS Study Conference*, May 1-6, Airlie, Virginia, 401-407.

Rimóczi-Paál, A., 1985: Determination of surface global radiation from METEOSAT images using relative brightness as new parameter to characterize the cloudiness. *Adv. Space Res. 5*, No. 6, 329-332.

Rimóczi-Paál, A., 1989: Relationship between cloudiness and surface global radiation obtained from METEOSAT images. *Adv. Space Res. Vol. 9*, No. 7, 101-104.

Salisbury, J.W. and *Milton, N.M.*, 1988: Thermal infrared (2.5 to 13.5 μm) directional hemispherical reflectance of leaves. *Photogrammetric Engineering and Remote Sensing 54*, 1301-1304.

Schmetz, J., 1984: On the parameterization of the radiative properties of broken clouds. *Tellus 36A*, 417-428.

Schmetz, J., 1991: Retrieval of surface radiation fluxes from satellite data. *Dyn. of Atmosph. and Oceans 16*, 61-72.

Sobrino, J.A. and *Caselles, V.*, 1991: A methodology for obtaining the crop temperature from NOAA-9 AVHRR data. *Int. J. Remote Sensing 12*, 2461-2475.

Tucker, C.J., 1979: Red and photographic infrared linear combination for monitoring vegetation. *Remote Sensing Environ. 8*, 127-139.

Yates, H.W., Tarpley, J.D., Schneider, S.R., McGinnis, D.F. and *Scofield, R.A.*, 1984: The role of meteorological satellites in agricultural remote sensing. *Remote Sensing Environ. 14*, 219-233.

IDŐJÁRÁS

Quarterly Journal of the Hungarian Meteorological Service
Vol. 97, No. 4, October–December 1993

Surface temperature derived from METEOSAT infrared data using atmospheric correction

J. Kerényi

Satellite Research Laboratory, Hungarian Meteorological Service,
P.O. Box 32, H-1675 Budapest, Hungary

(Manuscript received 11 August 1993; in final form 11 November 1993)

Abstract—The brightness temperature of the surface-air system can be determined from the METEOSAT IR window data, but the actual surface temperature cannot be established directly. Therefore a program has been developed to derive the true surface temperature. The brightness temperatures are corrected for effects of water vapour, ozone, uniformly mixed gases and aerosols in the atmosphere, reflected radiation, and sensor filter transmittance. Radiosonde data are used in the applied infrared transmission model. Comparison of satellite derived temperature with the ground measurements show differences of 2–3 degrees at water surface and 1–4 degrees at land surface. This discrepancy can be explained by the difference of two types of measurement methods.

Key-words: METEOSAT, transmittance model, surface temperature.

1. Introduction

A knowledge of surface temperature is strongly required for many applications, notably in agrometeorology, climate and enviromental studies.

The geostationary METEOSAT satellite observes the Earth in three channels in the infrared window (10.5–12.5 μm), in the visible (0.4–1.1 μm) and water vapour absorption band (5.7–7.1 μm).

The longwave radiance can be determined from the brigthness values using the calibration coefficient for METEOSAT. Atmospheric gases absorb energy radiated by the surface, and radiate according to their own temperature, which is typically lower than the surface temperature. Consequently, the radiance detected by satellite is less than the surface radiance and the derived surface temperature will be lower than the ground true value.

The correct temperature of the surface may be estimated by including an atmospheric correction scheme. At the determination of surface temperature the

LOWTRAN 7 transmittance model was used. The model relying on the radiosonde data, determines the longwave radiance at the top of the atmosphere taking into account the effect of the atmosphere. The determination of surface temperature is based on the comparison of the radiances calculated by model and measured by satellite.

Earlier, this method was applied for NOAA by *Irbe et al.* (1979). The water surface temperature was determined by the LOWTRAN 3B transmittance model using the radiosonde and AVHRR data from the NOAA-5.

The difference between the surface and the brightness temperature was investigated by *Tomasi et al.* (1992) using METEOSAT infrared data. At this calculation of the atmospheric correction the LOWTRAN 7 computer programme was applied for a wide set of atmospheric models. The radiance values, simulating the satellite signals and calculated by the model, and the surface temperatures determined in the lack of the atmosphere, were compared. These comparisons and the satellite signals define the value of brightness temperature for each simulated satellite signal, and then the corresponding value of temperature correction equal to the difference between the surface and brightness temperature.

2. Radiosonde data

The atmospheric correction varies with the amount and distribution of attenuators of infrared radiation in the atmosphere, the principal one of which is the water vapour. The calculation of water vapour distribution in the atmosphere was determined from upper air data of two radiosounding stations (Budapest, Szeged) in Hungary. To determine data for other areas of Hungary, a biharmonic spline interpolation was applied. Biharmonic spline interpolation is a special case of the more general multiharmonic spline. The interpolated value at any point of the territory is calculated by superposition of the impact of every measurement point, so the spatial structure of the meteorological field can well be described.

This method was applied for the Carpathian Basin. At the calculation the Hungarian and the neigbourhood radiosonde data (from 8 stations) were used. The interpolation technique produces a pseudo sonde in every gridpoint. Based on the pseudo sondes, the atmospheric transmittance model calculates temperature, humidity and pressure profiles.

3. Atmospheric transmittance model

The atmospheric correction program calculates the transmittance and radiance of the atmosphere from 0 cm^{-1} to 50,000 cm^{-1} at 20 cm^{-1} spectral resolution on a linear wavenumber scale with 5 cm^{-1} sampling.

The LOWTRAN 7 package includes transmittance functions for water vapour, unformly mixed gases and ozone, and absorption coefficients for the gaseous elements and aerosols.

In the present application, calculations are limited to the 800–950 cm^{-1} channel of the sensors on board METEOSAT.

The thermal radiation leaving the Earth's atmosphere at radiometer altitude and measured through a filter system can be formulated by the radiative transfer equation. The detected radiance consists of the surface emitted radiation, the reflected radiation and the radiation emitted by the atmosphere, respectively

$$N(Z,u) = \frac{1}{\pi}\int_{\nu_1}^{\nu_2} \phi(\nu)\varepsilon(\nu)B_\nu(T_0)t_\nu(0,Z,u)d\nu +$$

$$+\frac{1}{\pi}\int_{\nu_1}^{\nu_2}\int_{0}^{Z} \phi(\nu)(1-\varepsilon(\nu))t_\nu(0,Z,u)B_\nu(T(z))\frac{\partial t_\nu(0,z,u)}{\partial z}dzd\nu +$$

$$+\frac{1}{\pi}\int_{\nu_1}^{\nu_2}\int_{0}^{Z} \phi(\nu)B_\nu(T(z))\frac{\partial t_\nu(z,Z,u)}{\partial z}dzd\nu, \qquad (1)$$

where the following notation are used: $N(Z,u)$ detected radiance, θ zenith angle, u cos θ, Z satellite altitude, υ wave number, $\Phi(\upsilon)$ normalized response function, $B_\upsilon(T)$ Planck function at absolute temperature T, $\epsilon(\upsilon)$ emissivity of the radiating surface, T_0 surface temperature, $t_\upsilon(z_1,z_2,u)$ transmittance of the layer located between altitudes z_1 and z_2 for incidence θ and

$$t_\nu(z_1,z_2,u) = \exp\left(-\frac{1}{u}\int_{z_1}^{z_2} K_\nu(z)dz\right), \qquad (2)$$

where K_υ is the total absorption coefficient which is equal to sum of the aerosol and molecular absorption coefficient.

Formally integrating the radiative transfer equation along the atmospheric path, the upwelling infrared radiance at each wavelength measured by a satellite borne radiometer is given by the sum of the following three terms: (1) the surface contribution, depending on surface spectral emittance (also called emissivity), surface temperature and atmospheric transmittance; (2) the atmospheric contribution, which is given by the integral along the whole atmospheric path of the radiance emitted by each infinitesimal element of air volume attenuated by the overlying atmosphere; and (3) the contribution of the infrared radiation emitted downwards by the atmosphere and reflected by the surface. Therefore, the first contribution gives direct information about surface

temperature on the basis of the black-body theory; the second contribution partly compensates the loss of surface radiance caused by atmospheric attenuation; and the third contribution depends mainly on the surface reflection of downwelling infrared radiance, so it decreases as emittance increases and can be consequently neglected in all cases in which surface emittance is very close to unity at all wavelenghts. Since the second term, due to the atmospheric emission, masks the surface contribution, the apparent brightness temperature differs from surface temperature, in general.

The LOWTRAN model is used to calculate the transmittance including in (1), the normalized response function is incorporated into the program, and the emissivity is assumed to be unity in every case.

4. Determination of surface temperature by model

Since the surface temperature cannot be established directly from radiance measured by satellite, the LOWTRAN 7 model is applied. The model, using the pseudo sondes, determines the longwave radiance at the top of atmosphere.

The radiance measured by satellite and the data calculated by model were compared, and the measured values were grater than the calculated data. A reason for these deviations may be the fact that the model doesn't use the surface temperature itself, but rather value measured by the radiosonde near the surface. In order to accomplish this procedure, it is assumed that the calculated and the measured radiances are equal. An iteration method was employed for determining the near-surface temperature. The starting point was increased by 0.25 degrees, then the model calculated the longwave radiance using the corrected temperature. This procedure was continued until the difference between the measured and the calculated radiance values was less than the required precision. The temperature determined by the iteration method represents the actual surface temperature.

At the calculation TEMP measured at 12 UTC was used. The radiance measured by satellite was determined from the METEOSAT-4 infrared pictures received at 11 or 12 UTC.

5. Results

The emissivities were assumed to be unity in every case. This assumption is best for water and snow surfaces, therefore these surfaces were investigated first. For actual soil and vegetated surfaces the assumed emissivity may be incorrect and we have to estimate its value to calculate accurate temperatures. An error of only 1% in emissivity causes about 1K error in the determination of surface temperature. However, if the emissivity is equal to unity, the surface temperature will be underestimated.

One area examined was Lake Balaton and the temperature calculation was performed in clear weather in all cases. A gridpoint is near the Siófok Observatory where temperatures measured by resistance thermometer are available for comparison. The measured values, the brightness temperatures determined from the IR counts and the surface temperatures calculated with atmospheric correction scheme are shown for Balaton during 1992 in *Fig. 1.*

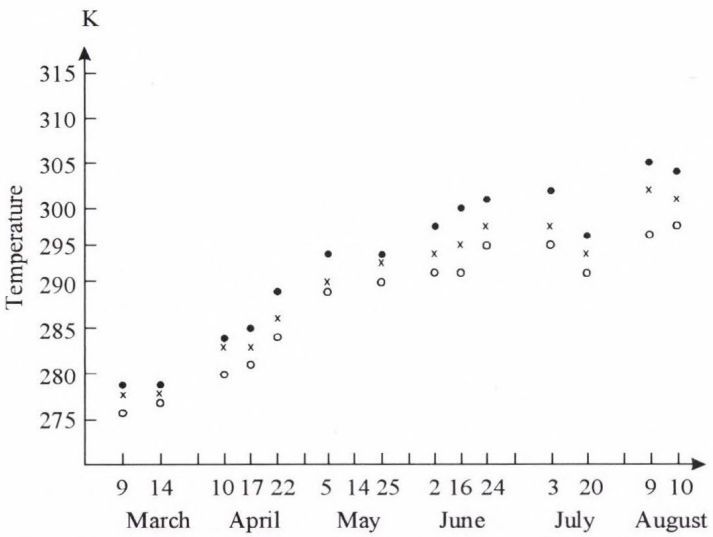

Fig. 1. Temperature values of Lake Balaton (denotations: × — measured temperatures, o — brightness temperatures, • — surface temperatures with atmospheric correction).

The calculated temperatures values were typically 2–3K lower, while the corrected temperatures were 2–3K greater than the measured water temperatures, which were confirmed by measurements (*Péczely*, 1974). The measurements showed, that the difference between the temperatures of water surface and lower layer (2 m) were around 2 degrees in the early afternoon. A possible reason for the difference is that the measurement is performed at only point, whereas the satellite temperatures are averaged over large areas, and the other reason may be that the measurement at the observatory is carried out in depth of 1.5 m, while the calculated temperature can be considered to be the skin temperature.

The region of Szarvas Agrometeorology Observatory was chosen for the other investigation, because it is situated in lowland territory and near the Szeged radiosonde station. Comparing the measured (mercury thermometer) and calculated temperatures, the calculated values were also lower than the measured data, as shown in *Fig. 2.*

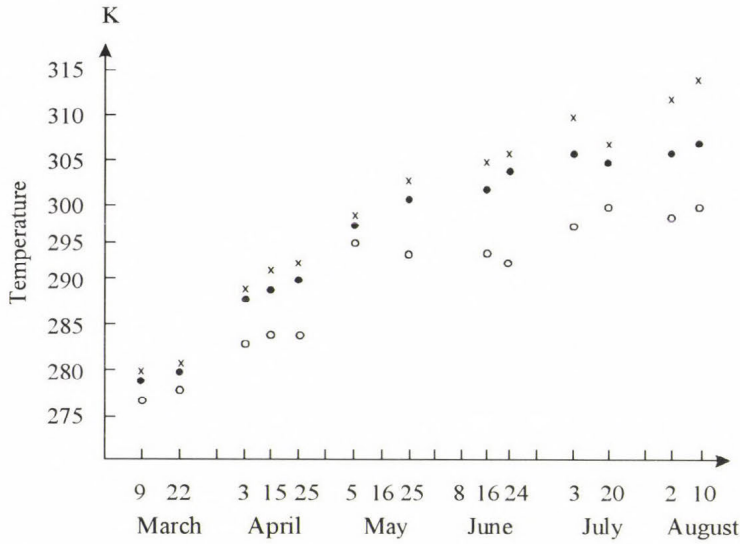

Fig. 2. Temperature values of land station, Szarvas (denotations are the same as in Fig. 1).

The early spring surface temperatures agree within 1–2K, but the differences increase gradually with the growth of vegetation, to 4–5K in summer. If the emissivity is unity, the calculated surface temperature will be lower. The difference between the calculated and measured temperatures can be partly explained by different emissivities of the surfaces in the examined region. The satellite measurements give average values, which are typical to the totality of surfaces. On the other hand, the surface temperatures are measured in one point on bare soil in Szarvas.

6. Summary

Summarizing the conclusions of the investigation, it can be stated, that on the basis of METEOSAT digital images using the radiative-transfer model, the surface temperature can be determined. The results obtained so far are promising for the future in spite of the existing deviations. In case of Lake Balaton, the difference between the measured and the calculated temperature is no more than 2–3K, which derives from the dissimilarity of the two types of measurements. At the land surface of Szarvas in early spring, the temperature difference was only 1–2K, although the difference increased with the growth of plants, due to neglecting emissivity and the different measuring method.

In the future, the determination of surface temperature will be made better, if the variation of emission will also be taken into account.

References

Irbe, G.J., Morcette, J.J. and *Hogg,W.D.*, 1979: Surface water temperature of lakes from satellite infrared data corrected for atmospheric attenuation. Canadian Climate Centre. *Report* No. 79-7.

Tomasi, C., Vitale, V. and *Bencivenni, S.*, 1992: Calculations if the atmospheric correction terms for surface temperature measurements from METEOSAT infrared data. *Proceedings of 9th METEOSAT Scientific User's Meeting*. Locarno, Switzerland, 15-18 September, pp. 369-375.

Péczely, Gy., 1974: *Climate of Lake Balaton* (ed.: B. Béll and L. Takács) (in Hungarian). Országos Meteorológiai Szolgálat Hivatalos Kiadványa, Budapest.

IDŐJÁRÁS

Quarterly Journal of the Hungarian Meteorological Service
Vol. 97, No. 4, October–December 1993

Surface temperature as an important parameter of plant stand

A. Anda

Pannon Agricultural University of Keszthely,
P.O. Box 71, H-8361 Keszthely, Hungary

(Manuscript received 16 September 1993; in final form 24 November 1993)

Abstract—Plants of diverse genetic origin may respond differently to the same environment. Our objective was to assess response of three different sugar beet varieties to the growing season drought during 1992, as inferred from surface temperatures (soil and foliage) and stomatal resistances. Together with diffusive resistance both the soil and foliage temperatures measured by infrared thermometer were sensitive indicators of plant physiological processes and production of sugar beet during the whole measuring period. Significant differences in such parameters as surface temperature and stomatal resistances of sugar beets of various genetic origin appeared only about solar noon. At low angle of solar radiation incidence there was no significant difference in temperature and resistance among the three beet cultivars. Because of well-known advantages of infrared thermometers (quickness and repeatability), they seem to have primary importance in comparative studies, mainly in such investigations where the number of treatments is generally high. In practice, one of this research areas is the plant breeding.

Key-words: canopy and soil temperatures, stomatal resistance, sugar beet varieties, LAI, sugar yield.

1. Introduction

Description and characterization of physiological properties of plant varieties is desirable, and provides a basis for the selection of the best genotype by plant breeders. Response of plants to their surrounding environment also involves interaction between genotypes and environment. One considers these responses when selecting the best genotype to respond under both favourable and non-favourable weather (*Hattendorf et al.*, 1990).

Similar to other plant species, in sugar beet stands water deficit caused stomatal closure (increased resistance and decreased transpiration) and rose canopy foliage temperature (*Brawn* and *Rosenberg*, 1970; *Lawlor* and *Milford*, 1975; *Huzulak* and *Matejka*, 1992). Determination of plant surface temperature

in assessing water status of plants has become quite common (*Pinter et al.*, 1979; *Idso et al.*, 1981; *Jackson*, 1982; *Keener* and *Kirchner*, 1983; *Walker* and *Hatfield*, 1983; *Tubaileh et al.*, 1986; *Smith et al.*, 1988; *Hattendorf et al.*, 1990). Infrared thermometers are often used to measure canopy foliage temperature because they provide precise and quick measurements and allow numerous nondestructive readings (*Halim et al.*, 1991). In plant breeding, the quickness has primary importance because the numerous treatments (plant cultivars) require instantaneous sampling. Many studies exist dealing with the use of plant surface temperature in determining plant physiological processes (mainly transpiration), but there is little information available on the importance of soil surface temperature, an important regulator of plant water loss.

Previous research has mostly characterized crop response to soil water deficit through the use of canopy surface temperature (*Mtui et al.*, 1981). The research reported here was devoted to an evaluation of the utility of both canopy and soil surface temperature measurements as quick indicators of plant response to surroundings. A means for evaluating temperature, the main cause of plant physiological processes could open the way to improved selection of varieties of different genetic origin that could ultimately lead to better yield production.

2. Experimental procedure

Field trials were conducted at Keszthely Agrometeorological Research Station during the growing season in 1992. Three sugar beet varieties of different genetic origin were planted in 4 m^2 plots (split-block design) with four repetitions on a Ramann type brown forest soil. The variety *Kawemaya* is the most frequent grown sugar beet cultivar in Western Europe. Originally, it was bred in Germany. The other two varieties, *Gála* and *Éva*, are breeding in Hungary. The plant population ranges between 10 and 12 plants per m^2.

Leaf area was measured by a LI-3000 type portable planimeter on 5 plants in each treatment every two weeks after emergence. Stomatal resistance was estimated with LI-60 type diffusive porometer on the exposed upper leaves with three to five repetitions. As significant differences in resistances of different sugar beet varieties occurred at high angles of solar radiation incidence only, these results will be presented as surface temperature measurements.

Canopy temperature readings – similar to those of soil surface temperature – were taken about solar noon each day when the radiation was undisturbed (clear sky conditions). At canopy temperature determinations the RAYNGER II.RTL type infrared thermometer was hand held at about 1 m above the canopy using an oblique angle of about 30°. In these cases, the sampling time was 30 seconds with three repetitions in each treatment. The average canopy temperature was calculated from temperature readings. The field of view of the instruments is 8°, the emissivity was assumed to be 0.98.

Because of the well-known heterogeneity of soil temperature measured by traditional mercury thermometers, soil surface temperature was measured with an infrared thermometer. This instrument takes 4 samples per second. The entire surface area of each plot was sampled by carrying the thermometer about 10 cm above the soil surface between the plant rows. From these readings, the surface temperature represented the average of the entire plot.

At the end of vegetative period, the sugar yield was determined by measuring both the root yield and sugar content of each sugar beet varieties.

3. Results and discussion

3.1 Assimilatory surface

The effect of change in plant biomass is twofold: the direct influence on size of photosynthetic area, and the indirect effect of plant architecture on canopy microclimate. The assimilatory surface can be therefore characterized easily by *leaf area index* (LAI).

There was no significant difference in LAI of sugar beet varieties in the first half of investigative period (from the middle of May to the end of June) when the weather was not dry and hot (*Fig. 1*). But as the drought in July occurred, the LAI curves of different beet cultivars separated. The largest assimilatory surface appeared in Kawemaya's canopy, where the size of LAI was almost two

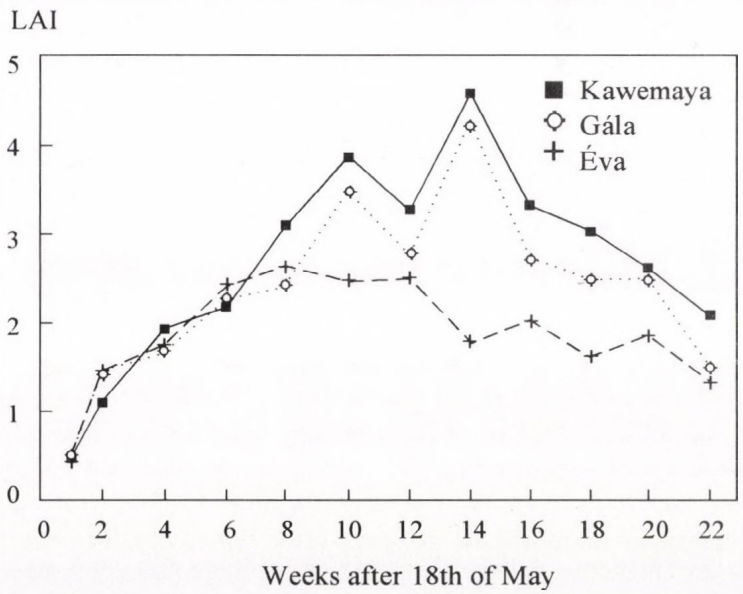

Fig. 1. Seasonal variation of leaf area index in 1992.

times higher than that of the LAI of Éva, the cultivar of lowest green area. Results of Gála were between the LAI of Kawemaya and Éva, but closer to the leaf area of Kawemaya.

4. Soil surface temperature

In May and June, when the LAI of the three beet varieties was nearby identical, the soil surface temperature of Kawemaya's plots increased significantly (*Fig. 2*). From the end of July, the higher the size of assimilatory surface, the cooler the soil surface temperature. Increased LAI of Kawemaya resulted in a 3 to 4°C decrease in instantaneous soil surface temperature compared to the values of Éva, the beet cultivar with the smallest assimilatory surface.

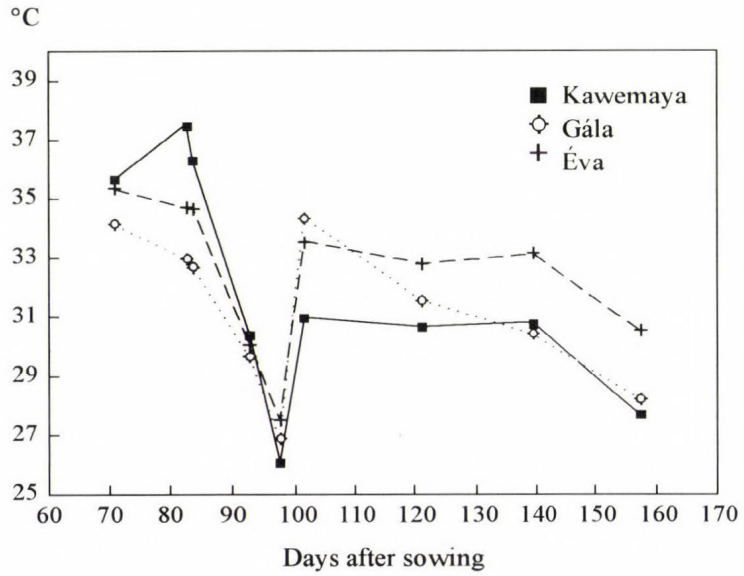

Fig. 2. Soil surface temperature about solar noon, 1992.

5. Canopy temperatures

There was little difference in plant canopy temperatures between the three varieties until the end of July (*Fig. 3*). Coincident with drought in August 1992, the canopy temperature curves separated according to the direction of change in soil temperatures. Coolest soil temperatures coincided with the treatment of the lowest instantaneous foliage temperature readings (Kawemaya).

The foliage temperature of Éva, the warmest treatment of the 3 varieties, was 3 to 6.5°C higher than the surface temperature of Kawemaya during the

dry and hot August of 1992. The degree of change in plant temperature seems to be high enough to modify the main plant physiological processes (photosynthesis, respiration and transpiration) and the production of dry matter.

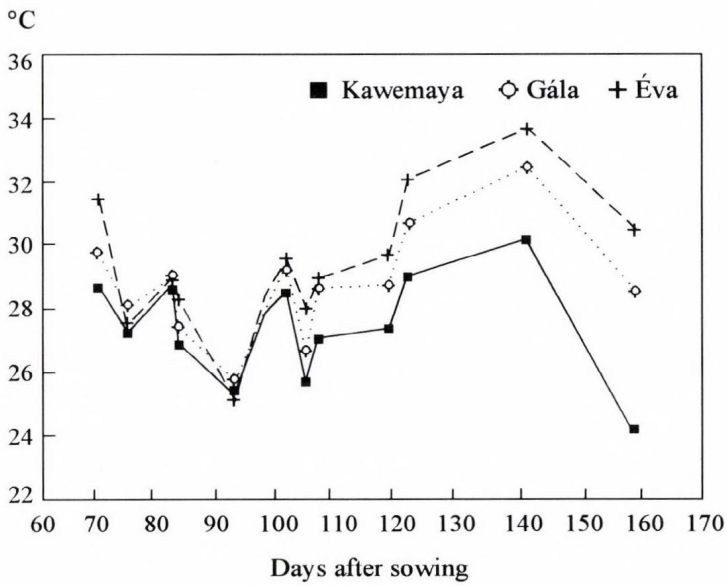

Fig. 3. Canopy temperature about solar noon, 1992.

6. Stomatal resistance

Independent of sugar beet cultivar, the instantaneous resistances measured at high incidence of solar radiation were two to three times larger than those resistance values determined earlier in the growing season. The likely explanation might be the occurrence of drought during the investigated period of 1992.

Hall et al. (1988) and *Mtui et al.* (1981) pointed out that difference in genotypes had no effect on stomatal conductances of alfalfa and corn varieties. In contrast, *Hattendorf et al.* (1990) found significant differences in stomatal conductance and water use efficiency among alfalfa cultivars with diverse origins.

In our study, there was a significant difference in stomatal resistances of different beet varieties during the dry and hot investigation period of 1992 (*Fig. 4*). The lowest resistances occurred in Kawemaya's canopy resulting in the largest transpiration and water losses. Mainly in the first half the data collection period Éva had larger stomatal resistances than the other two cultivars. As resistance decreases the pores open and the transpirational cooling is greater. It was concluded that soil temperature was one of the most important regulators

(driving force) of transpiration. At higher soil temperatures, transpiration intensity increases. In our study an opposite tendency occurred: the variation of warmest soil temperature and greatest stomatal resistance was the same (the cultivar Éva). The likely reason might have been the drought of 1992 growing season. Stomatal resistance of Kawemaya was the lowest, when the soil surface temperature was the coolest.

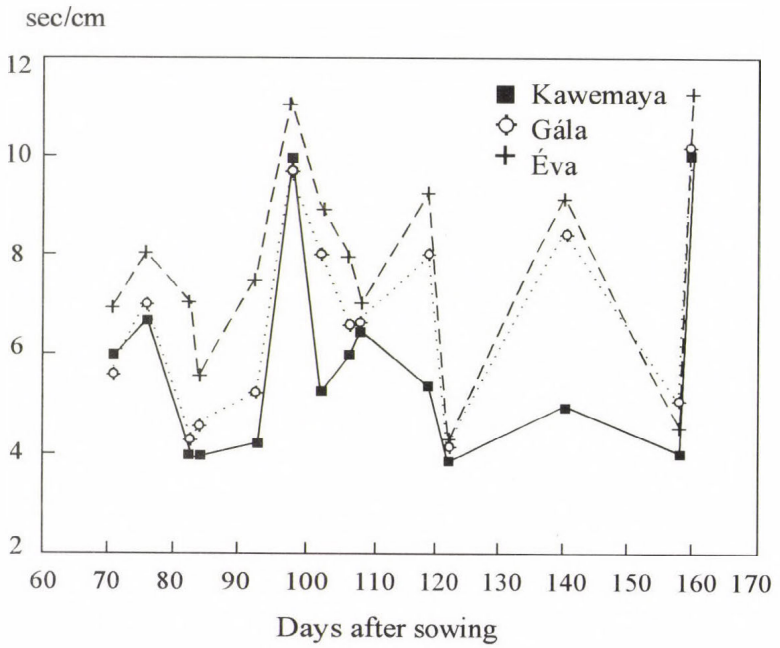

Fig. 4. Production of sugar beet varieties of diverse genetic origin.

7. Production of plants

In assessing sugar beet yield, two elements of yield, root mass and sugar content must be considered (*Fig. 5*). During the 1992 growing season, the variety Gála had the largest root yield of all. Decrease in root yield of Kawemaya and Éva were 8.1 and 36.7%, respectively compared to Gála.

There was no significant difference in sugar content between cultivars of Gála and Éva. The sugar percentage of Kawemaya increased by 10.2 and 10.3% compared to the sugar ratio of Gála and Éva varieties, respectively.

The goal of sugar beet production is to achieve the highest amount of produced sugar per unit area of soil. The cultivar with the highest production was Kawemaya. Decreases in sugar yield were 34.6 and 40.3% in Gála and Éva respectively, compared to Kawemaya.

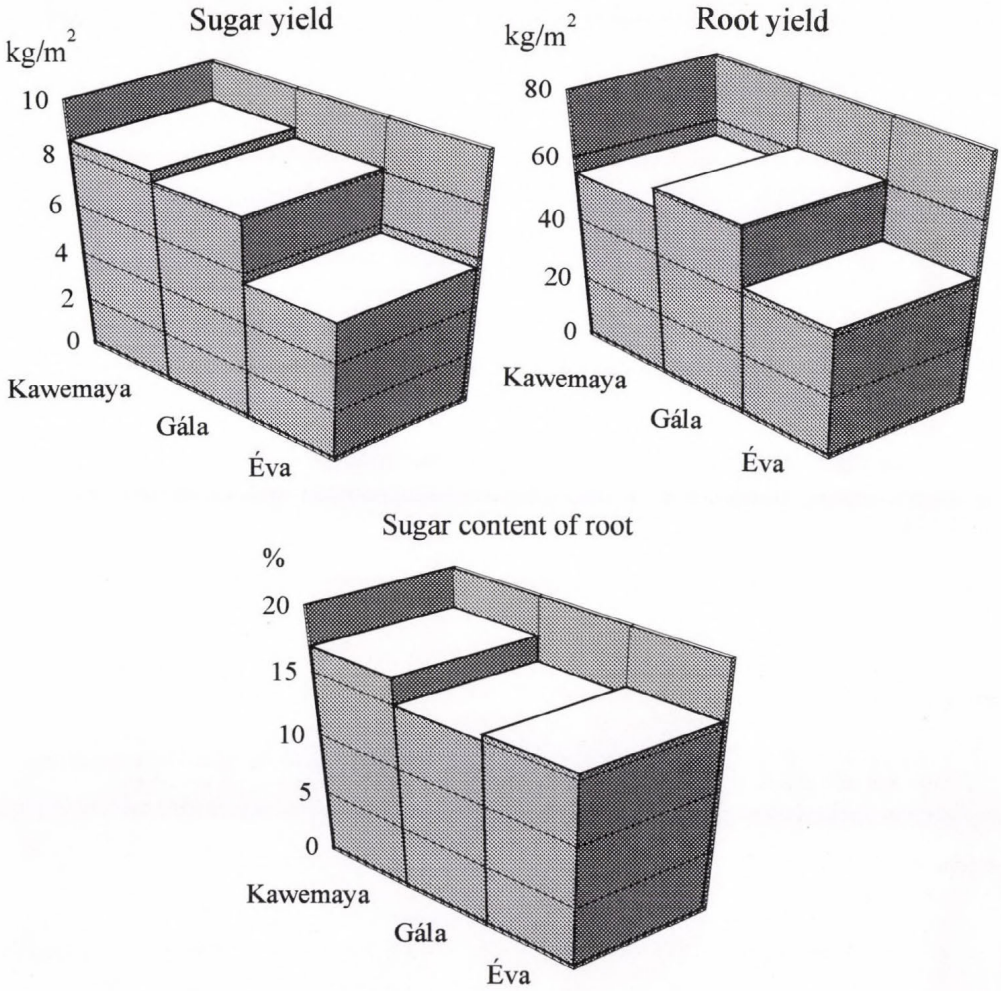

Fig. 5. Production of different sugar beet varieties.

The plant canopy and soil temperatures, and stomatal resistances were the most favourable in Kawemaya's canopy during the growing season in 1992. The greater sugar yield of the Kawemaya seems to be related to higher assimilatory surface resulting in an increased ability to produce more photosynthate. The greater biomass shadowed soil moderating soil surface temperature. At lower soil temperature the stomatal resistances decreased as transpiration increased. The cooler foliage temperature caused by low resistance values in Kawemaya's stand indicates greater transpirational cooling. In similar situations, one observes greater photosynthesis and subsequently greater yield (*Tanner* and *Sinclair*, 1981). Results of sugar production agree well with earlier investigations of *Sinclair et al.* (1981).

In our experiment, both canopy temperature and stomatal resistance values provided satisfactory results studying differences in parameters of sugar beet varieties of diverse genetic origin. As opposed to *Mtui et al.* (1981) stomatal resistance was as sensitive as canopy temperature, when non-irrigated field trial was carried out. Because of quickness of infrared thermometers, the canopy temperature seems to be a better indicator when assessing alterations of different plant varieties. The porometer use in comparative studies is time consuming, and since it is a point measurement, very uncertain. In contrast to stomatal resistance determinations, at infrared thermometer use the repeatability of temperature measurement is practically unlimited. In comparative studies (in plant breeding), when numerous treatments are investigated, the canopy temperature determinations should have primary importance. In our experiment, canopy temperature was sensitive indicator of physiological properties of sugar beet cultivars of diverse genetic origin. In practice, surface temperature measurements could serve a quick up-to-date method for plant breeders in selection of (sugar beet) varieties.

References

Brawn, K.W. and *Rosenberg, N.J.* 1970: Influence of leaf age, illumination, and upper and lower surface differences on stomatal resistance of sugar beet leaves. *Agron. J. 62*, 20-24.

Halim, R.A., Buxton, D.R., Hattendorf, M.J. and *Carlson, R.E.*, 1991: Crop water stress index and forage quality relationships in alfalfa. *Agron. J. 82*, 906-909.

Hall, H.M., Sheaffer, C.C. and *Heidel, G.H.*, 1988: Partioning and mobilization of photoassimilate in alfalfa subjected to water deficit. *Crop Sci. 28*, 964-969.

Hattendorf, M.J., Evans, D.W. and *Peaden, R.N.*, 1990: Canopy temperature and stomatal conductance of water stressed dormant and non-dormant alfalfa types. *Agron. J. 82*, 873-877.

Huzulak, J. and *Matejka, F.*, 1992: Stomatal resistance, leaf water potential and hydraulic resistance of sugar beet plants. *Biologia Plantarum 34*, No. 3-4, 291-296.

Idso, S.B., Reginato, R.J., Reicosky, D.C. and *Hatfield, J.L.* 1981: Determining soil-induced plant water potential depressions in alfalfa by means of infrared-thermometry. *Agron. J. 73*, 826-830.

Jackson, R.D., 1982: Canopy temperature and crop water stress. *Adv. in Irrig. 1*, 43-85.

Keener, M.E. and *Kirchner, P.L.*, 1983: The use of canopy temperature as an indicator of drought stress in humid regions. *Agric. Met. 28*, 339-349.

Lawlor, D.W. and *Milford, F.J.*, 1975: The control of water and carbon dioxid flux in water stressed sugar beet. *J. Exp. Botany 26*, 657-665.

Mtui, T.A., Kanemasu, E.T. and *Wassom, C.*, 1981: Canopy temperature, water use, and water use efficiency of corn genotypes. *Agron. J. 72*, 456-458.

Pinter, P.J. Jr., Stanghellini, M.E., Reginato, R.J., Idso, S.B., Jenkins, A.D. and *Jackson, R.D.*, 1990: Remote detection of biological stresses in plants with infrared thermometry. *Science 205*, 585-587.

Tanner, C.B. and *Sinclair, T.R.*, 1981: Efficient water use in crop production: Research or re-search. In *Efficient Water Use in Crop Production* (eds.: T.R. Sinclair, H.M. Taylor and W.R. Jordan). Amer. Soc. of Agron., Madison, Wisconsin.

Smith, R.C.G., Barrs, H.D. and *Fischer, R.A.*, 1988: Inferring stomatal resistance of sparse crops from infrared measurements of foliage temperature. *Agric. and For. Meteorol. 42*, 189-198.

Tubaileh, A.S., Sammis, T.W. and *Lugg, D.G.*, 1986: Utilization of thermal infrared thermometry for detection of water stress in spring barley. *Agric. Water Manag. 12*, 75-85.

Walker, G.K. and *Hatfield, J.L.*, 1983: Stress measurements using foliage temperature. *Agron. J. 75*, 623-629.

BOOK REVIEWS

H. B. Bluestein: **Synoptic-Dynamic Meteorology in Midlatitudes**. Vol. I: **Principles of Kinematics and Dynamics**. Oxford University Press, 1992, 431 pages; Vol. II: **Observations and Theory of Weather Systems**. Oxford University Press, New York, Oxford, 1993, 594 pages.

More than thirty years have elapsed since the publishing of the last edition of the two-volume textbook in synoptic meteorology by *Professor Sverre Petterssen* (*Weather Analysis and Forecasting*, Second Edition, Vol. I and II, McGraw-Hill, New York, 1956). The work of *Professor Howard B. Bluestein* provides a modern, updated replacement of the classical textbook of *S. Petterssen*. No other summarizing work has been published in synoptic meteorology since the middle of the fifties, meanwhile a series of good textbooks appeared in dynamic meteorology in the last three decades (e.g. *J.R. Holton*: *An Introduction to Dynamic Meteorology*, Third Edition, 1992; *A.E. Gill*: *Atmosphere-Ocean Dynamics*, 1982; *J.A. Dutton*: *The Ceaseless Wind*, 1986; *H. Pichler*: *Dynamics of the Atmosphere* (in German), 1984; *G.J. Haltiner* and *R.T. Williams*: *Numerical Prediction and Dynamic Meteorology*, Second Edition, 1980; *E. Palmén* and *C.W. Newton*: *Atmospheric Circulation Systems*, 1969).

This new, comprehensive textbook presents essential information about modern weather forecasting and analysis. It is based on *Professor Bluestein*'s fifteen years of teaching experience at the University of Oklahoma. *Professor Bluestein* received B.S. and M.S. degrees in electrical engineering and M.S. and Ph.D. degrees in meteorology from the Massachusetts Institute of Technology, he is a former *Oklahoma Professor of the Year*, and a recipent of the *Regents' Award for Superior Teaching*.

Vol. I of the book carefully examines the foundations of synoptic meteorology, from the analysis of scalar fields to atmospheric kinematics, dynamics and thermodynamics. Contemporary topics such as Q-vectors, and modern observing systems such as Doppler radar and lidar are discussed and the work emphasizes both physical understanding and mathematical analysis, and clearly explains observations in light of current theory.

Vol. II covers the interpretation of the behaviour of synoptic-scale systems in the context of both quasi-geostrophic theory in pressure coordinates and isentropic potential vorticity analysis. Frontal theory and observations are encompassed, along with mesoscale phenomena such as the coastal front, the dryline, and fronts that behave like trapped gravity currents. Semi-geostrophic theory, symmetric instability and jets are also detailed. Supercells, ordinary cells, mesoscale convective complexes, tornadoes, hail and microbursts are

discussed in the context of their larger scale environment. The text includes many helpful figures, photographs, selected problems and useful references for further readings.

This new, major textbook can be recommended for both undergraduate and graduate students of meteorology, workers of the weather forecast centres and for students of the new university postgraduate schools starting this year.

Gy. Gyuró

S. S. Butcher, R. J. Charlson, G. H. Orians and *G. W. Wolfe* (eds.): **Global Biogeochemical Cycles**. Academic Press, London, San Diego, New York, Boston, Sydney, Tokyo and Toronto, 1992. International Geophysical Series, Vol. 50, 367 pages.

During the last decade a new branch of sciences has been developed: the environmental science. In classical sense this science has a multidisciplinary character. However, the most important feature of this new science is that it wants to study the Nature as a global entity and does not bother with old classification of natural sciences. One of the main reasons for the development of this new discipline is the influence of mankind on our environment which has formed in close relationship with the biosphere during geological times. The most important subject area of environmental science is to investigate the huge material flow in Nature called the biogeochemical cycles.

The main aim of the present book is to discuss in one volume our knowledge of this essential field. The authors, coming from different research areas from biology to atmospheric science, try to summarize what we know about "the transport and transformation of substances in the natural environment, as seen in global context". The book is composed of sixteen chapters. After a short introduction the evolution of the Earth and the biosphere is presented. In two chapters the modeling of biogeochemical cycles and the chemical bases (e.g. equilibria, reaction rates) necessary for the study of the cycles are outlined. A separate chapter deals with tectonic processes playing an important role in shaping our planete. Then come four chapters discussing separately the pedosphere, the sediments, the ocean and the atmosphere. The next five chapters are devoted to a concise presentation of the biogeochemical cycles of such basic species like carbon, nitrogen, sulfur, phosphorus and different metals. The volume is closed with the discussion of human modification of global biogeochemical cycles.

Even this short enumeration shows the importance of this book. It should be added that these important subjects are treated in a fascinating way by the authors working mostly at the University of Washington (Seattle, WA, U.S.A.)

and the University of Stockholm (Sweden). Thus, they are congratulated for doing this not easy job. It goes without saying that some details in the text can be disputed. However, this does not touch the main merits of this work which is unique in this field. Different people can see differently the same subject. Briefly speaking, the use of this book is highly recommended to all scientists dealing with the study of biogeochemical cycles of different elements or compounds in the environment. It can be useful in particular for graduate students who want to get a specialization in environmental science.

E. Mészáros

ATMOSPHERIC ENVIRONMENT

an international journal

To promote the distribution of Atmospheric Environment *Időjárás* publishes regularly the *contents* of this important journal. For further information the interested reader is asked to contact *Dr. P. Brimblecombe,* School for Environmental Sciences, University of East Anglia, Norwich NR 7TJ, U.K.

Volume 27A Number 13 1993

Volume 27A Number 14 1993

R.T. McNider, M.P. Singh and *J.T. Lin*: Diurnal wind-structure variations and dispersion of pollutants in the boundary layer, 2199-2214.

P.M. Midgley and *D.A. Fisher*: The production and release to the atmosphere of chlorodifluoromethane (HCFC 22), 2215-2223.

A.J. Hayter and *M.M. Dowling*: Experimental designs and emission rate modeling for chamber experiments, 2225-2234.

Short Communication

G. Tidy and *J.N. Cape*: Ammonia concentrations in houses and public buildings, 2235-2237.

J. Padro, K.J. Puckett and *D.N. Woolridge*: The sensitivity of regionally averaged O_3 and SO_2 concentrations to ADOM dry deposition velocity parameterizations, 2239-2242.

Volume 27A Number 15 1993

G.J.H. Roelofs: A cloud chemistry sensitivity study and comparison of explicit and bulk cloud model performance, 2255-2264.

S.R. Hanna, J.C. Chang and *D.G. Strimaitis*: Hazardous gas model evaluation with field observations, 2265-2285.

A. Singer, Y. Shamay, M. Fried and *E. Ganor*: Acid rain on Mt Carmel, Israel, 2287-2293.

Xiaoming Zhang and *A.F. Ghoniem*: A computational model for the rise and dispersion of wind-blown, buoyancy-driven plumes-I. Neutrally stratified atmosphere, 2295-2311.

R.S. Thompson: Building amplification factors for sources near buildings: a wind-tunnel study, 2313-2325.

J.W. Spence, F.W. Lipfert and *S. Katz*: The effect of specimen size, shape, and orientation on dry deposition to galvanized steel surfaces, 2327-2336.

J. Baron and *A.S. Denning*: The influence of mountain meteorology on precipitation chemistry at low and high elevations of the Colorado Front Range, U.S.A., 2337-2349.

M. van Loon: Testing interpolation and filtering techniques in connection with a semi-Lagrangian method, 2351-2364.

S.J. Harrison, J.A. Vale and *C.D. Watts*: The estimation of aerial inputs of metals to estuarine waters from point pattern data using an isoplething technique: Severn Estuary, U.K., 2365-2373.

I.P. Bibby, G. Poots and *P.L.I. Skelton*: Theoretical aspects of iceload measurements on fixed rods and overhead line conductors: a transfer function for dry rime-ice accretion, 2375-2383.

I.M. Madany and *S. Danish*: Spatial and temporal patterns in nitrogen dioxide concentrations in a hot desert region, 2385-2391.

F. Fortezza, V. Strocchi, G. Giovanelli, P. Bonasoni and *T. Georgiadis*: Transport of photochemical oxidants along the northwestern Adriatic Coast, 2393-2402.

Volume 27A Number 16 1993

The Russian/American Desert Dust Experiment (Tadzhikistan) 1989

IDŐJÁRÁS

VOLUME 97 * 1993

BUDAPEST, HUNGARY

AUTHOR INDEX

TABLE OF CONTENTS

I. Papers

II. Book review

III. News

Contents of journal Atmospheric Environment, 1993

IV. SUBJECT INDEX

The asterisk denotes book reviews

NOTES TO CONTRIBUTORS

The purpose of *Időjárás* is to publish papers in the field of theoretical and applied meteorology. These may be reports on new results of scientific investigations, critical review articles summarizing current problems in certain subject, or shorter contributions dealing with a specific question. Authors may be of any nationality but papers are published only in English.

Papers will be subjected to constructive criticism by unidentified referees.

* * *

The manuscript should meet the following formal requirements:

Title should contain the title of the paper, the names(s) of the author(s) with indication of the name and address of employment.

The title should be followed by an *abstract* containing the aim, method and conclusions of the scientific investigation. After the abstract, the *key-words* of the content of the paper must be given.

Three copies of the manuscript, typed with double space, should be sent to the Editor-in-Chief: *P.O. Box 39, H-1675 Budapest,* Hungary.

References: The text citation should contain the name(s) of the author(s) in Italic letter or underlined and the year of publication. In case of one author: *Miller* (1989), or if the name of the author cannot be fitted into the text: *(Miller,* 1989); in the case of two authors: *Gamov* and *Cleveland* (1973); if there are more than two authors: *Smith et al.* (1990). When referring to several papers published in the same year by the same author, the year of publication should be followed by letters a,b etc. At the end of the paper the list of references should be arranged alphabetically. For an article: the name(s) of author(s) in Italics or underlined, year, title of article, name of journal, volume number (the latter two in Italics or underlined) and pages. E.g. *Nathan, K. K.,* 1986: A note on the relationship between photosynthetically active radiation and cloud amount. *Időjárás 90,* 10-13. For a book: the name(s) of author(s), year, title of the book (all in Italics or underlined with except of the year), publisher and place of publication. E.g. *Junge, C. E.,* 1963: *Air Chemistry and Radioactivity.* Academic Press, New York and London.

Figures should be prepared entirely in black India ink upon transparent paper or copied by a good quality copier. A series of figures should be attached to each copy of the manuscript. The legends of figures should be given on a separate sheet. Photographs of good quality may be provided in black and white.

Tables should be marked by Arabic numbers and provided on separate sheets together with relevant captions. In one table the column number is maximum 13 if possible. One column should not contain more than five characters.

Mathematical formulas and *symbols:* non-Latin letters and hand-written marks should be explained by making marginal notes in pencil.

The final text should be submitted both in manuscript form and on *diskette.* Use standard 3.5" or 5.25" DOS formatted diskettes for this purpose. The following word processors are supported: WordPerfect 5.1, WordPerfect for Windows 5.1, Microsoft Word 5.5, Microsoft Word for Windows 2.0. In all other cases the preferred text format is ASCII.

* * *

Authors receive 30 *reprints* free of charge. Additional reprints may be ordered at the authors' expense when sending back the proofs to the Editorial Office.

Published by the Hungarian Meteorological Service

Budapest, Hungary

INDEX: 26 361

HU ISSN 0324-6329